ICUS REPORT 2009-01

INTERNATIONAL CENTER FOR
URBAN SAFETY ENGINEERING

INSTITUTE OF INDUSTRIAL SCIENCE
THE UNIVERSITY OF TOKYO

2nd JOINT STUDENT SEMINAR ON CIVIL INFRASTRUCTURES
July 6, 2009

Edited by

Shinji Tanaka, Hyunmyung Kim, Kyung-Ho Park,
Muhammed Alamgir and Keh-Jian Shou
ICUS, IIS, The University of Tokyo, Japan

ISBN4-903661-30-0

Serial Number 37

2nd Joint Student Seminar on Civil Infrastructures

6 July 2009
Bangkok, Thailand

Co-Organized by

School of Engineering and Technology,
Asian Institute of Technology (AIT), Thailand

International Center for Urban Safety Engineering (ICUS)
Institute of Industrial Science
The University of Tokyo, Japan

BK-21 Global Leaders in Construction Engineering,
Korea University, Korea

Myongji University, Korea

King Monkut's University
of Technology North Bangkok, Thailand

National Chung-Hsing University, Taiwan

Khulna University of Engineering and Technology, Bangladesh

Chulalongkorn University, Thailand

and
Research Team for Maintenance Technology of Infrastructure,
Konkuk University, Korea

Edited by

Dr. Shinji Tanaka, Dr. Hyunmyung Kim, Dr. Kyung-Ho Park,
Prof. Muhammed Alamgir and Prof. Keh-Jian Shou

Organization Teams

Dr. Kyung-Ho Park (AIT, Thailand)
Dr. Pison Udomworrat (KMUT-NB, Thailand)
Dr. Hyunmyung Kim (AIT, Thailand)
Dr. Anat Ruangrassamee (Chula Univ., Thailand)
Dr. Jaroon Rungamornrat (Chula Univ., Thailand)
Dr. Kunnawee Kanitpong (AIT, Thailand)
Mr. Zaw Zaw Aye (SEAFCO, Thailand)
Dr. Adisorn Owatsiriwong (ALPS, Thailand)

Dr. Shinji Tanaka (UT, Japan)
Dr. Wataru Takeuchi (UT, Japan)
Dr. Kawin Worakanchana (UT, Japan)
Dr. Shinya Hanaoka (TIT, Japan)
Dr. Sano Kazushi (Nagaoka Univ. Of Tech, Japan)
Prof. Atsushi Koizumi (WU, Japan)
Dr. Koichiro Mizuno (EJRC, Japan)

Prof. Young-Uk Kim (MJU, Korea)
Dr. Jung-Sik Kong (KU, Korea)
Dr. Seok-Won Lee (KKU, Korea)
Prof. Ikki Kim (HYU, Korea)
Prof. Young-Ihn Lee (SNU, Korea)
Dr. Gye-Chun Cho (KAIST, Korea)
Dr. Gun-Ha Kim (HNU, Korea)
Dr. Yong-Taek Lim (CNU, Korea)
Dr. Chang-Yong Kim (KICT, Korea)
Dr. Dong-Hoon Shin (K-water, Korea)
Dr. Ik-Soo Ha (K-water, Korea)

Prof. Keh-Jian Shou (NCHU, Taiwan)

Prof. Muhammed Alamgir (KUET, Bangladesh)

Dr. Borinara Park (Illinois State Univ., USA)
Dr. Jung-Seok Oh (Wastern Michigan Univ., USA)
Dr. Eckhard Kraft (BU Weimar, Germany)
Dr. Semih Kuchkarslan (Istanbul Technical Univ., Turkey)

2^{nd} JOINT STUDENT SEMINAR ON CIVIL INFRASTRUCTURES

July 2009

PREFACE

As our activities expand beyond the border, international collaboration becomes more and more important. And, to build up a good relationship with other communities during young school days will be of advantage in the future. Considering this background, we held the 1^{st} seminar in July 2008, and following this success, "the 2^{nd} joint student seminar on civil infrastructures" was held on 6^{th} July 2009.

The objectives of this seminar are,
1) to experience the organization of international seminar,
2) to improve the presentation skill,
3) to share the research information and friendships.

The number of participants was 34, consisting of 16 faculties and 18 students from Korea University, Chonnam National University, Seoul National University, Suranaree University of Technology, Chulalongkorn University, Asian Institute of Technology, Khulna University of Engineering & Technology and The University of Tokyo. In this seminar, there were 4 faculties' lectures and 18 students' presentations. The topics were varied from all areas of civil engineering and every student did their best in his/her presentation as well as in the discussion. At the end of the seminar, excellent presentation awards were given to the following 3 students.

1. Ms. Hoang Thuy Linh from Japan
2. Mr. Jung-Yub Lee from Korea
3. Mr. Md. Reaz Akter Mullick from Thai

The student participants played the major role of this seminar, discussing on their research topics and communicating with students from other countries. The seminar was quite successful and fruitful in that this seminar gave not only knowledge and information but also a lot of other stimuli to the students. We hope to continue to hold this kind of interchange activities in the coming years.

Finally, we would like to express our sincere gratitude for those who kindly supported and contributed to the success of this seminar.

SHINJI TANAKA, HYUNMYUNG KIM, KYUNG-HO PARK,
MUHAMMED ALAMGIR AND KEH-JIAN SHOU

Table of Contents

Booth at seminar

Opening ceremony (Dr. Joydeep Dutta)

Prof. Muhammed Alamgir

Prof. Youngtaek Lim

Prof. Haruo Sawada

Dr. Thirayoot Limanond

Ms. Hee-Joo Kim

Mr. German A. Pardo R.

Ms. Bupavech Phansri

Mr. Vu Viet Hung

Ms. Sun-Ae Yi

Ms. Mari Sato

Mr. Md. Abdur Razzaque

Ms. Hoang Thuy Linh

Mr. Dee-Sik Nam

Mr. Pramuk Prabjabok

Mr. Jun-Seok Jang

Ms. Theonette Ruba Maribojoc

Mr. Jung-Yub Lee

Mr. Tawin Tiratanapakhom

Mr. Shumon Mori

Mr. Taiki Kou

Mr. Md. Reaz Akter Mullick

Excellent Presentation from Japan

Excellent Presentation from Korea

Excellent Presentation from Thai

Group Photo

Invited Lectures

INDIGENOUS APPROACH FOR THE CONSTRUCTION OF A PILOT SCALE SANITARY LANDFILL IN BANGLADESH

MUHAMMED ALAMGIR and MD. REZAUL ISLAM
Department of Civil Engineering
Khulna University of Engineering & Technology, Bangladesh
alamgir63dr@yahoo.com

ABSTRACT

This paper describes the process employed for the construction of a Pilot Scale Sanitary Landfill (PSSL) at the ultimate disposal site of Municipal Solid Waste (MSW) at Rajbandh, Khulna, Bangladesh. A very simple but technically compatible design is considered here to use local building materials and to avoid any imported materials such as any kind of geosynthetics. A local contractor having no field experience in the construction of sanitary landfill is entrusted for the construction. The available indigenous approach mostly manual labour intensive was employed to complete the construction of landfill base and the daily operation during waste deposition period. This field experience described in the paper will help in establishing the sanitary landfill construction standard for Bangladesh based on the local conditions, socio-economic settings and technological capabilities.

1. INTRODUCTION

Insufficient and ineffective government policy and response, lack of political will, lack of required economic and human resources, weak local institutions and in absence of appropriate & integrated system result in poor waste management in Bangladesh, especially in the big cities. These cities therefore face major problems relating to public health and environmental pollution (Alamgir et. al 2005a). Among the various problems exist in the Municipal Solid Waste (MSW) management tiers such as poor collection and unpleasant scenario at the secondary disposal sites, uncontrolled open dumping remains as one of the major striking environmental issues in Bangladesh. Like other Least Developed Asian Countries (LDACs), ultimate disposal sites of MSW are situated in and around the city areas at low-lying open spaces, unclaimed land, riverbanks and roadsides (WasteSafe 2005). Uncontrolled dumping of solid waste around the world becomes one of the major striking social and environmental issues. There are no controlled/engineered/sanitary landfills in Bangladesh; however, recently Dhaka City Corporation has taken an initiative to convert 'Matuail Open Dumping Site' into the Engineered Landfill (Ahmed 2008). Due to severe financial constraints and the priorities to other sectors such as food, shelter, health and education, central and local governments are not able to address this social and environmental issue despite the realization that the only affordable disposal solution in Bangladesh for the foreseeable future – is to establish engineered landfills (WasteSafe 2005, Alamgir et al. 2008).

By considering this, the Pilot Scale Sanitary Landfill has constructed and being operated to establish landfill construction technology in Bangladesh. Locally available construction techniques, equipments and building materials were used for the excavation of earth, construction of various components of the landfill such as approach road, site office, base liner and leachate collection system, leachate holding tank, leachate treatment tank etc. In every phase of PSSL construction such as material processing, maintaining slope, placement, remolding and compaction work manual labors are used where female participant was viewed a focus because 70% of labors were female. The deposition of waste has been monitoring and other necessary aspects have been controlling to ensure the quality management of daily operation. In spite of a pilot scale sanitary landfill, this is the second experience of the construction of sanitary landfill in Bangladesh. It is observed that using locally available construction materials and methods using manual labor intensively, the sanitary landfill can be constructed successfully with necessary components such as compacted clay liner, leachate detection and collection system. This small scale but real experience using indigenous method will provide confidence to the city authority and the concerned stakeholders about landfill technology in the contrast of presently practicing crude open dumping.

2. PILOT SCALE SANITARY LANDFILL IN BANGLADESH

To establish appropriate construction technology for Bangladesh conditions using local building materials, technical capabilities and the available technology, a pilot scale sanitary landfill is designed and hence constructed during the first-half of 2008 and currently is being operated. In the design and construction, very simple approach relevant to the condition of LDACs is considered, the details are discussed in the following sections.

2.1 Background

To address one of the most striking environmental and social issues in the urban areas of LDACs i.e. MSW management, a 12 months feasibility study project entitled *as "Integrated management and safe disposal of municipal solid waste in LDACs - WasteSafe*", was conducted by the Department of Civil Engineering, Khulna University of Engineering & Technology (KUET), Bangladesh during the period of 2004 to 2005, co-financed by Asia Pro Eco Programme of the European Commission. The project proposed a system named as '*WasteSafe Approach*' with some specific guidelines to address the MSW issues in an integrated and sustainable way. An appropriate method of MSW management can be established for any specific location/region of LDACs considering local conditions with the analysis and evaluation of practical application of this approach. To develop a safe and sustainable management of MSW in

Bangladesh through the practical application of *WasteSafe Approach* with required reality check and evaluation of the implemented parts, a three years (2007 to 2009) partnership project entitled as "*Safe and Sustainable Management of MSW in Bangladesh through the Practical Application of WasteSafe Proposal – WasteSafe II*" has been conducting since January 01, 2007 co-financed through a grant received from EU-Asia Pro Eco II Programme of the European Commission. One of the key activities of this research project is to establish the landfill construction technologies suitable for Bangladesh conditions as realized from field level experience through a pilot scale sanitary landfill (WasteSafe II 2007). To this endeavour, the landfill cell of the dimension of 50x50x6m, which is 3m below and 3m above the existing ground surface, has been constructed with the necessary components, at Rajbandh, Khulna, the ultimate disposal site of MSW of Khulna City Corporation (KCC).

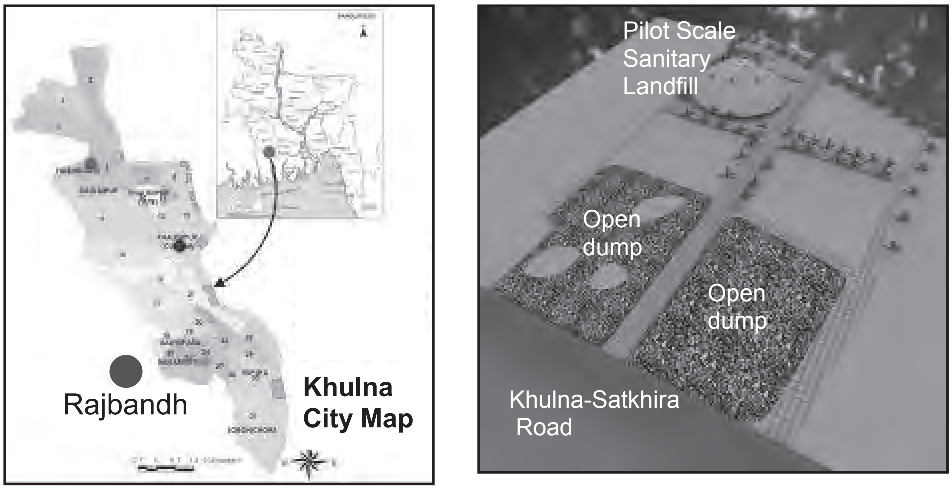

Figure 1: Location and layout of pilot scale sanitary landfill (PSSL) at Rajbandh as shown with respect to Khulna city map

2.2 Location and sub-soil conditions of the landfill sites

The site located at Rajbandh, Khulna with an area of 5 acres, is 8km far from the city centre i.e. Royal & Castle Salam Square of Khulna city and situated along the North-side of Khulna-Satkhira highway as shown in Figure 1. Actually, it is known as New Rajbandh, the second ultimate open disposal site of MSW of KCC, just 700m away from the older one, know as Old Rajbandh of 20 acres land. The New Rajbandh consists of 5 cells where paddy plantation and fish cultivation were continued till the waste deposition started. Despite the partial filling of MSW in the older one, KCC started to dump MSW in the New Rajbandh since January 2007 and first two cell cells along the Khulna-Satkhira Highway were started to fill. The site of the PSSL is located at the north-west cell as shown in the Figure 1.

The performance of Geoenvironmental structures such as landfill liners, covers, impoundments of vertical barriers depends mainly on the basic characteristics of the soils. The geotechnical characteristics of the sub-soils were determined in the laboratory using conventional test methods after collecting the soil samples through a sub-soil exploration by wash boring method up to a depth of 17m. The existing ground surface exists at a depth of 1m from the road level, while the ground water table is encountered at a depth of 2m. The fine-grained soils predominated in the site till the executed depth with the presence of significant portion of organics in the depth of 2 to 3.5m. The laboratory result shows that in the depth of 0-2m, the average value of liquid limit, plastic limit and the plasticity index are 53%, 33% and 20, while in the subsequent layers, these values vary from 36-71%, 22-37% and 13 to 41, respectively.

Hydraulic conductivity is a main indicator to judge the suitability of clay to prepare Compacted Clay Liner (CCL) for the construction of landfill. Liner soil should have at least 30% fines and 15% clay to achieve hydraulic conductivity in the range of $1x10^{-7}$cm/s (Benson et al.1994). In this context, it is revealed that the clay available in the site can be used for natural barrier to achieve a hydraulic conductivity in the range of $1x10^{-7}$ cm/s, as it possesses suitable amount of clay and fine fractions. But the soil must not be placed at too high water content as it results low shear strength and may be great risk of desiccation cracks forming if the soil dries, and ruts may form when construction vehicles pass over the liner.

The hydraulic conductivity varies as the water content changes and it is measured that as the molding water content increases from 12 to 28%, the hydraulic conductivity reduces from $25x10^{-7}$ to $15x10^{-5}$cm/s. The water content of CCL material at the time of compaction is the most important variable that controls the engineering properties of the compacted material. For this soils, it is observed that soils compacted at water content less than optimum tend to have a relatively high hydraulic conductivity: soils compacted at water contents greater than optimum tend to have a low hydraulic conductivity.

2.3 Waste streams

In Bangladesh the solid wastes mainly consists of food and vegetables waste (Alamgir et al. 2005b). Other items are presents in negligible percentages. For a basic understanding of the nature of the wastes that are generally encountered, the type distribution of particle sizes must be known. The particle size distribution of waste was determined by sieve analysis of the sieve of openings are 400, 300, 200, 100, 75, 38.2, 19.1, 9.52, 4.76 and 2.38mm. The result shows that the average percent finer in Bangladesh are 100% in 200mm sieve openings whereas 83% in 100mm, 72% in 76.2mm, 53% in 38.2mm and 33% in 19.1mm and gradually decreases for smaller sieve openings. Physical properties of wastes are determined before the deposition in the pilot scale sanitary landfill. The average moisture content of the waste deposited in the sanitary landfill is 64.48%. The typical composition is shown in Figure 2, which represents the percentage of solid waste as food & vegetable 93%, plastics 3%, demolition 2% and others 2%.

Figure 2: Composition of MSW in Khulna

2.4 Design aspects and various components of PSSL

Despite a pilot scale sanitary landfill cell, the WasteSafe II Team decided to consider all the relevant aspects of a standard sanitary landfill while designing the cell and the components. Emphasis is also given for the best use of locally available building materials and construction techniques. However, scientific and technical considerations, guided by field experiences, are given while fixing up the dimensions and materials specification of the various components of the landfill. The PSSL consists of the main components of a standard landfill such as (i) Waste deposition cell, (ii) Compacted clay liner on a geological barrier with a drainage layer on top (iii) Top Cover with compacted clay liner, drainage layer, top soil as vegetation cover, surface run-off and percolated water collection system, (iv) Gas measurement and management facility, (v) Leachate detection and collection system with leachate holding tank, (vi) Leachate pond with leachate treatment facility, (vii) Vehicle inspection and washing facility,

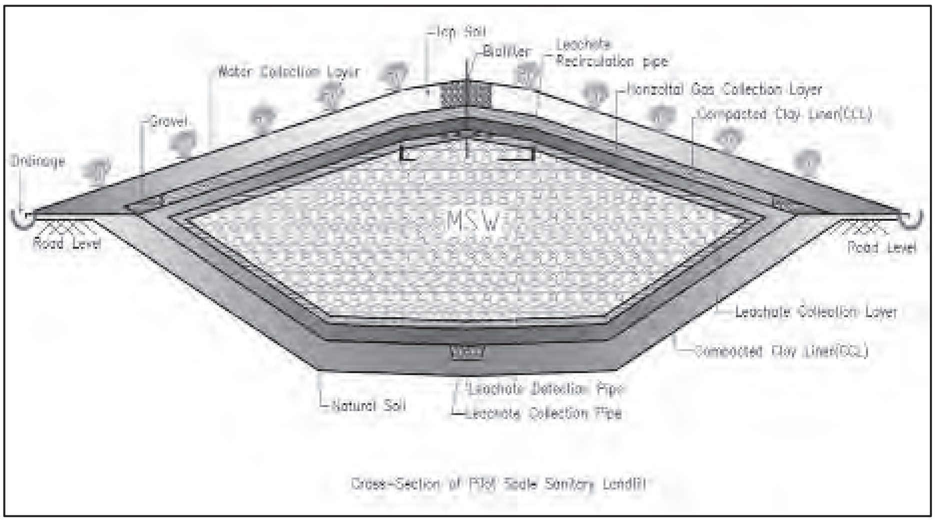

Figure 3: Schematic diagram of the pilot scale sanitary landfill

(viii) Access Road and Site office, (ix) On-going and post closure monitoring facilities.

Analysis and Design of the PSSL was completed by WasteSafe Team members by December 2007 guided by field experiences, local condition and project provision while fixing up the dimensions and materials specification of the various components of the landfill. The MSW collected from Khulna city will be deposited in shortest possible time with moderate compaction efforts. It is decided to follow the standard landfill operation system with local perspectives will be followed during the construction, waste deposition and operation, and monitoring phases. Post closure monitoring will be conducted till the end of the project, which will be continued by KUET till the active period of the landfill.

The size of the waste containment is 50x50x6m, which is 3m below and 3m above the ground surface with a side slope of 26^o the schematic diagram is presented in Figure 3. The base liner, the most important component, includes a leak detection sump system, compacted clay liner, leachate collection pipe system with a leachate collection layer. It is designed considering hydrological data of the site, the size of landfill, suitability of construction and locally available of material as shown in Figure 4. The base liner has a 400mm thick of CCL just above the geological barrier of 15m clay deposits, over which 200mm thick sand layer as drainage layer. Leachate collection pipe is placed in the drainage layer, while the leachate detection pipe is placed just below the CCL. The generated leachate will be stored in leachate holding tank of 2x2x4m and later transfer to the leachate treatment pond of 10x20x3.5m. The system is designed in such a way so that the leachate can be collected and thus stored in the tank through gravity flow. The leachate detection pipe is also designed and connected in the leachate holding tank by ensuring gravity flow. From tank the leachate will be transferred to the pond using pump.

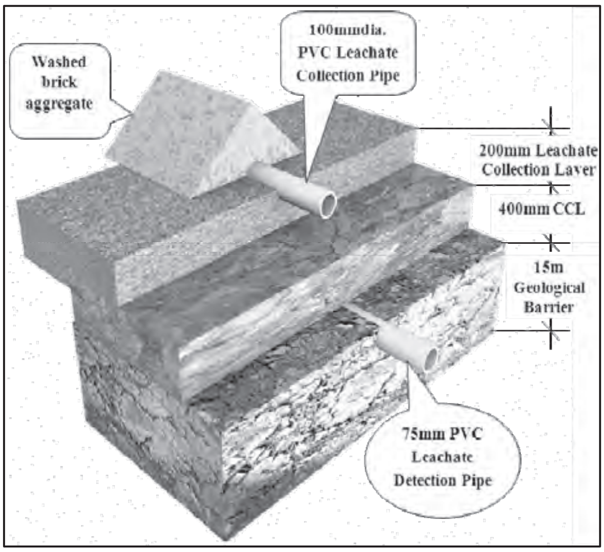

Figure 4: Schematic diagram of base liner

The final cover of PSSL as shown in Figure 5, consists of top soils, percolation water collection layer, compacted clay liner and gas collection pipe system with gas collection layer. The inclusion of biofilter for methane oxidation is kept as possible inclusion in the top cover. The top has gas collection layer at the top of 200mm thick just over the waste, then 300mm CCL, 150mm fine sand and 150mm sand plus brick aggregates as percolation and drainage layer which is followed by 600mm top soil. The combination of fine sand layer and then sand and brick aggregates is given to ensure capillary rise of water for the keeping CCL wet as much as possible to prevent possible desiccation and cracking. Top soil layer of 600mm thick will help to support and maintain the growth of vegetation by retaining moisture and providing nutrients. There is a Leachate Recirculation System that will maintain moisture and enhance degradation of waste. To control possible soil erosion, mild slope is maintained at the top cover, which is 15^o at the edge to middle and then 7^o from middle to top.

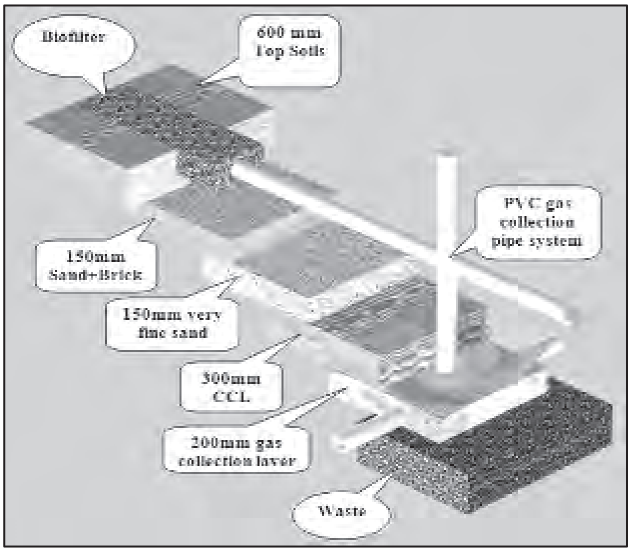

Figure 5: Schematic diagram of the cap liner

3. CONSTRUCTION OF LANDFILL

This PSSL is the first of this kind of construction in Bangladesh. The construction works have been conducted based on the design ensuring close monitoring by the project engineer. Another important aspects is that the locally available construction techniques, equipments and building materials were used for the earth excavation, construction of various components of the landfill such as approach road, inspection point, site office, base liner, leachate collection and detection systems, leachate holding tank, leachate pond and the small scale leachate treatment option.

3.1 People's participation

In a waste management system, social issue plays very important role and sometimes overrule the technical requirements and aspects. Moreover, as there is no sanitary landfill in Khulna, it is necessary to inform the people about this pilot project, which might play very important role for taking decision about actual one. From this view point, after completion of necessary official requirements, an inauguration ceremony was arranged on 19th March 2008 at the site, as shown in the Figure 6 to demonstrate the salient features of the project, positive impacts on the environment and its future on waste management. The Hon'ble Mayor of KCC, Ward Councilors, KCC officials, local people, civic societies, academicians, researchers, NGOs/CBOs, journalists and other relevant stakeholders were present. In the site, project coordinator graphically presented all the relevant elements and the related aspects of the sanitary landfill. This demonstration played a very positive role in the next course of actions as realized during construction and operation phases.

Figure 6: Demonstration on PSSL at site

3.2 Appointment of the contractor

An open tender for the construction of the PSSL was published on January 03, 2008 by KCC in the major local and national both the English and Bengali newspapers. It also launches in the website: www.wastesafe.org. The tender documents kept available both in KCC and KUET for the interested bidder. The closing date for the submission of document was 27 Jan., while the opening date was 28 Jan. 2008. Meeting of Technical Evaluation Committee was held at KCC Bhaban, Khulna on 22nd February 2008. Among the four bidders for the construction of pilot scale sanitary landfill, considering all the relevant aspects, it was decided to select the lowest bidder for the construction works. None of the firm has the experience of the construction of sanitary landfill. However, acknowledging the reality and the volume of works, selection was made. The work order was given to the selected construction company on March 12, 2008 and the construction works started on March 19, 2008.

3.3 Layout and site preparation

The site consists of five shallow ponds having earth embankments in all sides; those have been using for traditional agriculture and fish cultivation before the starting of waste dumping from the beginning of January 2007. For the PSSL construction, the pond located in the north-west corner is considered. As per the design and location of various components, layout was completed using traditional civil engineering survey equipments and the site was cleaned by removing grass, existing paddy plants and others unplanned trees as shown in the Figure 7.

Figure 7: Layout and preparation of site to start construction

3.4 Earth excavation

The main volume of works is the excavation of earth for the construction of landfill cell till the required depth. The ground surface was existed at the depth of 1m from the road level. Firstly, it was decided that the excavation will be conducted mechanically using the excavator, however, the non-availability of the machine, the alternate option came into mind. Moreover, due to the existence of very soft soil and the size of the land, it was decided to conduct the excavation works using manual labour and traditional digging tools as shown in the Figure 8. Daily about 50 to 100 people works at the site and nearly 70% of the work force were female. The excavation of earth was completed successfully maintaining proper slope of the cell as per the design and specification. Very close monitoring was conducted by the project engineer for the proper execution of the works. During the execution of the earth excavation, the soil from the top 2m, which seems to be suitable for the preparation of CCL, were collected with care and deposited in the middle of cell as well as on the bank, those were used later. During excavation, soils were also placed properly in the north side and south-west corner for the construction of the earth embankment surrounding the cell. Initially, it was thought that manual work might not be suitable for such sophisticated works, however, finally it was proved that, this kind of work at small scale can be done properly within reasonable timeframe if proper level of monitoring can be ensured. However, such works will not be suitable in the monsoon season.

Figure 8: Manual excavation of earth using traditional digging tools

3.5 Preparation of compacted clay liner

Liner on the bottom and sides of landfills that contain solid wastes has been considered necessary in many countries since the late 1970s. The main requirements of liners are the minimization of pollutant migration, high adsorption capacity and retardation of pollutants, resistance to chemicals and low swelling and shrinkage potential (Brandl 1992). Compacted Clay Liner (CCL) is the most important element of a sanitary landfill to prevent migration of leachate from landfill (Daniel & Keorner 2007). Clay and clay minerals play an important role in increasing containment removal capacity as well as in reducing hydraulic conductivity of soil because of their large specific surface area and high Cation Exchange Capacity (CEC) (Oweis & Khera 1998; Czurda & Cranston 1991).

The low hydraulic conductivity of clay minerals makes them potential materials to use as CCLs in sanitary landfill for environmental protection. The attenuation positively charged chemical species in leachate through a clay liner is a function of CEC of the liner material. Higher CEC of a clay liner material will result in greater amount of cationic containments being removed from the leachate (Kayabali 1997); Rowe et. al. (1995) recommended that soils with a minimum CEC of about 10 meq/100g of soil might be specified for clay liner. Soils classified as inorganic clay with high plasticity (CH) is considered as the suitable material for landfill liner (Oweis & Khera 1998). The clay liner is typically designed to have a hydraulic conductivity $\leq 1 \times 10^{-7}$cm/s. The origin of this design criterion is unclear; 1×10^{-7}cm/s was evidently selected on the assumption that this was an achievable value that would result in negligibly small seepage through the liner. In the PSSL, the clayey soils collected from the depth of 0 to 2m of the site, were used for the construction of CCL as the test results revealed the suitability of the clay. The stock pile of clay used to construct CCL and later its spreading over the bed for compaction are shown in Figure 9.


Figure 9: Stock pile of appropriate and its spreading to prepare CCL

The compaction of soil was done manually in three layers by using locally manufactured hammer made of cast iron connected with timber handle. The clay were placed uniformly over the bed and then compacted by adding required amount of water as shown in Figure 10. To ensure uniformity of compaction, a locally practiced technique is maintained while applying the hammer drop by a group of female worker. The thickness of the layer was maintained in such a way that the resultant thickness of the CCL reached as 400mm. The degree of compaction of the CCL was checked in the field by sand cone test method as shown in Figure 11, usually used as field compaction test. Initially, it was planned to prepare the CCL by using Sheep foot or smooth wheeled roller, however, due to the soften nature of soils; later compaction was done using manual intensive practice and equipments. However, finally a very impressive CCL was constructed with locally available technology and equipments without heavy machineries and skilled people as shown in Figure 12.

Figure 10: Manual compaction of clay to prepare CCL of the PSSL

Figure 11: Field compaction test of the prepared CCL of the PSSL

Figure 12: Partial view of completed CCL

3.6 Leachate detection pipe System

To depict the applicability of simple liner system and the functionality of CCL, leachate was collected through a leachate detection pipe placed just below the CCL. A long trench of 0.75mx0.75m starting from the center point of the cell till the leachate storage tank was dug in the bed of natural soil barrier of the landfill site to accommodate the pipe. A No. 10 perforated PVC filter pipe of 38mm in diameter used as leachate detection pipe system was placed in the trench which was surrounded by 150mm thick layer of granular soil to ensure free drainage of detected leachate. To ensure the gravity flow of the collected leachate, 1% slope towards the sump was maintained as shown in Figure 13. A vertical pipe having larger diameter is connected with the outlet end of the pipe, which is just at the inner surface of the tank, so that the leachate can be collected and the flow can be measured by removing leachate from the top. In all these works, local materials and traditional techniques were used and the performance so far is found quiet satisfactory.

Figure 13: Placement of leachate detection pipe

3.7 Leachate collection system

Figure 14: Jointing of leachate collection pipe in the field

Figure 15: Preparation of bed to place leachate collection pipe

Leachate Collection System (LCS) is considered as one of the most important components of sanitary landfill. The system commonly comprises perforated pipe at regular spacing in a continuous blanket of granular material to collect leachate. The primary function of leachate collection system is to control the leachate head acting on the liner system. Controlling of leachate head minimizes the advective transport of contaminants and also controls side slope leachate breakouts. Lowering height of leachate mounding, leachate seeps can be minimized. Leachate pressure head on liner gets reduced, hence gradient through liner gets reduced resulting flow reduction through liner. Finally, removing contaminants from the landfill reduces the available amount contaminants for transport.

To collect the leachate through gravity the bed was constructed maintaining a 3^{o} slope and the leachate collection pipe is placed at the middle of the cell. The leachate collection layer of 200mm thick was construction to accommodate a perforated leachate collection pipe with 100mm dia. and surrounded by washed brick aggregates as shown in the Figures 14-17. The collection was laid maintaining a slope of 3^{o} towards the leachate holding tank to ensure the easy movement of leachate through gravity flow as mounded on the leachate collection pipe.

Figure 16: Placement of leachate collection pipe at bed

Figure 17: Leachate collection pipe with brick aggregates as filter media

A Leachate holding tank of 2x2x4m size was constructed with brick masonry and properly connected with both the leachate collection and detection pipes as shown in Figure 18. From the tank, the leachate can be transferred to the treatment tank before discharge to natural streams as shown in Figure 18. Leachate pond has the size of 10x20x3.5m which was excavated, lined with locally available polythene sheet with double layer and compacted clay liner, using local technique as adopted from the construction of cell.

Figure 18: Leachate holding tank & treatment pond

Figure 19: Washing platform for waste carrying vehicle

A vehicle washing platform of 4x7m size was constructed just in front of site office to wash the outgoing vehicle to prevent any possible littering of waste while running out in the street as shown in Figure 19. For the construction of this platform very strong reinforced cement concrete was used. The access road was also constructed by the compacted brick bats and sands for the easy movement of vehicles.

The site office as shown in Figure 20 was constructed using local material such as *golpata* and bamboo for roofing, wooden pile (*bullah)* and *terrazzo* for column support and fencing around the periphery and brick masonry and concrete work for foundation and floor. The entire area is protected by constructing a boundary using bamboo pillar and barbet wire. The site office has been using to control and to inspect incoming vehicles and the wastes quality and quantity, office recording, demonstration of landfill construction and operation to the visitors and to conduct other relevant works.

Figure 20: Site office & control room

4. WASTE DEPOSITION AND DAILY OPERATION

MSW generated in KCC areas has been deposited in the PSSL. The incoming waste carrying vehicles are being counted, volume of waste measured roughly, weighted indirectly, inspected and hence recorded properly. Initially, deposited wastes were spreaded manually, later KCC's vehicle such as Back-wheeled Compactor cum Excavator and Chain-dozer, were employed for the spreading of wastes and hence compacted by the self-weight of vehicle and repeated passes. In some instances, for convenience, the manual labor and the compactor worked together for waste plantation and compaction as shown in Figure 21. At the beginning polythene sheet was used for temporary daily cover and presently sand is used irregularly as daily cover. Heavy rainfall during monsoon created special problem to operate the landfill properly, such as damage of approach road, movement of vehicle on the wastes, difficulties of waste plantation and compaction and generation of huge amount of leachate. During monsoon, to relieve the pressure of contaminants in the landfill, leachate was transferred to the nearest pond temporality; those were evaporated during dry season. One of the most difficult tasks is to keep the landfill free from birds, flies and dogs. A traditional system is being used to keep the landfill free from birds. However, in spite of limitation of resources and due to inexperience of landfill operation in local as well as Bangladesh condition, the waste deposition and daily operation have been running satisfactorily.

Figure 21: Manual spreading waste

5. CONCLUSION

The existing practice of crude open dumping in Bangladesh leads to irrecoverable environmental hazards throughout the country. The country needs to convert the existing ultimate disposal sites of MSW through the development of sustainable landfill based on its prevailing socio-economic settings, technological capabilities and the local conditions. The success history of the studied PSSL achieved so far, based on local building materials, available techniques, locally available traditional equipments, manual labor intensive works and simple design, will bring a positive change in the attitude of the local authority to switch from existing practice of crude opening dumping to sanitary landfill.

ACKNOWLEDGEMENTS

The financial supports provided by European Commission through the project of EU-Asia Pro Eco II Programme (Grant Contact No. ASIE/2006/122-432) are gratefully acknowledged.

REFERENCES

Ahmed, M.F. 2008. Improvement of solid waste facilities at Matuail in Dhaka City. *Proc. of the National Seminar on Solid Waste Management – WasteSafe 2008*, 9-10 February 2008, Khulna, pp.1-12.

Alamgir, M. Ahsan, A., McDonald, C.P., Upreti, B.N. and Islam, R. 2005a. Present Status of Municipal Solid Wastes Management in Bangladesh. *Proc. International Conference on Waste-The Social Context*, May 11-14, Edmonton, Alberta, Canada. Pp 11-20.

Alamgir, M., Chowdhaury, K.H., Roehl. K.E., Stentiford, E.I. and Bari, Q.H. 2005b. Basic Characteristics of Municipal Solid Wastes of Bangladesh. *Proc. International Conference on Waste-The Social Context*, May 11-14, Edmonton, Alberta, Canada. Pp 21-26.

Alamgir, M., Bidlingmaier, W., Hossain, Q.S., Mohiuddin, K.M. and Islam, M.R. 2008. Future Prospects of CDM Framework to Develop a Sustainable Landfill System in Bangladesh to Replace Open Dumping. *Proc. of 6th Intl. ORBIT Conf. on 'Moving Organic Waste Recycling Towards Resource Management and Biobased Economy'*, October 13-15, 2008 at Wageningen, the Netherlands, pp. 246/1-10.

Bensen, C.H., Zhai, H. and Wang, X. 1994. Estimating hydraulic conductivity of clay liners. *Journal of Geotechnical Engineering*, ASCE, Vol.120, No.2, pp.366-387.

Brandl, H. 1992. Mineral liner for hazardous waste containment, *Geotechnique*, Vol 42, No. 1, pp. 57-65.

Czurda, P. and Cranston, M. 1991. Observation on the performance of composite clay liners and covers", *Proceedings of Geosynthetic Design and Performance*. Vancouver Geothechnical Society, Vancourver, British Columbia.

Daniel, D.E. and Koerner, R.M. 2007. *Waste Containment Facilities*, 2nd Edition, American Society of Civil Engineers, 978-0-7844-0859-9, Reston, Virginia.

Kayabali, K. 1997. Engineering aspects of a novel landfill liner material: bentonite amended natural zeolite", *Engineering Geology*, Vol. 46, pp. 105-114.

Oweis, I.S. and Khera R.P. 1998. *"Geotechnology of waste management"*, 2nd Edition, PWS Publishing Company, USA.

Rowe, R.K., Quigley, R.M. and Booker, J.K. 1995. *Clayey barrier system for waste disposal facilities*", E& FN Spon, London.

WasteSafe 2005. *Integrated Management and Safe Disposal of Municipal Solid Waste in Least Developed Asian Countries: a feasibility study.*

M. Alamgir, C. McDonald, K.E. Roehl and A. Ahsan Edited WasteSafe Report, KUET, Bangladesh.

WasteSafe II 2007. *Annual Report 2007 of WasteSafe II – Safe and Sustainable Management of Municipal solid waste in Bangladesh through the Practical Application of WasteSafe Proposal.* A project of EU-Asia Pro Eco II Programme of EC, KUET, Khulna, Bangladesh.

A TARGET-ORIENTED NETWORK DESIGN MODEL FOR TRANSPORTATION MODE CHOICE PROBLEM

YONGTAEK LIM
Dept. of Transportation & Logistics
Chonnam National University, Korea
limyt@chonnam.ac.kr

ABSTRACT

The network design problem (NDP) is to determine a set of design parameters that leads the transportation system to an optimal state after allowing for travellers' responses. This paper presents a modified NDP for transport mode choice problem, called target-oriented NDP, which contains a target that we try to arrive in real world. Unlike general NDP which seeks an optimal value to minimize or to maximize objective function, in target-oriented NDP traffic manager or operator can set a target level and then try to find an optimal design variable to attain this target. An example for simple transportation mode choice problem is given to test the model.

1. INTRODUCTION

In order to alleviate traffic congestion, the network design problem (NDP) has been used because it is to determine a set of design parameters that leads the road network to an optimal state. The scope of the NDP includes traffic signal control, traffic information provision, congestion charge and new transportation modes as well as road expansion. In general, the NDP usually formulated a bi-level problem, which has an upper level part that represents system design and a lower level one that represents travellers' responses, try to find an optimal value to minimize or to maximize objective functions such as total travel time or net social benefit.

We have a long list of network design problems, which can be classified into the two classes of discrete network design problem (DNDP) and continuous network design problem (CNDP) according to the nature of the design parameter. For solving such CNDP, the sensitivity analysis of user equilibrium was introduced by Tobin and Friesz (1988) and has been used for the static network design problem by Yang (1995; 1997) and in the dynamic case by Heydecker (2002). Various sensitivity analysis-based heuristic algorithms are also proposed for the CNDP and relevant problems (Friesz et al, 1990; Yang and Yagar, 1994;Yang et al, 1994, Lim et al, 2005). Recently Maher et al (2001) proposed a bi-level problem for trip matrix estimation and traffic control problem with stochastic user equilibrium (SUE), and their solution algorithms in which SUE assignment map was approximated as a linear relationship. More detail and wider literature reviews and their algorithms are described in the paper of Yang et al (1998).

This paper presents a modified NDP for transport mode choice problem, called a target-oriented NDP, which contains a target that we try to arrive in real world. Unlike general NDP described above, the target-oriented model sets a target level in advance and then try to find an optimum under this constraint, which represents a sub-optimum, compared to general NDP. To reach the target, two methods have been developed such as direct sensitivity design model and cross sensitivity design model that use derivative information. This paper has been organized as follows. In next section, the basic idea of target NDP is given, and its formulation and solution algorithm are also described. An equilibrium condition for transportation mode choice problem is defined in section 3. In section 4, an example for a simple mode choice problem is given to test the model. Finally, conclusions are drawn in section 5.

2. TARGET-ORIENTED NDP FOR TRANSPORTATION MODE CHOICE PROBLEM

2.1 Basic idea of target network design model

The main difference between general NDP and the target NDP is that in target NDP traffic managers set a prior specific level, a target, which they wish to attain for the transportation system. On the contrary, in general NDP they try to optimize the system without setting a target. For instance, congestion pricing is introduced to maximize net social benefit of transportation system and search optimal design parameter (pricing rate) in general NDP. But in target NDP traffic managers set a target level of service (LOS) in advance, like LOS C, and then try to search an optimal design parameter able to reach the target. Hence the target NDP may be a variant of the general NDP. This kind of target NDP can be expressed as follows.

$$\begin{aligned} \min \quad & L(p(X)) = L(F - F^*) \\ subject \quad & F = p(X) \end{aligned} \tag{1}$$

Where, X is design parameter and F^* is target level. F is a function of the design parameter, which represents traffic assignment or mode choice mapping in transportation problem. Equation (1) is similar to traffic control model for attaining desired goal, for example ramp metering on expressway system, in that case the parameter X can be interpreted as a control variable and F as a state variable.

2.2. Model formulation for transportation mode choice problem

In this section we present a target NDP for mode choice problem. If we set a target value as p_r^*, target split of mode r, then the design parameter can be determined by following mathematical minimization program given equation (2), which minimizes the difference between target modal split and estimated modal split derived from logit mode choice model in constraint.

$$\min \quad L(p(t(d))) = \frac{1}{2}(p_r - p_r^*)^2 \tag{2}$$

$$\text{Subject to } \; p_r(t) = \frac{e^{-\theta t_r}}{\sum_u e^{-\theta t_u}}$$

Where $t_i = \sum_j v_{ij} + d_i$, v_{ij} is the j^{th} attribute (travel time or travel cost, etc.) of mode i, and d_i is design parameter of mode i. θ is a scale parameter of the logit model. This minimization program can be solved by two types. The first is direct sensitivity design method, which use the sensitivity of change of probability with respect to its own attributes to achieve its target. The other is cross sensitivity design method, which use indirect sensitivity of other transportation mode.

Consider the first method. By using the direct sensitivity, equation (2) can be linearly expanded at d_r^0 into equation (3).

$$L(p(t(d_r))) \approx L(p(t(d_r^0))) + \left.\frac{\partial L}{\partial p_r}\frac{\partial p_r}{\partial t_r}\frac{\partial t_r}{\partial d_r}\right|_{d_r = d_r^0} (d_r - d_r^0) \tag{3}$$

Here notes that this linear equation should be equal to zero at minimum, so we get following formulation.

$$L(p(t(d_r^0))) + \left.\frac{\partial L}{\partial p_r}\frac{\partial p_r}{\partial t_r}\frac{\partial t_r}{\partial d_r}\right|_{d_r = d_r^0} (d_r - d_r^0) = 0$$

$$d_r = d_r^0 - \left[\left.\frac{\partial L}{\partial p_r}\frac{\partial p_r}{\partial t_r}\frac{\partial t_r}{\partial d_r}\right|_{d_r = d_r^0}\right]^{-1} L(p(t(d_r^0))) \tag{4}$$

Finally we get optimal design parameter of d_r^* for reaching the target modal split through equation (4), which is a recursive formula computed with ease. Where, $\frac{\partial L}{\partial p_r} = (p_r(t) - p_r^*)$ and $\frac{\partial p_r(t)}{\partial t_r}$ can be derived from logit model as,

$$\frac{\partial p_r(t)}{\partial t_r} = \frac{-\theta e^{-\theta t_r}(\sum_u e^{-\theta t_u}) - e^{-\theta t_r}(-\theta)e^{-\theta t_r}}{(\sum_u e^{-\theta t_u})^2} = -\theta p_r(t) + \theta(p_r(t))^2$$
$$= -\theta p_r(t)(1 - p_r(t))$$

Following the same way, we get cross sensitivity design method for transportation mode r with regard to design parameter $d_a, (a \neq r)$ of other mode a, as given in equation (5).

$$d_a = d_a^0 - \left[\frac{\partial L}{\partial p_r} \frac{\partial p_r}{\partial t_a} \frac{\partial t_a}{\partial d_a} \bigg|_{d_a = d_a^0} \right]^{-1} L(p(t(d_a^0))) \tag{5}$$

Where, $\frac{\partial L}{\partial p_r} = (p_r(t) - p_r^*)$, and $\frac{\partial p_r(t)}{\partial t_a} = \theta p_r(t) p_a(t)$.

Based on the equation (4) and (5), solution procedures for direct and cross sensitivity methods can be listed as follows.

[step 0] initialization

set iteration number $n = 0$

set initial design parameter $d_i^n, (i = r, a)$

and target value of mode r as p_r^*

[step 1] $n = n + 1$

[step 2] calculate $p_r(t(d_i^{n-1}))$ by logit model with d_i^{n-1}

[step 3] update

(3.1) direct sensitivity design method

$$d_r^n = d_r^{n-1} - \left[\frac{\partial L}{\partial p_r} \frac{\partial p_r}{\partial t_r} \frac{\partial t_r}{\partial d_r} \bigg|_{d_r = d_r^{n-1}} \right]^{-1} L(p(t(d_r^{n-1})))$$

(3.2) cross sensitivity design method ($a \neq r$)

$$d_a^n = d_a^{n-1} - \left[\frac{\partial L}{\partial p_r} \frac{\partial p_r}{\partial t_a} \frac{\partial t_a}{\partial d_a} \bigg|_{d_a = d_a^{n-1}} \right]^{-1} L(p(t(d_a^{n-1})))$$

[step 4] convergence test

If $\left| d_i^n - d_i^{n-1} \right| < \kappa$, then stop; otherwise, proceeds [step1]

Where κ is a predetermined small value for convergence criteria.

3. TRANSPORTATION MODE CHOICE EQUILIBRIUM IN LOGIT MODEL

Consider a transportation network with one origin-destination (OD) pair w connecting two transport modes of auto and transit, then the flows of auto, f_a, can be calculated by following logit model.

$$f_a = q_w \frac{e^{-\theta t_a}}{\sum_u e^{-\theta t_u}}$$

Where q_w is travel demand for OD pair w. Following the same way, for rail f_r is computed.

$$f_r = q_w \frac{e^{-\theta t_r}}{\sum_u e^{-\theta t_u}}$$

If we divide f_a by f_r, then

$$\frac{f_a}{f_r} = \frac{e^{-\theta t_a}}{e^{-\theta t_r}}$$

Take logarithm on both sides.

$$\ln\left(\frac{f_a}{f_r}\right) = -\theta t_a + \theta t_r$$

And then we finally get following equation.

$$t_a + \frac{1}{\theta}\ln(f_a) = t_r + \frac{1}{\theta}\ln(f_r) \qquad (6)$$

Equation (6) represents a transportation mode choice equilibrium condition in logit model. Let the condition define equivalent travel time for mode i,

$$Ec_i = t_i + \frac{1}{\theta}\ln(f_i), \qquad \forall \text{ mode } i \qquad (7)$$

in which Ec_i is constant for each mode at equilibrium mode choice condition.

4. NUMERICAL CALCULATIONS

In order to illustrate use of the model and the solution algorithm suggested in the paper, a simple example for mode choice problem is used. As shown in figure 1, this example has two transportation modes of auto and rail serving travellers between one origin-destination pair. We assume that the travel time of auto is a function of flows on the roads, but that of rail is constant (fixed value) irrespective of passengers on board. Travel demand for the OD pair is 5 units.

Travel time of auto : $t_a = 2 + f_a$

Travel time of rail : $t_r = 5$

Travel demand : $q_w = f_a + f_r = 5$

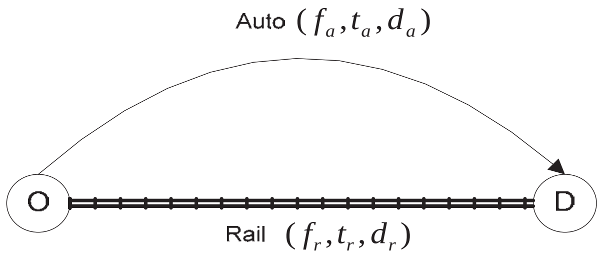

Figure 1: Example for target mode choice problem

In initial stage with no design parameter, the modal splits for each mode are divided by $p_a = 0.52$, $p_r = 0.48$ with $f_a = 2.6$, $f_r = 2.4$ and $t_a = 4.6$, $t_r = 5$. Now consider target problem. Let target modal split of rail set 0.6, or $p_r^* = 0.6$, and the parameter of logit model $\theta = 0.2$. If we introduce the design parameter to the travel time of auto or rail, then the function can be rewritten as follows.

$$t_a = (2 + f_a) + d_a$$
$$t_r = 5 + d_r$$

4.1 Direct sensitivity design parameter

Figure 1 depicts the change of modal split of rail (p_r), design parameter (d_r), and travel time of rail (t_r). As iteration number increases, p_r converges to the target modal split ($p_r^* = 0.6$) and design parameter decreases from zero to the value of -2.4274, which leads the travel time of rail to the value of 2.5726 from 5. These findings show that the model proposed in this paper produces correct solution and converges to steady state. Table 1 shows some major findings from the model with varying target modal split of rail from 10% to 70%. The optimal design parameter (d_r^*) decreases according to increasing the target mode split of rail as we expect. Among figures in the table, the partial derivative of rail split with regard to travel time of rail, $\frac{\partial p_r}{\partial t_r}$, has negative sign, which represents that model split of rail decrease as increase of travel time of rail. Note here that Ec_a and Ec_r last two rows in the table have the same value, which represents transportation mode choice equilibrium described in section 3.

Figure 3 illustrates some sensitivities of objective function with respect to design parameter for varying θ in logit model. All sensitivities are going down to zero point, which represents that no more increments of objective with regard to increment of travel time exist.

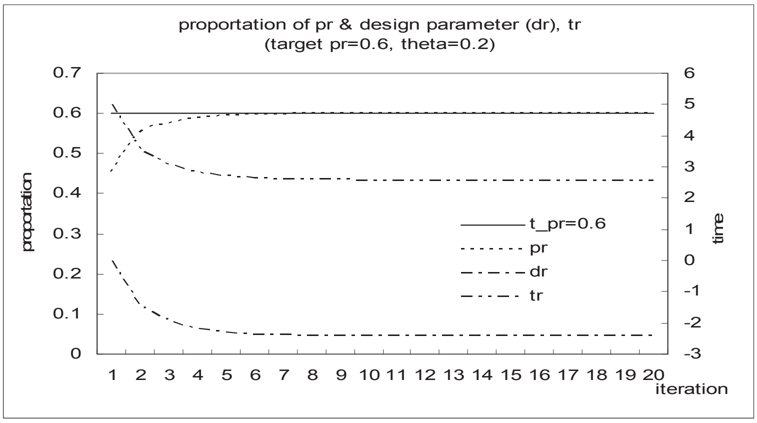

Figure 2: Change of modal split of rail (p_r) and design parameter (d_r) as iteration number increases : direct design

Table 1: Some key finding with varying target split of rail (p_r^*) : direct design

	target split of rail, p_r^*						
	0.1	**0.2**	**0.3**	**0.4**	**0.5**	**0.6**	**0.7**
d_r^*	10.5861	6.5314	3.8364	1.6273	-0.4000	-2.4274	-4.6365
f_a	4.3223	3.7951	3.3401	2.9222	2.5200	2.1170	1.6963
f_r	0.6777	1.2049	1.6599	2.0778	2.4800	2.8830	3.3037
t_a	6.3223	5.7951	5.3401	4.9222	4.5200	4.1170	3.6963
t_r	15.5861	11.5314	8.8364	6.6273	4.6000	2.5726	0.3635
p_a	0.9	0.8	0.7	0.6	0.5	0.4	0.3
p_r	0.1	0.2	0.3	0.4	0.5	0.6	0.7
$\frac{\partial p_r}{\partial t_r}$	-0.018	-0.032	-0.042	-0.048	-0.05	-0.048	-0.042
$Ec_a(auto)$	13.6411	12.4636	11.3702	10.2839	9.1413	7.8669	6.3386
$Ec_r(rail)$	13.6411	12.4636	11.3702	10.2839	9.1413	7.8669	6.3386

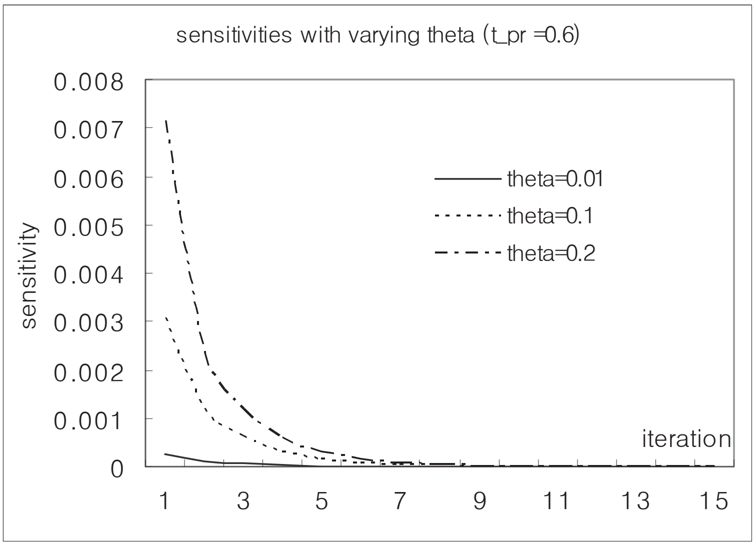

Figure 3: Sensitivities of $\frac{\partial L}{\partial d_r} = \left[\frac{\partial L}{\partial p_r} \frac{\partial p_r}{\partial t_r} \frac{\partial t_r}{\partial d_r} \bigg|_{d_r = d_r^{n-1}} \right]$ *for varying* θ *in with* $p_r^* = 0.6$

4.2 Cross sensitivity design parameter

Figure 4 shows the change of modal split of rail (p_r), design parameter of auto (d_a), and travel time of auto (t_a). The rail split also converges to the target split ($p_r^* = 0.6$) as iteration number increases. After several iterations, we get steady stable values of d_a and t_a shown in the figure. Compared to the figure 2 of direct sensitivity design parameter, the design parameter of auto (d_a) gradually increases, which leads to increment of travel time of auto, and finally to increase of split of rail in system.

Table 2 explains key findings derived from the cross sensitivity design method, which includes optimal cross design parameter (d_a^*), travel times, modal splits for each mode, and derivative of rail split ($\frac{\partial p_r}{\partial t_a}$). This table also shows that Ec_a and Ec_r has the same value, which represents the existence of mode choice equilibrium. Note here also that in case of $p_r^* = 0.1$ and $p_r^* = 0.2$, travel times of auto (t_a) has negative values, which does not exist in real world. This result comes from the fact that under fixed rail travel time ($t_r = 5$), auto travel time should be decreased below zero for reducing the split of rail to 0.1 or 0.2. So this phenomenon implies that we can not achieve such target splits just by reducing travel time of auto.

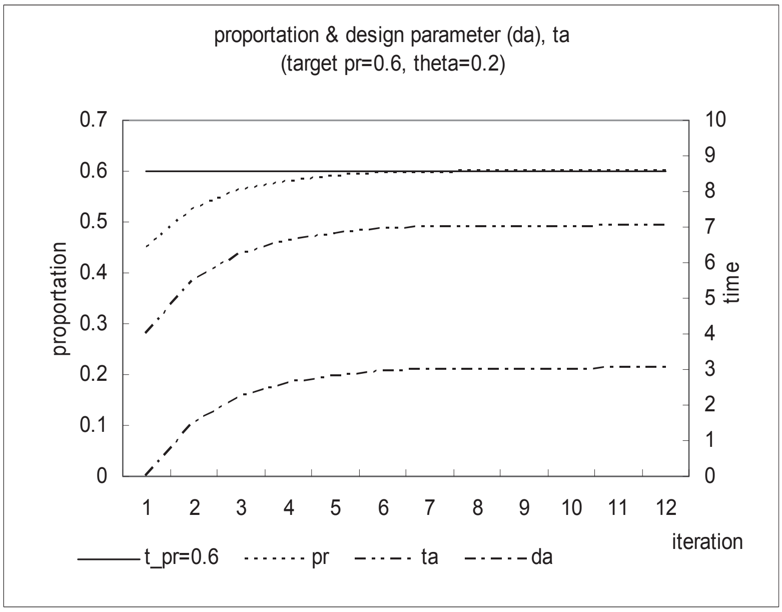

Figure 4: Change of modal split of rail (p_r) and design parameter (d_a) as iteration number increases : cross design

Table 2. Some key finding with varying target split of rail (p_r^*) : cross design

	target split of rail, p_r^*						
	0.1	**0.2**	**0.3**	**0.4**	**0.5**	**0.6**	**0.7**
d_a^*	-9.9861	-5.9315	-3.2365	-1.0273	1.0000	3.0273	5.2365
f_a f_r	2.0000 3.0000	2.0000 3.0000	2.0000 3.0000	2.0000 3.0000	2.0000 3.0000	2.0000 3.0000	2.0000 3.0000
t_a t_r	-5.9861 5.0000	-1.9315 5.0000	0.7635 5.0000	2.9727 5.0000	5.0000 5.0000	7.0273 5.0000	9.2365 5.0000
p_a p_r	0.9 0.1	0.8 0.2	0.7 0.3	0.6 0.4	0.5 0.5	0.4 0.6	0.3 0.7
$\frac{\partial p_r}{\partial t_a}$	0.018	0.032	0.042	0.048	0.05	0.048	0.042
$Ec_a(auto)$ $Ec_r(rail)$	1.5343 1.5343	5.0000 5.0000	7.0273 7.0273	8.4657 8.4657	9.5815 9.5815	10.4931 10.4931	11.2638 11.2638

5. CONCLUSION

In this paper, we propose a target-oriented network design model for transportation mode choice problem, which is a variant of general network design problem. To reach the target, two methods have been developed such as direct sensitivity design and cross sensitivity design model. Due to the existence of explicit function between travel demands of each mode and design parameter in logit model, we can easily derive the derivative and introduce it to the solution procedures. From the numerical examples, we calculate optimal design parameters, sensitivity and some other key findings as well as equivalent travel time (Ec_i), which represents the equilibrium condition among transportation modes. These results show that the model converges to steady state and its algorithm is feasible and advantageous in terms of real world applications.

REFERENCES

Friesz, T.L.,Tobin, R.L.,Cho, H.-J. and Mehta, .J. 1990. Sensitivity analysis based heuristic algorithms for mathematical programs with variational inequality constraints. Mathematical Programming, **48**, 265-284.

Heydecker, BG 2002. Dynamic equilibrium network design. **In**: Transportation and Traffic Theory in the 21st Century (ed MAP Taylor). Oxford: Pergamon, 349-70.

Lim, Y., BG. Heydecker, S. Lee 2005. A continuous network design model in stochastic user equilibrium based on sensitivity analysis, Journal of Advanced Transportation, Vol 39 No. 1, 63-79, Winter

Maher, M.J., Zhang, X, and Van Vliet, D. 2001. A bi-level programming approach for trip matrix estimation and traffic control problems with stochastic user equilibrium link flows. Transportation Research, **35B**, 23-40.

Tobin, R.L. and Friesz, T.L. 1988. Sensitivity analysis for equilibrium network flows. Transportation Science, **22**, 242-250.

Yang, H. 1995. Sensitivity analysis for queuing equilibrium network flow and its application to traffic control. Mathematical and Computer Modeling, **22**, 247-258.

Yang, H. 1997. sensitivity analysis for the elastic demand network equilibrium problem with applications. Transportation Research, **31B**, 55-70.

Yang, H and Yagar, S. 1994. Traffic assignment and traffic control in general freeway-arterial corridor systems. Transportation Research, **28B**, 463-486.

Yang, H, Yagar, S.,Iida, Y. and Asakura, Y. 1994. an algorithm for the inflow control problem on urban freeway networks with user-optimal flows. Transportation Research, **28B**, 123-139.

Yang, H.and Bell, M.G.H. 1998. Models and algorithms for road network design: a review and some new developments. Transportation Reviews, **18**, 257-278.

CURRENT REMOTE SENSING FOR LAND ENVIRONMENT AND DISASTER

HARUO SAWADA
International Center for Urban Safety Engineering
Institute of Industrial Science, The University of Tokyo, Japan
Department of Civil Engineering, The University of Tokyo, Japan
sawada@iis.u-tokyo.ac.jp

Current Remote Sensing for Land Environment and Disaster

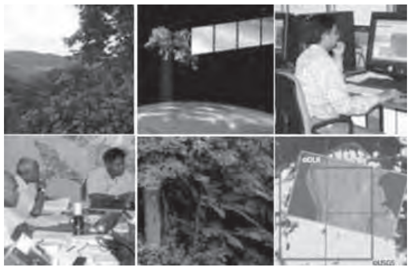

ICUS, IIS
The University of Tokyo

1

International Center for Urban Safety Engineering (ICUS)

(Established on April 1, 2001 for a 10-year period)

Director: MEGURO, Kimiro

The International Center for Urban Safety Engineering (ICUS) was established in April 2001 with the objective of developing new systems and methods to protect individuals from various accidents and disasters that could possibly occur in everyday life, mostly in urban areas throughout the world. ICUS works in collaboration with researchers and engineers from around the world.

The research areas of this center are :
1) Sustainable Engineering
2) Urban Safety and Disaster Mitigation
3) Infrastructure Information Dynamics

International Activities/ ICUS and RNUS

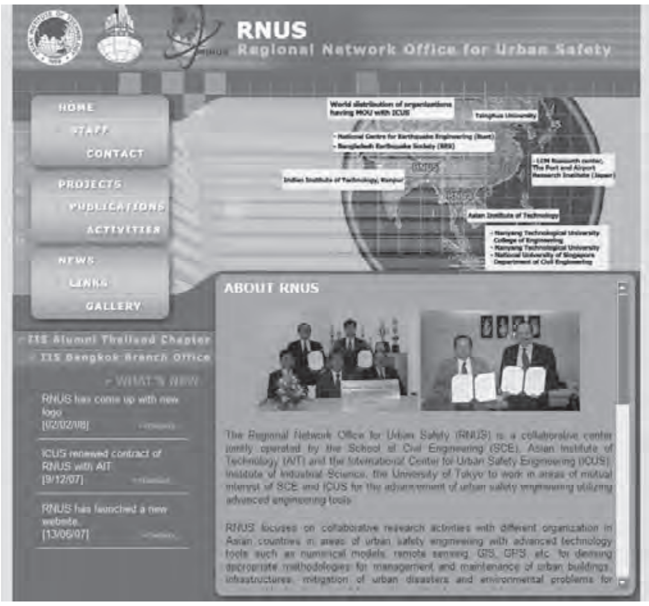

Construction Material Management – Kato lab

Study on providing durable infrastructures as well as maintenances of existing infrastructures while reducing cost, resource consumption, and environmental impact; A sustainable design philosophy is necessary to develop the new concrete materials to meet this challenge.

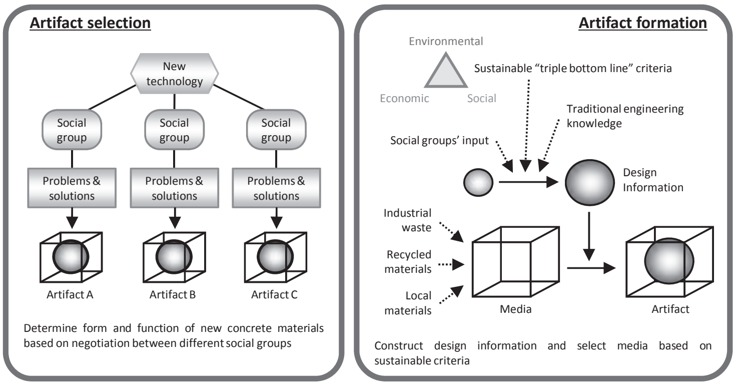

Framework for sustainable concrete materials

Life-Cycle Management of Urban Infrastructure – Yokota lab

Study on the Life-cycle management which includes a series of actions to evaluate the grade of deterioration and structural performance degradation by inspection, to predict the future progress of performance degradation, and to propose the alternatives of appropriate intervention.

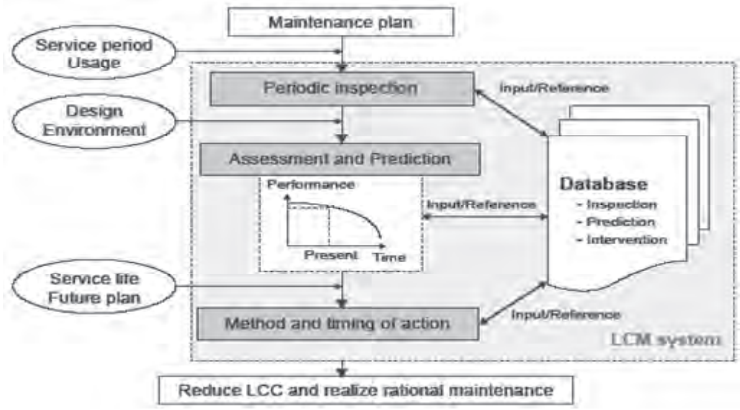

Geotechnical and Geoenvironmental Engineering – Kuwano lab

Studies on the mechanism of generation and the process of expansion of cavities and the loosening of the surrounding ground in order to evaluate the degree of ground looseness and also the resistance of the ground against being washed away.

Cave-in in the road caused by an old sewer pipe

Urban Earthquake Disaster Mitigation Engineering – Meguro lab

Study on Integrated Information System for Urban Earthquake Risk Assessment as a tool to increase the disaster situation awareness of individuals and to effectively reduce disasters; a 3D-GIS database in which each structure in an urban area are clearly identified.

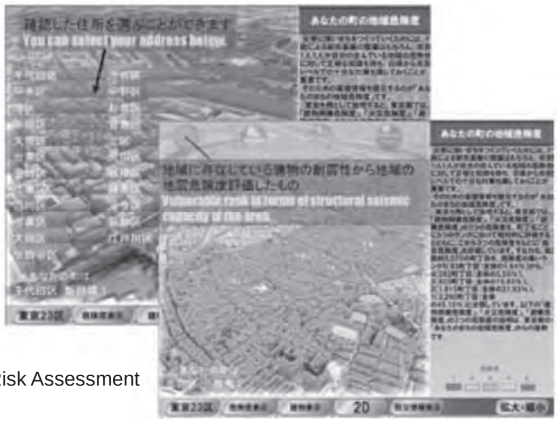

Urban Earthquake Risk Assessment using 3-D Micro GIS

Numerical Simulations – Huang lab

Studies on urban safety and environmental issues using numerical simulations, experiments, and measurements; The research is designed to simulate, explain, and design the urban safety and environment over multi-scales from human scale, indoor, outdoor to meso-scale.

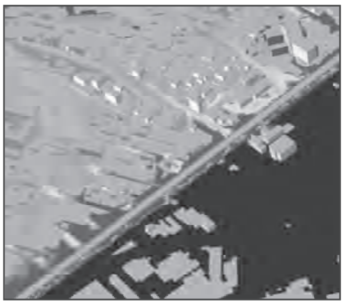

Numerical simulation of air pollutant dispersion

Experiment of urban fire spread

Integrated Disaster Management Engineering – Ohara lab

Development of the e-learning system to increase emergency medical responses from doctors and nurses; ICUS is conducting a joint-research program on the disaster manual of the hospital with the Division for Environment, Health and Safety and the Hospital of the University of Tokyo.

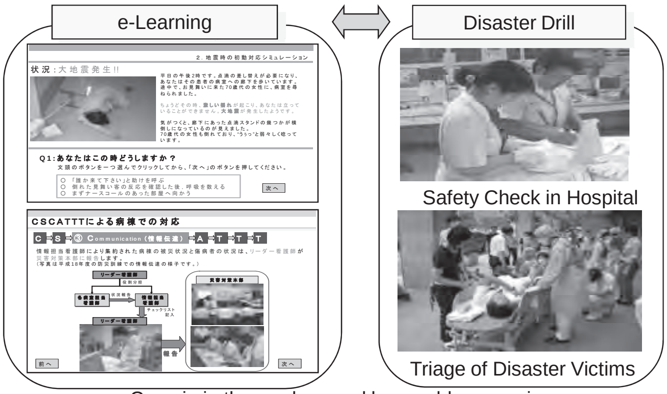

Cave-in in the road caused by an old sewer pipe

Wood Engineering – Koshihara lab

Studies on the possibilities of wooden structures; By revising the building standards, new medium-rise and high-rise wooden buildings can be built.

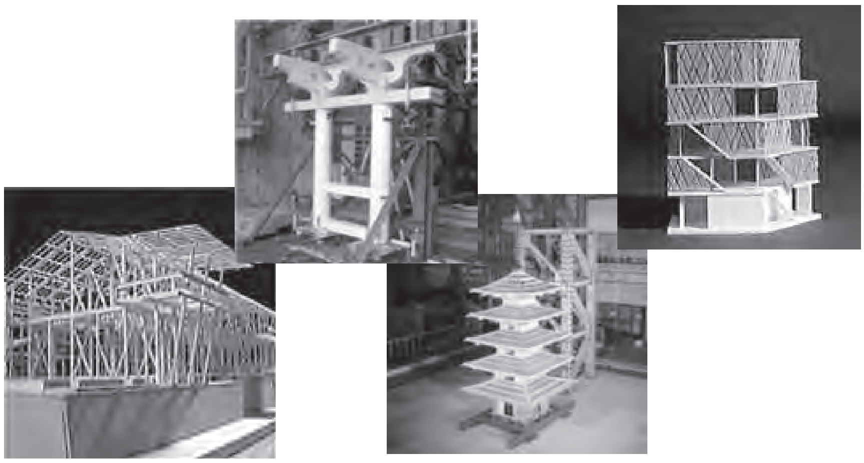

Urban Traffic Management – Tanaka lab

Study on the appropriate estimation of lost time in signal control that affects the length of a signal cycle, which, in turn, affects the delay in signalized intersection. We estimated the total lost time by observing the traffic flow using a video camera to shorten the signal cycle time.

video observation

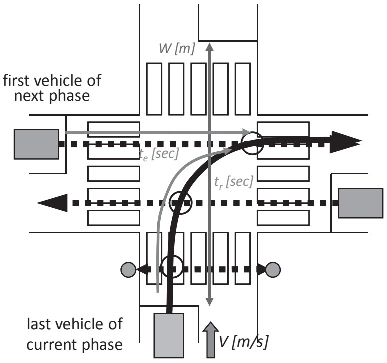

Observation and analysis of conflict points of traffic flows

Applied remote sensing – Sawada lab

Studies on systematic data processing methodologies spatially and timely for remote sensing data such as satellite data, aerial photo, and Lidar; Field observation systems are also integrated for vegetation management on a global as well as on a local scale.

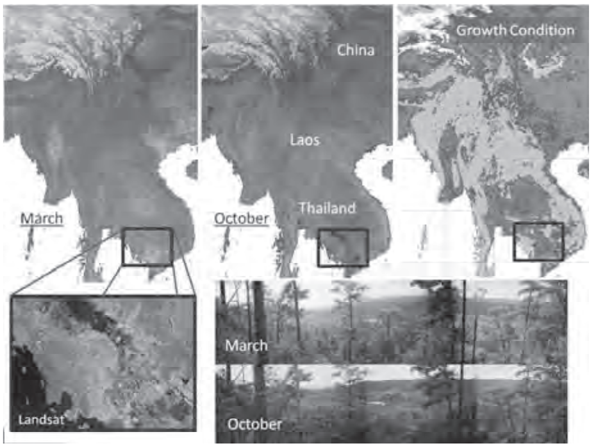

Vegetation environment map derived from satellite data (Indochina)

Remote Sensing for FRA

"Differences among data sets from the various countries can be great owing to the methods applied, the terms and definitions employed and the currency of the information in the individual inventories. Therefore RS is introduced for standardize the information qualities.

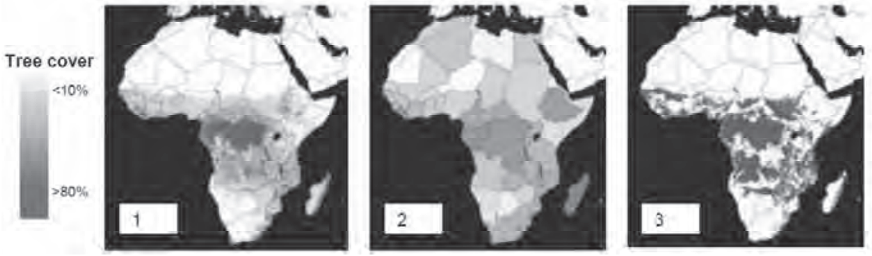

- Comparison of remote sensing and national reporting for Africa.
- 1: 1997 percent tree cover classification for Africa (Hansen, 2005).
- 2: Percent tree cover threshold which yields a forest area estimate for each country which matches that reported to FRA 2000. This map was created by starting at the densest tree cover per country and sliding the threshold down from there until the forest areas matched that reported for FRA 2000 (Hansen, 2005).
- 3: Resulting forest map where per country forested area match FRA 2000 totals. Green = forest, white = non-forest (Hansen, 2005). Pictures 1 through 3 confirm that national reporting and remote sensing analysis diverge for Africa (Mayaux et al., 2005).

Reliable and up-to-date information on the sate of forest resources

Sustainably managed forests have multiple environmental and socio-economic functions which are important at the global, national and local scales, and they play a vital part in sustainable development.

Reliable and up-to-date information on the state of forest resources is crucial to support decision-making for policies and programmes in forestry and sustainable development at all levels:
- not only on area and area change,
- but also on such variables as

growing stock,
wood and non-wood products,
carbon,
protected areas,
use of forests for recreation and other services,
biological diversity and
forests' contribution to national economies.

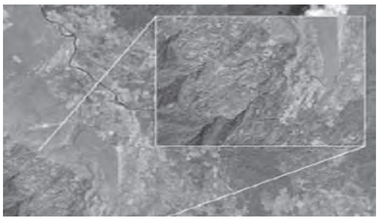

Sampling units of the FRA 2000 and the planned FRA 2010 RSS.

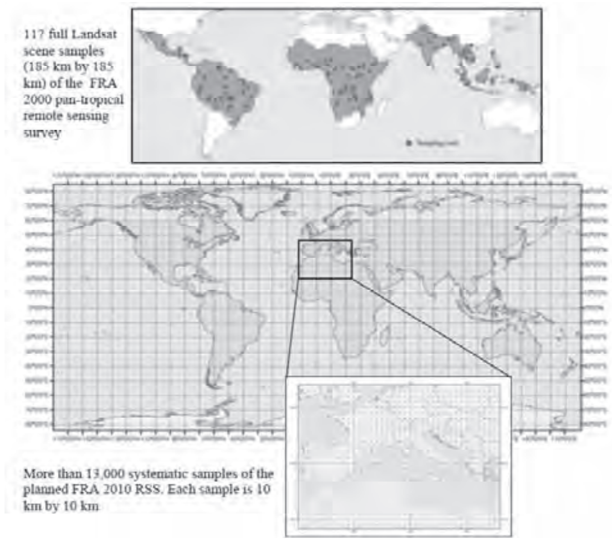

1 degree by 1 degree lat./long. grid system

- The latitude-longitude grid is easy to understand and to communicate to national governments.
- Sample locations can be easily identified on every map.
- The FAO supported National Forests Assessments (NFA) use this latitude/longitude grid; so information from field plots located within the sample units will be available to support the interpretation for many countries.

・ The 'degree confluence project' is posting photos of each latitude and longitude integer degree intersection on the Internet (see http://www.confluence.org). These photos can provide a substantial support to the FRA 2010 RSS sample interpret

Further reasons to promote FRA2010

- Accurate and timely information on forest and forest area change is essential for policy relevant at various levels.
- The new RSS approach promises to provide the best possible globally consistent data on forest cover by ecological zone which can provide valuable input information to biomass and carbon stock assessments.
- Institutions involved in sector of wide policy and structural adjustments can use frequently updated forest monitoring information to check if changed policies do or do not have the intended impact on forests.
- The Survey is expected to advance science in global natural resources monitoring.

National Forest Resources Database – NFRDB –

- Two servers
  - Main system in Forestry agency
    - Ordinary use
  - Sub system in FFPRI
    - Backup system
    - Research and development

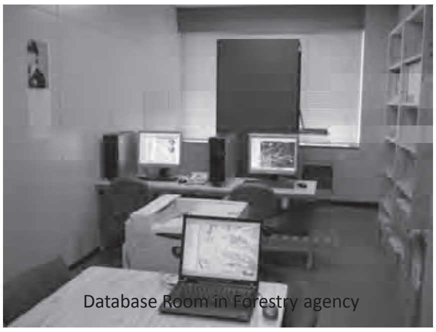

18

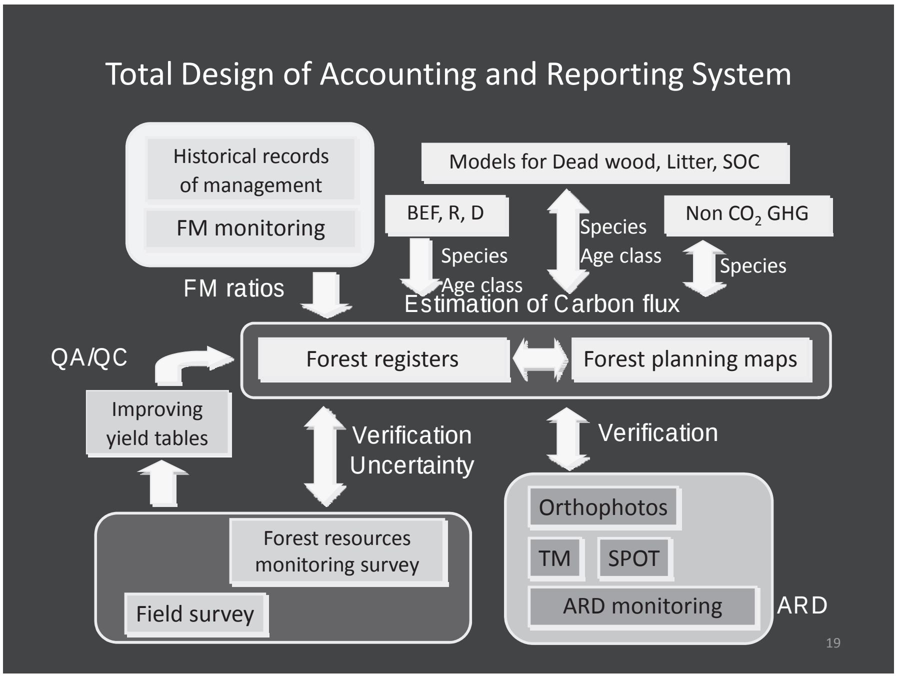
Total Design of Accounting and Reporting System
Historical records of management
FM monitoring
Models for Dead wood, Litter, SOC
BEF, R, D
Species
Age class
Species
Age class
Non CO_2 GHG
Species
FM ratios
Estimation of Carbon flux
QA/QC
Forest registers
Forest planning maps
Improving yield tables
Verification
Uncertainty
Verification
Forest resources monitoring survey
Field survey
Orthophotos
TM
SPOT
ARD monitoring
ARD
19

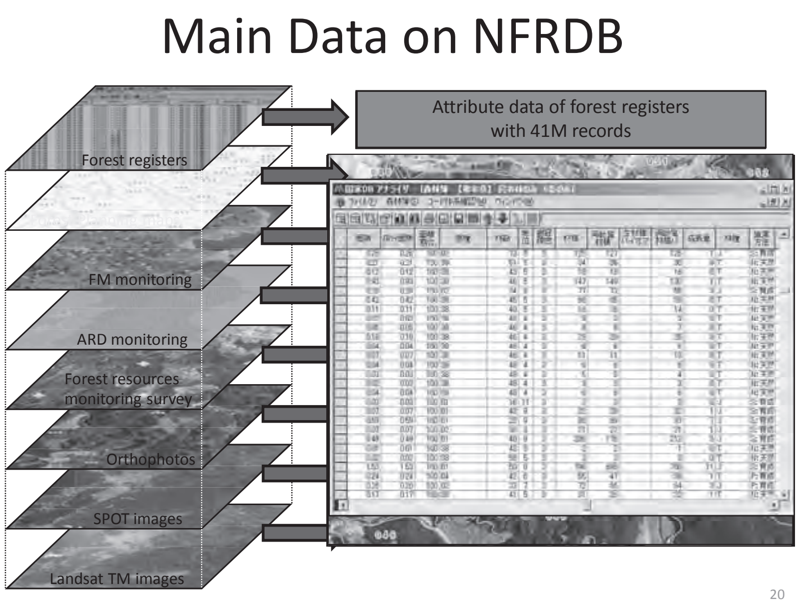
Main Data on NFRDB
Attribute data of forest registers with 41M records
Forest registers
FM monitoring
ARD monitoring
Forest resources monitoring survey
Orthophotos
SPOT images
Landsat TM images
20

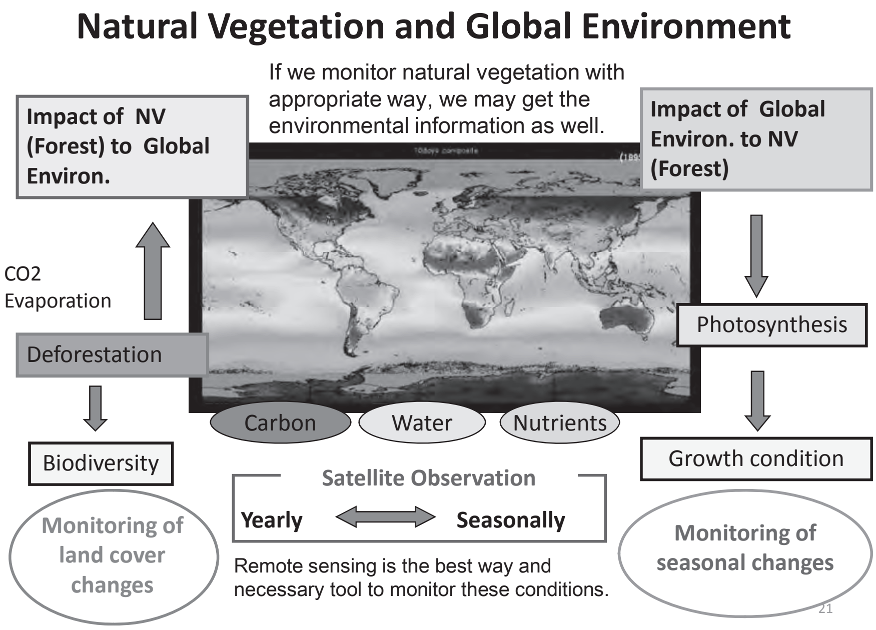

Natural Vegetation and Global Environment
If we monitor natural vegetation with appropriate way, we may get the environmental information as well.
Impact of NV (Forest) to Global Environ.
Impact of Global Environ. to NV (Forest)
CO2
Evaporation
Deforestation
Biodiversity
Monitoring of land cover changes
Carbon
Water
Nutrients
Photosynthesis
Growth condition
Monitoring of seasonal changes
Satellite Observation
Yearly
Seasonally
Remote sensing is the best way and necessary tool to monitor these conditions.
21

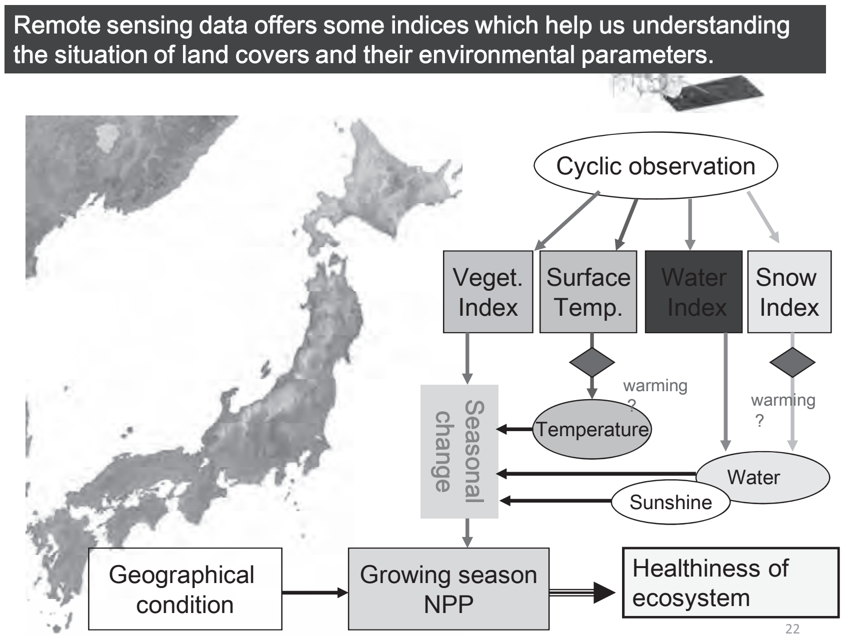

Remote sensing data offers some indices which help us understanding the situation of land covers and their environmental parameters.
Cyclic observation
Veget. Index
Surface Temp.
Water Index
Snow Index
warming ?
warming ?
Seasonal change
Temperature
Water
Sunshine
Geographical condition
Growing season NPP
Healthiness of ecosystem
22

Cloud-free dataset of 10 day interval

Surface Temperature and NDVI

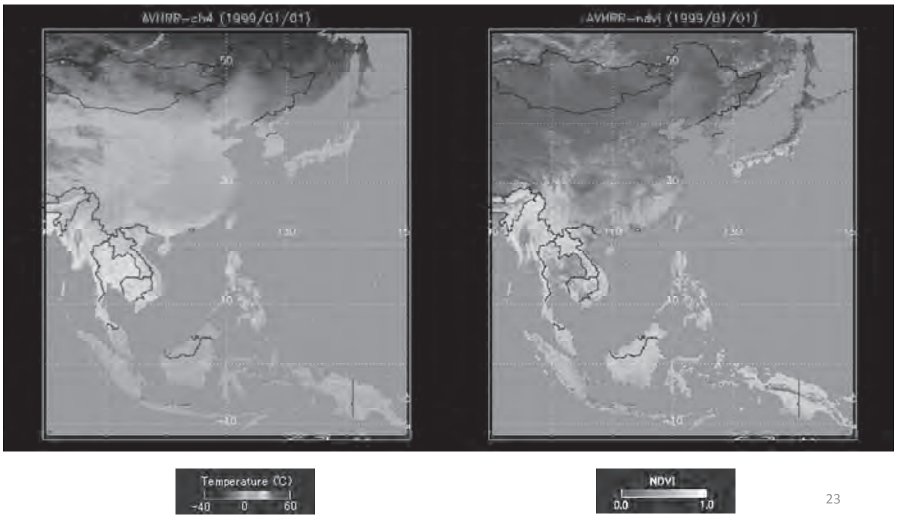

23

Seasonal Changes observed by the cloud-free10-day composite NOAA NDVI

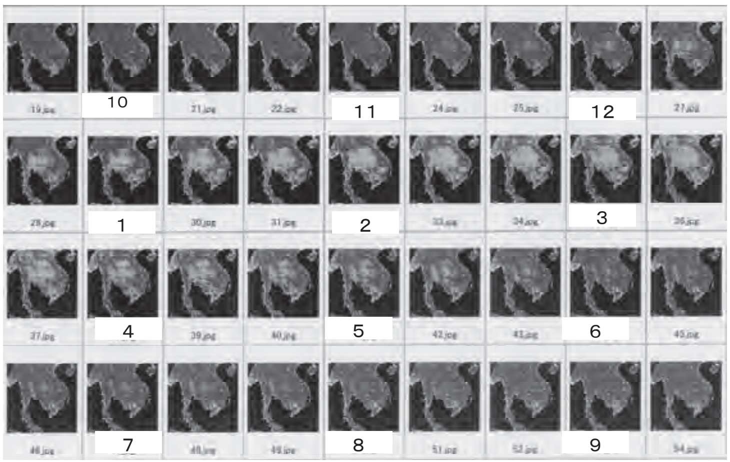

From these images, the duration of the leaf shedding of each pixel is estimated, which indicates the dryness and the amount of fuels on the ground.

24

Detection of Anomalies

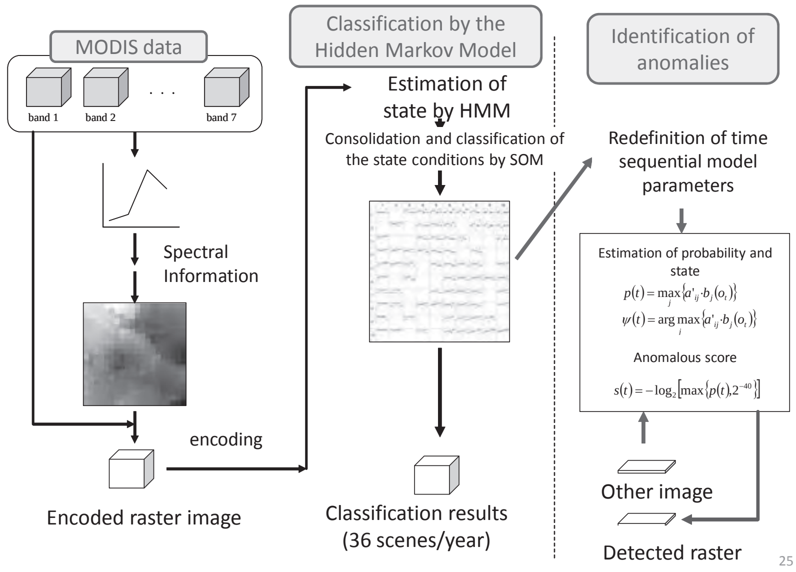

Time series processing and anomaly score

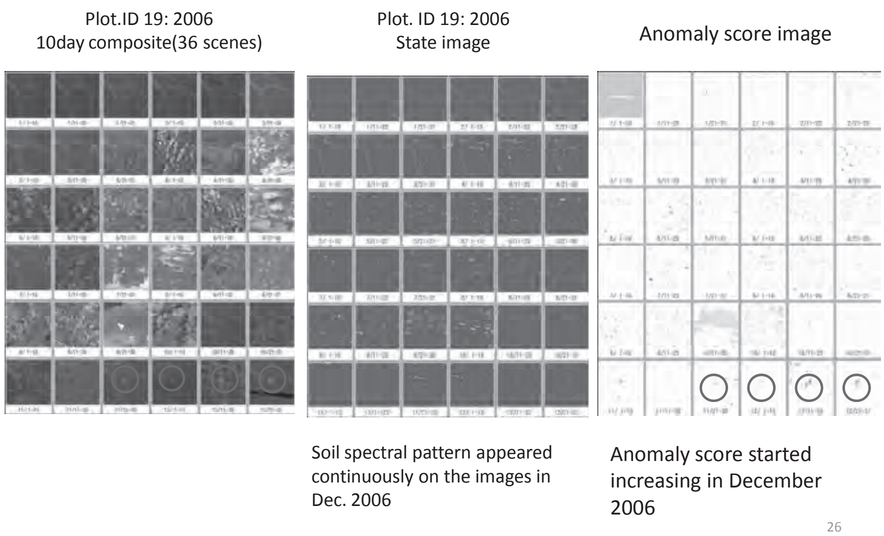

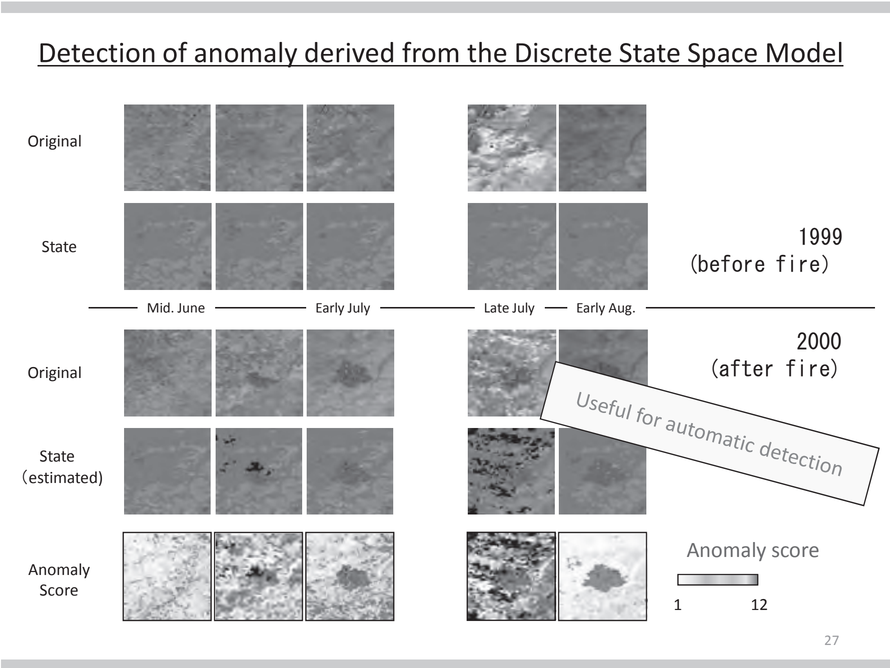
Detection of anomaly derived from the Discrete State Space Model
Original
State
1999
(before fire)
Mid. June
Early July
Late July
Early Aug.
2000
(after fire)
Original
State
(estimated)
Useful for automatic detection
Anomaly
Score
Anomaly score
1
12
27

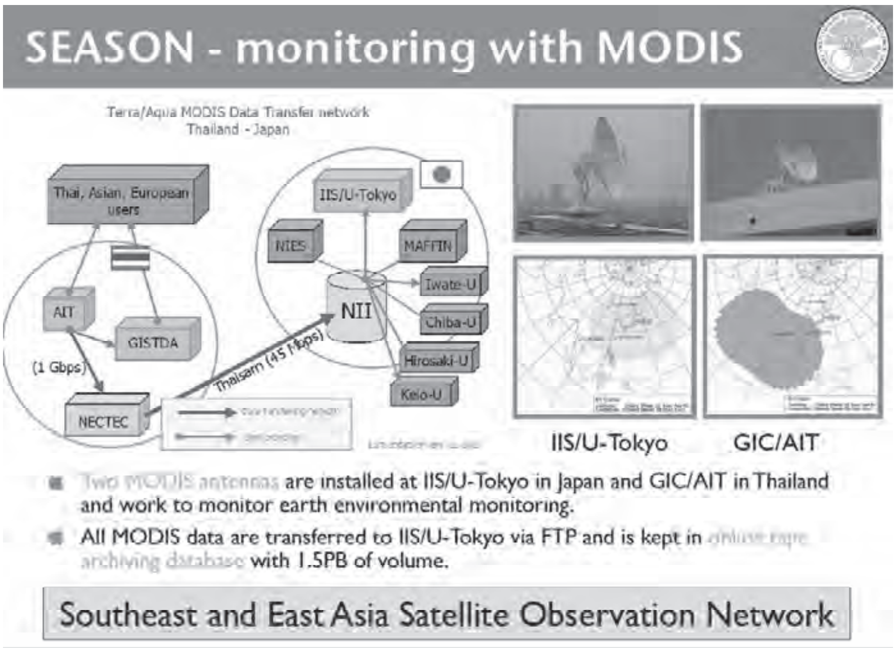
SEASON - monitoring with MODIS
Terra/Aqua MODIS Data Transfer network
Thailand - Japan
Thai, Asian, European users
AIT
GISTDA
(1 Gbps)
NECTEC
Thaisarn (45 Mbps)
IIS/U-Tokyo
NIES
MAFFIN
NII
Iwate-U
Chiba-U
Hirosaki-U
Keio-U
IIS/U-Tokyo
GIC/AIT
Two MODIS antennas are installed at IIS/U-Tokyo in Japan and GIC/AIT in Thailand and work to monitor earth environmental monitoring.
All MODIS data are transferred to IIS/U-Tokyo via FTP and is kept in online tape archiving database with 1.5PB of volume.
Southeast and East Asia Satellite Observation Network

MTSAT technical specification

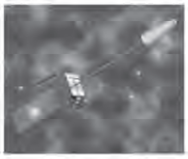

MTSAT-1R

Table 1. MTSAT-1R technical specifications.

Channels	Wavelentgh	IFOV	Quant.
IR1	10.5-11.5 μm	4 km	10 bit
IR2	11.5-12.5 μm	4 km	10 bit
IR3	6.5-7.0 μm	4 km	10 bit
IR4	3.5-4.0 μm	4 km	10 bit
VIS	0.55-0.90 μm	1 km	10 bit

Japanese geostationary satellite (MTSAT HRIT)

(a) IR1 (b) IR2 (c) IR3 (d) IR4 (e) VIS

IR4 (4μm) and IR1 (11μm) are used to monitor fires

MODIS fire product at IIS

- The are are mainly two ways to obtain our MODIS fire products;
  - Anonymous FTP at WebMODIS
  - Currently fire product in hdf and ascii text format is available online during 2002 Jan - present over IIS and AIT coverage (22,514 scenes).

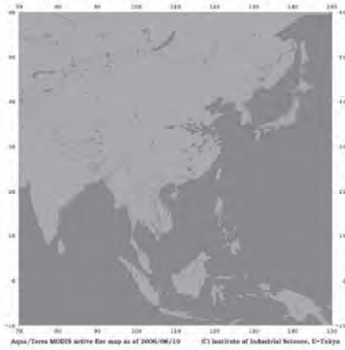

http://webmodis.iis.u-tokyo.ac.jp/FIRE/

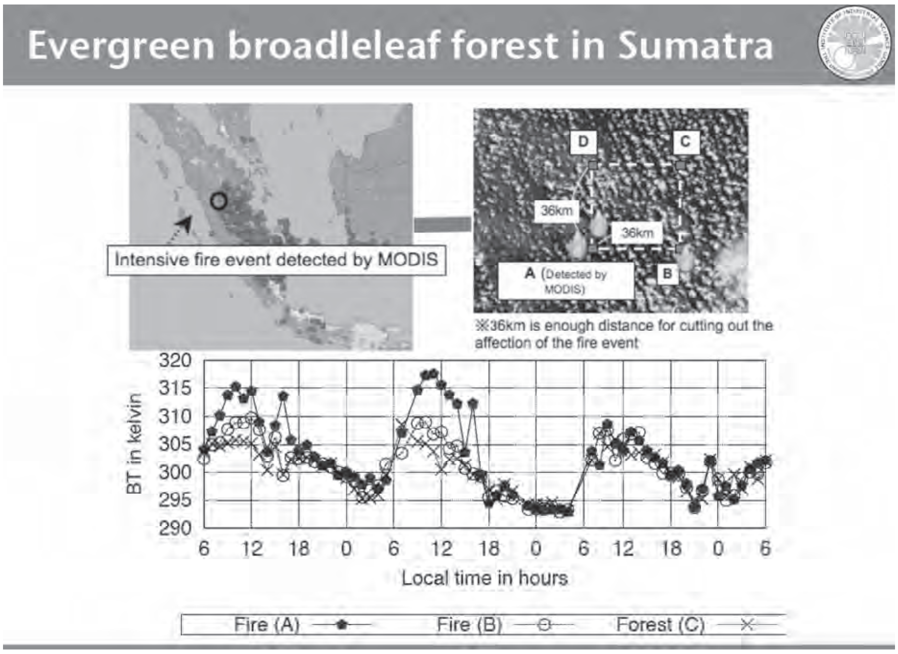
Evergreen broadleleaf forest in Sumatra
Intensive fire event detected by MODIS
D
C
36km
36km
A (Detected by MODIS)
B
※36km is enough distance for cutting out the affection of the fire event
BT in kelvin
Local time in hours
Fire (A)
Fire (B)
Forest (C)

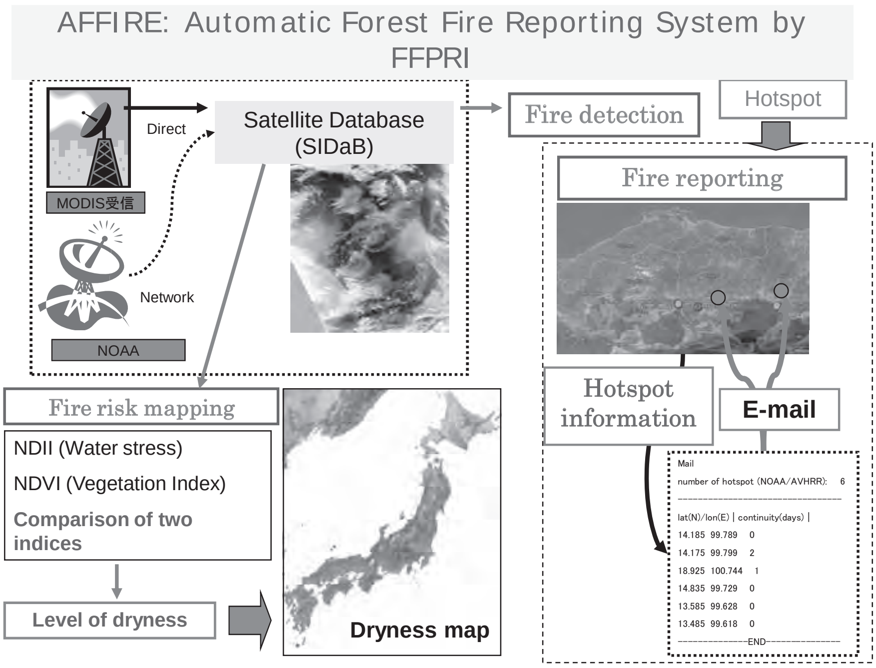
AFFIRE: Automatic Forest Fire Reporting System by FFPRI
Direct
Satellite Database (SIDaB)
MODIS受信
Network
NOAA
Fire detection
Hotspot
Fire reporting
Hotspot information
E-mail
Fire risk mapping
NDII (Water stress)
NDVI (Vegetation Index)
Comparison of two indices
Level of dryness
Dryness map

ALOS・PALSAR /Japan

Mode	High Resolution		Direct Downlink	SCANSAR	Polarimery
	Single Polarization	Dual Polarization			
Frequency	L band (1270MHz)				
Chirp Bandwidth	28MHz	14MHz	14MHz	14/28MHz	14MHz
Polarization	HH or VV	HH/HV or VV/VH	HH or VV	HH or VV	HH/HV +VV/VH
Incidence Angle	8-60deg (typ 39deg)	8-60deg (typ 39deg)	8-60deg (typ 39deg)	18-43deg	8-30deg (typ 24deg)
Range Resolution	7-44m 10m@39deg	14-88m 20m@39deg	14-88m 20m@39deg	100m (Multi-look)	24-89m 30m@24deg
Swath Width	40-70km	40-70km	40-70km	250-350km	20-65km
Bit Length	5 bits	5 bits	3/5 bits	5 bits	3/5 bits
Data Rate	240Mbps	240Mbps	120Mbps	120/240Mbps	240Mbps

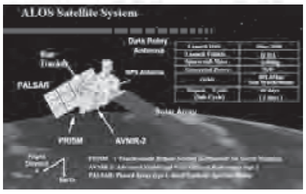

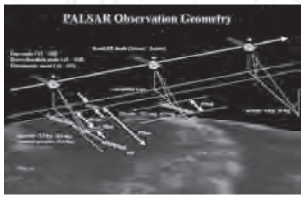

Detection of Forest development by RADAR

Optical sensors (Landsat, CBRES, etc.)

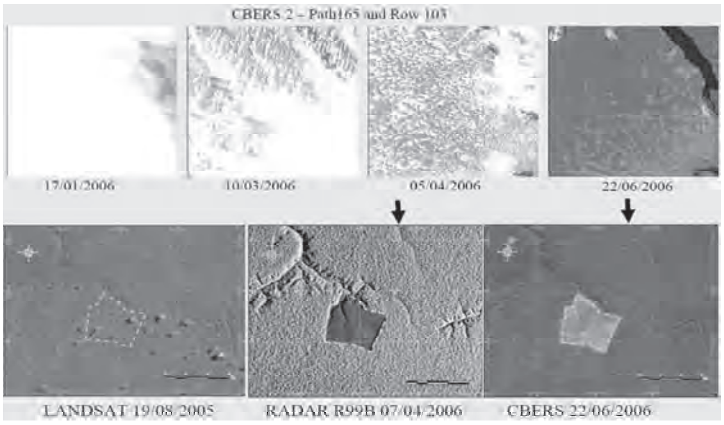

Forest(Landsat2005) -> Cutover(RADAR2006) -> (CBRES2006年)

SCAN SAR (Cycle20 & Cycle21)

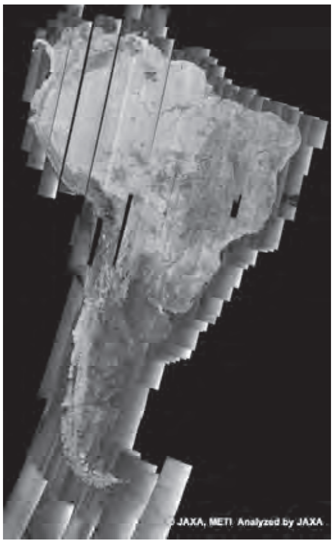

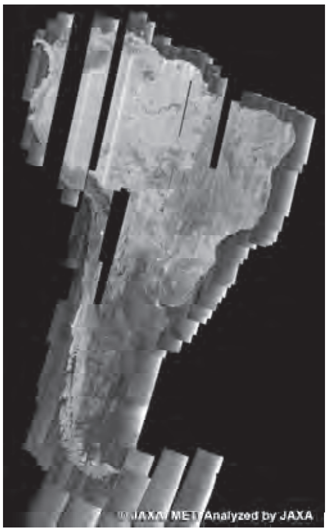

Flood monitoring by RADARSAT

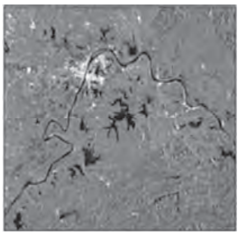

Dec. 1997, ScanSAR Narrow

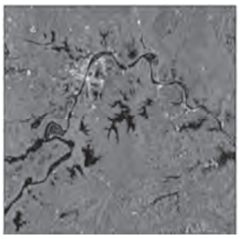

Aug. 1998 ScanSAR Narrow

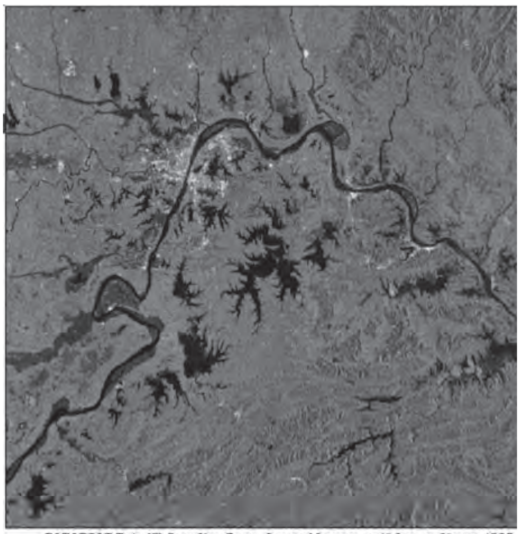

RADARSAT Data (C) Canadian Space Agency/Agence spatiale canadienne 1998. Received by the Canada Centre for Remote Sensing. Processed and distributed by RADARSAT International.

Four airborne sensors, aboard R99-B and R95-B aircraft, operating in the microwave, visible spectrum and infrared bands:

- SAR sensor (Synthetic Aperture Radar);
- HSS Hyperspectral sensor (Hyperspectral Scanner System);
- MSS Multispectral sensor (Multispectral Scanner System);
- OIS infrared sensor (Optical Infrared Sensor).

Aeronave R95-B e imagens do sensor HSS

What is important…

- Integration of reliable RS information with evaluation system
- Time series information as a simple layer of GIS
- Modeling for prediction
- International collaboration for global environment issues and disaster mitigation
- International Friendship through RNUS

PUBLIC TRANSPORTATION IN BANGKOK

THIRAYOOT LIMANOND
School of Transportation Engineering
Suranaree University of Technology, Thailand
tlimanond@yahoo.com

Public Transportation in Bangkok

Thirayoot Limanond
Suranaree University of Technology

2nd Joint Student Seminar on Civil Infrastructures

AIT Center 6 July 2009

Bangkok

Ranks as one of the top twenty mega cities in the world

- Population: 11 million people (15% of the country population)
- 5.9 million vehicles registered
- Locates all gov. agencies and many important business enterprises
- 50% of Country's economic activity
- Current Traffic Conditions:
  Seriously congested!!!

Center for Transport Study and Technology Transfer (CT3)

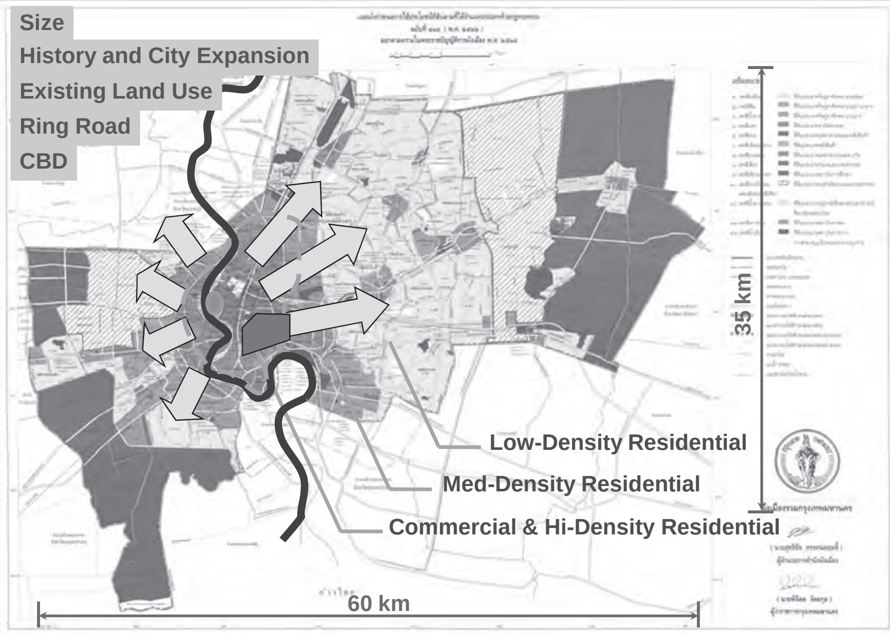

Greater Bangkok Area

Bangkok +
5 Adjacent Provinces

- ☐ Population: 15 million people
- ☐ 6.8 million vehicles registered

Center for Transport Study and Technology Transfer (CT³)

Vehicle Registration

- In Greater Bangkok Area (6.8 mill veh.)

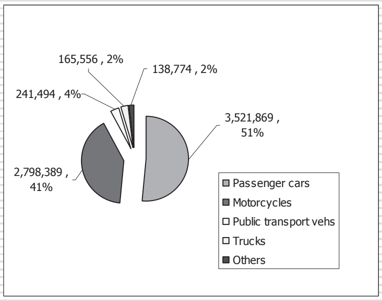

104,000 veh.

84,000 veh.

42,000 veh.

12,000 veh.

Center for Transport Study and Technology Transfer (CT³)

Bus Service

Center for Transport Study and Technology Transfer (CT³)

Bus Service

- Service for the entire Greater Bangkok Area
- Service Lines: 200+ major routes
- Service Hours: 5:00 – 23:00
- Bus Fare: 7 – 24 Baht

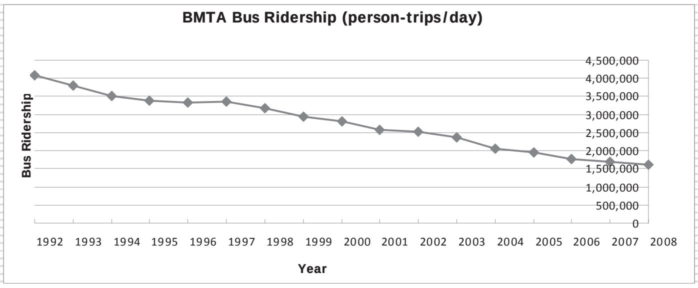

Center for Transport Study and Technology Transfer (CT³)

Ferry along Chao Praya

Center for Transport Study and Technology Transfer (CT³)

Suburban train

Center for Transport Study and Technology Transfer (CT³)

Current Heavy Rail System

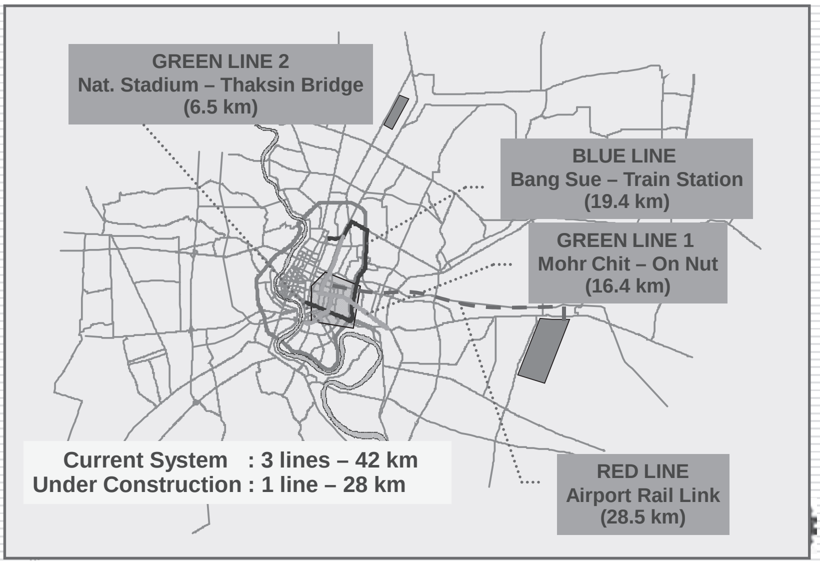

Current Heavy Rail System

- Green Lines (BTS sky train)
  - 22.9 km
  - Service hours: 6:00 – 24:00
  - BTS Fare: 15 – 40 Baht
  - Ridership: 450,000+ Passengers/d

- Blue Line (MRTA subway)
  - 19.4 km
  - Service hours: 6:00 – 24:00
  - BTS Fare: 16 – 41 Baht
  - Ridership: 200,000+ Passengers/d

Center for Transport Study and Technology Transfer (CT³)

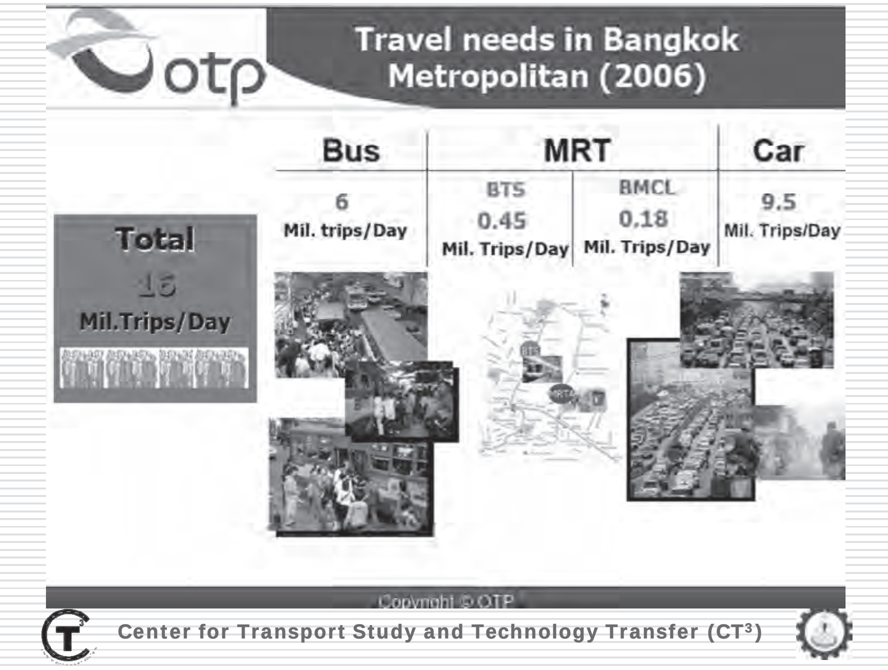

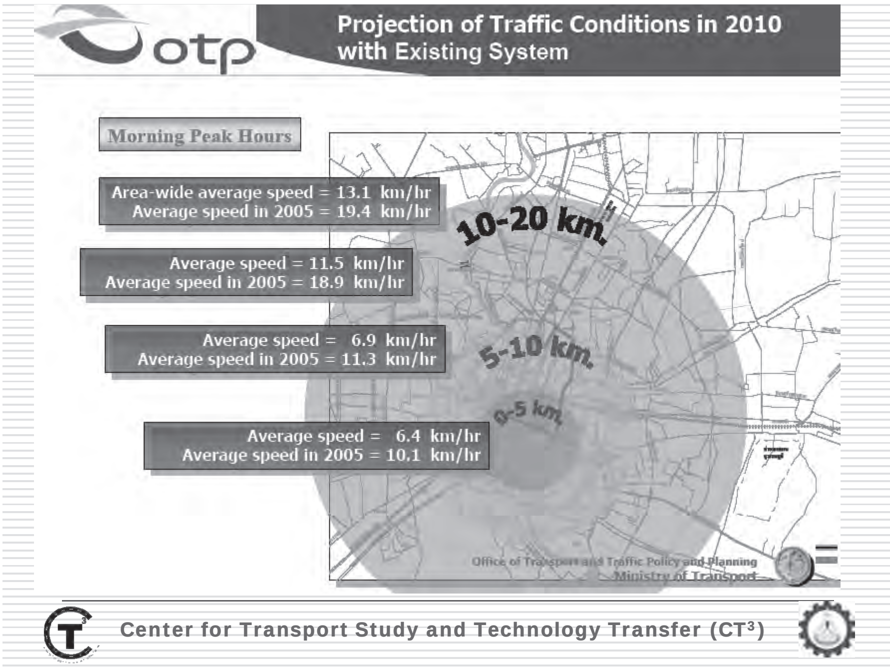
Projection of Traffic Conditions in 2010
with Existing System
otp
Morning Peak Hours
Area-wide average speed = 13.1 km/hr
Average speed in 2005 = 19.4 km/hr
Average speed = 11.5 km/hr
Average speed in 2005 = 18.9 km/hr
Average speed = 6.9 km/hr
Average speed in 2005 = 11.3 km/hr
Average speed = 6.4 km/hr
Average speed in 2005 = 10.1 km/hr
10-20 km.
5-10 km.
0-5 km.
Office of Transport and Traffic Policy and Planning
Ministry of Transport
Center for Transport Study and Technology Transfer (CT3)

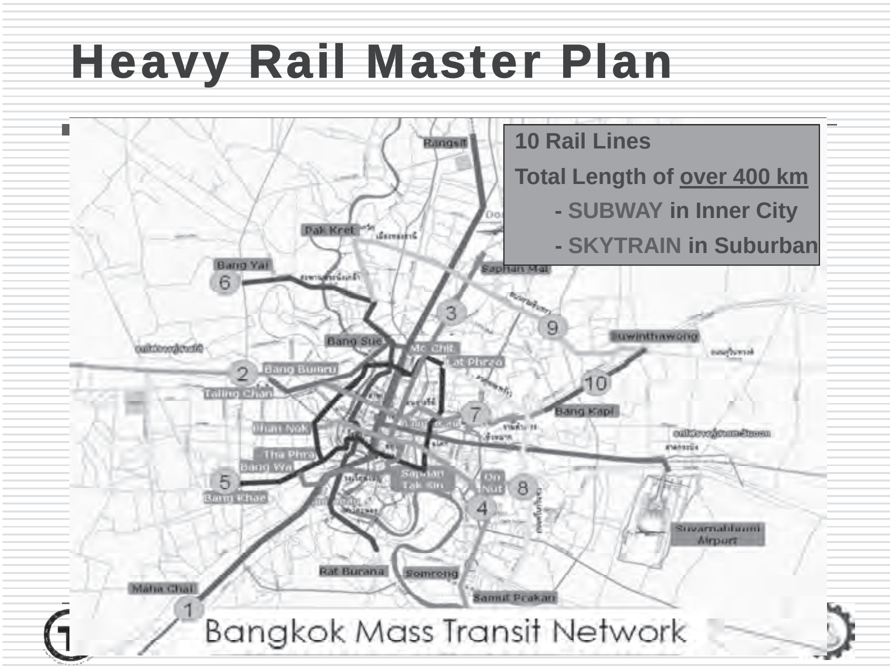
Heavy Rail Master Plan
10 Rail Lines
Total Length of over 400 km
- SUBWAY in Inner City
- SKYTRAIN in Suburban
Rangsit
Pak Kret
Bang Yai
Saphan Mai
Bang Sue
Mo Chit
Lat Phrao
Suwinthawong
Bang Bumru
Taling Chan
Bang Kapi
Tha Phra
Bang Wa
Bang Khae
Saphan Tak Sin
On Nut
Suvarnabhumi Airport
Rat Burana
Samrong
Samut Prakan
Maha Chai
1
2
3
4
5
6
7
8
9
10
Bangkok Mass Transit Network

Bus Rapid Transit (BRT)

Other names

Rapid Bus, Metro Bus, High Capacity Bus Systems, High Quality Bus Systems, Express Bus Systems, Busway Systems, etc.

Bus Rapid Transit is a mass transit system that mimics the rapidity and performance of metros but utilises buses rather than rail vehicles.

Characteristics

- ✓ Segregated busways
- ✓ Rapid boarding and alighting
- ✓ Efficient fare collection
- ✓ Comfortable stations
- ✓ Clean bus technologies
- ✓ Modal integration
- ✓ Competitively-bid concessions
- ✓ Sophisticated marketing
- ✓ Excellence in customer service

BRT Projects

BRT is an attempt to achieve a metro-level of transit quality using bus technology.

BRT Vs Heavy Rail

"How much US$1 billion can buy?"

Bus Rapid Transit

- Less Expensive
- Fast Construction Time
- Greater Flexibility
- Greater Accessibility

7 km. of Subway

426 km. of BRT

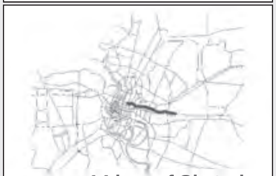

14 km. of Skytrain

BRT Project

BRT was introduced in 2003
(Heavy Rail Master Plan
is available since 1997)
-**OTP** (9 lines)
-B

OTP: 9 lines of BRT
2004 – Feasibility study, Prelim. Design
Current Status:
On-hold, waiting for a new heavy rail system master plan

BMA: 2 lines of BRT
2005 – Feasibility study, Detailed Design, Bidding
Current Status:
One line is recently completed, but need to wait for BRT buses

Bangkok BRT

Center for Transport Study and Technology Transfer (CT³)

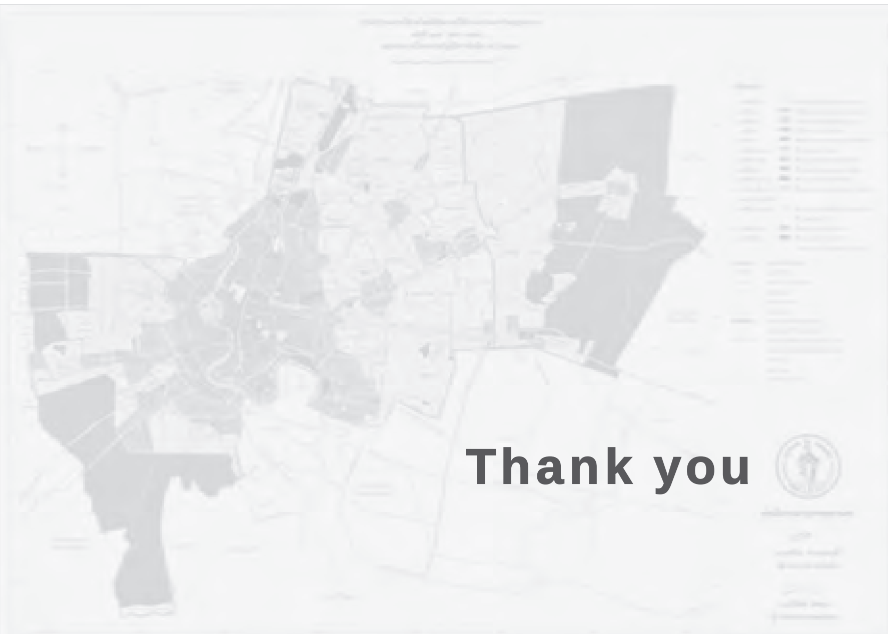

Invited Papers

METHODS FOR DETERMINING PHYSICAL, PARTICLE-RELATED CHARACTERISTICS RELEVANT TO FLUID FLOW PHENOMINA IN BIOWASTE

ECKHARD KRAFT
Bauhaus-Universität Weimar, Germany
eckhard.kraft@uni-weimar.de

ABSTRACT

The characterisation of biowaste and its influence on the fluid flow in packed beds of biowaste has been researched in . For the first time a considerable number of experiments have been done to measure particle density. The particle density can be used to estimate the amount of pores in the biowaste. Particle size distributions have been examined from the organic material. Possibilities have been tested to specify characteristic classification numbers and effective particle diameters in order to study the properties of the material. Using the knowledge of the specific surface, conclusions can be drown about interaction of Newton`s fluids in porous media. Certainly there has been an interdependence between viscosity, current properties, biodegradation and adsorption processes. At the moment it is impossible to determine specific surfaces of packed columns by using proved methods. Although this could help to improve process engineering in a range of technical fields. This study provides a statistical to estimate specific surfaces of packed columns. The results of a test of this method executed on defined materials and on organic waste are presented. Based on these results the accuracy of the method is discussed.

1. INTRODUCTION

The amount of waste in Germany has been estimated 1993 in a range of about 338,5 Mio Mg (Umweltbundesamt, 1998). The mainly part of waste accrues as a material mixture of different properties. This happens even to source separated waste. Waste, containing or consisting of organic matter, is incinerated or treated physically and biologically, at the moment. In 1999, 594 biological treatment plants have been existing in Germany with a cumulative capacity of about 8,4 Mio Mg (Wiemer and Kern, 1999). In March 2000 395 biological treatment plants with an input of 4,5 Mio Mg conformed with the RAL-quality standard (Bundesgütegemeinschaft Kompost, 2000).

The properties of gases and fluids greatly influences the rate of biological degradation of organic substances, the production rate of leachate and gas as well as biological filters. The concerning materials like untreated waste, physically biological treated waste, source separated organic waste and biological filters are examples of packed beds and piles. The characteristics of a material and its storage, which specify the behaviour of fluids, vary in a big range of space and retention time in heterogeneous waste materials.

In the domain of organic waste treatment a lot of forced aerated composting systems exist, which have a high aeration demand. This courses a high energy consumption. Often design and operation of composting plants are heavily based on empirical knowledge lacking scientific reasoning.

The inhomogenity of the feedstock certainly has an influence to this situation. Hence, it appears useful to study those characteristics of waste materials which effect fluid flow in packed beds.

2. CONCEPTUAL CONSIDERATIONS

To research in fluid flow through packed beds of waste the following three factors need to be taken in account:

1. the material; 2. the packed bed and 3. the flow pattern

The properties of these elements are strongly related to each other and determine in correspondence with the properties of the fluid the behaviour of the flow pattern. In packed beds of waste matrixes with huge pores and matrixes which have small pores, like the soil matrix, could be expected. Particles with internal pores can be expected additional.

Important characteristics in examining fluid flow phenomena in organic waste are provided in table 1. It is vital to adequately define procedures for sampling, sample handling and sample examination by using appropriate analytical methods. This would enable to describe the degree and quality of particle heterogeneity of organic waste. Such a description would profoundly contribute in composting process design and management.

Table 1: Important characteristics relevant to fluid flow in waste materials

material	**packed bed**	**perfusion**
hydrophobility	saturation of soil	effective pores
water content	pores	space, area load
specific weight	pore size distribution	retention time of fluid
particle size distribution	particle distribution	fluid distribution
particle size	Pore continuing	
specific surface	tortuosity	
roughness		

3. SPECIFIC WEIGHT OF ORGANIC WASTE

The specific weight ρ_S of a material is defined as the ratio of the mass the solid single particles m_d to the volume of the solids V_k, including possibly existing of inner pores, which cannot be reached from outside.

The specific weight ρ_S of a material can be measured by using the following methods (Brüggemann, 1982):

- estimation of the specific weight ρ_S by the common pyknometer; (DIN 18124, 1989)
- estimation of the specific weight ρ_S by submersible balance;
- estimation of the specific weight ρ_S by air pyknometer.

The methods applied to soil mechanics of estimating the specific weight ρ_S of organic waste cannot be used without any adaptation. Related to the German regulation DIN 18124 comparable experiments in four variations have be realised:

- heated in sand bath,
- heated in water bath,
- evacuated at 1000 ml Pyknometer
- evacuated at 2000 ml and Pyknometer.

Caused by the properties and the composition of the organic waste modifications are necessary (Kraft and Schwind 1996). According to the method of pyknometer, 192 experiments to estimate the specific weight ρ_S were realised. They included 96 experiments with a maximum particle size of 80 mm(original size) and 96 experiments with shredded material with a maximum particle size of 4 mm. Table 2 shows the results of the experiments conducted to the material.

Table 2: specific weight ρ_S of organic waste for a maximum particle sizes of 80 mm and of 4mm

experimental method	**specific weight ρ_S [g/cm³]**	
	average shredded 4 mm	**average original 80 mm**
heated in sand bath	1,80	1,76
heated in water bath	1,68	1,62
evacuated at 1000 ml pyknometer	1,87	1,74
evacuated at 2000 ml pyknometer	1,80	1,61

The specific weight of the shredded material is always higher than the specific weight of original material. That has been expected, because inner pores, which could not be reached before shredding the material, could be reached after that. The difference regarding the results of the evacuation method “water bath” is significantly wider than any of the methods. The evacuation methods “sand bath” and “1000 ml pyknometer” estimate, independently of the particle size, the highest specifics of weight. This may be assigned to an incomplete evacuation of the samples , when using these. The differences of the results of the methods of “sand bath” and “water bath” are caused by the different temperatures of the bath. The temperature of the sand bath was 275°C and of the water bath 100°C. Even the quality of heat transfer is varying with the material of the bath. The time of evacuation, which is prescribed by the technical standard between 25 minutes to 1 day, has to be extend for the method of “water bath”, as a result the lower maximum temperatures and the slower heat transfer involved.

Overall the aforementioned results indicate, that only the methods of “sand bath” and “1000ml pyknometer “ can reflect true results of specific weight of organic waste. Also, the experiments have to be done by using original material. Hackling the material to a size smaller than 5 mm, as prescribed by the standard method, is not appropriate for the purposes of our work. The specific weight of the material examined in this study reached a range between 1,72 and 1,77 g/cm³. It should be mentioned that the method of evacuating by using a pyknometer for estimating the specific weight of organic waste and residual(MSW after separate collection of organic waste and other secondary resources) waste has been established at most of the German universities. Mostly 2000 ml pyknometers are used, because their content can be evacuated by modern and stronger pumps within a working day. Figure 1 pictures the relationship between the specific weight and the particle size of an additional study. The results apply to material composted for a period of 40 days. The average specific weight is 1,51 g/cm³.

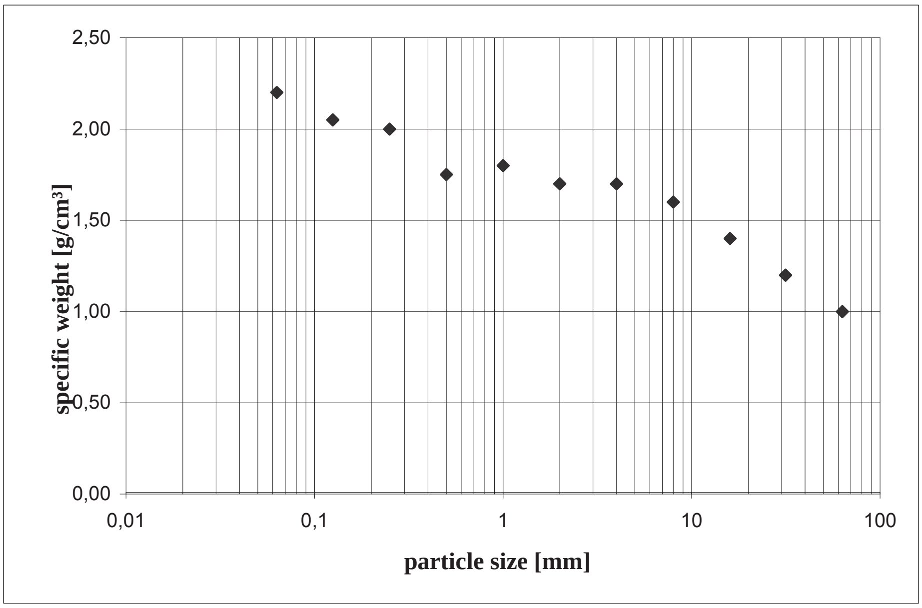

Figure 1: Specific weight of different particle sizes in organic waste

5. PARTICLE SIZE AND PARTICLE SIZE DISTRIBUTION

At the composting process the material is usually stored like loose gravel or as a packed bed. Generally, such groups of particles are named “disperse systems”. They contain mostly of a lot of single particles, the so-called disperse phase, and the surrounding media, the so-called continuos phase. Both the disperse phase and the continuos phase can be solid or fluid. Particle size and particle size distribution are strongly influencing the properties of particle groups.

The figure 2 shows 7 different particle size distributions, i. e. five single charges, the average of all charges and the corresponding distribution as defined by Fuller(Lang et.al). Each line represents the average of four replicates for each charge. Eight kg of material have been used for each single particle size distribution, which, indeed, guarantees the representative power of these results.

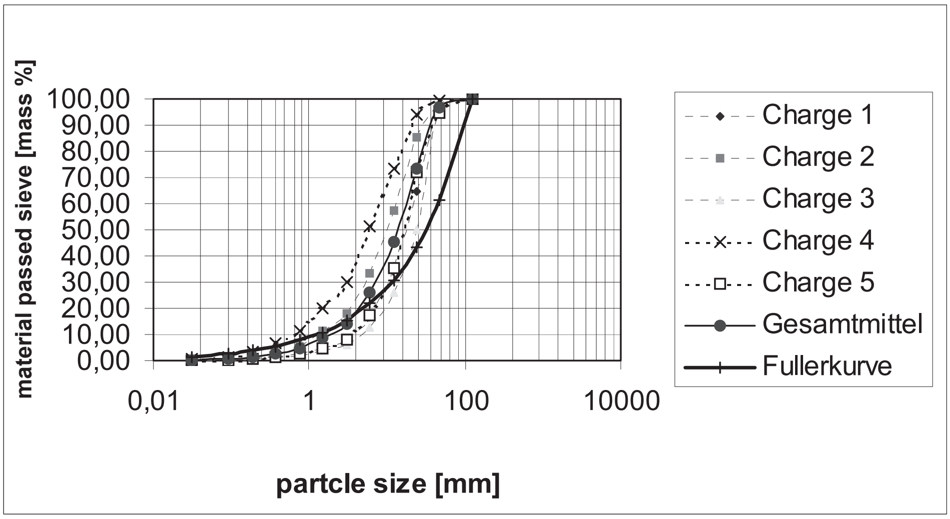

Figure 2: Particle size distributions of organic waste according to DIN 18123 (1996)

Using the particle size distribution the effective particle size d_w, the coefficient of uniformity C_U, and the coefficient of curvature(C_K) can be used as classifying parameters(Table 3). C_U and C_K of the particle size distribution of the "Fuller" curve are given coefficients. The parameter d_x shows the diameter(d) of the particles, where x- mass % of the sieved material passed.

Table 3: Classifying parameters of organic waste

	charge 1	charge 2	charge 3	charge 4	charge 5	avera.	Fuller
d_{10} [mm]	3,8	1,4	5,0	0,6	3,8	1,9	1,3
d_{30} [mm]	10,0	5,3	15,0	3,0	10,0	7,0	11,7
d_{60} [mm]	21,7	13,5	28,3	8,0	19,0	18,0	46,8
C_U	5,71	9,64	5,66	13,33	5,00	9,47	36,00
C_K	1,21	1,49	1,59	1,88	1,39	1,43	2,25
d_w [mm]	6,65	3,97	5,03	1,54	5,51	3,48	1,22

At a next step the 5 particle size distributions of the charges are compared to the one of Fuller(Table 4). They close a particle size distribution to the particle size distribution as per Fuller, the higher should be the estimated flow inhibition for this specific particle size distribution; the particle size distribution as per Fuller indicates the most densiest packed bed.

Table 4: Comparison of specific particle size distribution to the particle size distribution as per Fuller

	charge 1	**charge 2**	**charge 3**	**charge 4**	**charge 5**	**avera.**	**Fuller**
$A=C_U/C_{U,Fuller}$	0,159	0,268	0,157	0,370	0,139	0,263	1
$B=C_K/C_{K,Fuller}$	0,539	0,661	0,707	0,833	0,616	0,637	1
$C=d_w/d_{w,Fuller}$	5,468	3,263	4,133	1,269	4,534	2,859	1
D=(A+B+C)/3	2,055	1,397	1,666	0,824	1,763	1,253	1
E=D-1	1,055	0,397	0,666	-0,176	0,763	0,253	0
	6	3	4	2	5		1

The highest flow inhibitions could be expected at the charges 2 and 4, followed by the charges 3, 5 and 1.

Generally, particle size distributions of heterogeneous materials involve a substantial degree of error, when based on mass calculation. Using the results of particle size-based specific weights of organic waste, the particle size distributions, on a volume base, can be calculated. From those, the effective particle size, on a volume basis, can be calculated. Table 5 shows the comparison between effective particle size on a mass (d_w) and volume ($d_{w,v}$) basis.

Table 5: Comparison between effective particle size on a mass (d_w) andvolume ($d_{w,v}$) basis

	charge 1	**charge 2**	**charge 3**	**charge 4**	**charge 5**	**Fuller**
d_w [mm]	6,65	3,97	5,03	1,54	5,51	1,22
$d_{w,v}$ [mm]	8,51	4,79	7,16	1,90	7,24	1,22
Δd [%]	27,9	20,6	42,3	23,4	31,4	0

The difference between d_w and $d_{w,v}$ is apparently more then 20 %.

6. SPECIFIC SURFACE

A method developed by Chalkley et al. (1949), gave an estimation for the ratio of volume to surface of particles. This method was originally developed for speeding up the analysis of quantitative morphologic properties of human cells. Also, this method moves along the lines, the idea and results realised by Crofton (Encyclopaedia Britannica, 1875-1889).

If a room contains a number of each objects with different volume and surface, the following equation is valid (Chalkley et al., 1949):

$$\frac{r_1 \cdot h}{c} = \frac{4 \cdot \Sigma volume}{\Sigma surface} \quad [1]$$

Where:

c is the number of cuts of an independent and randomly dropped bar
r_1 length of the bar

Chalkley et al. (1949) verified the equation 1 by using geometric objectives with given sizes. During the course of our experiments an adaptation of the method of Chalkley et al (1949) has been developed, in order to apply the procedure to heterogeneous packed beds of organic waste. At a packed bed the single particles are laying strictly side by side. That requires a method to show clearly the border between the particles and the pores. The most suitable method is to have the print of a plane and coloured surface of frozen material on paper. That makes sure that deeper parts of the material(pores) cannot leave their print at the paper(Kraft, 2000; Schreiber, 1998). As copy only the coloured particles will be seen.

After preparing a copy of distributed particles and pores, the picture can be digitally scanned. The computerised interpretation of the specific surface according to the principle of Chalkley et al. (1949) has be developed and applied.

The program for simulation is able to create the print corresponding to the randomly dropped bar. The simulation can include up to 10000 prints. It can count the number of “cuts” and “hits”. The program produces a raster, which allows the localisation of every point at the co-ordinate system (Figure 3).

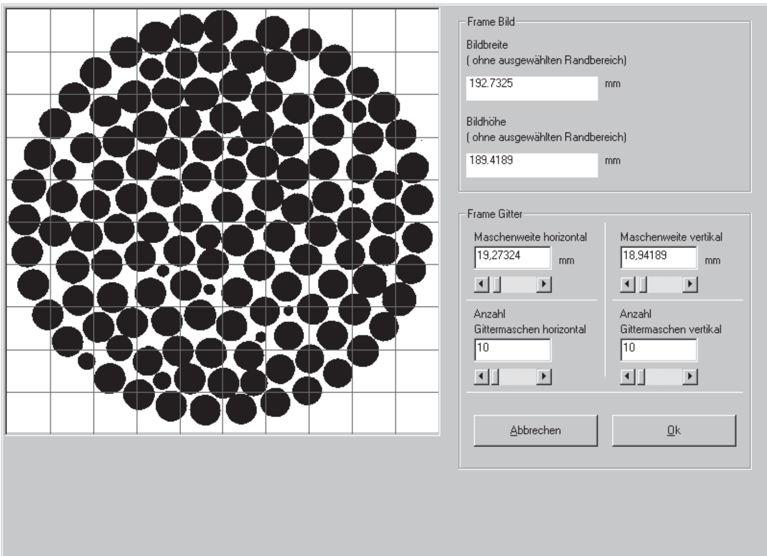

Figure 3: Program mask “establishing raster”(model of balls)

The prints of the bar is guaranteed to entirely fall in the designated area., because the main parameters, like the length of bar and the “hits” of the ends of the bar, are contributing in the equation for estimating the specific surface.

Figure 4 shows the result of experiments hold on a homogenous packed bed of balls with a length of the bar of 100 mm. The dotted lines at the figure illustrate the area of tolerance while showing the independent calculated specific surface between 0,4 mm²/mm³ to 0,4615 mm²/mm³(the used balls have an own tolerance of fabrication). At this experiment the approximation to one value due to the big number of independent samples is clearly to be seen. The estimation of the specific surface by the statistical method fluctuates between the valid borders of tolerance and stops at 0,424 mm²/mm³. A second experiment as been done at the them picture with the them length has been done in order to proof the reproduction and correctness of the procedure used. By comparing the result with the first experiment, almost the same estimation of the specific surface, which has been 0,426 mm²/mm³, could be found.

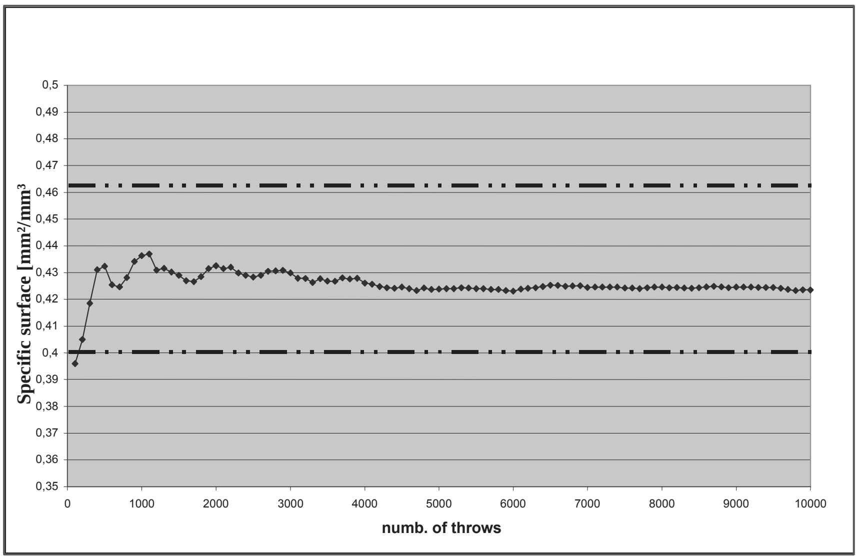

Figure 4: Statistically estimated specific surface of a homogenous surface of a packed bed of balls (length of the bar 100 mm)

7. CONCLUSIONS

Particle size distributions of organic waste according to DIN 18123 have been created. Possibilities of evaluating organic waste in consideration to characteristic numbers and effective particle size have been tested, to conclude to the properties of the packed bed.

The main results can be summarised as follows:

- the Kozeny-Köhler method is at the moment the most suitable one to estimate an effective particle size of particle size distributions,
- the uncritical derivative of an effective particle size on a mass basis according to the Kozeny-Köhler method contains for organic waste

at least a mistake of 20%, compared with an estimated effective particle size on a volume basis,

- in the case of rest waste the divergence in calculating an effective particle size on a mass basis will still increase, because of the even higher heterogeneity of rest waste,
- the use of characterising numbers, for instance the coefficient of curvature and uniformity, is suggestive to evaluate particle size distributions.

For practical use the following conclusions can be taken by the done research of particle size distributions of organic waste:

- in the cause of problems running the treatment process a detailed estimation of the particle size distribution and of the characteristic numbers, while sieving the material at least on 10 sieves, should be done,
- closely particle size distributions should be used,
- the recording of the test to the quality assurance system and the performance of the test in monthly distances is recommended especially in the case of recurring problems

Knowledge about the specific surface could cause new possibilities according to the calculation of the aeration system as well as to the degradation process of organic waste. Whiteout specific to the effective surface of organic waste, a further detailed calculation of the degradation process seems to be impossible. Recently a big number of different methods is available to estimate the specific surface of different materials, nevertheless there are now experiences on organic waste. A speciality of the considered research is, that the specific surface should be possibly estimated at the packed material and not at the loose gravel.

The estimated results, based on the introduced statistical method can be summarised as follows:

- two different samples of packed beds of organic waste have been searched,
- the sample with the higher amount on fine particles had a specific surface of 3,82mm²/mm³ to 4,22 mm²/mm³,
- the sample with the lower amount on fine particles had a specific surface of 1,34mm²/mm³ to 1,74 mm²/mm³.

For practical reasons a special importance approaches to the estimation of an effective particle size for planning the aeration system. Because the limited number of tests, comparing to the investment costs, the estimation of an effective particle size, based on specific weights of the particle size fractions should be done. Of course, the annual details of the composition of the organic waste according to the seasons of the different catchment areas have to be accounted. For the planning of plants, the realisation of the proposed experiments is recommended as part of the basic data’s. The tests should be take place in Europe at least in January and

September. In connecting with additional tests, like the water capacity, the proposed tests could be part of simple and fast optimisation of material properties, in the wider contents of a quality assurance system.

REFERENCES

Brüggemann, K. (1982). Die Bodenprüfverfahren bei Straßenbauten, Düsseldorf.

Bundesgütegemeinschaft Kompost e.V. (2000). personnel notice

Chalkley, H. W. (1949). A Method for Estimating Volume-Surface Ratios.- In: Science, Vol. 110, pp. 295-297, September 23, 1949.

DIN 18123. Bestimmung der Korngrößenverteilung.-Normenausschuß Bauwesen (NABau) im DIN Deutsches Institut für Normung e.V., 1996.

DIN 18124 T1. Bestimmung der Korndichte.-Normenausschuß Bauwesen (NABau) im DIN Deutsches Institut für Normung e.V., 1989.

Encyclopaedia Britannica (1875-1889). Probabaility.- 9. Auflage, Vol. XIX, S. 768-788, Edinburgh.

Kraft, E. (2000). Charakterisierung heterogener Abfallstoffgemische hinsichtlich ihres Einflusses auf das Strömungsverhalten Newtonscher Fluide, Dissertation Bauhaus-Universität Weimar.

Kraft, E., Schwind, B. (1996). Korn für Korn - Materialspezifische Kennwerte für Bioabfall ermöglichen Rückschlüsse auf das Durchströmungsverhalten von Abfällen, Müllmagazin 4/96.

Lang (1996): Bodenmechanik und Grundbau, Das Verhalten von Böden und Fels und die wichtigsten grundbaulichen Konzepte, Springer Verlag, Berlin.

Schreiber, P. (1998). Erarbeitung und Test einer statistischen Methode zur Ermittlung spezifischer Oberflächen von Abfallstoffen, Diplomarbeit GHS Essen, Fachgebiet Abfallwirtschaft.

Umweltbundesamt (1998) :Internet: www.umweltbundesamt.de, Abfallaufkommen, letzte Aktualisierung 18.11.98, abgefragt 02.06.2000.

van Genuchten, M. Th., Nielsen, D. R. (1985). On Describing and Predicting the Hydraulic Properties of Unsaturated Soils. Annales Geophysicae 3,5 S. 615-628.

Wiemer, Kern (1999). Bio- und Restabfallbehandlung III, Baeza Verlag, Witzenhausen, 1999.

ANALYSIS OF FLOOR ACCELERATION DEMANDS IN MULTISTORY BUILDINGS

SEMİH KÜÇÜKARSLAN and YALÇIN KUMBASAR
Department of Engineering Sciences
Istanbul Technical University, Istanbul
kucukarslan@itu.edu.tr

ABSTRACT

The floor acceleration demands in multistory buildings response as elastical when it is subjected to earthquake ground motion. In this paper, an approximate method is proposed in order to estimate these floor acceleration demands at any floor level. The dynamic characteristics of the building are investigated by using an approximated model combining a flexural beam and a shear beam. The dynamic properties of continuum system are considered to compute the modes of vibration of the building. The formulation is modeled including the effect of change of lateral stiffness along the height. Finite difference method with forward difference is used to estimate the acceleration demands in the building with non-uniform stiffness along height.

1. INTRODUCTION

During occurred earthquakes, a huge amount of nonstructural elements of the buildings are subjected to floor acceleration demands which result in damages and economic losses even when buildings go through nonstructural damage. As a result, it is important to estimate the distribution of maximum acceleration demands along the height to design correct and efficient non-structural components. Villaverde [1] states that not all elements, which have importance in the response of non-structural components, are taken into account in present design-oriented methods. He proposes a design-oriented method, which includes the dynamic properties of the first mode of vibration, to cover these limitations [2]. This method does not consider the contribution of higher modes of vibration to floor acceleration demands in buildings.

This paper presents an approximate solution to estimate floor acceleration demands in multistory buildings with non-uniform stiffness by using a small number of variables. While providing this, the contribution of the first three modes of vibration of the building are considered.

2. MULTISTORY BUILDINGS WITH NON-UNIFORM STIFFNESS ALONG HEIGHT

2.1 Simplified Model of Multistory Building

In the this method, the dynamic properties of multistory buildings are approximated by using an equivalent continuum model consisting of a flexural cantilever beam and a shear cantilever beam deforming in bending and shear configurations, respectively shown in Figure 1 [3-5].

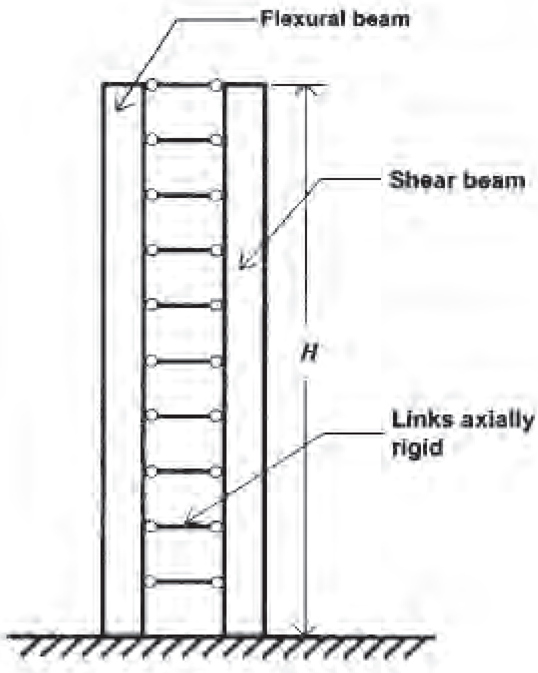

Figure 1: Simplified model to estimate dynamic properties of multistory buildings [5]

Miranda used the model shown in Figure 1 to estimate the maximum roof displacement and maximum interstory drift of uniform buildings responding primarily in the first mode of vibration [3]. This approximate method was more recently extended to buildings with non-uniform lateral stiffness [4]. That work shows that reductions in lateral stiffness along the height have a negligible effect on the ratio of spectral displacement to maximum roof displacement and only a small effect on the ratio of maximum interstory drift ratio to roof drift ratio. Non-dimensional ratios computed from the uniform case are accurate enough for computing approximate lateral drift demands in buildings subjected to earthquake ground motions. Miranda and Taghavi [5] give the response of the continuum system shown in Figure 1, when subjected to a horizontal acceleration at the base level, by the following equilibrium equation [5]

Eq. 2.1.1

$$\rho(x)\ddot{u}(x,t)+c(x)\dot{u}(x,t)+\frac{1}{H^4}\big(EI(x)u''(x,t)\big)''-\frac{1}{H^2}\big(GA(x)u'(x,t)\big)'=-\rho(x)\ddot{u}_g(t)$$

x: non-dimensional height varying between zero at the base of the building and one at roof level

t: time

$\rho(x)$: mass per unit length

u(x,t): lateral displacement at height x and time t

H: total height of the building

c(x): damping coefficient per unit length

EI(x): flexural rigidity of the flexural beam along the height

GA(x): shear rigidity of the shear beam

$u_g(t)$: ground displacement at time t

For a function y(x,t), partial differentiation with respect to x: $\frac{\partial y}{\partial x}=y'$

For a function y(x,t), partial differentiation with respect to t: $\frac{\partial y}{\partial t}=\dot{y}$

At the base level of the structure, the variation of flexural stiffness in the flexural beam can be expressed as a function of the flexural rigidity.

Eq. 2.1.2

$$EI(x)=EI_0S(x) \quad \text{and} \quad GA(x)=GA_0S(x)$$

EI_0: flexural rigidity at the base of the structure

GA_0: shear rigidity at the base of the structure

S(x): non-dimensional function which defines the variation of stiffness along the height of the building

It is assumed that a uniform mass and damping coefficient exist along the height of the building. Then, substitute Eq. 2.1.2 into Eq. 2.1.1 and divide by EI_0

Eq. 2.1.3

$$\frac{\rho}{EI_0}\ddot{u}(x,t)+\frac{c}{EI_0}\dot{u}(x,t)+\frac{1}{H^4}\big(S(x)u''(x,t)\big)''-\frac{\alpha_0^2}{H^4}\big(S(x)u'(x,t)\big)'=-\frac{\rho}{EI_0}\ddot{u}_g(t)$$

where α_0: non-dimensional parameter defined as

Eq. 2.1.4

$$\alpha_0 = H\left(\frac{GA_0}{EI_0}\right)^{1/2}$$

where α_0 controls the degree of participation of overall flexural and shear deformations in Figure 1.

2.2 Approximate Earthquake Analysis

The structure is supposed to act with elastic behavior, so the response can be calculated with superposition of the responses of all modes of vibrations. The displacement can be computed as a linear combination of all modal responses.

Eq. 2.2.1

$$u(x,t) = \sum_{i=1}^{\infty} u_i(x,t)$$

where $u_i(x,t)$: contribution of the i^{th} mode to the response

Assuming classical damping, Miranda and Taghavi propose the following equation for solution [5].

Eq. 2.2.2

$$u_i(x,t) = \Gamma_i \phi_i(x) D_i(t)$$

where Γ_i : modal participation factor of the i^{th} mode of vibration

$\phi_i(x)$: amplitude of the i^{th} mode shape of vibration at x.

$D_i(t)$: deformation response of a single-degree-of-freedom system corresponding to the *i*th mode to the ground motion

2.3 Dynamic Properties of Continuum System

For undamped (c=0) free vibration (u_g =0) Eq. 2.1.3 becomes

Eq. 2.3.1

$$\frac{\rho}{EI_0}\ddot{u}(x,t) + \frac{1}{H^4}\left(S(x)u''(x,t)\right)'' - \frac{\alpha_0^2}{H^4}\left(S(x)u'(x,t)\right)' = 0$$

Substituting Eq. 2.2.2 into Eq. 2.3.1 one can derive

$\ddot{u}_i(x,t)=\Gamma_i\phi_i(x)\ddot{D}_i(t)$, $u_i''(x,t)=\Gamma_i\phi_i''(x)D_i(t)$, $u_i'(x,t)=\Gamma_i\phi_i'(x)D_i(t)$ and Γ_i cancels out.

Eq. 2.3.2

$$\frac{\rho}{EI_0}\phi_i(x)\ddot{D}_i(t)+\frac{D_i(t)}{H^4}\left(S(x)\phi_i''(x)\right)''-\frac{\alpha_0^2}{H^4}D_i(t)\left(S(x)\phi_i'(x)\right)'=0$$

Then Eq. 2.3.2 is multiplied with $\dfrac{EI_0}{\rho\phi_i(x)D_i(t)}$. Using separation of variables two ordinary differential equations are obtained.

Eq. 2.3.3

a: $\ddot{D}_i(t)+w_i^2D_i(t)=0$

b: $\left(S(x)\phi_i''(x)\right)''-\alpha_0^2\left(S(x)\phi_i'(x)\right)'-\beta_i^2\phi_i(x)=0$

where $\beta_i=\left(w_i^2\dfrac{\rho H^4}{EI_0}\right)^{1/2}$ and ω_i : circular frequency of vibration of the system of i^{th} mode of vibration.

2.4 Uniform Stiffness Along Height

Eq. 2.4.1

$$\phi_i'^{V}(x)-\alpha_0^2\phi_i''(x)-\beta_i^2\phi_i(x)=0$$

Boundary conditions for the system, respectively. Zero displacement and rotation at the bottom, zero moment and shear forces at the top.

Eq. 2.4.2

a: $\phi_i(x)\Big|_{x=0}=0$ **b:** $\phi_i'(x)\Big|_{x=0}=0$

c: $\phi_i''(x)\Big|_{x=1}=0$ **d:** $\left[\phi_i'''(x)-\alpha_0^2\phi_i''(x)\right]\Big|_{x=1}=0$

From Eq. 2.4.1 and Eq. 2.4.2.a,b,c the solution for $\phi_i(x)$ is derived as

Eq. 2.4.3

$$\phi_i(x)=A_1e^{r_1x}+A_2e^{-r_1x}+A_3e^{r_2x}+A_4e^{-r_2x}$$

$$r_1 = \sqrt{\frac{\alpha_0^2 + \sqrt{\alpha_0^4 + 4\beta_i^2}}{2}} \qquad r_2 = \sqrt{\frac{\alpha_0^2 - \sqrt{\alpha_0^4 + 4\beta_i^2}}{2}}$$

where $A_1 = -\frac{r_1^2 + r_2^2}{2} e^{-r_1} + \frac{r_2^2\left(r_1 + r_2\right)}{2r_1} e^{-r_2} - \frac{r_2^2\left(r_1 - r_2\right)}{2r_1} e^{r_2}$

$$A_2 = -r_1 r_2 e^{r_1} - \frac{r_2^2\left(r_1 - r_2\right)}{2r_1} e^{-r_2} - \frac{r_2^2\left(r_1 + r_2\right)}{2r_1} e^{r_2}$$

$$A_3 = \frac{r_1\left(r_1 - r_2\right)}{2} e^{r_1} + \frac{r_1\left(r_1 + r_2\right)}{2} e^{-r_1} - r_2^2 e^{-r_2}$$

$$A_4 = -\frac{r_1\left(r_1 + r_2\right)}{2} e^{r_1} + \frac{r_1\left(r_1 - r_2\right)}{2} e^{-r_1} - r_2^2 e^{r_2}$$

and $r_1^2 + r_2^2 = \alpha_0^2 \Rightarrow r_2 = \sqrt{\alpha_0^2 - r_1^2}$, which gives a more simple equation.

Substituting Eq. 2.4.3 into Eq. 2.4.2.d gives the characteristic function with parameters α_0 and β_i .

Eq. 2.4.4

$$\begin{aligned}
&\left[\left(r_2^2 + \frac{r_2^3}{r_1}\right)\left(r_1^3 - \alpha_0^2 r_1\right) + \left(r_1^2 + r_1 r_2\right)\left(r_2^3 - \alpha_0^2 r_2\right)\right]\cosh\left(r_1 - r_2\right) \\
&+\left[\left(r_2^2 - \frac{r_2^3}{r_1}\right)\left(r_1^3 - \alpha_0^2 r_1\right) + \left(r_1^2 - r_1 r_2\right)\left(r_2^3 - \alpha_0^2 r_2\right)\right]\sinh\left(r_1 + r_2\right) \\
&-\left[\frac{\left(r_1 - r_2\right)^2}{2}\left(r_1^3 - \alpha_0^2 r_1\right) + 2r_2^2\left(r_2^3 - \alpha_0^2 r_2\right)\right] = 0
\end{aligned}$$

The three smallest roots of Eq. 2.4.4 correspond to the first, second and third modes of vibration of the building, respectively.

For the case α_0 =3, one can compute the first three roots as follows:
β_1^2 =38.5 , β_2^2 =792.57 , β_3^2 =4456.7

2.5 Non-uniform Stiffness Along Height

A close-form solution for a building with a non-uniform distribution of lateral stiffness along the height cannot be derived from Eq. 2.3.3.b. Therefore, finite difference method with forward difference is used in order to estimate the amplitudes of mode shapes for buildings with non-uniform stiffness along height. Miranda and Taghavi propose the following formula for variation of stiffness [5].

Eq. 2.5.1

$S(x) = 1 - (1-\delta)x^{\lambda}$

where δ: ratio of the lateral stiffness at the top to the lateral stiffness at the base

λ: non-dimensional parameter that controls the variation of lateral stiffness along the height.

For the case, λ=0.5, δ=0.25 Eq. 2.5.1 becomes $S(x) = 1 - 0.75x^{1/2}$. Substituting this in Eq. 2.3.3.b gives

Eq. 2.4.2

$$\left(1-0.75x^{1/2}\right)\phi_i^{IV} - 0.75x^{-1/2}\phi_i''' + \left[0.1875x^{-3/2} - \alpha_0^2\left(1-0.75x^{1/2}\right)\right]\phi_i'' + \alpha_0^2 0.375x^{-1/2} - \beta_i^2\phi_i = 0$$

Finite difference method with forward difference:

$${}^j\phi_i \rightarrow {}^j y$$
$${}^j y' = \frac{1}{h}\left({}^{j+1}y - {}^j y\right)$$
$${}^j y'' = \frac{1}{h^2}\left({}^{j+2}y - 2\,{}^{j+1}y + {}^j y\right)$$
$${}^j y''' = \frac{1}{h^3}\left({}^{j+3}y - 3\,{}^{j+2}y + 3\,{}^{j+1}y - {}^j y\right)$$
$${}^j y^{IV} = \frac{1}{h^4}\left({}^{j+4}y - 4\,{}^{j+3}y + 6\,{}^{j+2}y - 4\,{}^{j+1}y + {}^j y\right)$$

Substituting these in Eq. 2.5.2 and taking h=1/16 (dividing the height into 16 equal intervals, this number is optional, hence number of points can be increased) gives

Eq. 2.5.3

$$\left({}^j a + {}^j b + {}^j c - {}^j d - \beta_i^2\right){}^j y + \left(-4\,{}^j a - 3\,{}^j b - 2\,{}^j c + 16\,{}^j d\right){}^{j+1}y$$
$$+\left(6\,{}^j a + 3\,{}^j b + {}^j c\right){}^{j+2}y + \left(-4\,{}^j a - {}^j b\right){}^{j+3}y + a\,{}^{j+4}y = 0$$

where ${}^j a = 16^4\left(1 - 0.75\,{}^j x^{1/2}\right)$

$${}^j b = 16^3\left(0.75\,{}^j x^{-1/2}\right)$$
$${}^j c = 16^2\left[0.1875\,{}^j x^{-3/2} - \alpha_0^2\left(1 - 0.75\,{}^j x^{1/2}\right)\right]$$
$${}^j d = 16\alpha_0^2 0.375\,{}^j x^{-1/2}$$

Matrix form for Eq. 2.5.3: $\underset{\sim}{C}\underset{\sim}{Y} = \underset{\sim}{0}$

where $\underset{\sim}{C}$: coefficients matrix , (21x21) square matrix

$$\underset{\sim}{Y} = \begin{bmatrix} {}^{0}y \\ {}^{1}y \\ . \\ . \\ . \\ {}^{20}y \end{bmatrix} : \text{unknowns vector} \ , \quad \underset{\sim}{0} = \begin{bmatrix} 0 \\ 0 \\ . \\ . \\ . \\ 0 \end{bmatrix} : \text{constants vector, (21x1)}$$

2.6 Numerical Implementation

Finite difference method applied into boundary conditions gives the four extra equations needed, as follows:

Eq. 2.6.1

i) ${}^{0}y = 0$

ii) $4\left({}^{1}y - {}^{0}y\right) = 0$

iii) $4^{2}\left({}^{18}y - {}^{17}y + {}^{16}y\right) = 0$

iv) $64\,{}^{19}y - 192\,{}^{18}y + 156\,{}^{17}y - 28\,{}^{16}y = 0$

From Eq. 2.6.1.i,ii it is trivial that ${}^{0}y = {}^{1}y = 0$. Thus, the first two columns and first two boundary conditions can be omitted. Coefficient matrix reduces to a (19x19) matrix. Yet, a matrix with zero constants vector cannot be applied into Cramer method. It is assumed that at the top $\phi_i\left(x\right)\big|_{x=1} = {}^{16}y = 1$. Then, 14th (16th before elimination) column multiplied by -1 forms the new constants vector different than zero vector. In order to have a square matrix one more row, which can be written as a linear combination of the other rows, is eliminated. The most adequate row is the last boundary condition: Eq. 2.6.1.iv. In the end, a (18x18) coefficients matrix and a (18x1) constants vector are proposed to be applied into Cramer method.

2.6.2.1 First Mode of Vibration

Code used in command window in Matlab for β_1^2 =38.5:

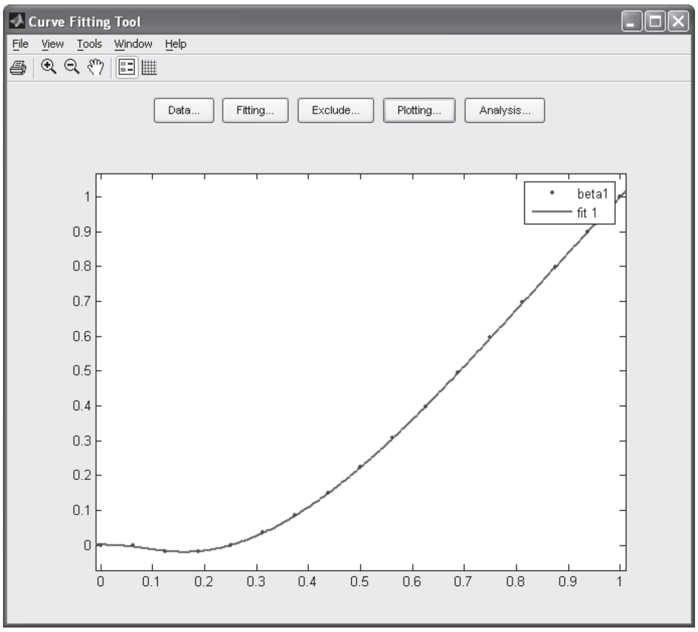

Figure 2: Matlab Curve Fitting Tool showing the spline for mode shape of 1st mode of vibration

In Figure 2, x-axis represents the height of the building (x), while y-axis represents the amplitude of the 1st mode of vibration (ϕ_1).

2.6.2.2 Second Mode of Vibration

Code used in command window in Matlab for β_2^2=792.57

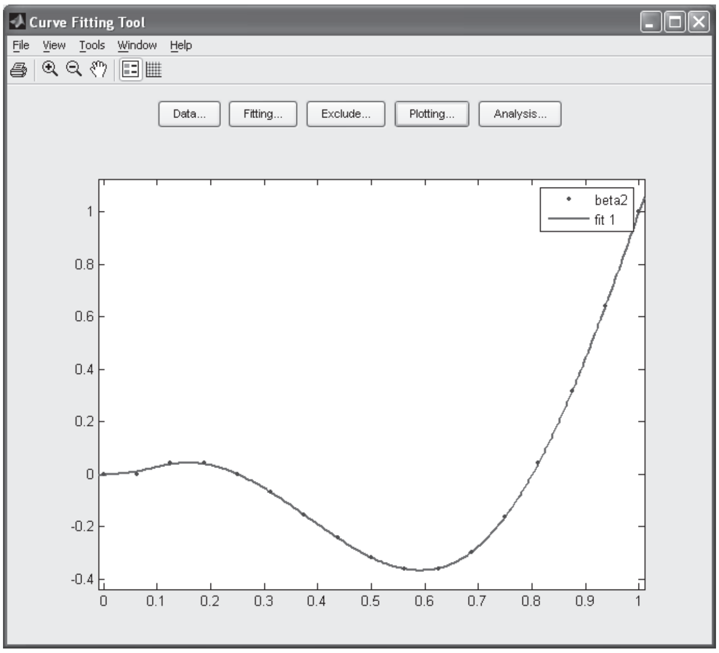

Figure 3: Matlab Curve Fitting Tool showing the spline for mode shape of 2nd mode of vibration

In Figure 3, x-axis represents the height of the building (x), while y-axis represents the amplitude of the 2nd mode of vibration (ϕ_2).

2.6.2.3 Third Mode of Vibration

Code used in command window in Matlab for β_3^2 =4456.7

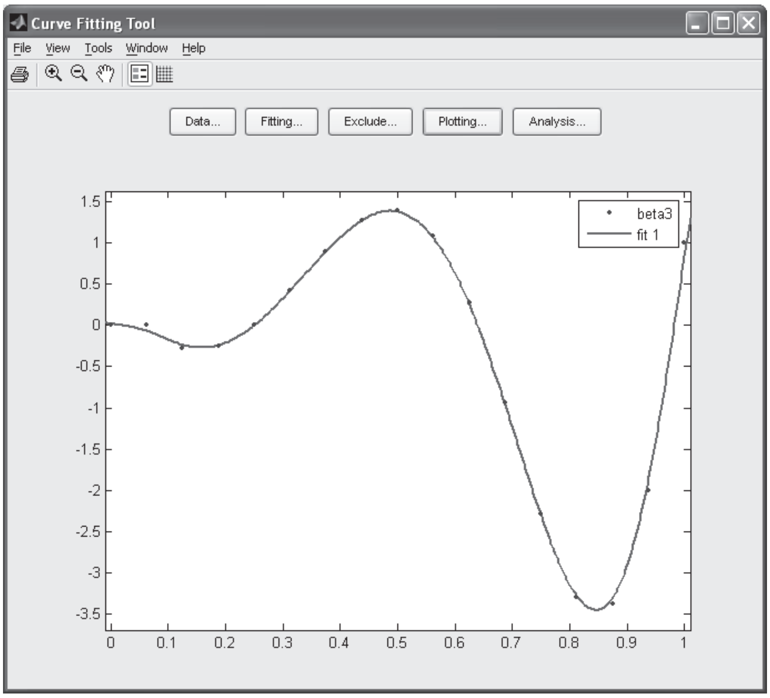

Figure 4: Matlab Curve Fitting Tool showing the spline for mode shape of 3rd mode of vibration

In Figure 4, x-axis represents the height of the building (x), while y-axis represents the amplitude of the 3rd mode of vibration (ϕ_3).

Miranda and Taghavi propose an approximating function for the mode shapes of the simplified model with non-uniform stiffness along height as follows [5]:

Eq. 2.6.2:

$$\phi_{i,nu}\left(x\right)=\phi_{i,u}\left(x\right)+\left[\left(-1\right)^{i} i^{1.3}\sin\left[\left(i-0.1\right)\pi x\right]\sqrt{\sin\left(\pi x\right)}\right]x\left[\sin\left(\frac{\pi\alpha_0}{60}\right)+0.4\right]\left(\frac{1-\delta}{9}\right)$$

where $\phi_{i,u}\left(x\right)$ is the function derived in Eq. 2.4.3. Besides, mentioned approximation method using finite difference method, Eq. 2.6.2 can be used to calculate the mode shapes of the building with non-uniform stiffness along height.

3. CONCLUSIONS

In this paper, an approximated model of a multistory building is presented to estimate the mode shapes of vibration when the building is subjected to ground motions. By using the model with uniform stiffness along height, the effects of first three modes of vibration are calculated. After that, finite difference method with forward differences is applied to approximate the points of the curve which represents the mode shapes of buildings with non-uniform stiffness along height when exposed to ground motions. The first three modes of vibration are considered separately. The calculations followed during the paper are an application of a general method, which can be applied into other situations with small modifications. Civil engineers can use and improve this method to approximate floor acceleration demands in multistory buildings with non-uniform stiffness along height.

REFERENCES

Villaverde, R. (1996). “Earthquake resistant design of secondary structures: a report on the state of the art.” *Proc., 11th World Conf. on Earthquake Engineering* (CD-ROM), Elsevier Science Ltd., Oxford, England.

Villaverde, R. (1997). “Method to improve seismic provisions for nonstructural components in buildings.” *J. Struct. Eng.*, 123(4), 432–439.

Miranda, E. (1999). “Approximate lateral deformation demands in multistory buildings.” *J. Struct. Eng.*, 125(4), 417–425.

Miranda, E., and Reyes, C. J. (2002). “Approximate lateral drift demands in multistory buildings with nonuniform stiffness,” *J. Struct. Eng.*, 128(7), 840–849.

Taghavi, S., and Miranda, E. (2005). “Approximate floor acceleration demands in multi-story buildings. I: Formulation.” *J. Struct. Eng.*, 131(2), 212–220.

IMPACTS OF BASE FLOW DISCHARGE ON NITRATE IN SURFACE WATER QUALITY

WOO SANGDEOK, HAN KYUNGMIN,
AND KIM GEONHA
Department of Civil and Environmental Engineering,
Hannam University, Ojungdong, Daedukku,
Daejeon, 306-791, Republic of Korea. [1]
kimgh@hnu

ABSTRACT

It is a well known fact that baseflow discharge of rainfall runoff impacts on water quality of surface water significantly. In this paper, impacts of nitrate discharged as base flow on stream water quality were studied by using a software, PULSE from USGS to calculate monthly ground water discharge from hydrograph. We used water quality and flow rate data for Ghapcehon2 site in Daejeon city for year 2005 as well as ground water quality data in the watershed acquired from government agencies. Agricultural and forestry land use are dominant for upstream of Ghapcheon2 in the watershed. Base flow contributes about 85~95% of stream flows during spring and fall while 25~38% of stream flow was induced by base flow during summer and winter. Monthly nitrate loading discharged as base flow for Ghapcheon2 was estimated by using averaged nitrate concentration of groundwater in the watershed. Nitrate loading induced by base flow at Ghapcheon2 was estimated as 5.4 ton of NO_3^-*-N/km*^{2}*, which is about 60% of nitrate loading of surface water, 9.2 ton of* NO_3^-*-N/km*^{2}*. From this study, it can be understood that ground water quality monitoring is important for the proper manage of surface water quality.*

Keywords
Base flow, Groundwater, Hydrograph separation, Nitrate, Water quality.

1. INTRODUCTION

For the proper management of the surface water quality, pollutant loadings are subjected to abatement. However, enough water quality improvements may not be achieved without proper management of groundwater discharge (Freeze and Cherry, 1979; Schilling and Zhang, 2004). If a watershed is covered by forestry and agricultural land use, surface water quality will be vulnerable to groundwater discharge of rainfall runoff.

Nitrogen, particularly in the form of nitrate, is the most common contaminants in aquifer systems (Freeze and Cherry, 1979; Kim et al. 2008). Muhammetoglu et al. (2002) points to agriculture as being the most substantial anthropogenic source of nitrate, and Burkart et al. (2002) suggests that this is caused by the intensive and extensive land use activities associated with crop production and animal raising. The Korean Ministry of Environment monitored groundwater that was used as source water and reported that up to 5 % of the 4,534 wells were polluted by nitrates (KMOE, 2008). This fact indicates that nitrate is emerging as one of primary pollutant in the groundwater.

Nitrates in drinking water cause *Methmoglobinemia* (Blue baby syndrome) and cancer. The US EPA promulgated nitrate concentration criteria for drinking water as 10 mg NO_3^--N/L, and 1.0 mg NO_2^--N/L (Plumb, 1998). Nitrates originated from various sources which included agricultural and industrial areas and percolated into ground aquifers. As nitrates are hardly removed naturally from the subsurface areas, they accumulate in the aquifers.

Flow rate of groundwater discharge may be separated from flow rate of surface water by hydrograph analysis. Frequently adopted hydrograph separation methodologies are master groundwater depletion curve method, straight line method, fixed base method, and variable slope method. Public domain software for hydrograph separation such as PULSE, PART, RECESS, RORA, HYSEP, BFI is available, and can be downloaded from the internet (U.S. Geological Survey, 2008) for free.

As discussed above, groundwater quality is of concern, but understandings about interactions between groundwater and surface water is still not enough. In this research, impacts of nitrate discharged from groundwater on surface water quality were estimated by means of hydrograph analysis for an agricultural-forestry watershed.

2. METHODOLOGY

For this study, one monitoring station named Ghapcheon2 was selected on the Ghap stream in the Daejeon city, Republic of Korea. Fig. 1 show the land uses of the Daejeon city and the location of the Ghapcheon2 site. Ghapchen2 station is located upstream of Ghap stream and before entering the center of the city and the watershed includes large portion of agricultural and forestry land uses. There are 4 groundwater monitoring wells located run by the government and shown in Figure 1. A site and G site are close to forestry while B site and F site are relatively close to agricultural land use.

Water quality data were obtained from Water Environment Information System (KMOE, 2008), groundwater quality data were obtained from National Groundwater Information Center (KOWACO, 2008), water level data were obtained from National Water Resources Management Information System (KMOLM, 2008). Rating curves between water level-flow rate were obtained from the Annual Report of Hydrology (KMOLM, 2008).

Hydrograph separation was carried out by PULSE developed by USGS (USGS, 2002: Rutledge, 1997). PULSE separates groundwater discharge from surface water flow rate based on master groundwater depletion curve, which is deletion curves are isolated from hydrograph and sorted to compose main groundwater depletion curve. PULSE can calculate flow rate of groundwater discharge and recharge rate based on recession index derived from hydrograph and watershed area.

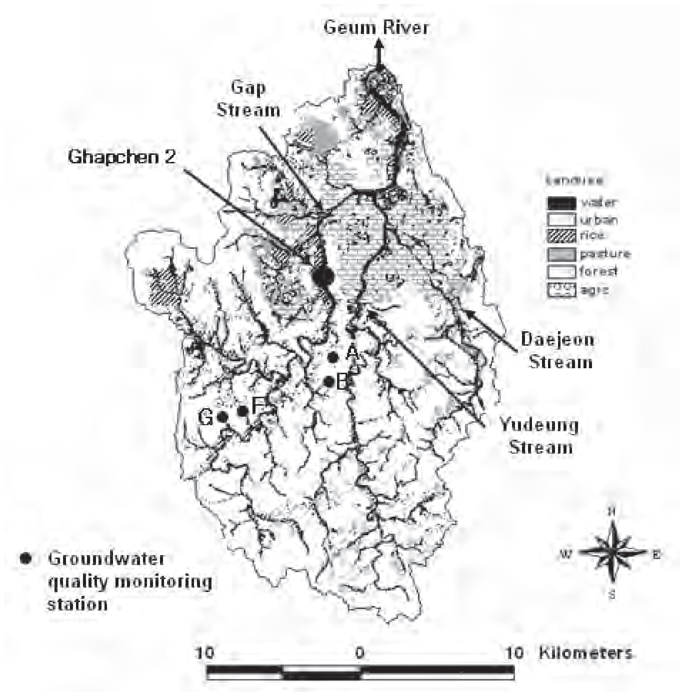

Figure 1: Land Use of the Daejeon city, Location of Ghapchen2, and Groundwater Monitoring Station for Domestic Use in Daejeon City.

3. RESULT AND DISCUSSION

Figure 2 shows flow rate of Ghapcheon2 site in the year 2005 and groundwater discharge calculated by PULSE. It can be understood that groundwater discharge largely constitute surface water. During January, February and December, contribution of groundwater on surface water are decreasing mainly due to defected flow rate data. During successive rainfall event in July, contribution of baseflow discharge are decreasing as well. If rainfall event was occur right after the previous one, groundwater discharge contribution is low, implying that more precipitation discharged via surface runoff.

Figure 3 is stream flow and groundwater discharge per unit area for Ghapcheon2 for year 2005 calculated by PULSE. In the figure, contribution of baseflow discharge are shown on top of the graph by dividing groundwater discharge by stream flow. During drought season, contribution of groundwater discharge is high while the contribution is low during wet season. During April and May, 90% of flow rate of surface water are discharged from groundwater while 30% of surface water was contributed by the groundwater during summer.

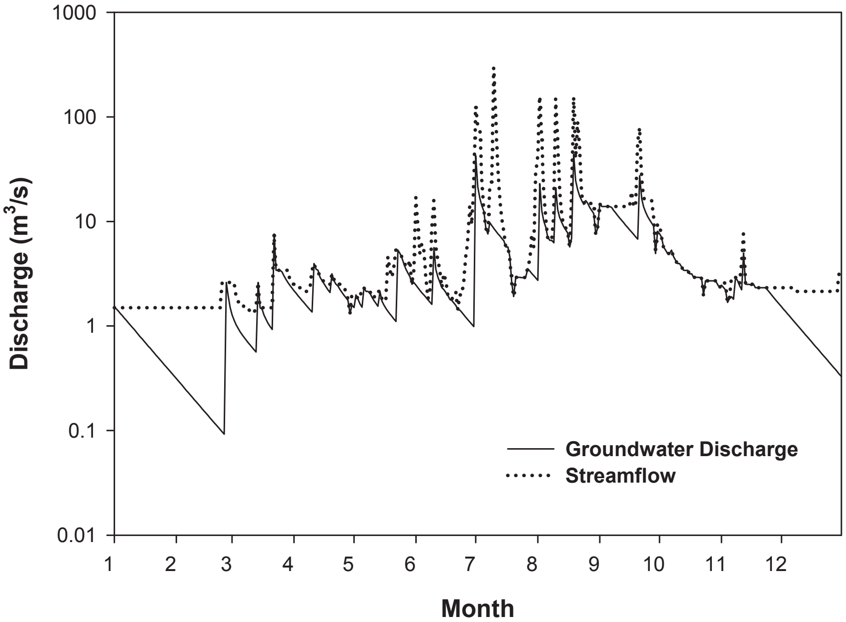

Figure 2: Measured Stream Flow for Ghapcheon2 and Calculated Base Flow Discharge by PULSE for Year 2005.

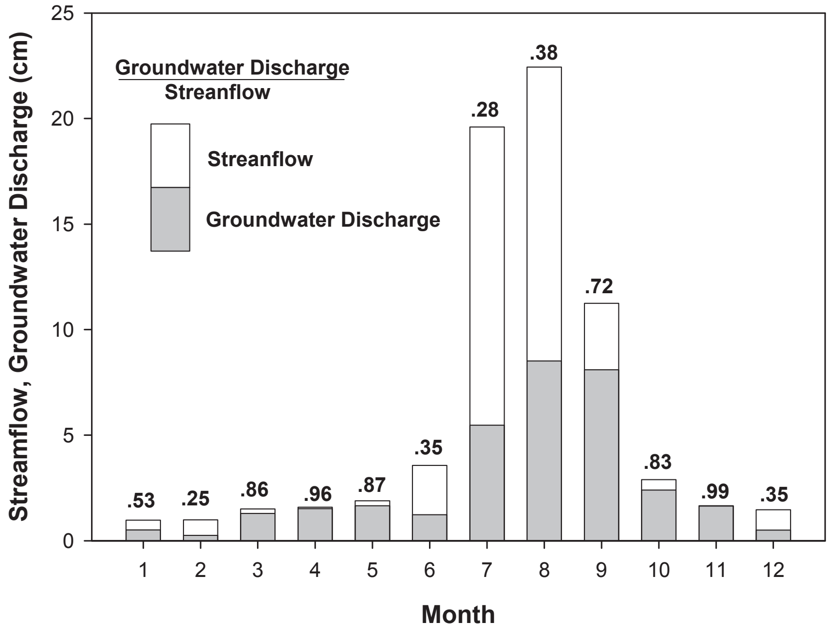

Figure 3: Stream Flow and Groundwater Discharge per Unit Area for Ghapchen2 for Year 2005.

Figure 4 shows nitrate and BOD concentration variations at Ghapchen2. In general, BOD concentrations were high during Spring and Summer while nitrate concentrations were high during drought season. Nitrates were leached more during winter as agricultural area is not enoughly managed and uptaked by plants.

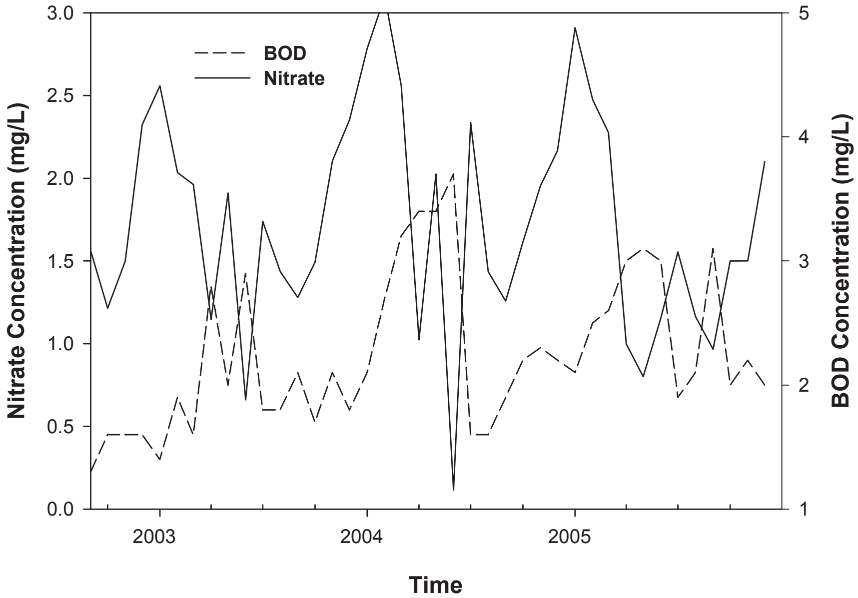

Figure 4: Nitrate and BOD (Biochemical Oxygen Demand) Concentration Variations at Ghapchen2 from September, 2002 to December, 2005.

Figure 5 is the comparison of nitrate loads of streamflow and base flow discharge for the Ghapcheon2 for year 2005. Nitrate concentration of ground water was assumed as averaged nitrate concentration of groundwater, 1.62 mg/L (data not shown here). In the figure, estimated loadings of baseflow were higher than those of surface flow for months as the averaged groundwater concentration were high. When converting data shown in Fig. 6 into annual loading, annual loading of surface runoff is calculated as 9.2 ton of $NO_3^-N/km^2{\cdot}yr$, while that of baseflow discharge is calculated as 5.4 ton of $NO_3^-N/km^2{\cdot}yr$, which is 59% of surface flow. While analyzing Fig. 6, one should note that the subjected area possess significant portion of agricultural land use, and groundwater concentration data contains high level of uncertainty (Diek, 2002).

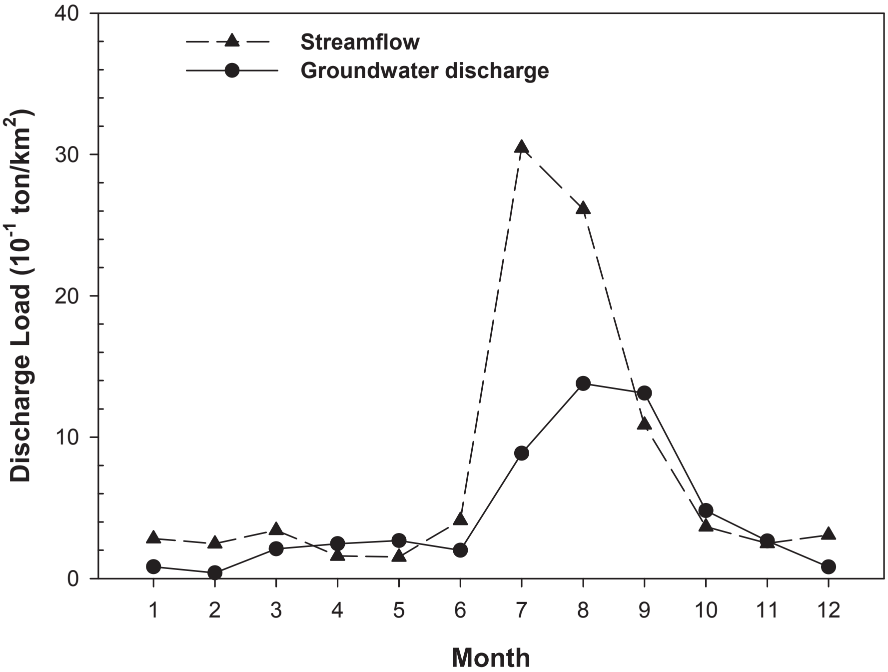

Figure 5: Comparison of Nitrate Loads of Streamflow and Base Flow Discharge for the Ghapcheon2 for Year 2005 (nitrate concentration of ground water was assumed as 1.62 mg/L).

4. CONCLUSION

To assess the impacts of nitrate discharged from groundwater on surface water quality, hydrograph analysis was carried out for an agricultural-forestry watershed. Nitrate loading for the year 2005 were 85-95% during Spring and Fall while 25-38% of loading during Winter.

When converting data into annual loading, annual loading of surface runoff is calculated as 9.2 ton of $NO_3^-N/km^2 \cdot yr$, while that of base flow discharge is calculated as 5.4 ton of $NO_3^-N/km^2 \cdot yr$, which is 59% of surface flow. In this study, it can be understood that base flow discharge impacts on surface water quality, but lack of monitoring data of groundwater quality cause significant level of uncertainty.

ACKNOWLEDGEMENT

The authors sincerely appreciate the financial support provided by the Han River Watershed Management Committee and Han River Environment al Research Center

REFERENCES

Burkart M. R., Stoner, J. D. (2002) Nitrate in aquifers beneath agricultural systems. *Water Science and Technology*. *45* (9), 19-29.

Diek R. H. (2002). *Measurement uncertainty: Methods and applications. 3rd ed.*, ISA, Research Triagle Park, NC.

Freeze A. R. and Cherry, J. A. (1979). *Groundwater*, Prentice Hall, London.

Kim T., Kim G., Kim S., and Choi E. (2008). Estimating riverine discharge of nitrogen from the South Korea by the mass balance approach. *Environmental Monitoring and Assessment*, 136(1-3), pp. 371-378.

KMOLM (2008). National Water Resources Information System, Korean Mistry of Land and Marine. http://wamis.go.kr., accessed December, 2008.

KMOE (2008). Water Environment Information System, Korean Ministry of Environment http://www.water.nier.go.kr/weis/, accessed December, 2008.

KOWACO (2008). National Groundwater Information Center, Korean Water Company, http://www.gims.go.kr, accessed December, 2008.

Muhametoglu H., Muhametoglu A., and Soyupak S. (2002) Vulnerability of groundwater to pollution from agricultural diffuse sources: a case study. *Water Science and Technology*, *45* (9), 1-7.

Plumb D. (1998) *Nitrates and Groundwater: A Public Concern*; Freshwater Foundation, 28 pp.

Rutledge A. T. (1997). *Model-estimated ground-water recharge and hydrograph of ground-water discharge to a stream*. U.S. Geological Survey. Water-Resources Investigations Report 97-4253.

Schilling K. and Zhang Y. K. (2004). Baseflow contribution to nitrate-nitrogen export from a large, agricultural watershed, USA. *Journal of Hydrology*, 295, pp. 305-316.

U.S. Geological Survey. (2002) *User guide for the PULSE program*. Open-File Report 02-455. Reston, Virginia, U.S. Geological Survey.

U.S. Geological Survey. (2008) *USGS Groundwater Information*. http://water.usgs.gov/ogw/gwsw.html.

Student Presentations

SUGGESTION OF PSC BOX BRIDGE PERFORMANCE PROFILE ACCORDING TO CORROSION OF TENDON.

KIM HEE JOO and KONG JUNG-SIK
School of Civil Engineering and Architecture
Korea University, Korea
smileball@korea.ac.kr

ABSTRACT

Generally, Bridge structure become superannuated by deterioration of system and environmental factor during service life. Decision making should reflects the maintenance management what prevent from physical lifetime of the bridge deterioration and damage. Making analysis system state what is the life cycle condition/ performance analysis by member deterioration is important part of decision making. Study of condition valuation is being done, but the study of performance valuation does not revitalize in domestic bridge system. Particularly, numerical analysis of the deterioration and repair and reinforcement effect is necessary for the maintenance Life Cycle Cost Profile (LCC) analysis. This study proposes the performance profile by using quantitative analysis of deterioration factor PSC Box bridge what is effected by corrosion.

1. INTRODUCTION

Generally, Bridge structure became superannuated by deterioration of environmental factor during service life. Therefore, the decision making should reflects the maintenance management what prevent from physical lifetime of the bridge deterioration and damage. Making analysis system state what is the life cycle condition/performance analysis is important part of decision making. Actually, condition valuation of domestic bridge is proposing the performance profile that reflected regression analysis and a professional advice to a basis to Database of the bridge. However, in case the bridge DB is insufficient, it is difficult to the precise regression analysis. In addition, the subjective nature of professional opinion, difficult to propose the objectively condition curve. The performance evaluation of the bridge which make up for the weak points and make a determination of maintenance management time is performed, but the research of the domestic is still insufficient. In this study, performance profile of the bridge using RSM(Response Surface Method) by apply to the deterioration factor of the principal member of the PSC Box bridge was proposed.

2. DETERIORASION OF THE PSC BOX BRIDGE.

For get to the performance profile of PSC Box bridges, it is very important that understood about the deterioration factor of bridge. There are many factors that work to the deterioration factors of PSC Box bridges. In the PSC Box, if the concrete and tendon are deteriorated, the intensity in which it operation of the bridge is decreased and it has an affect on a durability and reliability of the bridge. These deterioration of tendon are occurs at post-tensioned by pitting corrosion.

2.1. Corrosion of Post-Tensioned Steel Wire.

Generally, corrosion to occur at concrete bridges can be sectioned to Pitting Corrosion and General Corrosion. The pit is concerned to electrolysis reaction included anodic and cathodic reaction. Comparison with general corrosion, the pitting corrosion rate is higher four to eight times and causes the sudden failure of steel reinforcement. There are many reasons to cause the pitting corrosion in the tendon. Most of the popular mechanism is the presence of bleed water and chlorides at the surface of tendon. Chloride ions occurring in the tendon reduce the pH environment and making the passive film unstable. And it`s disperse the passive film and make the film permeable to Fe^{2+} ionsullowing the anodic reaction to occur as a catalyst. The rust will form from the presence of oxygen and water on the tendon surface, $Fe(OH)_2$ was created. Furthermore, $Fe(OH)_2$ reacts with oxygen and water again to create $Fe(OH)_3$. Hydrolysis of the corrosion product in the pit causes a decrease in pH. In acid condition and saline product, corrosion may occur rapidly. In this study, all corrosions are assumed to be occurred in the post-tendsined. Figure 1 explained the creative rust process and pit formation. The pitting process is self-propagating process in the nature as illustrated in Figure 2.

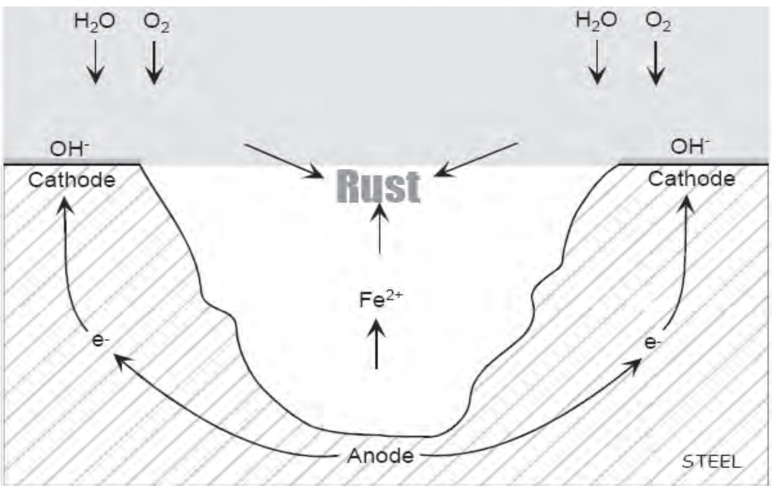

Figure 1: Anodic and cathodic reaction on the tendon surface

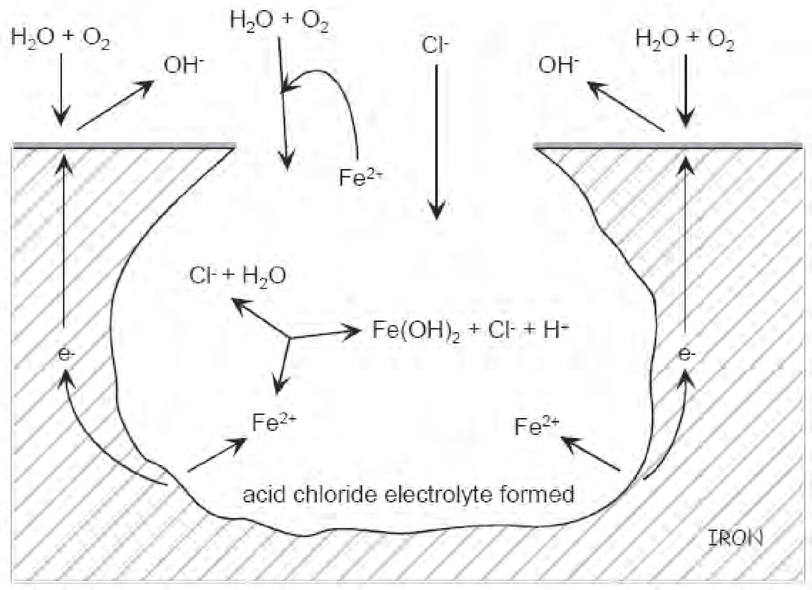

Figure 2: The self-propagating process of pitting corrosion

2.2. Analysis Model the Member of Major Deterioration.

(1) Pitting corrosion modeling.

PSC Box Bridge are when the pit propagates, the loss of tendon cross section area will be.

$$A_{S,C} = \frac{\pi=[D-2v(T-t)]^2}{4} \tag{1}$$

The equation is calculate the corrosion section according to time. The corrosion rate of rebar is different depend on environment. The corrosion rate specification in rebar was suggested by ting, Mori, Ellingwood`s each other $100\mu m/yr$, $50\mu m/yr$.
In this paper, the authors used the suggested equation from Stewart & Rosowsky (1998)

$$\upsilon = 0.00116\, R\, \acute{\iota}_{corr} \tag{2}$$

Where, R=Pitting corrosion coefficient, suggested by Gonzalez(1994), ranges from 4 to 6; $\acute{\iota}_{corr}$ =corrosion current density ($\mu A/cm^2$). Used in this study, Zhao-Hui Lu (1998) proposed the following expression.

$$\acute{\iota}_{corr} = \frac{T_k H_r(\omega/c)}{d_c} \tag{3}$$

That is suggested by Zhao-Hui Lu(1998); T_k=absolute temperature, average temperature 16° C/yr in Korea.; Hr=relative humidity; w/c=water/concrete ratio, assume 0.5; d_c=cover.

(2) Time variant reliability index.

Tendon and shear reinforcement corrosion lead to the deterioration of reliability index for moment and shear are respectively. Used in analysis the limit state equations are formulated base on AASHTO LRFD code. the depth of equivalent stress block is less than the thickness of top flange. Therefore, the distance between the neutral axis and the compressive face and nominal moment is used to calculate the reliability index.

3. MODEL SELECTION OF PSC BOX BRIDGE.

(1) Variable sesction

A PSC Box bridge is have a lot of ratios in bridge formats during domestic use. In this study, the bridge analysis to the bridges of 50m span length. A PSC Box bridge was classified according to the number of boxes, such as the single and multi-box, and etc. And selected the single box bridge in this research. Also, PSC Box bridge was classified into to various methods according to constructive methods. It classified as two methods of a FSM and ILM among many methods being applied to the national and it analysis. PSC Box bridge was assumed to the cross section was constant depth girger. And the bottom flange value separately classified the central part and support of the PSC Box bridge and analyzed. When used to analysis of bridge, The critical sections for moment of analysis used in the bridge is considered at the middle of the first span. The valuse of moment and random variables are listed in table 1.

Table 1: The valuse od moment of PSC Bos bridge

Factor	Mean	COV	Factor	Mean	COV
f_{pu}	1681.65 Mpa	0.0142	f_{ck}	34.5 Mpa	0.15
d_p (ILM method)	295cm	0.047	d_p(FSM method)	262.2cm	0.0054
Dead load	68230 KN.m	0.1	Live load	15700 KN.m	0.2

(2) Select performance profile constitution variable

Consider of environment factor, PSC Box bridge of 50m span length performance profile is calculated. It is different to the constitution variable according to constructive methods, but its kind is not different. RSM configuration variable of two methods is composed of humidity, reinforcement depth, corrosion factor R, and time. The diameter of post-tensioned tendon at midspan are 8x19x12.7 mm and slab tendon 19x9x12.7 mm for ILM bridge. In case of FSM bridge the post-tensioned tendon is 22x15x12.7 mm. PS Steel kind that used in two methods is different, but they are assumed to the average of 80mm and the deviation of 20mm.

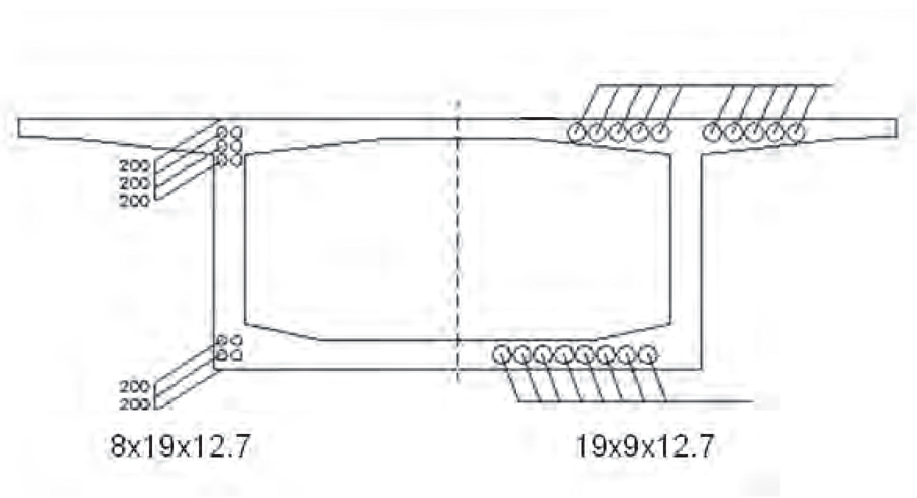

Figure 3: post-tensioned tendon of ILM bridge

In addition, the humidity of RSM configuration variable is assumed to be 60~100%, corrosion coefficient R is assumed to the average of 5 and the deviation of 1.

4. PERFORMANCE PROFILE.

Each variables to have been composed of to RSM operation as the independent variable, and it calculate reliability index along each condition. The coefficient values of RSM variables are calculated the performance profile by using the coefficient according to the application method. Following figure indicated performance profile of reliability index along the change of humidity by a method. It is different to the method, but RSM variable used the same values.

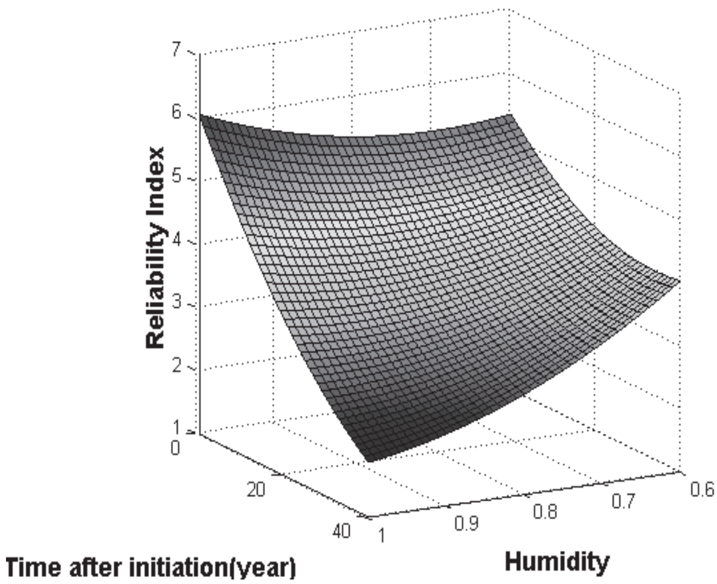

Figure 4: Performance profile as change of humidity in PSC Box bridge using ILM method .

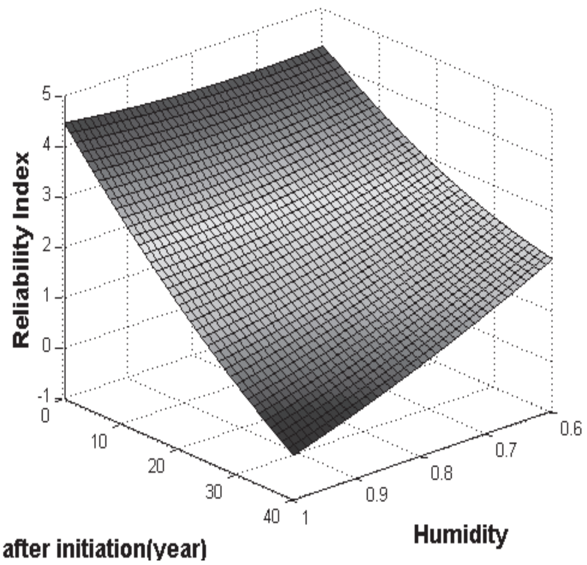

Figure 5: Performance profile as change of humidity in PSC Box bridge using FSM method.

This two graphs shows the performance profile by Pitting Corrosion, and it`s assumes to be reinforce depth 60mm, corrosion coefficient 5. The performance profile calculated form the two method appears that initial reliability and corrosion point along time is different. The bridges of used an ILM method appears to reliability index and safety to be high by thickness of girder deeper than the bridges of sued a FSM method. A maintenance reinforcement point of time of a FSM method appears more quickly an ILM method. Because, that is the starting point of the initial performance index lower than the ILM method.

5. CONCLUSIONS

In this study, the main member and deterioration factor of PSC Box bridge suggested to the performance profile by RSM. In this study assumed pitting corrosion in ILM method and FSM method from PSCB girder. It could be the base of the study what about calculation of performance profile assumed the various environmental factor that in this study calculation of performance profile result assumed the factor of tendon corrosion. The performance profile shown up in consideration of the tendon corrosion is proposed time of repair and reinforcement will be able to be predicted.

REFERENCES

KOREA INSTITUTE OF CONSTRUCTION RECHNOLOGY,. 2003. *Annual Report of Hydrologic Date,2002.,*

Doo-Kie,Kim, Ki Young Koo, Seo Hyeong Yeol. 2004 GY,. 2003. *Annual Report of Hydrologic Date,2002 Long- Term Effectiveness of*

Posttensioning in bridges. Korea Institute for Structural Maintenance Inspection, KSMI 2004.,

R.M.Salas, A.J.Schokker, J.S. West, J.E.Breen, M.E.Kreger, 2004. *Conclusion, Recommendations and Design Guidelines for Corrosion Protection of Post-Tensioned Bridges, Center for Transportation Research, University of Texas at Austin, 2004.*

Willian H. Hartt, *Corrosion Evaluation of Post-Tensioned Tendons on the Mid By Bridge in Destion Frorida*, *Frorida Department of Transportation Research Center, 2002*

ENVIRONMENTAL PERFORMANCE INDICATORS FOR CONCRETE CONTAINING HIGH VOLUME OF RECYCLED MATERIALS

GERMAN A. PARDO R.
Department of Civil Engineering, University of Tokyo, Japan
ger-pard@iis.u-tokyo.ac.jp

MICHAEL HENRY
Department of Civil Engineering, University of Tokyo, Japan
mwhenry@iis.u-tokyo.ac.jp

YOSHITAKA KATO
International Center for Urban Safety Engineering
Institute of Industrial Science, University of Tokyo, Japan
katoyosh@iis.u-tokyo.ac.jp

ABSTRACT

The role of concrete throughout the history has been to provide society with infrastructure and shelter. During this process, concrete itself has been in constant development and new factors have appeared and played different roles, with the environmental impact as one of the most important and recent. After becoming aware of the necessity of mitigating the negative environmental impact of concrete, the use of new materials for producing concrete with low environmental impact has been proposed.

To reflect this new consideration, it is necessary to implement a new assessment factor which considers the environmental effect of concrete as well as the mechanical performance. This paper shows the results of the environmental performance indicator, which considers both the mechanical performance and CO_2 emissions. It was found that implementing the environmental performance indicator results in a balance between mechanical performance and environmental performance, becoming in a useful assessment tool.

1. INTRODUCTION

To face the reality of global warming, the concrete industry can play an important role. Carbon dioxide (CO_2) is the primary GHG contributing to climate change, and the concrete industry is a major generator, with some researchers estimating that the manufacture of Portland cement is responsible for roughly 7% of the world's total emissions. Along with cement production, the utilization of natural resources like aggregates, water and sand, is also an important environmental concern, and since the concrete consumption in the world is enormous and increasing every year, the availability of these resources is endangered.

In order to mitigate the environmental effect of producing concrete and reduce the exploitation of natural resources, many researches on replacing cement and raw materials with by-products and recycled materials have been conducted. These works have shown that it is possible to obtain a good quality concrete with other benefits such us landfill reduction and concrete durability.

However, until now the construction industry has not taken these factors, such as CO_2 emissions, seriously into account or considered them as important as the mechanical performance when evaluating concrete materials. Therefore, is necessary to implement a new assessment factor, "environmental indicator," which considers both the mechanical performance and the CO_2 emissions.

2. RECYCLED MATERIALS

A durable concrete which replaces virgin materials with industrial waste or recycled products could provide a sustainable option for construction materials. Fly ash, a waste by-product of the coal industry, has been used to replace up to 70% of Portland cement in some concretes (Malhotra, 1999). Total replacement of normal coarse aggregates with recycled aggregates, produced from demolition waste, has also been investigated, and satisfactory concrete quality was observed (Meinhold et al., 2001). Fibers made from recycled plastics have also been successfully applied in concrete (Moriwake et al., 2004). These applications demonstrate the different possibilities which exist for utilizing alternative materials in develop sustainable concrete. However, these materials are often utilized individually, so the effect of combining recycled materials is not clear.

3. EXPERIMENTAL PROGRAM

3.1 Materials

Cement mortar and concrete were prepared using tap water (W), Type 1 Portland cement (C), river sand (S), normal (NG) and recycled (RG) aggregates, fly ash (FA), polypropylene (PP) and recycled fibers (RF), and air entraining (AE) and super plasticizer (SP) admixtures.

The fly ash used was type JIS II fly ash, which met requirements specified by JIS A 6201, and the coarse aggregates were low-grade.

Fiber properties are given in Table 1. The recycled fibers were manufactures from recycled polyethylene terephtalate (PET).

Table 1: Fiber properties

Type	**Dia. (mm)**	**Length (mm)**	**Density (g/cm^3)**	**Strength (MPa)**
PP	0.75	32	0.91	-
Recycled	0.70	30	1.35	450

3.2 Mix proportions and specimens

Mix proportions are given in Table 2. The term binder (B) is used to represent all cementitious materials – in this case, fly ash and Portland cement. All mixes used a constant water-binder ratio of 30%.

Table 2: Mix proportions

<table>
<tr><th rowspan="2">Series</th><th colspan="4">Material ratios (%)</th><th colspan="2">Admixtures (%binder)</th><th colspan="2">Fibers (%volume)</th></tr>
<tr><th>W/B</th><th>S/B</th><th>FA/B</th><th>s/a</th><th>AE</th><th>SP</th><th>PP</th><th>RF</th></tr>
<tr><td>SB60</td><td rowspan="9">30</td><td>60</td><td rowspan="3">30</td><td rowspan="9">-</td><td>0.04</td><td>0.4</td><td rowspan="6">2.0</td><td rowspan="6">-</td></tr>
<tr><td>SB80</td><td>80</td><td>0.04</td><td>0.5</td></tr>
<tr><td>SB100</td><td>100</td><td>0.04</td><td>0.6</td></tr>
<tr><td>FA30-PP</td><td rowspan="6">80</td><td>30</td><td>0.04</td><td>0.5</td></tr>
<tr><td>FA50-PP</td><td>50</td><td>0.06</td><td>0.4</td></tr>
<tr><td>FA70-PP</td><td>70</td><td>0.08</td><td>0.4</td></tr>
<tr><td>FA30-RF</td><td>30</td><td>0.04</td><td>0.5</td><td rowspan="3">-</td><td rowspan="3">2.0</td></tr>
<tr><td>FA50-RF</td><td>50</td><td>0.06</td><td>0.4</td></tr>
<tr><td>FA70-RF</td><td>70</td><td>0.08</td><td>0.4</td></tr>
<tr><td>FA50-sa60-NG</td><td rowspan="5">30</td><td rowspan="5">80</td><td rowspan="3">50</td><td rowspan="2">60</td><td>0.015</td><td>0.6</td><td rowspan="5">-</td><td rowspan="5">2.0</td></tr>
<tr><td>FA50-sa60-RG</td><td>0.015</td><td>0.6</td></tr>
<tr><td>FA50-sa80-RG</td><td>80</td><td>0.025</td><td>0.5</td></tr>
<tr><td>FA30-sa60-RG</td><td>30</td><td rowspan="2">60</td><td>0.015</td><td>0.6</td></tr>
<tr><td>FA70-sa60-RG</td><td>70</td><td>0.015</td><td>0.6</td></tr>
</table>

For mortar mixtures to investigate the effect of sand-binder ratio, a constant fly ash-binder ratio of 30% was used with PP fibers at 2% volume, and three sand-binder ratios of 60%, 80%, and 100% were chosen. For investigating the effect of fiber type and fly ash-binder ratio, mortar mixtures containing either PP or recycled fibers at 2% volume were mixed at a constant sand-binder ratio of 80% with three fly ash-binder ratios of 30%, 50%, and 70%. Testing was conducted 28 days after casting.

For concrete mixtures, sand-binder ratio (80%) and fiber type (recycled fibers) were selected based upon the results obtained from mortar series tests at 28 days. The effect of aggregate volume was obtained by varying the sand-aggregate volume ratio from 80 (lower volume of aggregates) to 60 (higher volume). Mortar (no aggregates) was also included. At the highest volume, both recycled and normal aggregates were tested to evaluate the effect of aggregate type. Finally, the fly ash-binder ratio was varied from 30% to 70% to see the effect of fly ash content.

AE and SP were varied as necessary to maintain satisfactory fresh mortar and concrete properties. Testing was conducted 28 and 91 days after casting.

Cylinder (10Øx20cm) and beams (10x10x40cm) specimens were cast for each mortar and concrete mix following JSCE-F 552-1999. Cylinder specimens were cast in two layers and beam specimens in one layer, with a vibrator applied to the outside of the mold after each layer was placed. After casting, molded specimens were covered in plastic wrap and cured in the molds for 24 hour, after which they were removed from the molds and moved to water curing.

3.3 Fresh mortar and concrete properties

The properties of fresh mortar and concrete are given in Table 3. Slump flow, flowability and air content were measured according to JIS A 1150, JSCE-F 512-1999 and JIS A 1128-2005 respectively.

Table 3: Fresh mortar and concrete properties

Series	Slump flow (mm)	Efflux time (s)	Air content (%)
SB60	495	6.5	-
SB80	495	5.7	-
SB100	585	5.7	-
FA30-PP	600	4.7	11.6
FA50-PP	360	10.7	12.1
FA70-PP	650	4.4	9.1
FA30-RF	595	5.5	9.9
FA50-RF	415	6.7	11.6
FA70-RF	660	4.6	8.6
FA50-sa60-NG	600	5.3	9.0
FA50-sa60-RG	570	5.4	10.0
FA50-sa80-RG	615	4.6	10.0
FA30-sa60-RG	600	5.3	10.0
FA70-sa60-RG	600	5.1	10.0

3.4 Specimen testing

Three properties of the mortar mixes were tested experimentally. Compressive strength f_c was measured according to JIS A 1108-2006, and flexural strength f_b was determined according to JSCE-G 552-1999. For all tests, reported valued are the average of three specimens.

Air permeability K was measured for concrete series at 91 days in order to better observe the effect of fly ash. Air permeability specimens were taken from cylinders by cutting a 40 millimeter-thick section from the center of the cylinder. Specimens were then placed in a drying machine for one week at 40ºC and checked by monitoring the weight change. After dry conditions were met, the specimens were set into an air permeability machine and the volume of air flow was measured under steady state conditions. The air permeability coefficient was calculated per Equation 1.

$$K = \frac{2P_2 \cdot h \cdot r}{P_1^2 - P_2^2} \cdot \frac{Q}{A} \tag{1}$$

Where:
K: air permeability coefficient (mm/s)
P_1: loading pressure (MPa)
P_2: atmospheric pressure (MPa)
h: specimen thickness (mm)
r: unit volume weight of air (1.205×10^{-6} MPa)
Q: air flow volume (mm^2/s)
A: sectional area (mm^2)

4. ENVIRONMENTAL PERFORMANCE INDICATOR

The environmental performance indicator was calculated as the ratio of the mechanical performance to the CO_2 footprint (MPa / kg of CO_2/m^3) (Nielsen, 2009). The CO_2 footprint is calculated from the mix proportions (Table 2), and the emissions of Portland cement, sand, aggregates and fly ash (Table 4). These values are determined from the emissions related to the manufacture of concrete and its constituent parts. In this research, only the contribution from cement, fly ash, sand, and aggregates were considered.

Table 4: CO_2 emissions by material (JCI, 2008)

Material	**CO_2 emissions (kg CO_2/ton)**
Portland cement	765.5
Fly ash	17.9
Natural river sand	3.4
Normal/Recycled aggregate	2.8

5. RESULTS AND DISCUSSION

5.1 Compressive and flexural strength

5.1.1 Mortar series

For sand-binder ratio effect, compressive and flexural strength results are shown in Figure 1. For compressive strength it can be seen that increasing the sand-binder ratio resulted in a marginal decrease in compressive strength. For flexural strength this effect is more pronounced; increasing the sand-binder ratio resulted in flexural strength increases. From these results, a sand-binder ratio of 80% is considered optimal for utilizing in concrete series, as it produces the best combination.

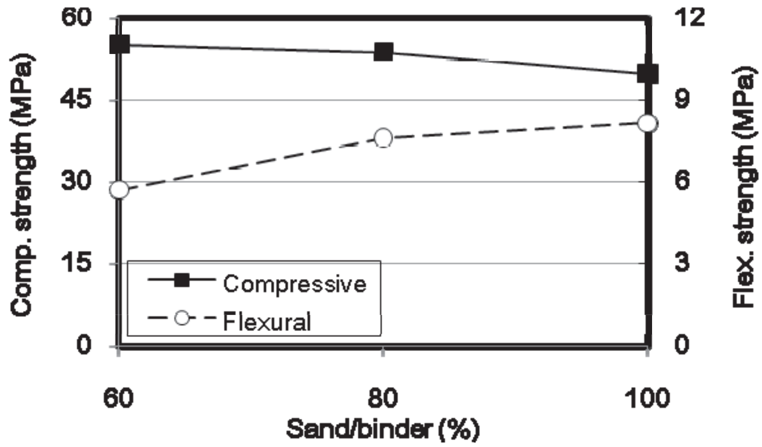

Figure 1: Compressive and flexural strength results by sand/binder ratio (Mortar)

For the fly ash-binder ratio and fiber type effect, compressive and flexural strength results are shown in Figure 2. For compressive strength a decreasing trend is observed when the fly ash-binder ratio is increased. For flexural strength the behavior is slightly different, with a decreasing tendency when fly ash content increases from 30% to 50% and no change from 50% to 70%. The effect of fiber type is almost negligible. Based upon this recycled fibers were selected for concrete series.

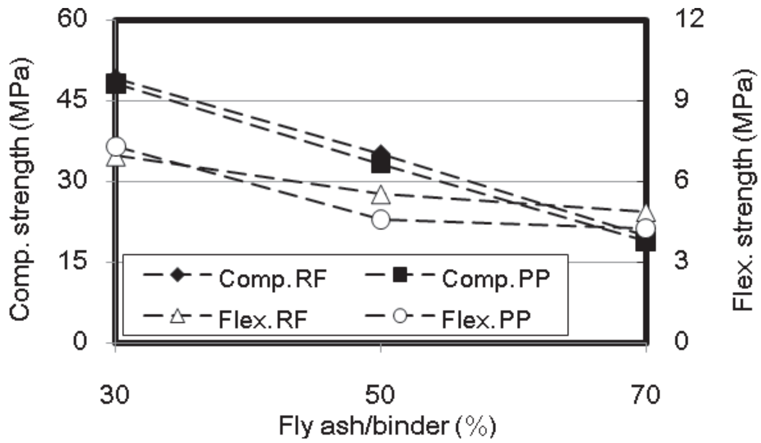

Figure 2: Compressive and flexural strength results by fly ash/binder ratio and fiber type (Mortar)

5.1.2 Concrete series

Compressive and flexural strength results for fly ash-binder ratio are shown in Figure 3. It can be seen that increasing the amount of fly ash has a significant effect on strength behavior. Increasing the fly ash-binder ratio results in a constant decrease in both compressive and flexural strength. The slow but steady strength development for high fly ash content can also be seen, as the slope is less for 91 days than for 28 days.

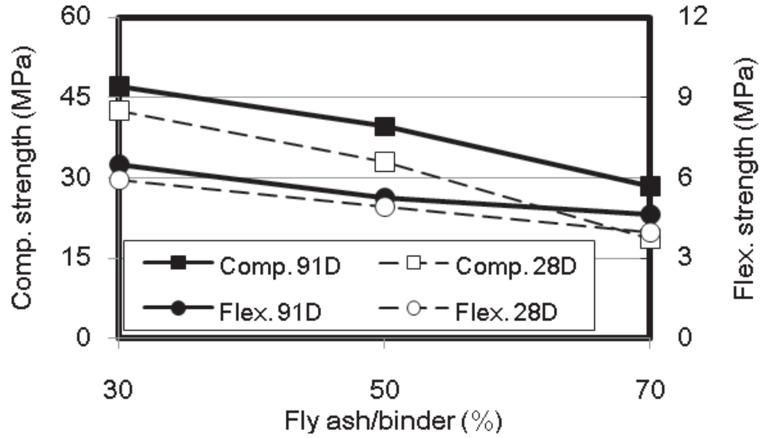

Figure 3: Compressive and flexural strength results by fly ash/binder (Concrete)

On the other hand, increasing the amount of aggregates does not considerably effect either the compressive strength or flexural strength. The compressive strength is highest for normal aggregate (Figure 4). The strength development seems quite good in time being more noticeable for compressive strength, showing the best increase the series with 6.4% aggregate volume; however for 0% aggregate volume and normal aggregate, there is slight unexplained reduction in flexural strength.

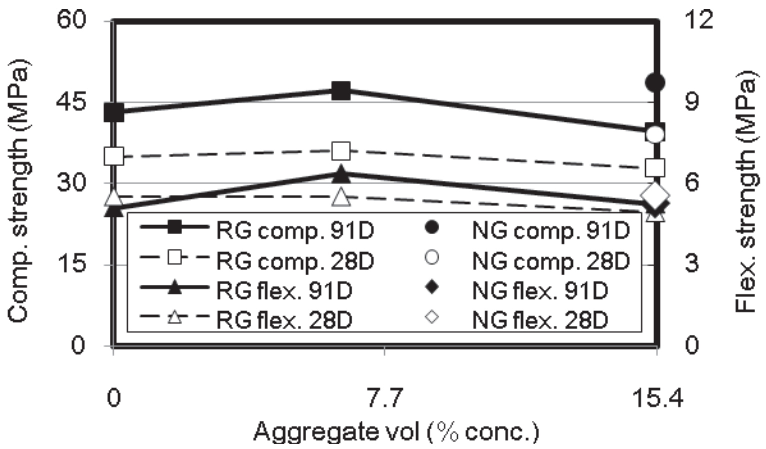

Figure 4: Compressive and flexural strength results by aggregate volume and type

5.2 Air permeability

As mentioned before, the air permeability test was conducted for concrete series at 91 days, and the results are displayed in Figures 5 and 6. It can be observed that increasing the fly ash-binder ratio from 30% to 50%, decreases the air permeability considerably, and increasing the fly ash-binder ratio from 50% to 70% results in a much smaller decrease in the air permeability (Figure 5). This can be explained by the large amount of fly ash content which reacts slowly but progressively as compared to the decreasing cement content which reacts faster up to 28 days.

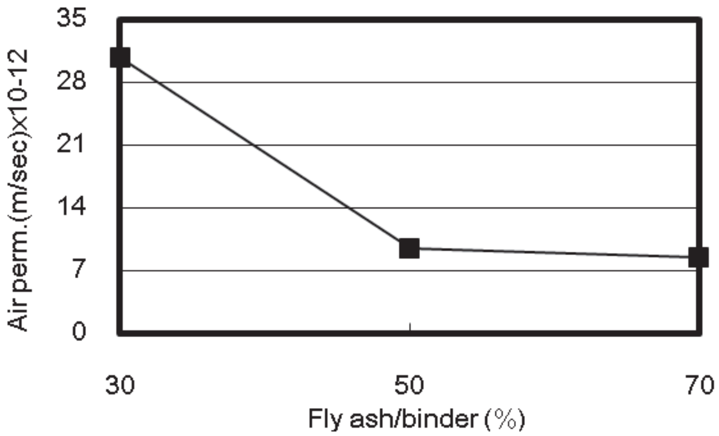

Figure 5: Air permeability by fly ash/binder

Conversely, increasing the amount of aggregate results in a constant increase in air permeability; in this case it can be explained by the constant increase in coarse aggregates (Figure 6). However, for aggregate type the lowest air permeability is for normal aggregate, due to the lower density and low grade recycled aggregate, which results in higher air permeability. It can be seen also that for 15% normal aggregate volume the air permeability is quite similar to that for 0% aggregate volume.

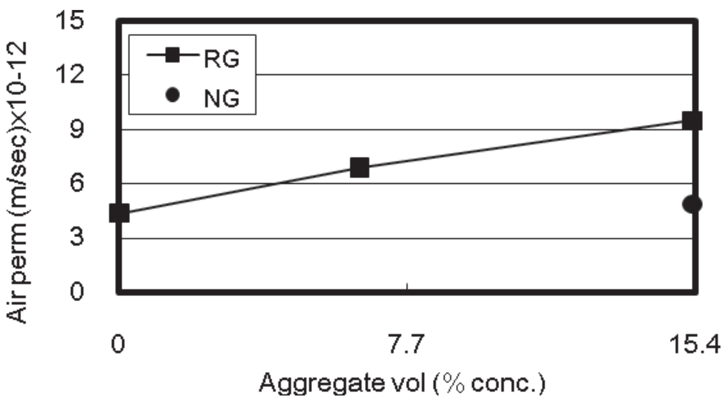

Figure 6: Air permeability by aggregate volume and type

5.3 Environmental performance indicator

The environmental performance indicators were calculated at 91 days for concrete series, and the results are displayed in Figure 7. For variable aggregate volume and type, the trend is similar to the mechanical performance, so there is little change when normalized by the environmental impact. For variable fly ash-binder ratio normalized by the environmental performance indicator, results in a reverse of the trend shown by the mechanical performance.

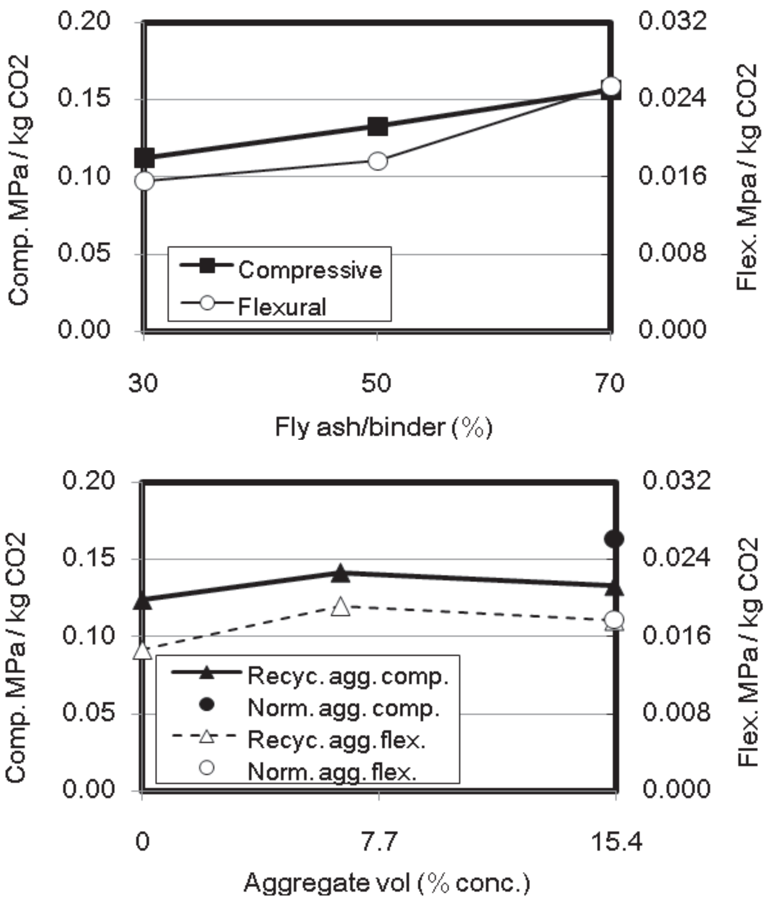

Figure 7: Environmental performance indicators by fly ash/binder (top) and aggregate volume and type (bottom)

The usage of fly ash has a more noticeable effect on the environmental indicator compared with recycled aggregates. Recycled aggregates have the same CO_2 emissions as normal aggregates, so the effect of aggregate type is difficult to evaluate by CO_2 alone. However, the effect of fly ash can be explained by the large difference in CO_2 between Portland cement and the other materials, and the effect is greater when more cement is replaced.

6. CONCLUSIONS

In this paper, environmental performance indicators were used to evaluate the mechanical & environmental performance of concrete containing high volume of recycled materials. It was seen that implementing the environmental indicator is a useful tool in order to assess both the mechanical performance and the CO_2 emissions of the concrete, and make it clear that concrete quality can be appraised taking into account the environmental impact as well.

The concrete with the highest environmental indicator for compressive strength had a fly ash-binder ratio of 50% and normal aggregates. The advantage of utilizing recycled aggregates is difficult to see in this case since recycled aggregates have the same CO_2 emissions as normal aggregates, but generally lower performance; therefore, to evaluate the effect of aggregate type it is necessary to introduce an additional factor which considers the effect of preserving raw materials as well.

The tendency of the environmental performance indicator for fly ash-binder ratio concrete is similar to that of air permeability, suggesting that the environmental performance indicator may be comparable to the durability of the concrete in this case.

The concrete with the highest environmental indicator for flexural strength had a fly ash-binder ratio of 70% and 100% replacement of normal aggregates with recycled aggregates. This value was driven by the extremely low CO_2 emissions achieved by replacing high volume of Portland cement with fly ash.

ACKNOWLEDGEMENT

The authors would like to express their thanks to Hirata Wataru, who developed a big part of the project; Shota Mizukami, who helped in the achievement of the final part; and all the other members of Kishi-Kato Laboratory who generously assisted in conducting these research works.

REFERENCES

Japan Concrete Institute, 2008. Concrete innovation in the environmental age. Technical Committee on Environmental Performance of Concrete Structures. (in Japanese).

Malhotra, V.M., 1999. Making concrete greener with fly ash. *Concrete Internationa* 21 No. 5, 61-66.

Meinhold, U., Mellamann, G., and Maultzch, M., 2001. Performance of high-grade concrete with full substitution of aggregates by recycled concrete. *Sustainable Development of Cement and Concrete.* ACI Special Publication SP-202, 85-96,

Moriwake, A., Habuchi, T., Kushida, M., Dec. 2004. Short fiber for concrete reinforcement produced from recycled PET bottles. *Cement Concrete* 694, 20-25 (in Japanese).

V. Nielsen, Clauss, January 2009. Toward sustainable concrete structures. Lecture on Sustainability in Concrete & Concrete Structures, University of Tokyo, Japan.

SEISMIC HAZARD MAPS OF THAILAND

CHITTI PALASRI and ANAT RUANGRASSAMEE
Department of Civil Engineering,
Chulalongkorn University, Bangkok, Thailand
p_chitti@yahoo.com, fcearr@eng.chula.ac.th

ABSTRACT

In this study, the probabilistic seismic hazard map of Thailand and neighboring areas is developed. Thailand is located close to the Andaman thrust in the west and the Sunda arc in the south which are the interaction between the Eurasian plate and Indo-Australian plate. Several active faults in the region contribute to earthquakes in Thailand. It is important to evaluate seismic hazard in the area for seismic design of structures. Earthquakes recorded from 1912 to 2006 by Thai Meteorological Department and US Geological Survey are used in the analysis. Two attenuation relationships developed for the western USA which give good correlations with actual measured accelerations are used for active tectonic zones in Thailand. Maps of peak horizontal accelerations at rock sites with 2% and 10% probabilities of exceedance in 50 years are developed. For the peak horizontal acceleration with 10% probability of exceedance in 50 years, the maximum value in Thailand is about 0.25 g in the northern part of Thailand. The peak horizontal acceleration is 0.02 g in Bangkok. For the peak horizontal acceleration with 2% probability of exceedance in 50 years, the peak horizontal acceleration is about 1.6 – 2 times of the 10% probability of exceedance in 50 years for most areas.

1. INTRODUCTION

In Thailand, earthquakes occasionally occur in the northern and western parts. Fenton et al. (2003) investigated several faults in the northern and western parts of Thailand. Maximum credible earthquakes were determined by using empirical relationships between rupture lengths of faults and magnitudes by Well and Coppersmith (1994). They found that the maximum credible earthquakes of the active faults in Thailand had moment magnitudes of 7 to 7.5. A maximum moment magnitude of 7.5 was estimated for Thoen, Mae Chan and Three Pagodas faults which were located in Chiang Mai and Kanchanaburi provinces, in the north and west of Thailand respectively.

Some earthquakes caused structural damages in local areas. For example, the September 11th, 1994 earthquake with a local magnitude of 5.1 had an epicenter around 15 km from Pan District, Chiang Rai province. The earthquake caused structural damage to the Pan hospital. The May 16th, 2007 earthquake with a moment magnitude of 6.3 had an epicenter near the

Thai-Laos border. The earthquake caused structural damage to a school in Chiang Rai province, located 109 km from the epicenter.

Warnitchai and Lisantono (1996) proposed the seismic hazard map of Thailand using the earthquake data and the seismic source zone map from South Asia Association of Seismology and Earthquake Engineering (Nutalaya et al., 1985) and the attenuation model of Esteva (1973). For the peak horizontal acceleration with 10% probability of exceedance in 50 years, the maximum value in Thailand is about 0.25 g in the northern part of Thailand. The peak horizontal acceleration is 0.05 g in Bangkok.

Petersen et al. (2004) developed seismic hazard maps for Sumatra, Indonesia and the southern Malaysian Peninsula using attenuation models for the active tectonic region and subduction zones such as Sadigh et al. (1997), Toro et al. (1997) and Youngs et al (1997). The researcher found that the peak horizontal acceleration with 2% probability of exceedance in 50 years was around 0.1 g to 1.0 g for Sumatra Island and less than 0.2 g for the southern Malaysian Peninsula and the peak horizontal acceleration with 10% probability of exceedance in 50 years is about 60% of that with 2% probability of exceedance in 50 years.

At present, up-to-date earthquake catalogs and accelerograms are available. So, the seismic hazard maps of peak horizontal accelerations can be developed with sound attenuation models and updated information. The seismic hazard map can be used as a guideline for earthquake-resistant design of structures in Thailand.

2. EARTHQUAKE CATALOGS

Thai Meteorological Department (TMD) has recorded earthquake events and complied earthquake records from several catalogs which consist of time, location, depth, and magnitudes. The earthquake events in the catalogs range from 1912 to 2006 in the area covering 0^oN to 30^oN and 88^oE to 110^oE. Magnitudes in the catalogs are presented in a body-wave magnitude (m_b), a local magnitude (M_L), a surface-wave magnitude (M_S) and a moment magnitude (M_W). The catalogs are obtained from US Geological Survey (USGS) with 9,794 events since 1954, International Seismological Centre (ISC) with 1,074 events since 1964, TMD with 3,794 events since 1976 and others with 98 events before 1964. Before using the earthquake data, the earthquake magnitudes were transformed to the moment magnitude (M_W). Various types of the magnitudes were converted to the moment magnitude using the relations proposed by Campbell (1985), Sipkin (2003), Heaton et al. (1986), and Hanks and Kanamori (1997).

The assumption in the seismic hazard analysis is that all earthquake events are independent. Thus, the earthquake events which are foreshocks and aftershocks must be eliminated before further analysis. The method proposed by Gardner and Knopoff (1974) was applied to eliminate foreshocks and aftershocks. After eliminating aftershocks and foreshocks, the numbers of earthquakes in the area ranging from 0^{o}N to 30^{o}N and 88^{o}E to 110^{o}E become 5,550, or about 37.6% of all events in the original catalog.

3. SEISMIC SOURCE ZONES

Seismic source zones are usually derived from tectonics, earthquake catalogs, and studies on active faults. Seismic source zones in Thailand was recently proposed by Saithong et al. (2000) as shown in Fig. 1, based on studies by Nutalaya et al. (1985) and Charusiri et al. (2000). Active tectonic regions in the north of Thailand consist of Zones E, F and I which there are Chiang Mai, Chiang Rai, Mae Hong Sorn provinces. Active tectonic regions in the west of Thailand consist of Zone J which is located in Kanchanaburi province. The previous study notes that active faults in the zone can generate an earthquake with a maximum magnitude of about 7.5 (Fenton et al., 2003). The subduction zones are Zones A, N and O in the Andaman Arc.

The earthquake data which were recorded in the past are incomplete because instruments could not detect small earthquakes. And incomplete data can result in the under-estimation of recurrence rates. The completeness of earthquake data was considered in this study by using the method proposed by Stepp (1972). The Gutenberg-Richter magnitude-frequency relation is used for each source zone as

$$\log \lambda_m = a - bm \qquad (1)$$

where λ_m is the mean annual rate of exceedance of a magnitude m, a and b are parameters of the relation. The result can be summarized in Table 1 which indicates the a and b values of Gutenberg-Richter relation and the maximum moment magnitude of each source zone. The maximum moment magnitude of each source zone is selected from 1) the study by Fenton et al. (2003) that estimated the maximum magnitudes of faults in Thailand from geomorphology, and 2) the maximum magnitude from the past seismic record.

4. ATTENUATION MODELS

Attenuation models are used for determining the ground motion parameters from the magnitude and distance. The attenuation models are important in predicting the peak horizontal acceleration at any sites. Petersen et al. (2004) modified the Youngs et al. (1997) relation for the subduction zone in Sumatra's outer-arc ridge, Indonesia and the Southern Malaysian Peninsula. The Youngs et al. (1997) relation and the modified Youngs et al. (1997) relation can be expressed as Eq. (2) and Eq. (3), respectively.

$$\ln Y = 0.2418 + 1.414M + C_1 + C_2(10-M)^3 + C_3\ln(R_{rup} + 1.7818\exp(0.554M)) + 0.00607H + 0.3846Z_r \qquad (2)$$
$$\text{Standard Deviation} = 1.45 - 0.1\,M$$

$$\ln Y_{Modified}(M,R) = \ln Y_{Youngs}(M,R) - 0.0038(R - 200) \qquad (3)$$

where Y is the median spectral acceleration for 5% damping (g), or peak ground acceleration (g), M is a moment magnitude, R_{rup} is the closest distance to the rupture plane (km), H is the depth of earthquake source (km), $Z_r = 0$ for crustal interplate region, $Z_r = 1$ for crustal intraplate region and C_1, C_2,…,C_7 are coefficients. In this study, the relation by Youngs et al. (1997) is used for the distance less than 200 km and the modified Youngs et al. relation is used for the distance over 200 km.

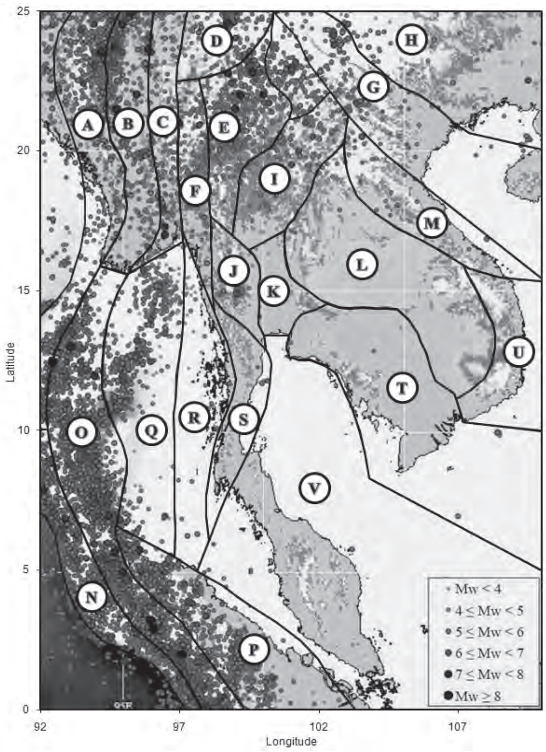

Figure 1. Seismic source zone map in Thailand and neighboring areas. (Saithong et al., 2004)

Table 1: Source zones and parameters of Thailand and neighboring areas.

Source Zones	**No. of Events (1912-2006)**	**Parameters of Gutenberg-Richter Equation**		**Maximum Moment Magnitude**
		a	**b**	
Zone A	457	6.111	1.148	7.2
Zone B	432	3.430	0.616	7.4
Zone C	207	3.177	0.700	7.7
Zone D	89	2.745	0.616	7.0
Zone E	645	2.927	0.582	7.3 (7.5)
Zone F	316	5.178	1.159	7.9
Zone G	97	3.629	0.805	6.6
Zone H	42	4.294	0.961	6.7
Zone I	534	4.032	0.923	6.7 (7.5)
Zone J	81	2.892	0.752	6.2 (7.5)
Zone M	31	3.387	0.883	6.7
Zone N	120	2.771	0.439	7.5
Zone O	908	4.953	0.784	9.0
Zone P	439	5.512	0.982	7.4
Zone Q	360	5.112	0.981	6.5
Zone R	43	3.548	0.906	5.6
Zone W	119	3.775	0.825	6.7

Remarks the value in the parenthesis is the moment magnitude from the study by Fenton et al. (2003).

Chintanapakdee et al. (2008) studied suitability of various attenuation models for Thailand by comparing measured ground accelerations with various available models. Peak horizontal accelerations were obtained from 163 ground motions recorded by Thai Meteorological Department from 45 earthquakes with magnitudes between 4.7 to 6.3 and distance ranging from 231 to 2090 km. Measured peak horizontal accelerations were compared with attenuation equations which are used in active tectonic regions. They found that Sadigh et al. (1997) and Idriss (1993) relationships gave peak horizontal acceleration close to measured peak horizontal accelerations. So, Sadigh et al. (1997) and Idriss (1993) equations are used for active tectonic regions and weighed equally for the peak horizontal acceleration. Sadigh et al. (1997) and Idriss (1993) equations can be expressed as Eq. (4) and Eq. (5), respectively.

$$\ln Y = C_1 + C_2 M + C_3 (8.5 - M)^{2.5} + C_4 \ln[R_{rup} + \exp(C_5 + C_6 M)] + C_7 \ln(R_{rup} + 2)$$
$$\text{Standard Deviation} = 1.39\text{-}0.14\, M \tag{4}$$

$$\ln Y = (\alpha_1 + \alpha_2 M) - (\beta_1 + \beta_2 M)\ln(R_{rup} + 10) + \varphi F$$
$$\text{Standard Deviation} = \begin{cases} \varepsilon_{\max} & ; M \le 5 \\ \varepsilon_1 - 0.12M & ; 5 < M \le 7.25 \\ \varepsilon_{\min} & M > 7.25 \end{cases} \tag{5}$$

where Y is the median spectral acceleration for 5% damping (g), or peak ground acceleration (g), M is the moment magnitude, R_{rup} is the closest distance to the rupture plane in km and $C_1, C_2, \ldots, C_7, \alpha_1, \alpha_2, \beta_1, \beta_2, \varepsilon_1, \varepsilon_{max}, \varepsilon_{min}, \varphi$ are coefficients.

5. PROBABILISTIC SEISMIC HAZARD MAPS

The effects of maximum magnitudes considered in each source zones on seismic hazard maps are investigated. The maximum magnitude is the upper limit set in the magnitude-frequency relation. From Table 1, maximum moment magnitudes from the study on active faults by Fenton et al. (2003) for source zones E, I, and J are larger than those from the catalogs. Sadigh et al. (1997) attenuation relationship is used in this comparison. The hazard maps using the maximum magnitudes determined from catalogs and active faults together with a case having no limit on maximum magnitudes are shown in Fig. 2.

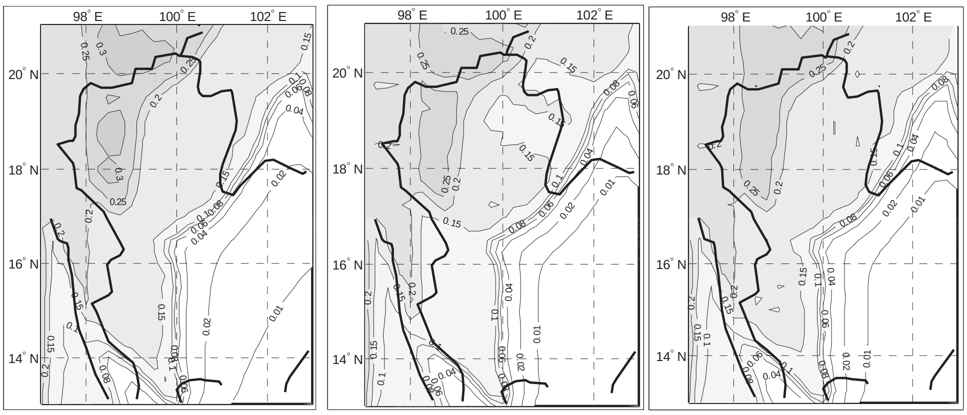

(a) (b) (c)

Figure 2: Sensitivity of hazard maps to the maximum magnitudes.

(a) Unbounded maximum magnitude

(b) Maximum magnitudes from the earthquake catalog

(c) Maximum magnitudes from study on active faults

The peak horizontal acceleration from the case with no limit on maximum magnitudes of earthquakes in Figure 2(a) are larger than the peak horizontal acceleration from the case with maximum magnitudes derived from active faults in Figure 2(c). The difference is about 0.01g - 0.04g in the north of Thailand and about 0.004g – 0.008g in the centre and west of Thailand.

The peak horizontal accelerations from the case with maximum magnitudes from earthquake catalogs in Figure 2(b) are smaller than that the peak horizontal acceleration from the case with maximum magnitudes from active faults in Figure 2(c) by 0.014g in the west of Thailand and 0.004g in the north of Thailand. It is seen that the effect of maximum magnitudes on seismic hazard is less significant because large earthquakes in Thailand have low probability. In developing hazard maps, the maximum magnitudes obtained from study on active faults are used for the maximum magnitudes in each zone.

The seismic hazard curve for all sources which is the relation between the annual rate of exceedance and the peak horizontal acceleration can be developed for any site. The seismic hazard curves for Chiangmai (Point A) Kanchanaburi (Point B) and Bangkok (Point C) can be obtained as shown in Figure 3. It is seen that the seismic hazard curve at Point A in the northern part of Thailand is close to the hazard of Zone E, while the seismic hazard curves at Point B (in the western part of Thailand) and Point C (in Bangkok) are governed by the hazard of Zone J. Therefore, the hazard in Bangkok is contributed from earthquakes in the western part of Thailand.

The probabilistic seismic hazard maps by Sadigh et al.(1997) and Idriss (1993) attenuation models are equal weighted. The seismic hazard maps using Sadigh et al.(1997) and Idriss (1993) attenuation models showing peak horizontal acceleration with 10% and 2% probability of exceedance in 50 years are shown in Figure 4. High seismic hazard is observed in the north and the west of Thailand.

For 10% probability of exceedance in 50 years, the maximum peak horizontal acceleration in the northern part of Thailand is about 0.25g, in the western part of Thailand is about 0.15g and in Bangkok is about 0.03g. The maximum peak horizontal acceleration for the 2% probability of exceedance in 50 years map increases in the same trend with the value of about 1.6 to 2 times the peak horizontal acceleration with 10% probability of exceedance in 50 years.

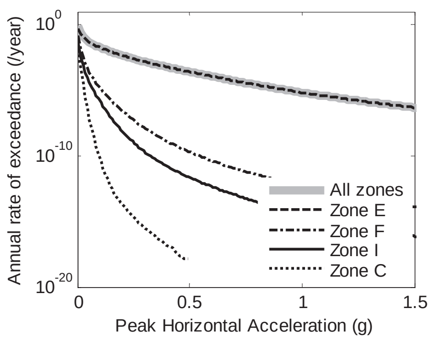

(a) Hazard curves at Point A

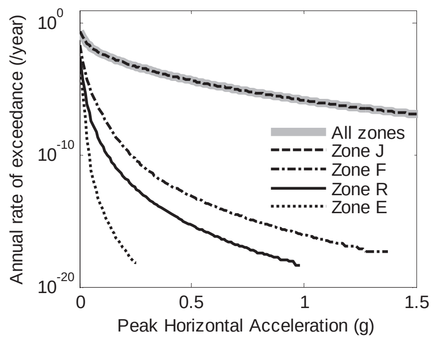

(b) Hazard curves at Point B

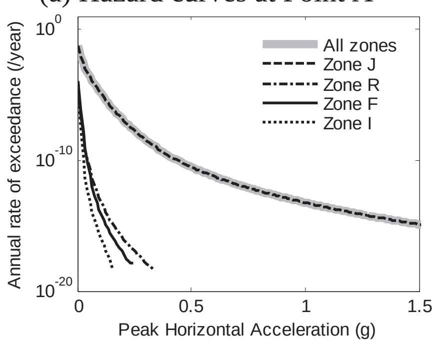

(c) Hazard curves at Point C

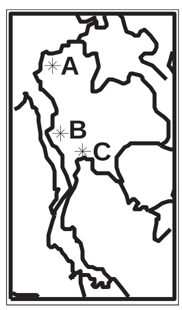

(d) The positions of Points A, B and C

Figure 3: Seismic hazard curves

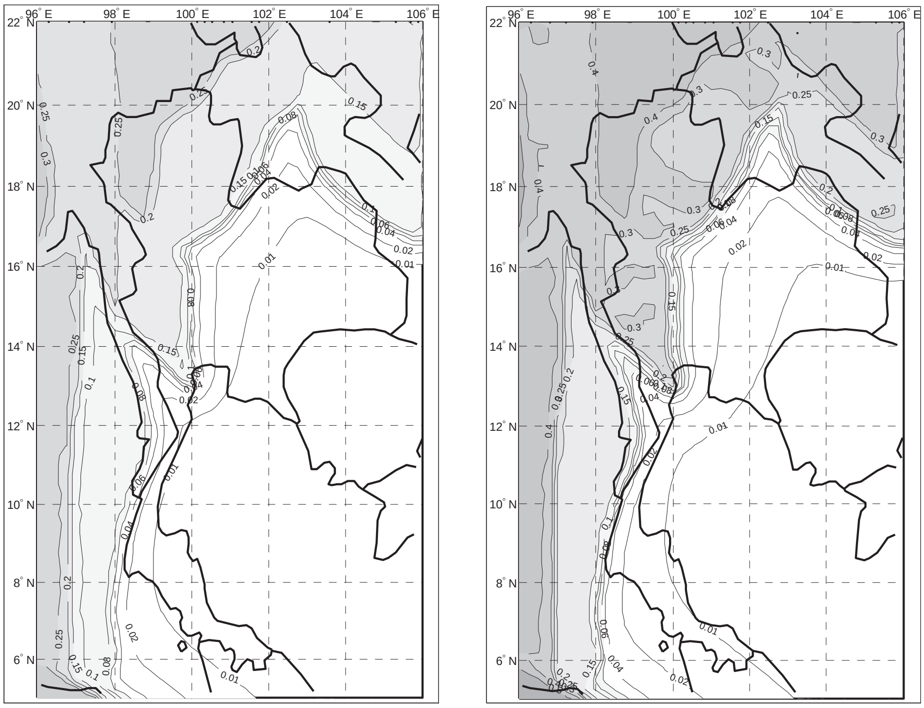

(a) 10% probability of exceedance in 50 years (b) 2% probability of exceedance in 50 years

Figure 4: Seismic hazard maps of peak horizontal accelerations (g)

Comparing this result with Wanitchai and Lisantono (1996), the maximum PHA from this study is close to that in Wanitchai and Lisantono (1996) but contour lines of PHAs do not cover in the same area. In Bangkok, the PHA from this study which is about 0.03g is less than the PHA from Wanitchai and Lisantono (1996) which is about 0.05g.

6. CONCLUSIONS

In this study, The seismicity of Thailand is collected from 1912 to 2006 by using the catalogs of Thai Meteorological Department and US Geological Survey. Probabilistic seismic hazard maps of Thailand are developed. It can be concluded that

1) Peak horizontal accelerations at a site are affected by the nearest sources. Kanchanaburi and Bangkok are governed by the hazard of zone J where Three Pagodas fault and Sri Sawat fault are located on this zone.

2) The seismic hazard maps of Thailand for the 2% and 10% probability of exceeedance in 50 years are proposed. Peak horizontal accelerations for 10% probability of exceedance in 50 years are approximately 0.15g in the western part of Thailand, 0.25g in the northern part of Thailand and 0.03g in Bangkok. For the peak horizontal acceleration for 2% probability of exceedance in 50 years, the peak horizontal acceleration is about 1.6 - 2 times of the 10% probability of exceedance in 50 years for most areas.

REFERENCES

Campbell, K.W. (1985), “Strong motion attenuation relations: a ten-year perspective,” *Earthquake Spectra*, Vol. 1(4), 759-804.

Charusiri, P., Kosuwan, S., Wechbunthung, B., Kutranon, S., Daorerk, V. (2000), *Earthquakes in Thailand and Areas in Southeast Asia*, Final report, Thailand Research Fund (in Thai).

Chintanapakdee, C., Naguit, M.E. and Charoenyut, M. (2008) “Suitable attenuation model for Thailand,” Proceedings, 14th World Conference on Earthquake Engineering, Beijing, China.

Esteva, L. and Villaverde, R. (1973) “Seismic risk, design spectra and structural reliability,” Proceedings, 5th World Conference on Earthquake Engineering, Rome, 2586–2597.

Fenton, C. H., Charusiri, P. and Wood, S.H. (2003) “Recent paleoseismic investigations in Northern and Western Thailand,” Annals of Geophysics 46(5), 957-980.

Gardner, J. K., Knopoff , L. (1974), “Is the sequence of earthquakes in southern California, with aftershocks removed, Poissonian?,” *Bulletin of the Seismological Society of America*, Vol. 64, 1363-1367.

Gutenberg, B., Richter, C.F. (1954), “Frequency of earthquakes in California,” *Bulletin of the Seismological Society of America*, Vol. 34(4), 1985-1988.

Hanks, T.C., Kanamori, H. (1979), “A moment magnitude scale,” *Journal of Geophysical Research*, Vol. 84, 2348-2350.

Heaton, T.H., Tajima, F., Mori, A.W. (1986), “Estimating ground motions using recorded accelerograms,” *Survey in Geophysics*, Vol. 8, 25-83.

Idriss, I.M. (1993), *Procedures for Selecting Earthquake Ground Motions at Rock Sites*, Report No. NIST GCR 93-625, Report to National Institute of Standards and Technology, Gaithersburg, Maryland, Center for Geotechnical Modeling, Department of Civil and Environmental Engineering, University of California at Davis.

Nutalaya, P., Sodsri, S. and Arnold, E.P. (1985) Series on Seismology-Volume II-Thailand, In E.P Arnold (ed.). Southeast Asia Association of Seismology and Earthquake Engineering: p 402.

Petersen, M.D., Dewey, J., Hartzell, S., Mueller, C., Harmsen, S., Frankel, A.D., Rukstales, K. (2004), “Probabilistic Seismic Hazard Analysis for Sumatra, Indonesia and Across the Southern Malaysian Peninsula,” *Tectonophysics*, v390, 141-158.

Sadigh, K., Chang, C.-Y., Egan, J.A., Makdisi, F., Youngs, R.R. (1997), “Attenuation relationships for shallow crustal earthquakes based on California strong motion data,” *Seismological Research Letters*, Vol. 68, 180-189.

Saithong, P., Kosuwan, S., Choowong, M., Won-in, K., Takashima, I. and Charusiri, P. (2004) “Preliminary study on morphotectonic evidences along Moei-Mae Ping fault zone, Tak province, Northwestern Thailand,” Asia Conference on Earthquake Engineering, Manila, Philippines.

Sipkin, S.A. (2003), “A correction to body-wave magnitude mb based on moment magnitude Mw,” *Seismological Research Letters*, Vol. 74(6), 739-742.

Stepp, J.C. (1972), "Analysis of completeness in the earthquake sample in the Puget Sound area and its effect on statistical estimates of earthquake hazard," *Proceedings, International Conference on Microzonation*, Seattle, Washington, Vol.2, 897-910.

Toro, G.R., Abrahamson, N.A. and Schneider, J.F. (1997) "Model of strong ground motions from earthquakes in Central and Eastern North America: best estimates and uncertainties," Seismological Research Letters 68, 41-57.

Wanitchai, P., and Lisantono, A. (1996), "Probabilistic Seismic Risk Mapping for Thailand," *Proceedings, 11th World Conference on Earthquake Engineering*, Acapulco Mexico.

Wells, D.L. and Coppersmith, K.J. (1994) "New empirical relationships among magnitude, rupture length, rupture width, rupture area, and surface displacement," Bulletin of the Seismological Society of America 84(4), 974–1002.

Youngs, R.R., Chiou, S.J., Silva, W.J., Humphrey, J.R. (1997), "Strong ground motion attenuation relationships for subduction zone earthquakes," *Seismological Research Letters*, Vol. 68, 58-73.

EFFECT OF OXYGEN AND WATER ON MACRO-CELL CORROSION

VU VIET HUNG,
OMINDA NANAYAKKARA and YOSHITAKA KATO
Department of Civil Engineering
University of Tokyo, Japan
viethung@iis.u-tokyo.ac.jp

ABSTRACT

In reinforced concrete structures, macro-cell corrosion with locally separated anode and very large cathode is dominant in chloride environment & repair patching. It causes very severe damage and suddenly destroys the real structures. Oxygen and water play an important role in corrosion process in terms of accelerating the corrosion rate during exposure period. Moreover, it was proposed that anodic-cathodic transformation of steel bar over the time was caused by spatial variation of oxygen and water concentration along the steel bar. This experimental study was designed to study the effect of oxygen & water on the behavior of macro-cell corrosion in concrete and repaired concrete based on different surface coating conditions. It was observed that the properties of macro-cell corrosion, such as maximum anodic current density and time dependent variation, mainly occur in regions closed to oxygen and water support. And macro-cell corrosion was clearly observed when there is a big variation of amount of oxygen and water concentration along the steel bar.

1. INTRODUCTION

In reinforced concrete structures, macro-cell corrosion with local anode and very large cathode (Elsener et al. 2002) is dominant in chloride environment & repair patching. It causes very local damage and finally destroys the real structures.

Corrosion is an electrochemical process in which both cathodic and anodic reactions occur simultaneously at the steel surface. Oxygen and water, consumed in cathodic reactions (1) when corrosion occurs, accelerate the corrosion rate during exposure period. The rate of oxygen and water diffused to concrete, however, is limited due to the sound of concrete structures. As a result, the rate of corrosion is restricted by the cathodic reaction rate (Shiyuan et al., 2006).

$$\text{Anodic reaction:} \quad Fe \rightarrow Fe^{2+} + 2e^-$$
$$\text{Cathodic reaction:} \quad H_2O + 1/2O_2 + 2e^- \rightarrow 2OH^- \qquad (1)$$

Moreover, according to our research (Ominda et al. 2009), it was proposed that anodic-cathodic transformation of steel bar against the time

(time-dependent variation of macro-cell corrosion) was caused by spatial variation of oxygen and water concentration along the steel bar. This behavior of macro-cell corrosion produces maximum corrosion rates periodically and causes misinterpreted by the transformation when corrosion current measurements are taken.

From these backgrounds, the aim of this experimental study is to identify the effect of oxygen & water on the behavior of macro-cell corrosion of steel bar embedded in concrete structures.

2. EXPERIMENTAL PROCEDURE

2.1. Methodology

Macro-cell corrosion was observed in both concrete and repaired concrete with different chloride content. Segmented steel bar was used to study macro-cell corrosion. To study the effect of oxygen and water, epoxy coating was used to disturb oxygen & water penetration into specimen.

2.2. Specimen

(1) Concrete specimen

Concrete specimens of 100×100×576 mm were cast in this experiment (Figure 1) and the mixture proportion of concrete is shown in Table 1.

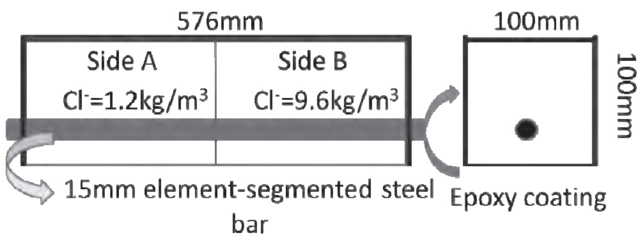

Figure 1: Outline of specimen

Table 1: Mixture proportion of concrete

W/C	s/a (%)	Weight per unit volume (kg/m^3)				AE(C x weight %)
		W	C	S	G	
0.55	45	190	345	770	966	0.008

Chloride ions were deliberately added during mixing the concrete in order to accelerate the corrosion process. Pure sodium chloride (NaCl) was used as the source of chloride ions.

A plain steel bar having a diameter of 10 mm was used. Segmented steel bar is composed of 28 elements, in which each has 15mm of exposure length (Figure 2).

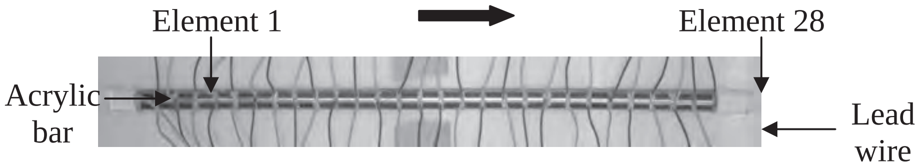

Figure 2: Segmented steel bar

In term of material aspect, the steel bar was separated by steel elements, however on the view of electrical aspect, it was assumed continuously by using lead wire connection. Two lead wires were welded to each steel element and then connected by epoxy. The total length of segmented steel bar embedded in concrete was 600 mm, even though the length of concrete specimen was 576 mm. Therefore both ends of steel bar were connected with acrylic bars as shown in Figure 2.

(2) Repaired concrete specimen

Same dimensional specimens were used (Figure 3) in which side A was repair material, EMACO ® S98P, with high resistance to oxygen and water penetration.

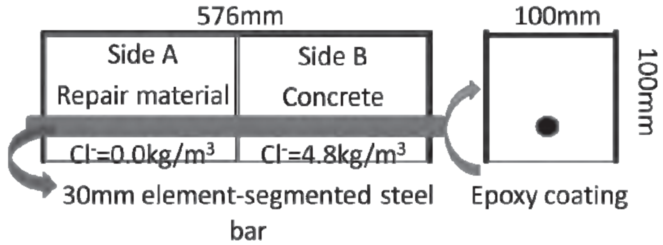

Figure 3: Outline of specimen

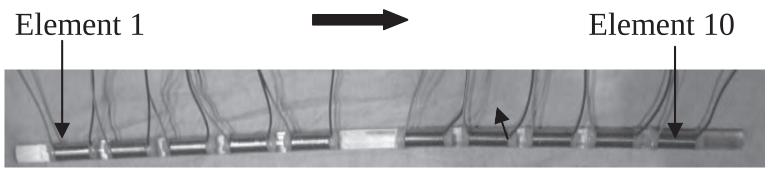

Figure 4: Arrangement of segmented steel bar

2.3. Experimental cases

Different bottom surface coating conditions were applied to investigate the influence of oxygen and water on the properties of macro-cell corrosion in concrete and repaired concrete structures (Table 2).

Table 2: Experimental cases

Specimen	No	Epoxy coating (bottom)	
		Side A	Side B
Concrete	1	-	covered
	2	covered	-
	3	-	-
Repaired concrete	4	-	covered
	5	covered	-
	6	-	-

2.4. Exposure condition

After casting, the specimens were sealed curing at a temperature of 20^{o}C in one week and then all the surfaces of the specimen except the bottom surface were covered by epoxy layer, to ensure that the penetration of moisture and oxygen through the bottom surface only. Then, all specimens were exposed to wet and dry cycling in chamber to accelerate the corrosion progress. Table 3 shows exposure condition in one cycle. The study was conducted on concrete & repaired concrete specimens for 16 weeks & 13 weeks, respectively.

Table 3: Exposure condition

Condition	Duration (days)	T (°C)	RH (%)
Wet	3	40	90
Dry	4	20	60

2.5. Item and method of measurement

By applying segmented steel bar inside concrete specimen (which was introduced by Miyazato. 2001, Thesis for Doctoral Degree), it is easy and direct to measure the electric current flowing from element to element to study the macro-cell corrosion (Figure 5). However, the lengths of steel element in the experimental cases were different therefore to compare and analyze the results the current is converted to current density, as calculated by:

$$a_i = \frac{I_{i,i+1} - I_{i-1,i}}{S_i} \tag{2}$$

where, a_i is macro-cell current density of element i (μA/cm^2), $I_{i,i+1}$,$I_{i-1,I}$ are macro-cell currents flowing from element i to i+1, i-1 to i respectively (μA), and S_i is surface area of steel element i (cm^2).

Periodic macro-cell corrosion current measurement was carried out twice a week (the end day of wet and dry exposure) by using a data logger.

The current values were then converted to current densities of each steel element along the specimen.

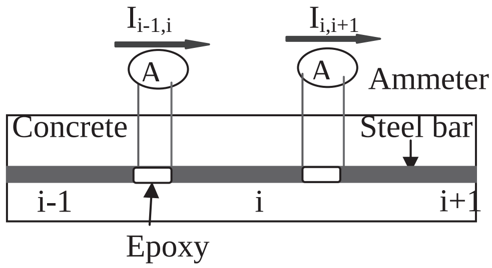

Figure 5: Macro-cell corrosion current measurement

3. RESULTS AND DISCUSSION

Macro-cell current was measured and then converted to current density. Figure 6 shows the results of current densities of concrete under dry exposure (a) (12th week), wet exposure (b) (12th week) and repaired concrete specimens under dry exposure (c) (9th week), wet exposure (d) (9th week) with different surface coating conditions (Table 2).

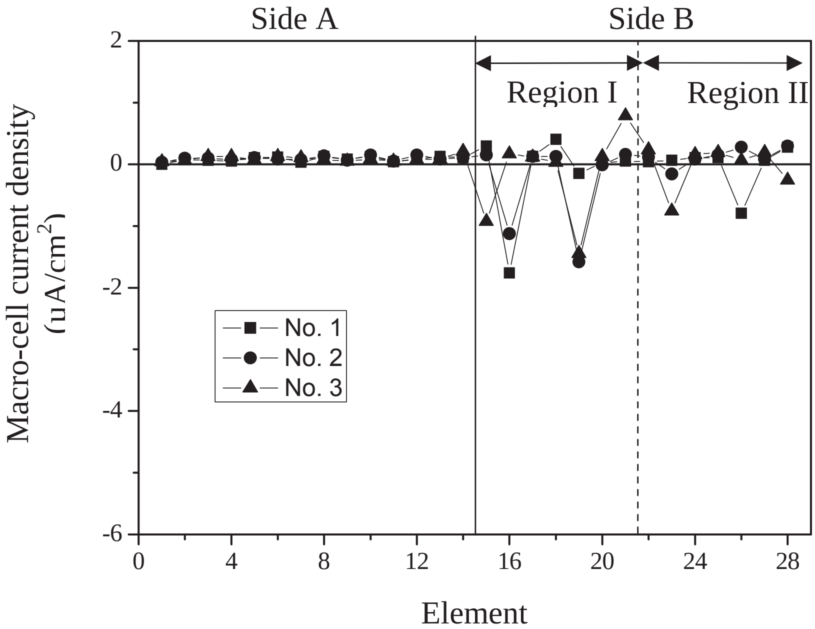

(a)

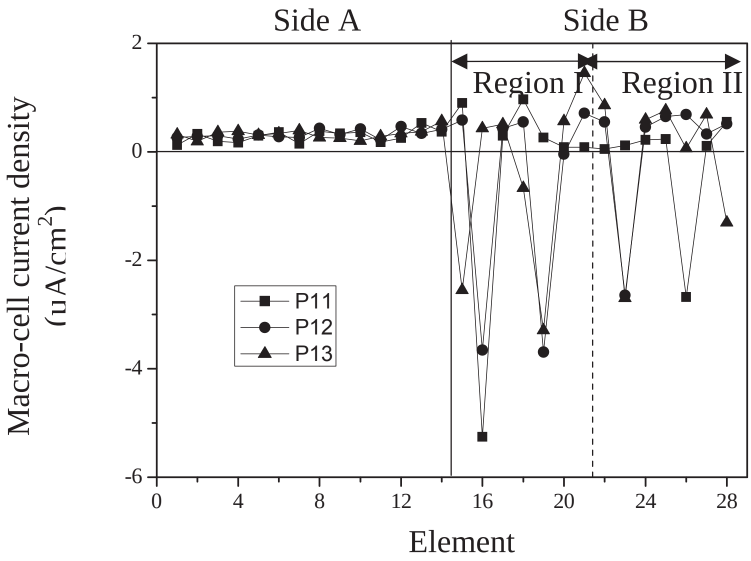

(b)

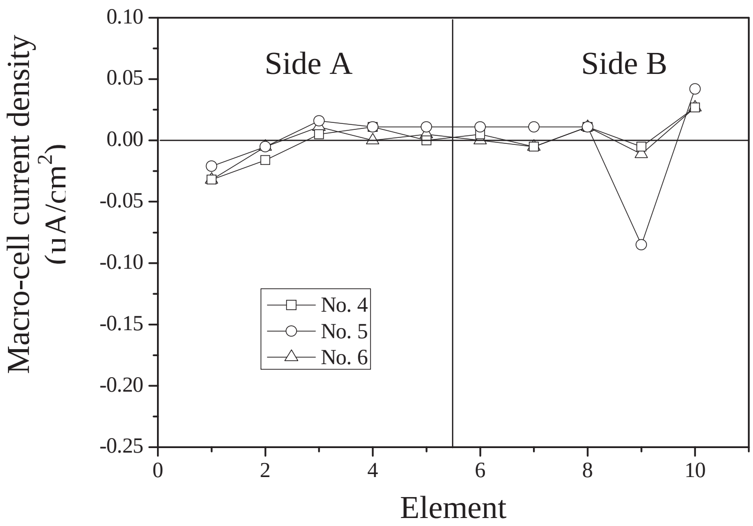

(c)

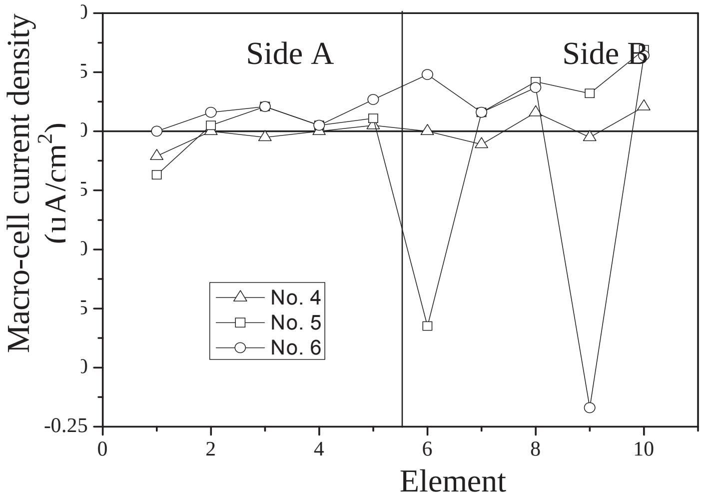

(d)

Figure 6: Macro-cell current density

In concrete specimens, it was imagined that side B was divided into two equal regions I & II, in which region I is close to the interface. Table 4 shows the comparison of specimens with different surface coating conditions based on maximum anodic current density & anodic-cathodic transformation in region I & II.

Table 4: Comparison of specimens with different surface coating conditions

Criteria	Specimen		
	No. 1	No. 2	No. 3
Maximum anodic density	I>>II	I>II	I>II
Anodic-cathodic transformation	mainly in I	mainly in II	mainly in I

It is widely accepted that oxygen and water play an important role in corrosion process. Wherever oxygen and moisture are available, corrosion becomes active. As can be seen from Figure 6 (a), local corrosion (anode) occurs near the interface (region I, side B) in specimen No.1 where it is supported by cathodic area in side A, while in specimen No.2 & 3, the appearance frequency of maximum anodic densities in region II is higher. Furthermore, the difference between specimen No.2 & No.3 is in region II, corrosive level in specimen No.3 is higher than that of in specimen No.2. It could be explained that elements of region II in specimen No.3 are much more supported from side A where cathodic reactions take place.

Time-dependent variation of macro-cell corrosion was also considered in this research. It is inferred that once an element changes from anode to cathode, another or other elements will switch from cathode to anode at the short time or simultaneously. In concrete specimen, generally, macro-cell corrosion and anodic-cathodic transformation occurs near the interface (region I), high "competitive" or the highest electrochemical potential difference zone. However, as can be seen from Table 4, time-dependent property was mainly observed in region II of specimen No. 2. The reason is, in author's opinion, region II not only acts as cathodic supporting area for region I but also contains anodic elements. Therefore, elements in region II are vulnerable to change their potentials due to different amount of oxygen and water along the steel bar caused by on-going corrosion process.

In repaired concrete, although magnitude is small, macro-cell corrosion continues happening in repair part (Figure 6 (c), (d)) because of the incompatibility between repaired and non-repaired parts. In this experiment, there are two factors causing potential imbalance between two sides of specimen: different material and different chloride content. This condition is the same with real repaired concrete structures subjected to chloride attack in which repaired part is free chloride content while concrete part is still contaminated by chloride.

According to previous researches (Ominda et al.2007, Barkey.2004, Ping et al.1997), it was proposed that different material induced macro-cell corrosion will be dominant and causes corrosion in repaired part when chloride concentration is less than 1.2 kg/m^3 while corrosion caused by different chloride content becomes significantly in concrete part if chloride content is higher than 1.2 kg/m^3. In this research, chloride variation of two sides of specimen was chosen as 4.8 kg/m^3 on the expectation that corrosion will occur in concrete part (side B).

Theoretically, it was assumed that repair material has higher resistivity to corrosive agents, such as oxygen and moisture, penetration compared to concrete part, and epoxy coating is used to totally disturb substances transporting inside specimen. On this basis, illustration of amount of oxygen and water content was drawn in series of repaired concretes (Figure 7).

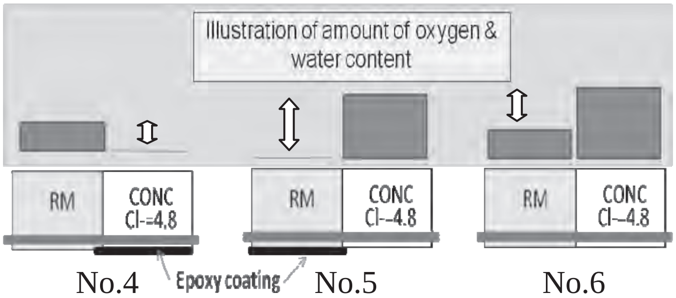

Figure 7: Image of oxygen and water content

The results from Firgures 6 (c) & 6 (d) confirm the above assumption. The rate of cathodic reactions in side A (repaired part) are very small compared to that of in side B (concrete part) in both dry and wet exposure. In the case of total bottom surface was exposed to experimental environment (specimen No. 6), corrosion occurred in concrete part. However, since concrete part was under coating condition in specimen No. 4, corrosion zone was reaching towards the interface where oxygen and water were supplied from side A. Another evidence to show the role of oxygen and moisture in corrosion process, for example, in specimen No.5, high variation amount of oxygen and water between two sides of specimen, in side A almost no corrosion occurs (current density less than 0.1 $\mu A/cm^2$) because of lack of oxygen and water while macro-cell corrosion appears clearly in side B. The most severe macro-cell corrosion observed in specimen No. 5 can be explained by the increasing in potential imbalance between two sides caused by oxygen and water concentrations.

4. CONCLUSIONS

The aim of this study was to identify the effect of oxygen and water on macro-cell corrosion. The research results are presented below:

Macro-cell corrosion occurs in higher chloride content side of concrete specimen. Depend on surface coating conditions, however, the behavior of macro-cell corrosion will different in both the position of maximum anodic current density and anodic-cathodic transformation.

Macro-cell corrosion is clearly observed when there is a big different amount of oxygen & water content along the steel bar in repaired concrete structures.

REFERENCES

Ominda N. and Kato Y., 2009. *Macro-cell corrosion in reinforcement of concrete under non-homogeneous chloride environment.* Journal of Advanced Concrete Technology, 7-1, 31-40.

Elsener, B., 2002. *Macro-cell corrosion of steel in concrete –implications for corrosion monitoring,* Cement and concrete composites, 24-1, 65-72.

Barkey, D.P. 2004. *Corrosion of steel reinforcement in concrete adjacent to surface repairs.* ACI Material Journal, 101-4, 266-272.

Ominda N. and Kato Y. 2007. *Macro-cell corrosion of partially repaired concrete members.* Seisan-kenkyu (University of Tokyo), 59-3, 263-266.

Ping Gu, J.J. Beaudoin, P.J. Tumidajski, and N.P Mailvaganam. 1997. *Electrochemical incompatibility of patches in reinforced concrete*. Concrete International, 19-8, 68-72.

Miyazato, S.2001. *Macro-cell corrosion induced by chloride and carbonation in reinforced concrete with defects*. Thesis for Doctoral Degree.

Shiyuan. Q., Jieying Z., Deyu Q., 2006. *Theoretical and experimental study of microcell and macrocell corrosion in patch repairs of concrete structures*. Cement and concrete composites, 28, 685-695.

CONSTRUCTION STEP ANALYSIS AND COLLOSION SIMULATION OF CFTA

YI SUN-AE, JUNG MIN-CHUL and KONG JUNG-SIK
School of Civil Engineering and Architecture
Korea University, Korea
capritio@korea.ac.kr

ABSTRACT

Recently, many studies about high-strength concrete and composite structures are progressed to get more economic and stable result in the construction of structure all over the world. One of those studies is about CFTA(Concrete Filled and Tied Steel Tubular Arch) girder that applies an arch structure and a pre-stressed structure to CFT(Concrete Filled Steel Tubular) Structure which is filled with a concrete and improve the stiffness and strength of the structure by the confinement effect of fillers to maximize the efficiency of structure and economic. In this study, construction step analysis of CFTA girders by using ABAQUS. And one of the weak points of CFTA girder is pre-stressed tendon exposed outside of structure. Therefore, collision simulation of heavy projectile with CFTA girder was also performed to check the safety of tendons by using ABAQUS 6.5-1.

1. INTRODUCTION

In recent years, many studies about shape of bridge's superstructure, efficiency of materials and complex structure are being progressed for bridges, which are more safety, economical and well harmonized into nature, in the construction for structure all over the world. SCP Girder, as an example, which has similar cross section shape of PSC girder is filled with a pre-stressed concrete. In this manner, studies about new types of bridge superstructure which can minimize shortcomings of the existing superstructure of bridge by performance improvement from rearranging of structure shapes and materials, using tensile force, and being beneficial for economic as well as aesthetic part are being progressed.

As mentioned above, the studies about new types of synthetic structure and girder system of bridges are being progressed these days. However, as it is hard to be used on actual construction field immediately, it is needed to develop new structure types which can be applied without further delay and minimize some weak points of existing structure stuffs. 'Concrete Filled steel tubular Tied Arch composite (CFTA) girder, one of the new types of complex structure girder, is studied for this purpose. In CFTA girder, the construction step has 4-steps. And the constructor has to consider about the stress and displacement in each step. In this study make the process for construction by using ABAQUS program and check the limit stress and displacement.

There is an increasing number of severe accidents, some of these are the accident between the transportation means or the merchandises and our structure systems such as bridge girders, bridge piers or barriers. In this case, if no officially is considered, there will be seriously affect not only to the performance of the structure but also the economic issue and public safety. In this part of the research, numerical simulation of collision has therefore an imperative method for testing the CFTA girder. A hypothesis projectile was created from an I shape steel girders or wood trees which the truck is carrying were thrown out and collides the girder. Both the object and the CFTA girder were modeled using finite element method (FEM) to simulate the dynamic impact performance. The results will then be used to invoke for the on-site full scale experiments later on and for further studying.

2. CFTA GIRDER AND PROPERTIES

The top side of CFTA girder filled with concrete in steel tube maintains constant height, while the bottom side of CFTA girder is the arch shape. Besides, pre-stress is put on steel tendons exposed at the lower part of CFTA girder to improve its safety and reduce its weight.

The solid drawing and the constituent material of CFTA girder are showed figure 1 and 2. As shown figure 1, the height of CFTA girder at both ends is 620mm and filled with concrete. As going to the center part, the shape of the inner filled concrete is the arch shape with maintaining 180mm thickness. Tendons are inserted until 520mm from both ends, and then they are exposed to outside because of the arch shape of CFTA girder. The steel box on the concrete arch is the empty and transmits the load from upper part of steel box to the concrete arch. The length of the whole span is 12.2m, the width is 500mm and the displacement control load is applied to perform the non-linear analysis. Besides, material properties and scale are as following table 1.

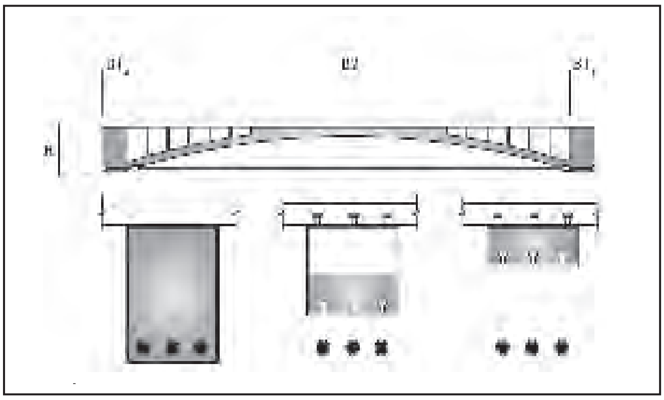

Figure 1: The solid drawing of CFTA girder Figure

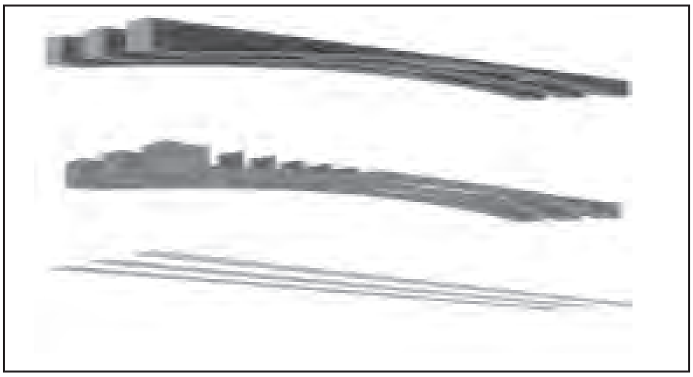

Figure 2: The constituent material of CFTA girder

Table 1: Material Properties and Scale

Part	**Density (kg/m^3)**	**Young's Modulus (Mpa)**	**Poisson's Ratio**
Concrete Slab	2500	21,500	0.167
Concrete Block	2500	29,885	0.167
Steel Plate	7850	210,000	0.3
Tendon	8000	210,000	0.3

Part	**Length(mm)**	**Wide(mm)**	**Height(mm)**
Slab	30600	3500	240
Steel	30500	198.6 ㎟	
Concrete	30600	2000	1476
Steel Plate	30600	2000	1476
Tendon inside	30600	2635.5 ㎟	
Tendon outside	30600	1664.4 ㎟	

3. CONSTRUCTION STEP ANALYSIS

Construction step has 5 steps and each step has different stress and strain. If the constructor does not consider about that actual state, it could be makes critical fracture. In this study the stress and strain were checked in from top to bottom at middle of bridge.

Figure 3.1 shows the displacement of CFTA in step 1 by color, and the detail value appears in table 3.1. In the first step of CFTA girder construction, there are only self-weight of concrete and steel plate. So the girder has -124.16mm displacement. It is the largest displacement in whole construction step.

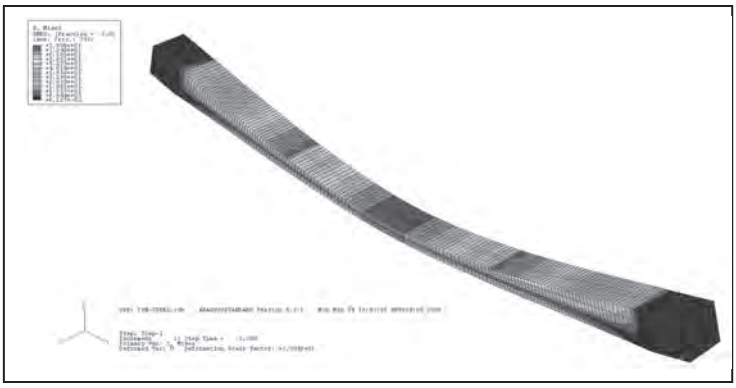

Figure 3.1: Displacement of Step 1

Table 3.1: Stress and Strain of Step 1

Part		Center	
		Strain	**Stress (MPa)**
Filled concrete	Upside	-0.00036	-10.2477
	Downside	0.000357	10.2567
Steel plate	Upside	-0.00049	-104.027
	Downside	0.000487	104.365
Displacement (mm)		-124.16	

The Second Step has first tension for inside tendon 775.9Mpa each and the whole tension is 4300kN. So CFTA girder gets 37.94mm camber. Self-weight of steel plate and concrete will be applied with the first tension.

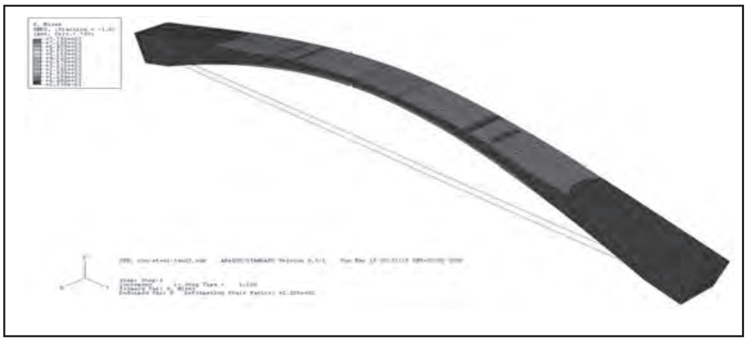

Figure 3.2: Displacement of Step 2

Table 3.2. Stress and Strain of Step 2

Part		Center	
		Strain	Stress(MPa)
Filled concrete	Upside	2.20E-05	0.617965
	Downside	-0.00018	-5.1912
Steel plate	Upside	5.81E-05	12.2881
	Downside	-0.00022	-46.7539
Displacement (mm)		37.94	
1st tendon stress(Mpa)		775.9	

There are slab self-weight in third step. In this step, the slab stiffness is not revelation yet, so the girder displaced caused by the slab weight.

Figure 3.3: Displacement of Step 3

Table 3.3: Stress and Strain of Step 3

Part		Center	
		Strain	Stress(MPa)
Filled concrete	Upside	-0.00018	-5.05392
	Downside	-9.37E-07	-0.03545
Steel plate	Upside	-0.00021	-44.5875
	Downside	3.05E-05	6.4032
Displacement (mm)		-27.07	
1st tendon		863.287	

At the last step of construction, the second tension applied on CFTA girder 420.6MPa each of step. Total tension force is 1400kN. The forces in the last step are the self-weight of concrete, steel plate, slab and the tension of tendon. Figure 3.4 shows the displacement of step 4 by color. CFTA model's displacement shows blue color, it means the whole model is in safety displacement range.

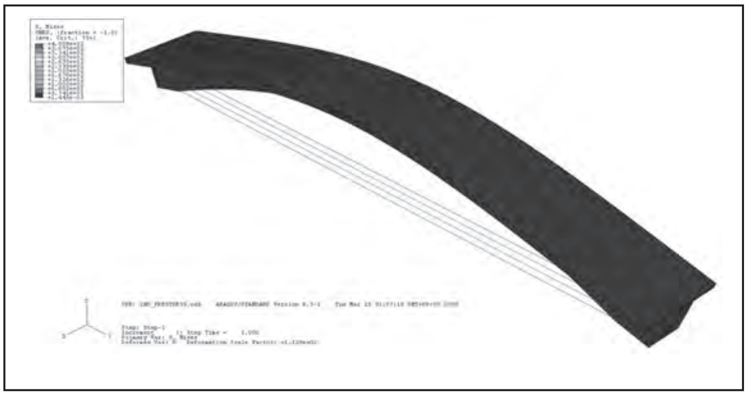

Figure 3.4: Displacement of Step 4

Table 3.4: Stress and Strain of Step 4

Part		Center	
		Strain	**Stress(MPa)**
Filled concrete	Upside	-36.7257	-4.70566
	Downside	-25.7211	-3.60818
Steel plate	Upside	-0.00017	-3.17482
	Downside	-0.00012	-3.18767
Concrete slab	Upside	9.81E-05	2.43468
Displacement (mm)		23.8977	
1st tendon		822.548	
2nd tendon		420.6	

4. COLLISION MODEL NUMERICAL SIMULATION OF PHYSICAL TESTING

The projectile model is allowed to impact the CFTA girder at the most dangerous part, the tendon area through transverse to the longitudinal axis of the tendon. The impact event is simulated using ABAQUS/Standard 6.5-1 for a period of 20 ms using automatically time increment. Various quantities of interest are extracted from the finite element results including: impact force versus time relationship, stress and strain values and rates at key points, deformations at critical sections.

According to the speed limit on expressways managed by the Korea Expressway Corporation, the range is 100 km/h and 120 km/h. This velocity will be used in the study to examine the performance of the tendon first and then the working state of the whole structure.

4.1 Numerical Models

The numerical model of the impact test comprises of two main parts: the projectile (object) and CFTA girder. The first part represents the steel rectangular beam which had a length of 3000 mm, width of 800 mm and height of 400 mm (Figure. 4.1). The projectile contains 120 solid elements; type C3D8R, an 8-node linear brick, reduced integration and hourglass control have been used. The second part of the model, the CFTA girder, was maintained unchanged as in the static analysis behavior. The tendon was considered as cable element, which is an inextensible cable that supports only tensile loads (initial stresses). It can be simulated as hybrid beam element type 3-D beam linear B31 or the 2-node linear 3-D truss, T3D2 element. The mechanical properties and values of the system are displayed in the same values in the static analysis step.

4.2 Contact analysis algorithm

When two objects collide, contact stresses are transmitted across their common interface. In the analysis of contact problems, the contact area needs to be defined and the stress transmitted through the contact must be calculated.

Contact problems can be simulated using contact elements. In advanced numerical programs, it is not necessary to define contact elements. Instead, the interaction between contacting surfaces consists of two components: one normal to the surfaces and on tangential to the surfaces. This study uses slave surface and master surface to simulate the interaction between two objects. The properties interaction was also defined (with finite sliding, small sliding or with friction).

Because in finite element analysis the bodies to be analyzed are discretised, a discretised formulation should be used in which the nodes on one surface (the slave surface on the softer body) contact the discretised segments on the other surfaces (the master surface on the hard body). The distances between the corresponding locations are determined to examine whether they are in contact or not.

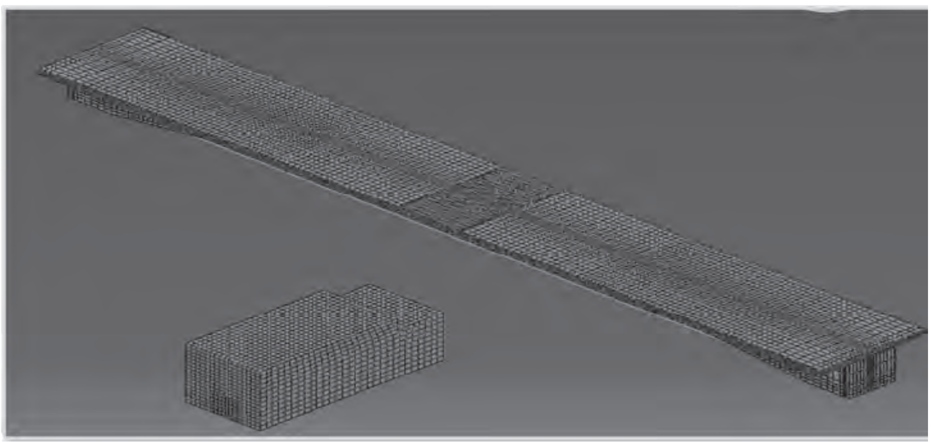

Figure 4.1: Impact simulation model between truck and girder

4.3 Results of Numerical Simulation Test

For the impact analysis, an implicit direct integration dynamic approach, called the Hilber- Hughes- Taylor operator, has been used to solve the non-linear equations of motion. Dynamic impact responses are usually involved with severely discontinuous non-linearity. With the range of the velocity and duration of impact specified in this research, the event can be specified as an intermediate dynamic impact phenomenon.

Figure. 4.3 shows the selection of frames taken from the finite analysis at the time of collisions. These numerical figures will then be compared with the corresponding experiment results.

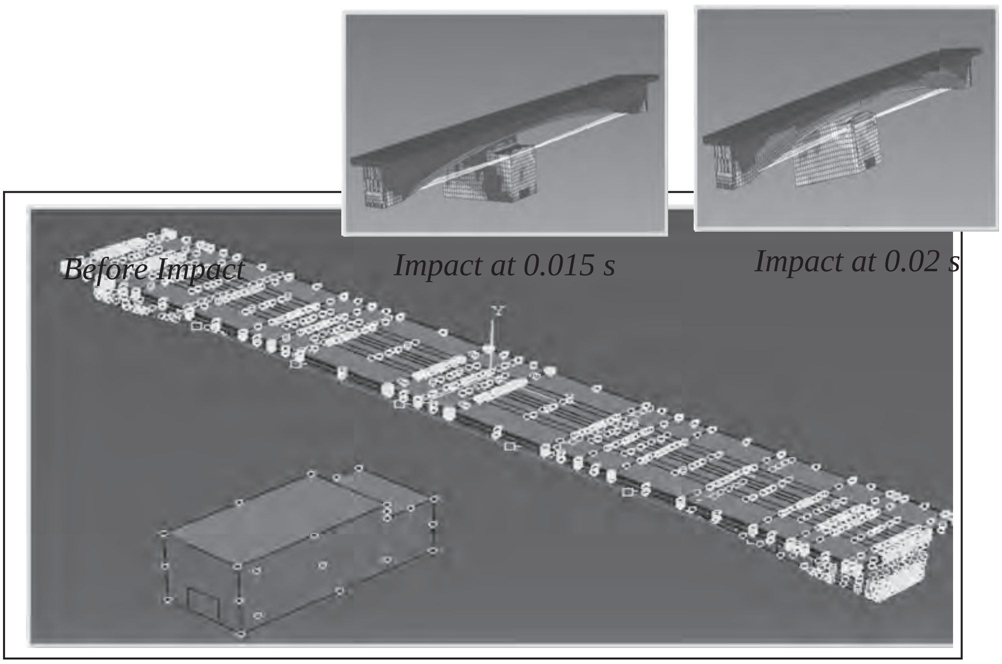

Figure 4.2: Model representing Master and Slave surfaces on the project tile and the tendon member respectively

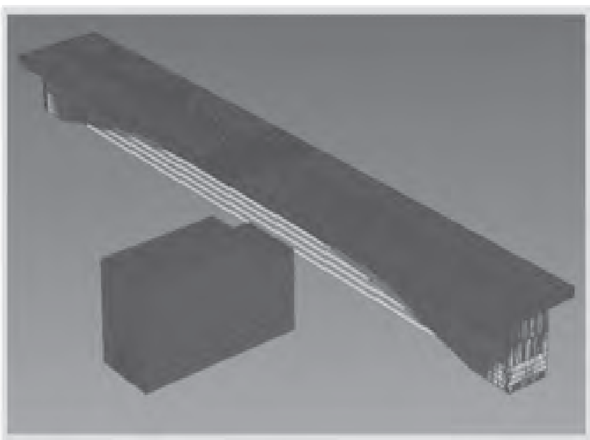

Figure. 4.3: Impact performance of the projectile to the tendon of the girder at (a) 0.0s, (b) 0.015s and (c) 0.02s

Strain rate is one of the important factors in order to investigate the behavior of the structure. In this study, the strain rate of the most critical points on the longitudinal side of the tendon was observed. Figure 4.4 shows the strain of the tendon as time goes. The tendon yield strain assumed 0.002, so the tendon 1 and 4 will be within the plastic strain range. But, there are not be rupture by crash.

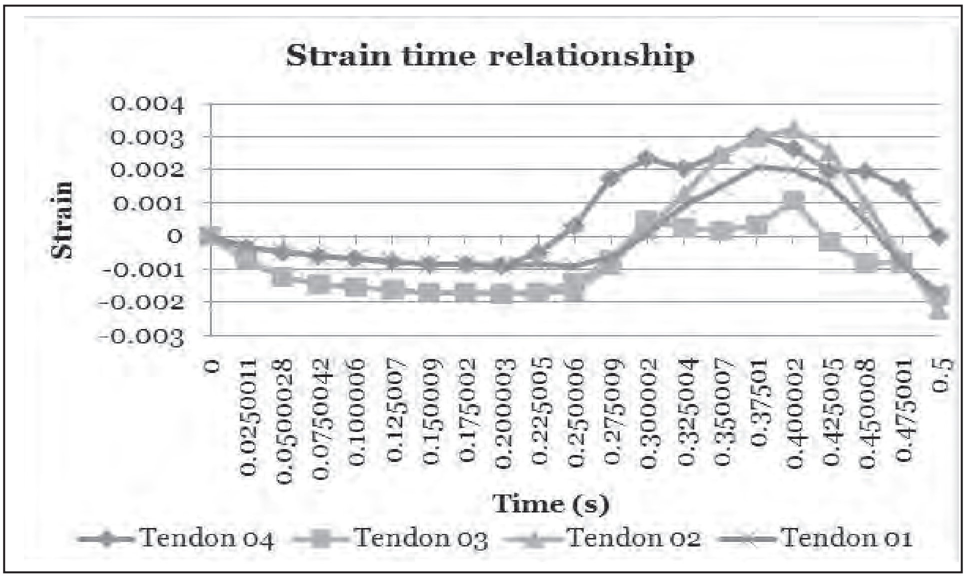

Figure 4.4: the tendon strain for collision simulation

6. CONCLUSIONS

This study is carried out to verify the performance characteristic of the innovation type of the composite girder, CFTA girder. In order to comprehend the characteristic, ABAQUS 6.5-1 is used. The conclusion by the FE analysis of the CFTA girder is summarized as follows:

1) CFTA construction step has different load and stiffness in each step. In this study concern about the material will be rupture or large stress in that step, so check the stress and strain in 5 steps.

2) The first step displacement and stress are the largest value in whole steps, it is not make rupture concrete and steel-plate. So the CFTA girder is safe in the construction state.

3).The tendons are deformed through the impact by truck. And the tendons deformed within the plastic range. But there are no rupture by the crash, so CFTA is in service after the collision

An investigation into the impact behavior of the CFTA girder has been presented. Using the hypothesis projectile resulted from the assumed accident of the truck in the expressway. The simulations presented in this research demonstrate that numerical modeling could serve as a power tool to investigate the vulnerability of new types of bridge or to improve general design criteria. These results will be used effectively in comparison with the next research steps including on-site full impact experiments, vulnerability assessment and fragility analysis.

ACKNOWLEDGEMENT

This study was supported by the Construction Core Technology R&D(05 Construction Core D11 and 06 Construction Core D14) of Ministry of Construction and Transportation (MOCT).

REFERENCES

Hak, Lee., Ho, Park., Eun Ho, Lee., Jung Ho, Kim., Jung Sik, Kong., 2007. *Behavior of Concrete-Filled and Tied Steel Tubular Arch Girder. Spring Conference Paper Book 668-693*. Computational Structural Engineering Institute of Korea.

Ho, Park., Myung Kyun, Park., KyungHun, Park., JungHo, Kim., 2006. *Development of Concrete-Filled and Tied Steel Tubular Arch Girder. Conference Paper Book 2289-2292*. Korean Society of Civil Engineers.

SungWon, Yoo., KyungWook, Hong., 2000. Bending Analysis and *Improvement of Bending Capacity of Pre-stress Concrete Beam Using the Partly Attached Rigid Model. The collection of learned papers 813-821*. Korean Society of Civil Engineers.

ByungHwan, Oh., SungWon, Yoo., 2000. *Bending Behavior Test of PSC Beam Which has the External Steel Wire according to the Shape of Steel Wire and the Number of deflection side. The collection of learned papers 795-804*. Korean Society of Civil Engineers.

ABAQUS 6.5-1 analysis user's manual

EXPERIMENTAL STUDY ON THE EVALUATION OF A CAVITY AND LOOSENING IN SOIL

MARI SATO
Graduate Student
Department of Civil Engineering, The University of Tokyo, Japan
msato@iis.u-tokyo.ac.jp

REIKO KUWANO
International Centre for Urban Safety Engineering,
Institute of Industrial Science, The University of Tokyo, Japan
kuwano@iis.u-tokyo.ac.jp

ABSTRACT

Damaged old sewer pipes are known to often cause void/cavity or loosening in the surrounding soil, which may lead to a cave-in in the road. In this research, in order to understand the mechanism and governing factors of cavity formation/expansion in the ground, a series of model tests simulating flow out of soil through a crack/gap in a buried pipe was conducted.

It was found that a cavity and surrounding loosening in the ground can extend rapidly upward when the ground consists of poorly graded, high water content, and low relative density sand.. Quantitative evaluation was also given to the loosening around a cavity.

1. INTRODUCTION

An old deteriorated sewer pipe, when it is damaged, may eventually cause local subside or a cave-in in the road. Recently, the number of pipes which are older than the service life time of 50 years, has been rapidly increasing. Accordingly, incidents of a cave-in are found to be more frequent in urban areas. In spite of the significance, full investigation of the road cave-in is often skipped as the urgent road restoration is usually priotised. It is difficult to clearly identify the real cause by the fact that eventual cave-in is likely to occur long after the initial formation of a cavity in soil. The congested underground lifeline structures also make it complicated.

Kuwano et al. (2006a) conducted a survey to obtain basic information on how the damaged sewer pipes were related to the collapses of road, which occurred from 2001 to 2003. The survey was performed by sending questionnaires and interviewing local government officers in seven cities where the sewerage system had started more than 30 years ago and the management and maintenance of old sewer pipes are likely to be the concerned issues. It was found that even small gaps or cracks could lead to road cave-in and the rainfall appears to be one of the most important factors, as schematically shown in figure 1. Based on the survey results, Kuwano et al. (2006b) performed a series of model tests to investigate how a cavity initially forms in soil and how it progresses up to the ground surface. In this paper, the typical pattern of cavity formation/expansion in sandy soil and the quantitative evaluation for the loosening surrounding the cavity is shown.

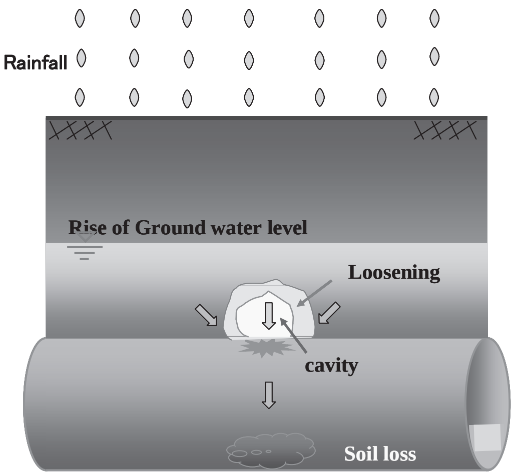

Figure 1: A cavity and loosening formed above the defect of buried pipe

2. TEST APPARATUS AND PROCEDURE

A test apparatus used in this study is shown in Figure 2. Model ground of 300m wide, 50mm long and 200mm high was made in a small soil chamber having an opening of 5mm in a base plate. A cavity was formed above the opening at the base, after the water flow in and out of the opening repeatedly. Water of approximately 100cc was supplied into the opening with 1m head difference. After pausing 1 minute, the drainage valve was opened to let water and soil flow out. This cycle of water supply/drainage was repeated until the cavity or loosening reached the ground surface.

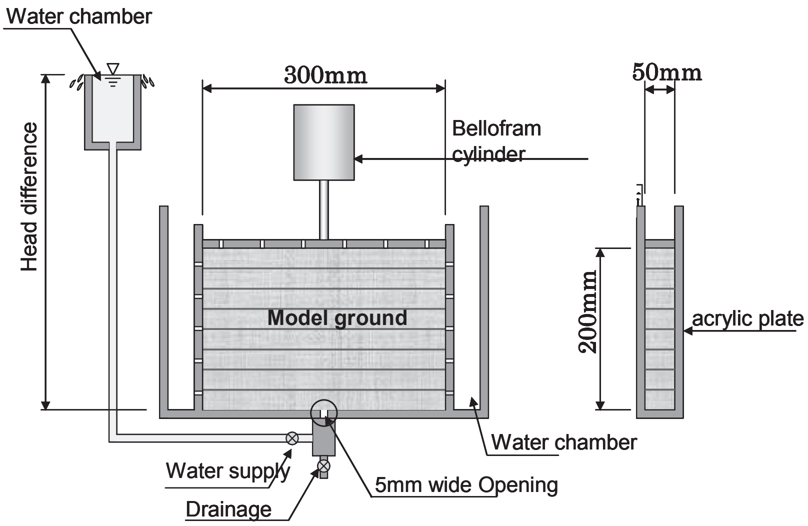

Figure 2: Model test apparatus for generating cavity/loosening in soil

The details of experimental conditions are shown in Table 1. Three sandy materials were used for the model ground; Toyoura sand, Natural sand and silica sand. Both Toyoura sand and silica sand are clean uniform sand but average particle size of silica sand is larger than that of Toyoura sand. Natural sand contains fines of around 3%. Particle size distributions are shown in Figure 3.

Table 1: Experimental conditions

Code	**Materials**	**Initial water content** (%)	**Relative density** (%)
$T_{14,80}$ $T_{14,60}$	Toyoura sand	14 14	80 60
$K_{10,80}$ $K_{0,80}$ $K_{5,80}$ $K_{10,60}$	Silica sand	10 0 5 10	80 80 80 60
$E_{15.5,80}$ $E_{0,80}$ $E_{7.8,80}$	Natural sand	15.5 0 7.8	80 80 80

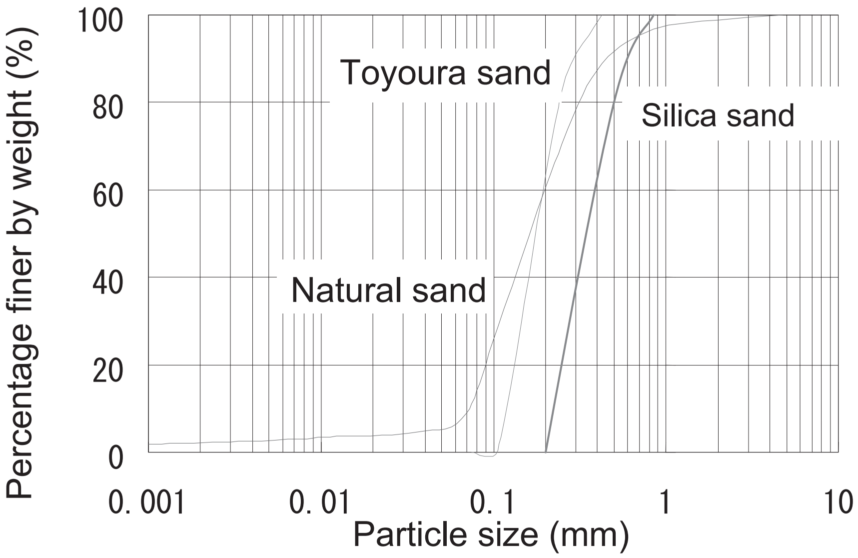

Figure 3: Particle size distribution of tested materials

For the preparation of model ground, soil was placed into the chamber and compacted by eight layers. At each layer, colored soil was placed in order to observe the deformation of ground. A load equivalent to an overburden of 60cm was applied on the surface of model ground.
At each cycle of water supply/drainage, a photograph was taken to observe a cavity and deformation of the model ground. The weight of soil frown out of the opening was also measured.

3. DEFINITION OF INDICES

In order to evaluate a cavity and loosening developed in the ground, some indices were proposed as shown in Table 2.

Table 2: Definition of Indices in this research

Index	Definition and description
Weight of soil loss	Cumulative dry weight of lost soil
Cycle	One cycle is from the beginning of water supply to the end of water out flow.
Area of loosening	Area of deformation area, not including a cavity
Area of a cavity and loosening	Area of cavity + area of loosening.

4. TEST RESULTS AND EVALUATION OF CAVITY AND LOOSENING AREA

4.1 common features observed in all the experiments

Typical forms of a cavity and loosening created in the model ground are shown in Figure 4. A cavity of fan-like shape, having slope at both sides and arching ceiling, was generated above the opening. After repeating some cycles, cavity and loosening above cavity were expanded.

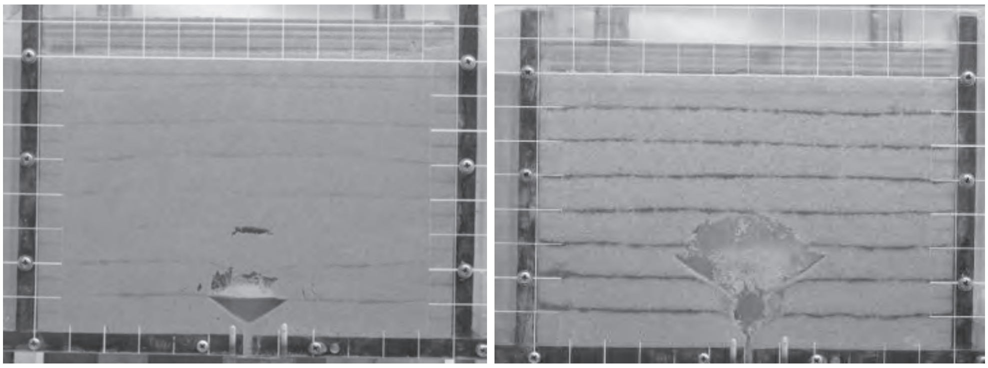

(a) $T_{14,80}$ after 7 cycles (b) $K_{10,80}$ sand after 6 cycles

Figure 4: Cavity and loosening formed in the model ground

4.2 Comparison between different materials

Three different material conditions ($T_{14,80}$ $K_{15.5,80}$ & $S_{10,80}$) which had optimum initial water content and same relative density (80%) were compared. Weight of soil loss and cavity and loosening areas are plotted against the number of cycles in Figure 5 and Figure 6. From figure5, it is revealed that soil drainage was most rapidly in silica sand and was most slowly in natural sand. On the other hand, Figure 5 and Figure 6 suggested that expansion of loosening tended to followed by rapid growth of a cavity. Loosening area expanded even if cavity hadn't expanded so much, especially in Toyoura sand.

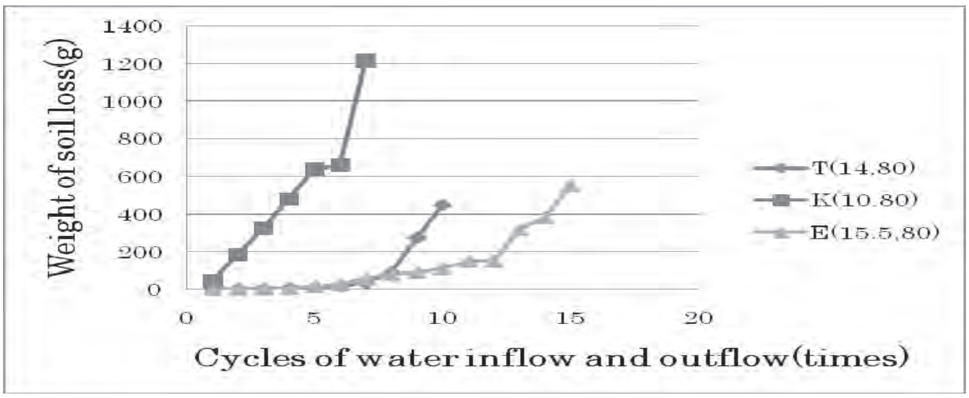

Figure 5: Weight of soil loss in different materials

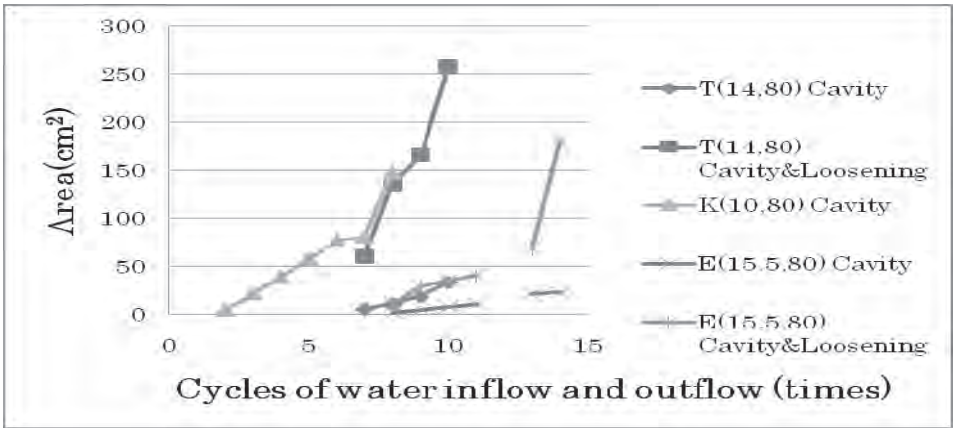

*Loosening area was not observed in Silica sand.

Figure 6: Process of cavity/loosening formation in different materials

4.3 Comparison between different initial water content

Weight of soil loss in three different water content conditions in natural sand ($E_{15.5,80}$ $E_{7.8,80}$ &$E_{0,80}$) is plotted against cycles in Figure7 and the details of Figure7 is shown in Figure8. Referring to Figure7 and Figure8, it is clean that soil was drained more rapidly in larger amount of initial water content especially in early stages. Similar result was shown in silica sand ($K_{10,80}$ $K_{5,80}$ &$K_{0,80}$). Cavity and loosening areas of plotted against cycles in Figure9. Figure9 showed that cavity expanded rapidly after loosening area expanded sharply at a certain cycle.

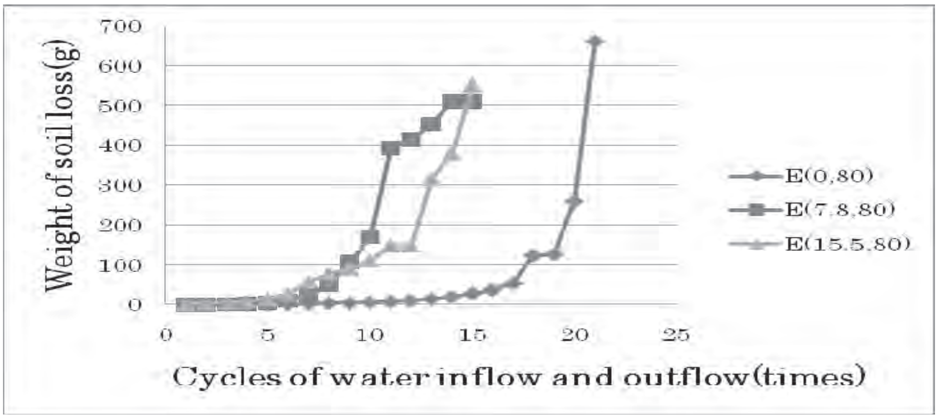

Figure 7: Weight of soil loss in different water content

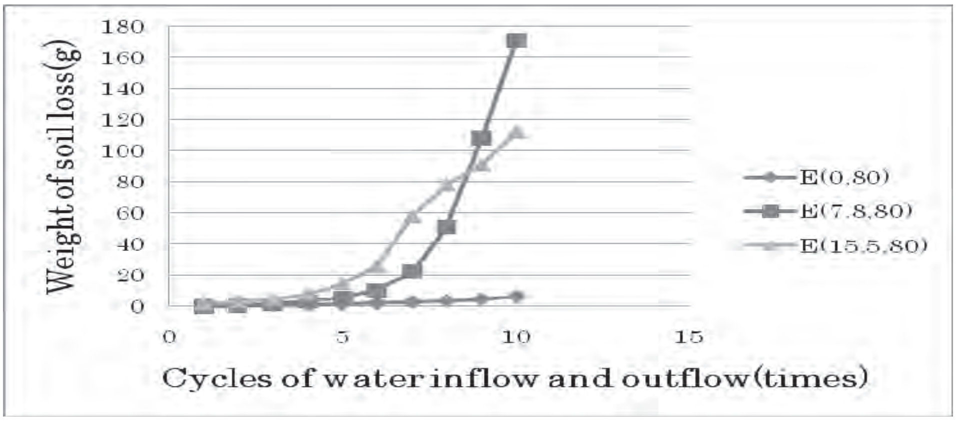

Figure 8: Details of Figure 7

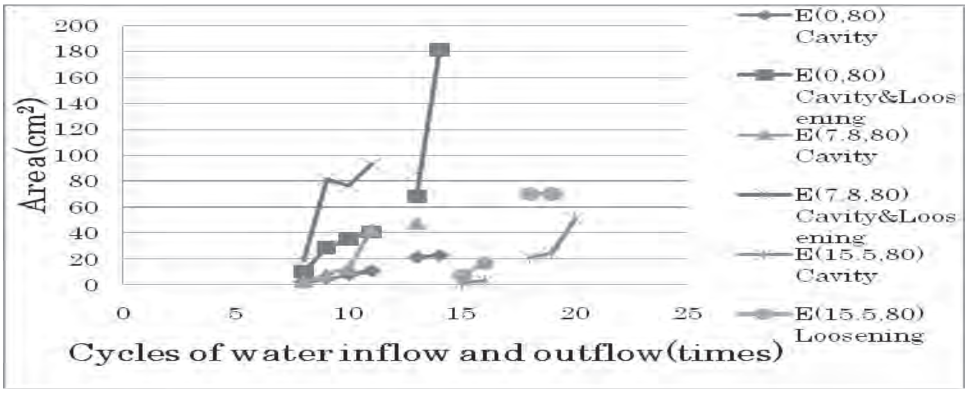

Figure 9: Process of cavity/loosening formation in different water content

4.4 Comparison between different relative densities

Two different relative density conditions ($T_{14,80}$ &$T_{14,60}$) were compared. Weight of soil loss and cavity and loosening areas are plotted against the number of cycles in figure11. Referring to Figure10, weight of soil loss increased rapidly through cycles in a high relative density condition. Figure11 showed that speed of loosening expansion was similar in both conditions, but that of cavity expansion was specifically different. Low relative density condition caused large cavity more immediately.

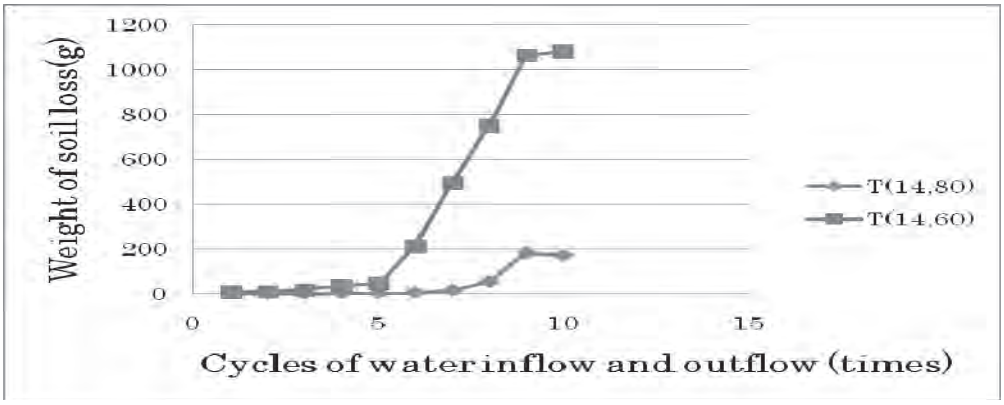

Figure 10: Weight of soil loss in different relative density

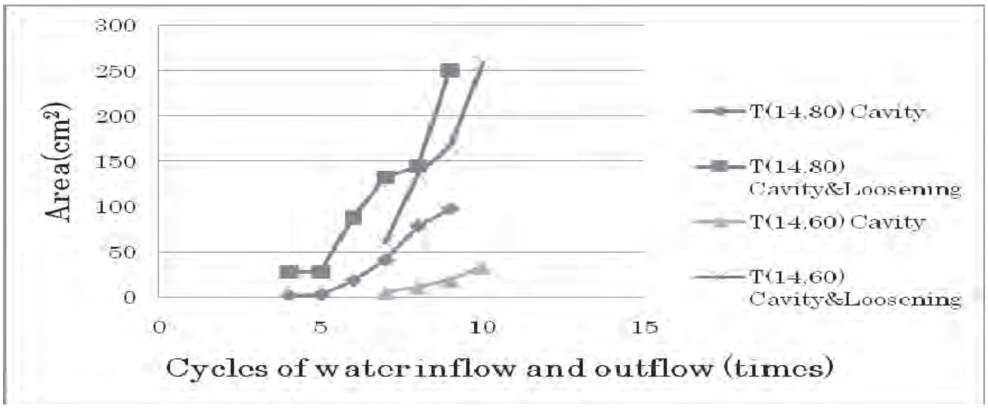

Figure 11: Process of cavity/loosening formation in different relative density

4.5 Summary

Summary of observations and comparisons between different experimental conditions is shown below.

- Weight of soil loss corresponded well to expansion of cavity.
- 1) Larger particle, 2) smaller relative density, 3) lower water content, and 4) clean uniform sand caused cavity rapidly.
- In Toyoura sand and silica sand, weight of soil loss rapidly increased at a certain cycle.

After rapid expansion of cavity was caused, large part of the ground was collapsed. This phenomenon was suggested from data of expansion of cavity and loosening area in natural sand. (Referring to Figure9)

5. ADDITIONAL EXPERIMENTS FOR EVALUATING FINES DRAINAGE

“Weight of soil loss from a cavity” was estimated from observed cavity area in photographs, and it was found that estimated soil loss from cavity was much less than measured soil loss. This result suggested that soil was drained not only from a cavity, but also from loosening. To reveal more details about soil drainage from loosening, Content ratio of fines in whole drained soil in each cycle was examined.
The examined results are shown in Figure12. Initial content ratio of fines means original content ratio of fines in natural sand. Figure12 referred that fines were drained more easily than larger particle soil even in the early stage. In addition, ratio of fines loss was increasing as the number of cycles. These two results suggested that much fines were drained from the ground which hadn’t caused a cavity yet.

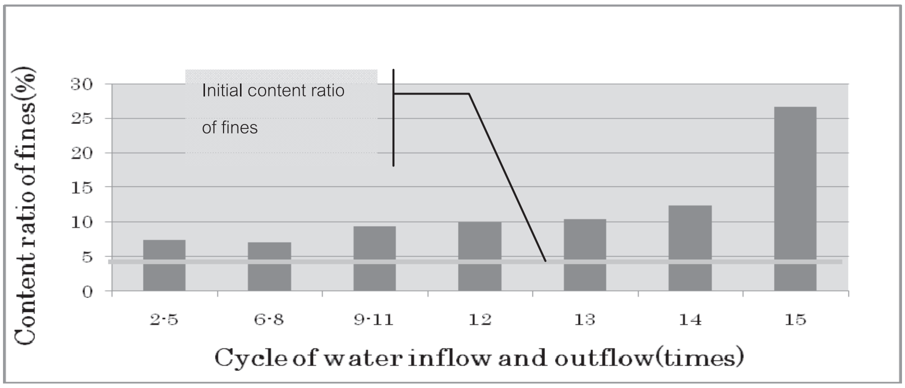

Figure 12: Change of content ratio of fines

6. PROCESS AND MECHANISM OF EXPANSION OF A CAVITY AND LOOSENING

General process of expansion of cavity and loosening is suggested like as follows.

A) Cavity is expanded due to soil collapse from a limited small area surrounding a cavity, which happens mainly after stopping water supply.
B) Deformation and cracks gradually developed in large area of the ground as cycle progress.
C) Deformation area of the ground is collapsed. This collapse area is wide and was not near to the cavity.
D) Fines drainage (Referring to chapter4)

Process (A) was observed from initial cycles. Process (B) and Process (C) often happened after cycles progressing. If once Process (B) happens, cavity expands and weight of soil loss increases very rapidly.
Then, Principal factors which caused (A) ~ (D) Processes were proposed as below.

- **Factor of Process (A) and (B): Saturation**

Due to water inflow, soil surrounding a cavity is saturated. Saturation causes increasing of pore water pressure and decreasing of effective stress. Ground collapse is almost prevented during water is supplying, because upward water seepage force due to water inflow is still working. When water supply is stopped, collapse occurs.
On the other hand, during initial cycles, ground is stable due to suction in un saturated conditions. However, due to repetition of water inflow, water content of large area of the ground increases. This rise of water content makes large part of ground unstable and causes deformation.

- **Factors of Process (C): Water seepage**

Unstable area in the ground collapses due to a downward penetration which works most strongly during water outflow.

- **Factors of Process (D): Fines drainage**

Even the ground is still stable and not caused collapses, fines are drained due to water inflow and outflow. Fines drainages causes decrease of soil density and promote generation of a cavity and loosening.

Ground situations which caused by these four factors are shown in Figure13.

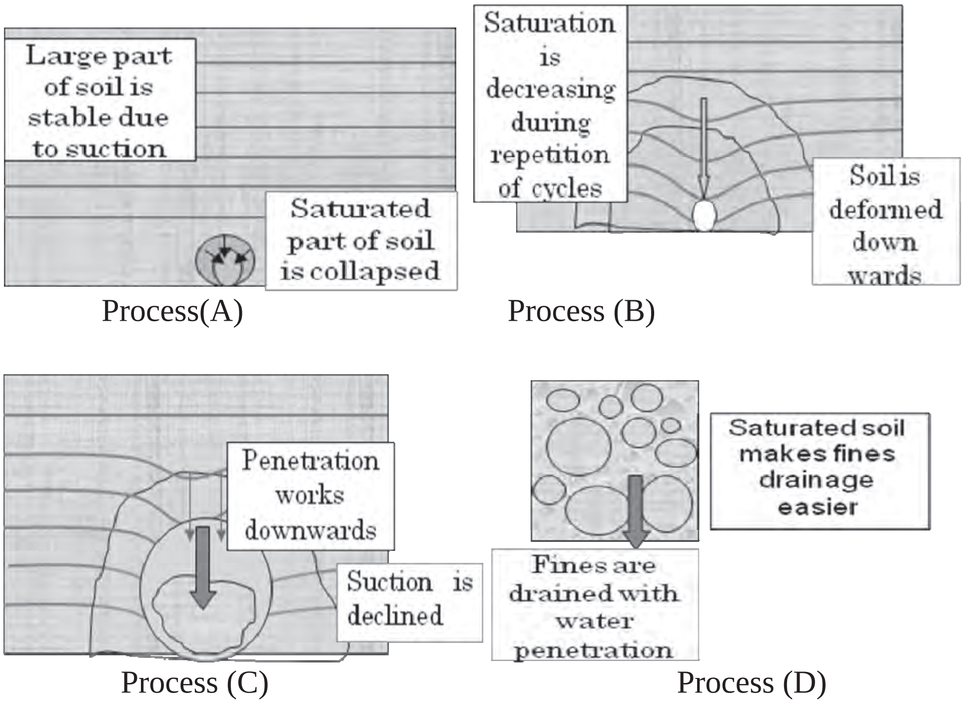

Figure 13: Ground situations caused by four main factors

7. SUMMARY AND FUTURE PLAN

Factors which cause a cavity and loosening are 1) saturation, 2) water Penetration and 3) fines drainage. Combination of these factors causes generation of cavity or loosening. In addition, it is revealed that there are some particular conditions which cause cavity and loosening very rapidly. On the basis of this research, development of effective method for investigating cavity and loosening is aimed.

REFERENCES

Kuwano, R, Yamauchi, K., Horii, T. and Kohashi, H. 2006. *Defects of sewer pipes causing cave-in's in the road,* Proc. of 6th International Symposium on New Technologies for Urban Safety of Mega Cities in Asia, Phuket, November 2006.

Kuwano, R., Horii, T. and Kohashi, H., 2006. E*valuation of loose ground surrounding a cavity due to the outflow of soil*, Proc. of 41th annual conference, Japanese Geotechnical Society, Kagoshima, 1785-1786 (in Japanese).

FOUNDATION SYSTEM ADOPTED TO CONSTRUCT THE CIVIL INFRASTRUCTURES IN KHULNA UNIVERSITY OF BANGLADESH

MD ABDUR RAZZAQUE
Deputy Chief Engineer, Khulna University
Ph.D. Student
Khulna University of Engineering & Technology (KUET)
Khulna, Bangladesh

MUHAMMED ALAMGIR
Professor
Department of Civil Engineering
Khulna University of Engineering and Technology (KUET)
Khulna, Bangladesh

ABSTRACT

This paper describes the case studies of different foundation systems adopted in Khulna University campus for the construction of civil infrastructures. The sub-soil of South-West region of Bangladesh, especially in the campus of Khulna University consists of very soft fine grained soil with significant percentage of organics. The buildings in this region are experienced huge amount of total and differential settlements while constructed on conventional shallow foundation, as a result the constructed infrastructures lost their utility and abandoned in some cases. Geotechnical engineers have been facing such difficulties for the last few decades as in the recent years the rate of construction of civil infrastructures on such ground have been increased. Based on field experiences and requirements, different types of foundation have been practiced in Khulna University Campus for the construction of Academic Building-I, II and III, Students Dormitory, Vice Chancellor's, Teachers' and Staffs' Quarter and other infrastructures. Brief accounts of the construction and the findings on the practical performance of the constructed buildings are illustrated here.

1. INTRODUCTION

Three mighty rivers - the Ganges, the Brahmaputra and the Meghna and their associated tributaries contributed very much in the formation of sub-soil profiles of Bangladesh which is situated in the lower reaches of Bengal Basin. The South-West costal region of Bangladesh contains fine grain soil deposits with the presence of significant percentage of organics. The presence of organics is due to the fact that vast of these coast regions were part of the Sundarbans, the world largest mangrove forest which extends over an area of 577,285 hectares as recorded (Vishnu & Gupta 1972, Sen & Banerjee 1984, Das & Siddiqui 1985, Naskar & Bakshi 1987, Mukharjee

1992). During the geological changes in the past, some parts of the Sundarbans were submerged by the weathered and sedimentary deposits resulting in the present peat deposits in these regions. In this region peat soils is found in different layers and in different depth. Also this soil has low bearing capacity below the peat layer. For that purpose all infrastructures are settled by large amount. Due to these inherent limitations, the foundation system for the construction of civil infrastructures is designed with special consideration and employed very carefully, which leads to high cost for the preparation of sub-structures in this region of Bangladesh.

Khulna University, located in the south-western region of Bangladesh situated along the Khulna-Satkhira Highways, just 4km from the city center, was established in 1991. The campus is situated in a low-lying topography with a very thick soft and organic soil deposits up to a great depth. The first construction of a new building named as Academic Building-I was started in the year of 1992 in the designated location as per the layout plan of the campus. This building suffered very large settlement, which leaded to rethink about the types of foundations. In a series of construction, in the recent years, several new buildings have been and/or are being constructed such as Academic Building-II, Academic Building-III, Khan Jahan Ali Hall, Khan Bahadur Ahsanullah Hall, Administrative building, Vice-chancellor's, Teacher's and staff's quarters and Mosque, in which different types of foundation systems are considered based on the sub-soil profiles, building types, purpose and the consultant preference. The performance of the constructed buildings are evaluated and discussed here.

2. LOCATION AND LAYOUT OF THE UNIVERSITY CAMPUS

Khulna University is situated in Khulna, the South-West region of Bangladesh considered as coastal zone. The University Campus is located in the western side of Khulna City Corporation (KCC) area. It covers 105 acres of land. It is beside Khulna-Satkhira highway. Many years ago it was the

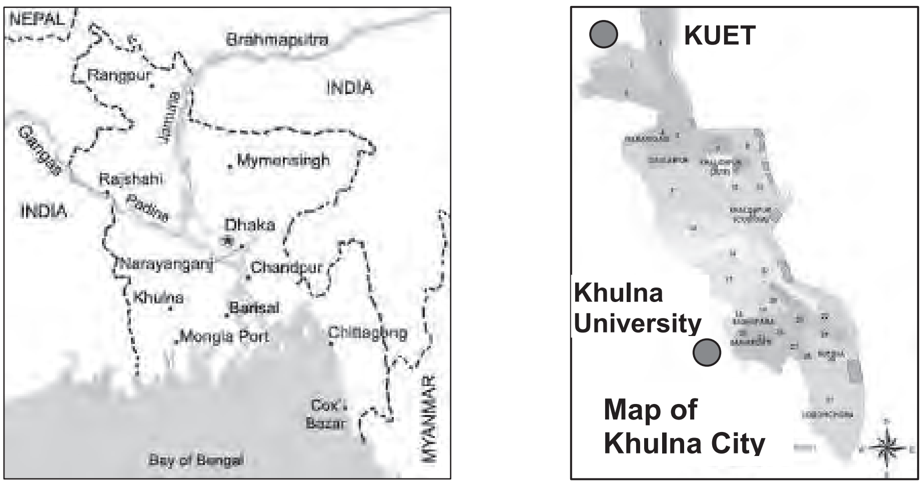

Figure 1: Location Khulna university campus in Bangladesh map and the map of Khulna city

part of the biggest mangrove forest, the Sundarbans. In course of time some part of Sundarbans were submerged by sediment deposits resulting in the present peat layer in this region. The layout of Khulna University Campus is presented in Figure 2. A lake passes through the campus and the locations of the important civil infrastructures have been constructed recently and planned to construct in future are shown in the figure and hence listed as marked from no. 1 to 14.

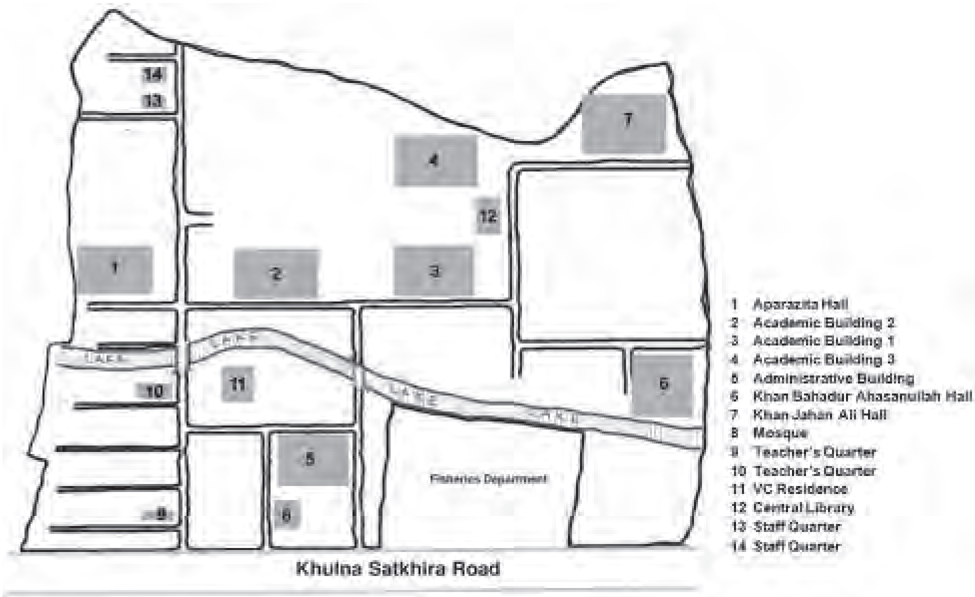

Figure 2: Layout of Khulna university campus and location of case study sites.

3. SUB-SOIL CONDITIONS

To investigate the sub-soil condition of the sites at Khulna University campus, sub-soil exploration programme was conducted by different geotechnical engineering consulting firms, soil samples were collected and tested through conventional laboratory tests (BRTC 1998, SAAR 1992 and NSE 1995). Despite the differences of sub-soil profiles and the values of soil parameters in different locations within the campus, a typical sub-soil profile is shown in Table 1, which can be treated as general one from the geotechnical viewpoint. In the sub-soil profile, it can be seen that the top soil layer about 1.5m is soft clay. Next layer depth exists from 1.5 to 7.5m i.e. 6m thick layer of dark grey organic clay with decomposed woods and vegetations. In the university campus, organic layer varies from 5 to 6m thick. Here N value is very low. In some layers it shows zero penetration resistance. Below this organic layer, at the depth of 7.5 to 19.5m, grey medium plastic clay having N values vary from 3 to 6 exists. Next to this, a layer of light grey medium compressible silt, trace fine sand is encountered at 19.5 to 23.5m depth with N value varies from 8 to 9. Here soil consistency is medium to stiff. In the bottom of the sub-soil profiles as executed, 23.5 to 30.5m depth, soil of light grey of non plastic silt, trace fine sand having N value varies from 18 to 28, is countered.

Table 1: Typical sub-soil profile at Khulna University campus

Depth (m)	Thickness (m)	Strata	Classification of Soil	N-Value
0-1.5	1.5		Light brown medium plastic CLAY (soft)	3
1.5-7.5	6.0		Dark grey organic CLAY, trace decomposed wood (very soft)	1
7.5-19.5	12.0		Grey medium plastic CLAY (Soft)	3-6
19.5-23.5	4.0		Light grey medium compressible SILT, trace fine sand. (medium stiff)	8-9
23.5-30.5	7.0		Light grey non plastic SILT, trace fine sand (medium dense)	18-28

4. DESCRIPTION OF THE ADOPTED FOUNDATION SYSTEM

There is no typical or standard or unique foundation system that can be applied for the construction of any civil infrastructures in Khulna region as well as in Khulna University Campus. Moreover, different consultants were also employed for different types of buildings for the construction at various times. Performance of foundation system already adopted in the campus, experiences in the similar situation, sub-soil condition in the particular site, super-structures requirements and finally consultant preference, lead to select the foundation type, those are described in the following sections.

4.1 Sand cushion with mat foundation

In Khulna University campus, the first major construction works was started in 1992 with the adopt of mat foundation system with sand cushion to build Academic building –I, a four storied building as shown in Figure 3. The schematic diagram of the foundation system is presented in Figure 4. From this figure it can be seen that the top soft soils layer was removed up to 4.5m depth measured from the existing ground surface. Here peat deposit situated at 1.5 to 4.5m from top was removed by excavation. Then excavated area was refilled by compacted sand. Two types of sands having the fineness modulus (FM) of 1.2 and 2.2 were mixed properly at a ratio of 1:1. The filling sands were compacted in layers and the required degree of compaction was achieved. At the top of the filled and compacted sand layer, several mat foundations were provided. The thickness of the mat foundation varies from 300 to 450mm. At the top of the mat, a foundation beam was provided to reduce mat thickness. Despite the consideration of such special precaution in the foundation, the building suffered from very large settlement which mostly occurred during the first three years after the completion of the building. The long term measurement showed that the building was settled as much as nearly 800mm. However, it was found that settlement is uniform, as a result there was no damage in the building although the pipe lines and other utility services hampered due to large settlement and needed to replace and reconstruct to ensure the proper function of the system, the details are given in Razzaque & Alamgir (1999). Similar foundation systems were also employed to construct the buildings of Khan Jahan Ali Hall and Associate Professor Quarter.

Figure 3: Pictorial view of Academic Building-I

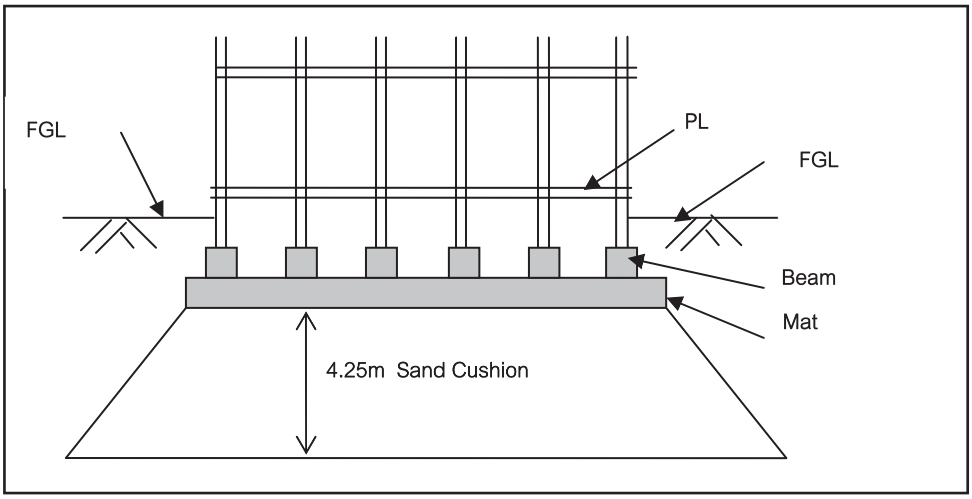

Figure 4: Schematic diagram of sand cushion with mat foundation

4.2 Floating foundation

Academic Building–I showed huge settlement due to the implementation of mat foundation with a sand cushion. As a result the university authority and the consultant looked for alternative solution to minimize the settlement while constructing the Academic Building-II. After looking on the various possible alternatives, finally consultant decided to use floating (compensated) foundation, hence designed the foundation and the building was constructed accordingly as shown in Figure 5. The schematic diagram of the foundation system used for the construction of this building is also presented in Figure 6.

Figure 5: Pictorial view of Academic Bldg.-II

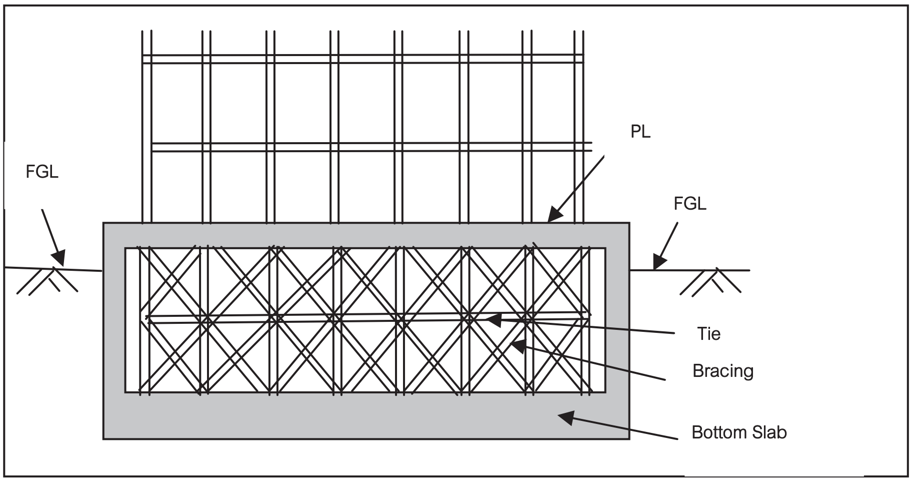

Figure 6: Schematic diagram of floating foundation- Academic Bldg-II

Based on the design requirements, the sub-soil was excavated and hence removed till the depth of 4.5m measured from original ground level. Due to the excavation till the designated depth, the peat deposits were removed from the site. Then a concrete box which has the inner clear space of 5.2m was provided. In the bottom, 450mm thick base was constructed. Side wall is 300 to 200 mm from bottom to top. Top slab is 125mm thick acted as ground floor. For water protection outside of the concrete box three layers of Hessian cloth with tar was placed. Inside the box a height 5.2m is available which stabilized by providing column, concrete bracing and concrete tie inside the foundation box (SAL 1996, Hossain & Razzaque 1999). To provide bracing and tie, the section of column was reduced, so that the box was not tilted. Top of the box is the Plinth level of the building. The settlement of this building was observed as insignificant, which is about

20mm. Similar type of foundation system was also used in the construction of the Female student's dormitory named as Aparajita Hall.

4.3 Pile foundation

Pile foundation is commonly practiced in Bangladesh for the construction of buildings in the soft soil region and even in moderate to hard soil for high rise building. In Khulna, since there is an existence of very soft compressible soil layer and peat deposits in the upper layer, the pile constructed in this region is subjected to negative skin friction due to the faster compression of these compressible upper layers surrounding the pile.

Figure 7: Pictorial view Admin. Building

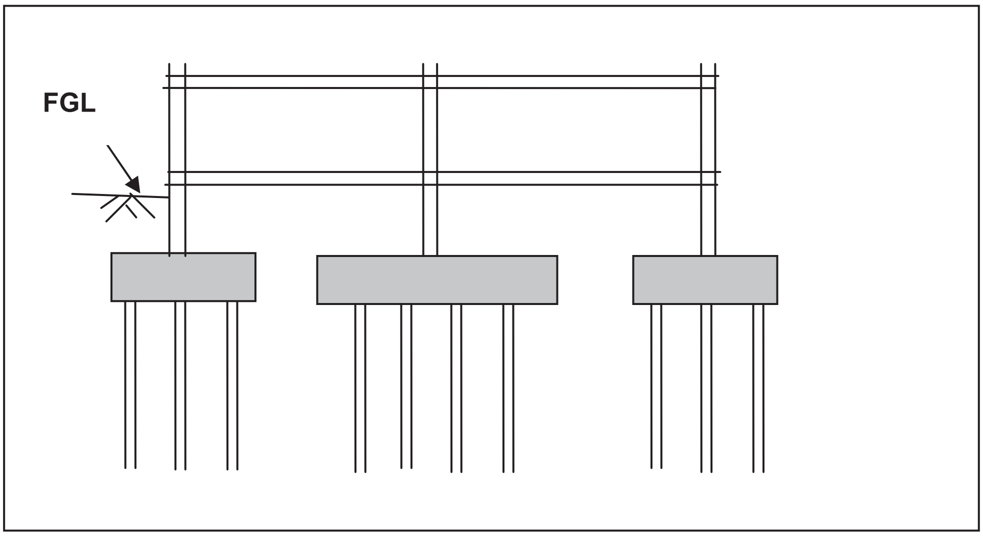

Figure 8: Pile foundation used for the construction of Admin Building

Table 2: Information of pile specification used in different buildings

Sl No	Name of the Buildings	Plinth Area (m^2)	Storied	Pile length (m)	Pile Diameter (mm)	Design load (Tons)
1.	K.B. Ahsanullah Hall	581	4	26	450	55
2.	Administrative Bldg.	1,488	4	24	450	40
3.	Asst. Prof. Quarter	242	4	30	500	53
4.	Staff Quarter	223	4	30	450	46
5.	Staff Quarter	316	4	30	500	50
6.	Lecturer Quarter	214	4	30	500	44
7.	Professor Quarter	218	4	30	500	46
8.	Central Mosque	1,115	3	26	500	38
9.	Academic Building III	10,446	4	26	450	40
10.	Central Library	5,562	4	27	500	45

In the Khulna University Campus, the first pile foundation was employed for the construction of student's dormitory named as Khan Bahadur Ahsanullah Hall. This is a four storied building constructed on cast *in-situ* bored pile made of Reinforced Cement Concrete (RCC) having cylindrical shape of diameter 450mm and length 24m. In the design, the possible development of skin friction due to the compression of surrounding soft soil layers and peat deposits and its impacts on the reduction of pile capacity was considered. One of the constructed buildings on pile foundation in the campus is shown in Figure 7. The piles are configured in a group with RCC pile cap based on the layout of the locations of different columns of the buildings and loads as shown in Figure 8. Later, additional nine buildings named as Administrative Building, Academic Building-III, Central Library, Central Mosque, Professor's, Assistant Professor's, Lecturer Quarters, Staff Quarter-I and Staff Quarter-II were constructed and planned to construct using pile foundation. Table 2 shows the comparison of various aspects such as dimension and design load of the pile foundation used and/or planned for the construction of different buildings, till now ten buildings, in the Khulna University campus for pile foundation. Although pile types, materials and construction process are similar, there dimensions and capacity are different. The plinth areas of the buildings vary from 214 to 10,446 sq.m, length, diameter and designed load of pile foundation are varied from 24 to 30m, 450 to 500mm, 38 to 55 Tons, respectively. The actual pile capacity were also established conducting pile load test after the installation of pile. Sufficient days were allowed in between the pile construction and load test due to the remolding influence of the clayey soil.

4.4 Sand cushion with continuous footing

Some buildings were also constructed using spread footing i.e. Continuous type Reinforced Cement Concrete (RCC) footing resting on 4.25m compacted filling sand cushion. One of the such buildings is shown in Figure 9, the Vice Chancellor's Quarter. The building was constructed through load bearing wall resting on the footing. Sub-soils till the depth around 4.5m from the existing ground surface were excavated and removed and then filled by sand in layers ensuring proper compaction to provide a sand cushion of 4.25m thick. On the top of sand cushion, continuous footing by RCC was constructed over which load bearing wall of 380mm below and 250mm above the ground level were provided. The performance of such foundation system is found satisfactory.

Figure 9: Vice Chancellor's quarter

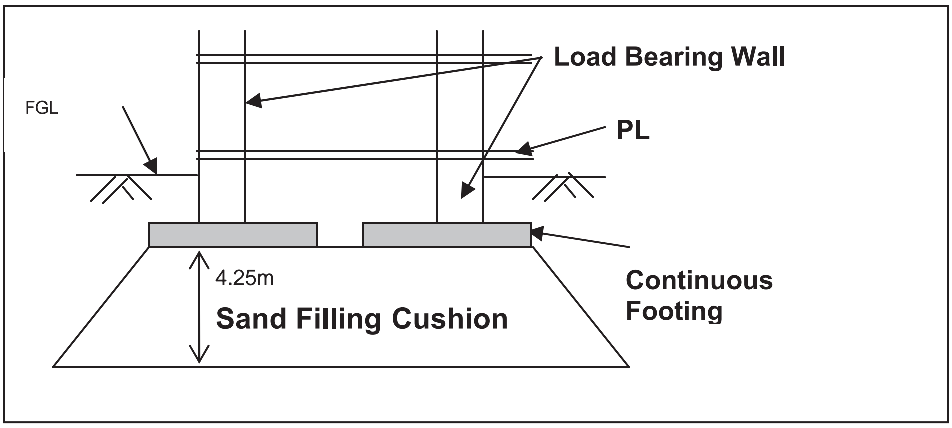

Figure 10: Sand cushion with continuous footing and load bearing wall

In Khulna University campus, very simple foundation is also used for the construction of one to two storied buildings despite the existence of very soft clayey soil deposition. One of such foundation system is continuous Brick Wall Footing, known as brick foundation. For lower bearing capacity higher width of brick wall is required at the base which gradually decreases as it reached to plinth level and finally ended with 250mm thick brick wall. Khulna University Mosque as shown in Figure 11 was constructed on such foundation and the schematic diagram of the employed foundation system is shown in Figure 12. Here, the bottom width of the foundation is 1.5m. Despite the implementation of simple foundation mostly used in low-rise building, it is observed that the performance of the foundation is quite satisfactory.

Figure 11: Mosque at Khulna University

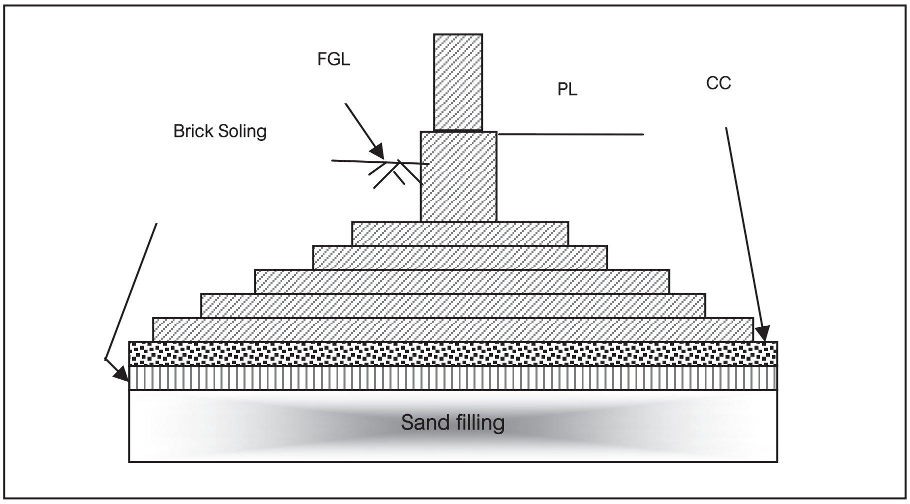

Figure 12: Strip footing constructed by continuous brick wall

5. DISCUSSION

In Khulna University campus different types of building was constructed with various foundation system based on soil conditions, super-structural requirements, client's choice and consultant preference. Despite the similarity of sub-soil conditions, super-structures types and requirements, different types of foundation systems have already been constructed and planned as described in the above sections. From the illustration it is revealed that the settlement is quite large while mat foundation in conjunction with soil replacement with a well compacted sand cushion although differential settlement was not noticed and there no cracks observed in the buildings. However, due to very large settlement which is as much as about 800mm, the utility appliances lost their serviceability and needed to replace. However, it was realized that such foundation technique is easier than other counterparts to satisfy fundamental criterion for the construction of buildings in the similar sub-soil conditions. Significant amount of settlements were also observed while continuous footing made of Reinforced Cement Concrete (RCC) and Brick masonry resting on sand cushion with varying thickness were used for the construction of even one or two storied building.

To overcome the inherent limitations of the shallow foundation (except floating foundation), pile foundations have been adopted in ten buildings. Most of them are four storied except central mosque which will be a three storied structure. It is observed that pile foundation served better and fulfilled the requirements despite higher cost than the shallow foundation counterpart. It is also observed that the floating foundation also performed well and the settlement remains within the tolerable limit.

In Khulna University Campus, as an alternative of conventional foundation system (e.g. pile foundation), ground improvement technique may be adopted to examine the applicability in such compressible ground condition. In this region, sand compaction piles with a diameter of 200 to 300mm and the depth of 6 to 8m were constructed successfully in several projects and the performance are satisfactory. In some cases, geosynthetics was also used successfully to reinforce the ground under shallow foundation (Alamgir & Chowdhury 20003; Haque et al. 2001). In future, instead of conventional pile foundation, ground improvement techniques suitable for the sub-soil conditions exist in Khulna University Campus may be considered to overcome the inherent limitations of conventional foundation.

6. CONCLUSION

Special care need to be taken while choosing a foundation system to construct civil infrastructures in the site of soft compressible ground with the existence of peat deposits, like Khulna University campus. It is not proper to implement a unique system considering general sub-soil profile, appropriate foundation system might be chosen based on the soil conditions in the specific location, type of superstructures and relevant requirements. Field investigation shows that the rate and amount of settlement is insignificant while Pile foundation and Floating foundation were used. However, on the other hand mat foundation with sand cushion resulting very large total settlement and damaged the utility fittings, although it is less expensive and easy to construct with locally available logistics. Ground improvement technique such as sand compaction piles, cement columns, etc. may be adopted to judge the applicability of such techniques in this sub-soil conditions.

ACKNOWLEDGEMENT

The authors express their deep gratitude to the Engineering Section of Khulna University to provide required information on the design and construction of Civil Infrastructures illustrated in this paper.

REFERENCES

Alamgir, M. and Chowdhury, K.H. 2003. Ground Improvement Methods Recently Practiced to Solve the Geotechnical Engineering Problems in Bangladesh. *Proc. Fifth International Conference on Case Histories in Geotechnical Engineering,* April 13-17, 2004, New York.

BRTC 1988. *Soil investigation and constructing building foundation repost of proposed Khulna University of selected Gollamary area*. Bureau of Research, Testing and consultancy (BRTC), BUET, Dhaka.

Das, S. and Siddiqui, N.A. 1985. The mangroves and mangrove forests of Bangladesh, Mangrove silviculture division Bullatin No. 2.

Haque, M.A., Alamgir, M., Salim, M. and Kabir, M.H. 2001. Performance of Geotextile-Reinforced Shallow Foundations used in Bangladesh. *Proc. International Seminar on Earth Reinforcement (IS Kyushu 2001)*, 16-18 Nov. 2001, Fukuoka, Japan, pp.565-570.

Hossain, M.M., and Razzaque, M. A., 1999. Structural Advantages of Floating foundation over traditional mat foundation for soft clay: A case study. *Proc. Pre-conference symposium or Ground improvement and Geosynthetics*. 5 Nov, 1999, Bangkok. pp. 201-210.

Mukherjee, B.B 1992. Quaternary pollen Analysis as a possible indicator of prehistoric Agriculture in the Deltaic part of West Bengal, *J. Playnol,* Vol.8 : 144-51.

Naskar, K.R. and Guha Bakshi, D.N. 1987. *Mangrove swamps of the Sundarbans.*

NSE 1995. *Subsoil Investigation for proposed 4 storied 2nd Academic Building at Khulna University*., National Soil Engineering, Dhaka.

Razzaque, M.A. and Alamgir, M. 1999. Long-term settlement observation of a building in a peat deposits of Bangladesh. *Proc. of the Intl. Conf. on Civil & Environmental Engineering – New Frontiers and Challenges,* 8-12 November 1999, Bangkok. Vol.2, pp.III-85 to IV-94.

SAAR 1992. *Consultants reports about the design and construction of Academic Building-I at Khulna University*, SAAR Association Ltd, Dhaka.

Sen, P. and Banerjee, M. 1984. *On the occurrence of Raptilian Remnants in the peat bed of Barrackpore, 24-Parganas*, West Bengal, *Paleobot. Soc. Ind*. Vol. 29: 47-51.

SAL 1996. *Consultants reports about the design and construction of Academic Building-II at Khulna University*, Shaheedullah and Associates Limited, Dhaka.

Vishnu M. and Gupta, H.P. 1972. Pollen Analysis study of Quaternary Deposit in the Bangla Basin, *Paleobotanist,* vol, 19: 297-306.

A REPRESENTATION OF MOTORBIKE DOMINATED TRAFFIC USING CELLULAR AUTOMATA

HOANG THUY LINH,
MARC MISKA, and MASAO KUWAHARA
Traffic Engineering Laboratory,
Department of Civil Engineering,
The University of Tokyo, Japan
ht-linh@iis.u-tokyo.ac.jp

ABSTRACT

This study aims to develop a network scale, microscopic simulation model for mixed traffic, where motorbikes dominate the traffic composition (more than 70%) as in Vietnam, Malaysia, or Thailand. Therefore, cellular automata, with modified cell size, time step and rule set are used to simulate three different vehicle classes (motorbike, car and bus). Surrounding vehicles (type, speed, distance) are considerably affecting the motorbikes' behavior, they have more freedom in movements, and hence, can continue their way, while other modes already came to a stop. To capture these special behavior patterns, a utility function is introduced, to determine preference positions and movements. A first prototype of the model is implemented to investigate queuing and dispersion behavior of mixed traffic at an intersection approach. Future work will extend the model to network scale

1. INTRODUCTION

Up to now, large numbers of traffic simulation models have been developed. However, those are mainly for lane-based traffic, in which vehicles remain in a certain restricted area where lateral movements are only considered during lane changes. This is not applicable for motorbike dominated traffic of some developing countries such as Vietnam, Thailand, etc. In these countries, the share of motorbikes in the traffic stream is more than 70% and link utilization is not lane-based.

Motorbikes can travel with more freedom than other modes, therefore, they can advance using small spaces between vehicles. Besides, being the most unsafe mode in the stream, their behavior is strongly affected by surrounding vehicles. These circumstances cause differences in road space utilization between normal lane-based traffic and non lane-based traffic (Figure 1).

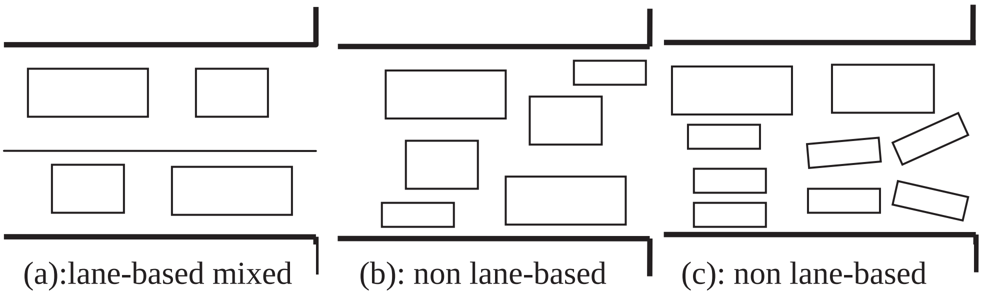

(a):lane-based mixed traffic | (b): non lane-based mixed traffic | (c): non lane-based mixed traffic

Figure 1: Mixed traffic types

Hence, this study aims to develop a network scale model using Cellular Automata method (CA); to represent this type of traffic in order to investigate possible effects and to evaluate ITS measures in those countries.

2. SIMULATING MIXED TRAFFIC

Conventionally, traffic models are divided into microscopic, mesoscopic, and macroscopic models. The major difference is the detail of how vehicles and their drivers are represented. In macroscopic models, single vehicles do not exist, and instead, a traffic stream is considered with dynamics based on a fundamental diagram, describing the relationships between speed, flow and density. On the other hand, microscopic models deal with individual vehicle driver combinations and the dynamics are based on individual behavior. Most commonly, the behavior is incorporated into two separate models for car following and lane changing. As the name suggests, mesoscopic models are something between the other two models and exist and various set-ups. However, usually they represent single vehicles or platoons (microscopic), which move according to macroscopic relationships. Since the specifics of mixed traffic - are hard to describe in macroscopic terms - that is without extensive measurements a microscopic approach has been chosen. CA models belong to microscopic approaches, using crude microscopic parameters to obtain correct macroscopic patterns. Therefore, the CA approach - a computationally efficient microscopic model (Maerivoet 2005) - is chosen for this study.

2.1. Network representation

The cellular automaton is a well known mathematical concept and used in many researches on traffic flow phenomena. The CA model is a dynamic, discrete system in space and time. Road space is discretized into a lattice of cells and each cell is either empty or occupied by a vehicle. In this system, vehicles move by hopping from cell to cell based on a rule set, reflecting car – following and lane changing behavior (see Figure 2). Therefore CA models are sometimes called “particle hopping models”.

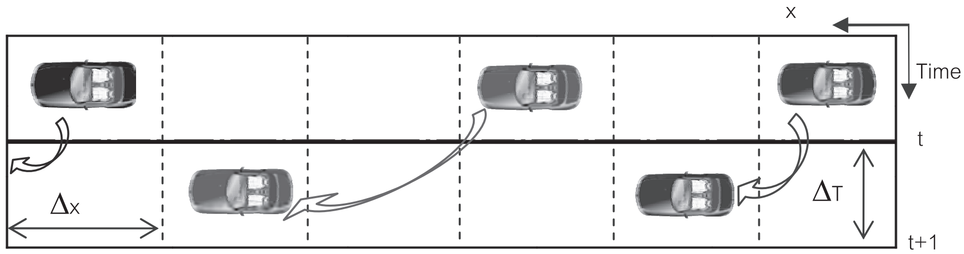

Figure 2: Schematic diagram of the operation of a single-lane traffic CA

Applying above scheme to the mixed traffic situation, we chose a 2D lattice which is a square grid of 0.25mx0.25m (see Figure 3) for a unidirectional link, 3.75m wide and 400m long. The time step is 1/20 second. Therefore the increment speed is 5m/s. Each line paralleling to road direction is defined as a “virtual lane”.

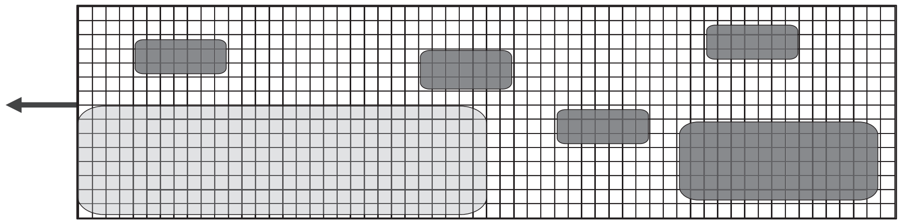

Figure 3: Illustration of Road stretch with 2D grid

Traversing through the intersection, vehicles are assumed to be bounded within a “virtual link” - marked by two green curves in Figure 4a. The virtual link will be straightened and discretized into a 2D grid as a normal road stretch, in this case the left turning grid. It will be connected with the grids of in-going and out-going links (see Figure 4b). The movement of traffic on this grid is similar to that on a link. Now to determine the actual situation inside the intersection, the traffic flow on each turning grid is projected onto the intersection grid. See Figure 4c as an example.

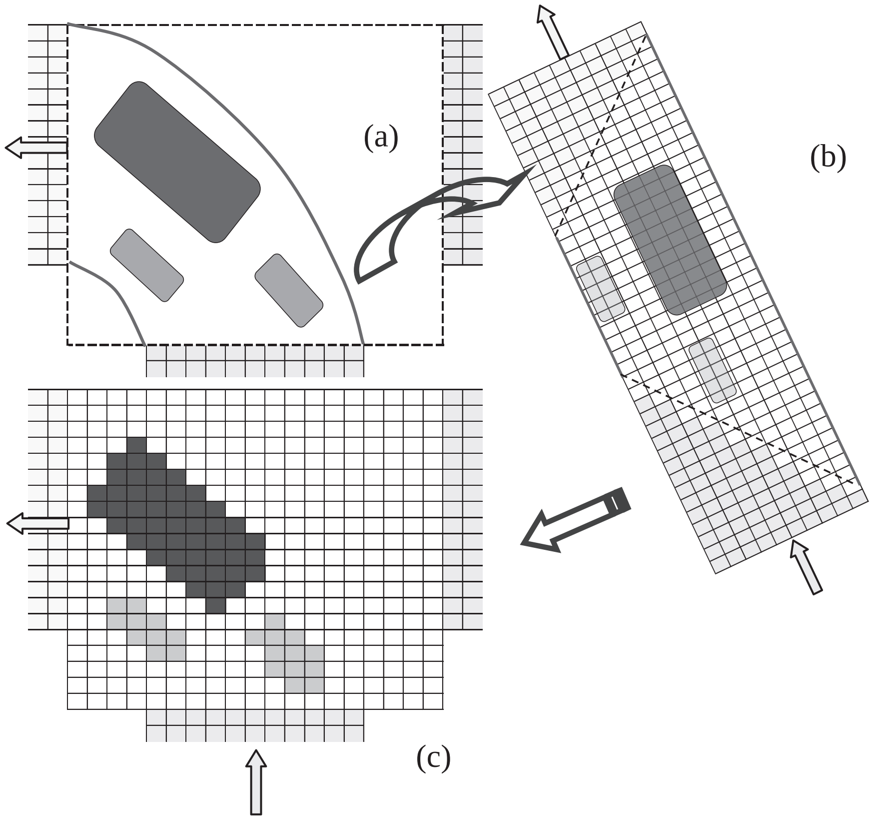

Figure 4: Illustration of Intersection and traversing grid

2.2. Representative vehicle classes

Our modified CA model is developed for the mixed traffic with three representative vehicle-classes which are significantly different in their specifications, such as length, width and speed. Table 1 shows the vehicle class specification in CA model units.

Table 1: Parameters of model

Vehicle Type	Maximum speed		Dimension			
	cells/time step	m/s	Width		Length	
			cells	m	cells	m
Motorbike	3	15	3	0.75	8	2
Car	6	30	6	1.5	15	3.75
Bus	4	20	10	2.5	40	10

2.3. Driving behavior

There has been research on behavior of mixed traffic, and we have integrated findings from studies by Hsu et al. 2003 and Hien 2007 into the model. Those findings were:

- Cars and bus at desired speed travel on the left road side

- Motorbikes at low speed prefer the right road side and at high speed they prefer middle to left road side
- In congestion, buses, cars and motorbikes can be at any position in lateral direction
- Motorbikes do not have preference either following buses or cars or followed by buses or cars
- At intersection approach, the vehicles have mandatory lane changing therefore they will make their effort to be on the desired position to perform the turn.
- For each turning direction through the intersection, vehicles are assumed to travel in an virtual
- First vehicles will traverse though intersection with higher speed than the followers.

In opposite to traditional CA models, we substituted the rule set for a psychological driving logic approach to describe the drivers' decision making process. This includes the following steps:

- Scanning driving environment
- Determining the safe speed
- Determining possible direction

Scanning driving environment

Here, the driver scans his visible area to get information of surrounding vehicles: gap distance, speed and type (Figure 5).

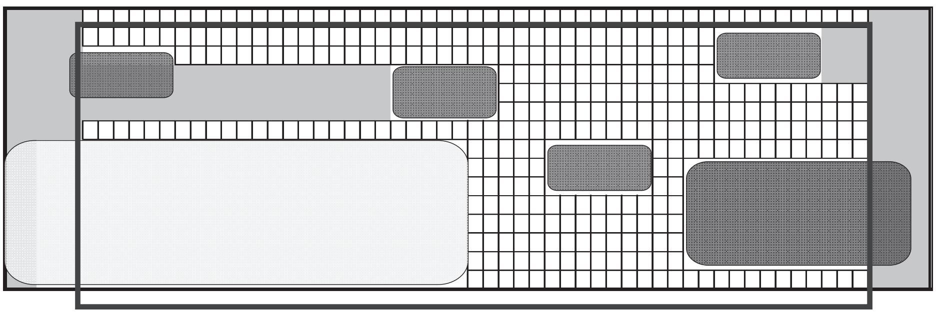

Figure 5: Scan area

Determining the safe speed

Based on the driving environment, he or she will determine his or her safe speed - maximum speed in order to avoid collision with other vehicles. The safe speeds are representations of the gap acceptances to the left, straight or right side of the vehicle (Figure 6).

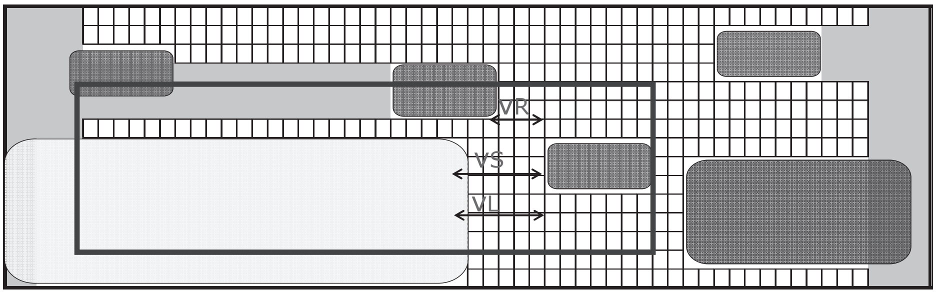

Figure 6: Determining the safe speed

Determining possible direction

Changing direction to the left, or right depends on the preferred "virtual lane". This lane is determined by a utility function taking into account a set of possible reasons for lane changing. The next section will describe this function in more detail.

Above process is represented in CA model as one evolution of each vehicle in the traffic stream to the next time step. Within the scope of this model, the term "virtual lane" changing, which is used instead of lane-changing, explains any change in the lateral position of a vehicle. At every time step, the longitudinal position *x* is increased by the vehicle's speed calculated in the current step *t*.

$$x(t) = x(t-1) + v(t) \tag{1}$$

The lateral position *y* is adjusted to the left or right by a maximum of one cell of the vehicle's current position, with the boundary condition that the vehicle does not leave the road stretch, determined by the lane marking.

$$y(t) = \begin{cases} \min(y(t-1) + vehicle's\ width; road\ \ width) & if \quad move\ to\ left \\ \max(y(t-1) - vehicle's\ width; 0) & if \quad move\ to\ right \\ y(t-1) & if \quad go\ straight \end{cases} \tag{2}$$

Formula (1) describes the longitudinal position where:

$$(*): v(t) = \max(v_{left}^{safe} \vee v_{right}^{safe} \vee v_{straight}^{safe}, 0)$$

$v_{left}^{safe}, v_{right}^{safe}, v_{straight}^{safe}$: Speed if vehicle moves to the left, right side or straight, respectively.

2.4. Utility function and decision making rule

The utility function shows the level of satisfaction a driver perceives at every "virtual lane" at a certain time; taking all the possible reasons of lane changing as its parameters to describe how the driver is attracted by each position over the cross section. Virtual lane changing behavior is performed based on two parts, which are the reasons to change and the safety criteria (Nagel 2002). Both are differentiated between car/bus and motorbike (see assumptions in section 2.3).

We assume that the decision of choosing a lateral position of motorbikes depends on all the vehicles in his front and back within his observable area, and also depends on the distance to the next desired turning point (Gipps 1986). Within a road stretch (without any effect of bus stop, intersection…), in free flow traffic, motorbike drivers can freely use all road space. However, from observation, motorbike drivers do not like following big, slow vehicles (buses, cars). In congestion, vehicles attempt to use every road space or in other words, they are stimulated by free space in front. Vehicles want to adjust their lateral position when they do not like following the leading vehicles or find appropriate free space. But those changes are not necessary to be performed – discretionary lane changing. While at an intersection approach, both with and without clear turning split, the turning direction forces the driver to change lane from a certain distance to the intersection – mandatory lane changing.

Therefore, the utility function contains variables such as gap distance, type and speed of those observed vehicles. Further, depending on the subject vehicle type and speed, the effect of the desired lateral position in the link and intersection approach is also taken into account by the lane factor and turning factor respectively. Variables of this function and their explained factors are shown in Table 2.

Table 2: Variables and factors of Utility function

Variable	Factor
Speed, vehicle type	Lane_factor
Front vehicle speed+gap; type	Front_factor
Back vehicle speed+gap; type	Back_factor
Turning direction	Turning_factor

The ranges or boundaries in which each factor varies due to personal preferences is still to be determined (see future work) and is for now set according to personal perception. The utility function can be written as:

$$
\begin{aligned}
U(i) = \{ & (front\_gap + front\_speed) \times Front\_factor \\
& + (back\_gap - back\_speed) \times Back\_factor \} \\
& \times Lane\_factor \times Turning\_factor
\end{aligned}
$$

Where $U(i)$: Utility of virtual lane i

$$P \text{ is a preferred lane} \Leftrightarrow \forall\, U(P \pm k) \geq U(i)$$

Where:

k: integer; k= 0÷vehicle' width ("+": range at the left side; and "-": rang at the right side)

i: current virtual lane

To make the contents of the utility function easier accessible let us consider the situation at the bottom of Figure 7. A motorbike with the speed of 2 cells /time-step evaluates first the attractiveness of each virtual lane by the gap size, incorporating the speed of leading vehicles (Figure 7a). Since following a bus or car is less desirable for the motorbike than driving among other motorbikes or without a leader, the utility function get adjusted on these lanes (see Figure 7b). Additional, in this situation, the motorbikes get followed by a bus. Feeling unease about the situation as the weakest member of the traffic stream, the utility gets lowered in the width of the bus (Figure 7c), resulting in the final shape of the cross section utility (see Figure 7d).

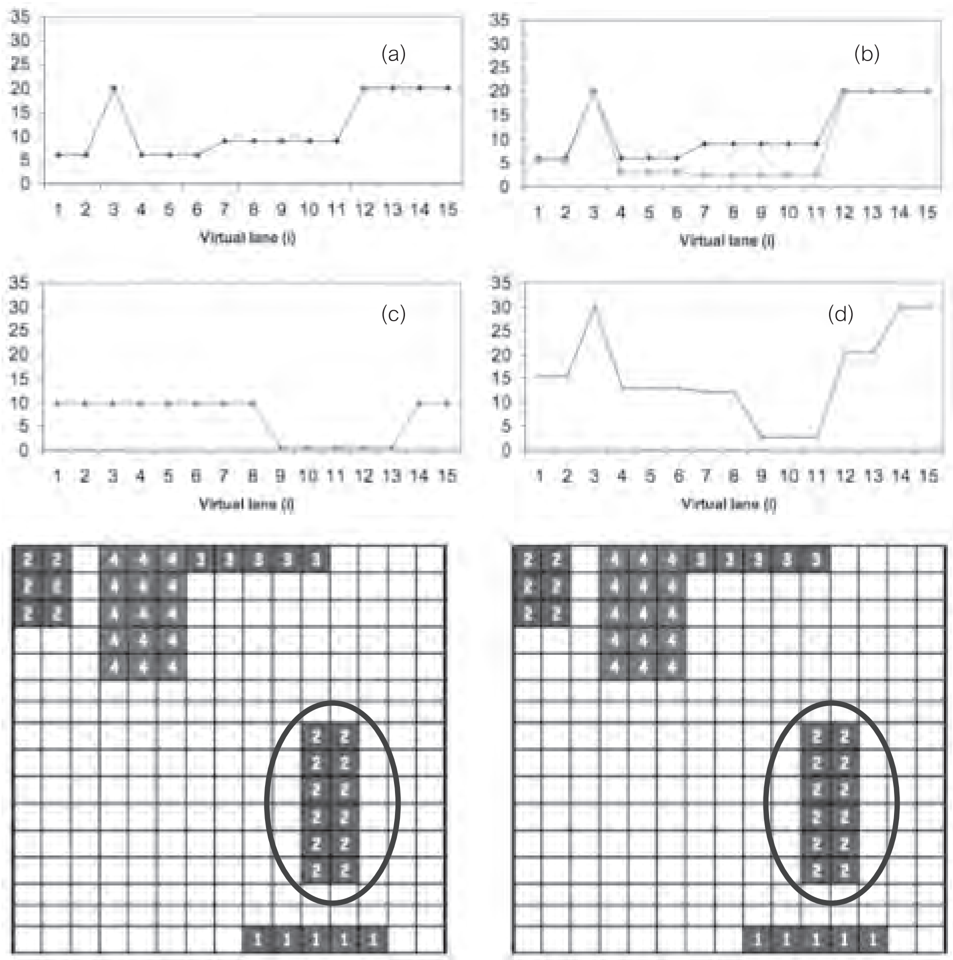

Figure 7: Illustration of Utility Function

The vehicle will choose the position where not only the utilities are higher than in current position but also the number of consecutive higher utility cells must not be smaller than the vehicle's width. The preference lane is the most left or most right boundary of those cells. In this example, the driver will set the new preferred lane to 15 and hence try to move to the right inside the road stretch.

3. PROTOTYPE APPLICATION AND FUTURE WORK

To investigate the possibilities of such a model, we have implemented a prototype. This first application shows already realistic driving behavior among all three vehicle types and is the basis for further developments (see Figure 9).

Figure 9: Model prototype

All in all, we could proof the feasibility of such a model and in the next step it will be calibrated and validated with video footage from Vietnam.

REFERENCES

Gipps, P.G., 'A model for structure of Lane changing decisions', Transport Research 20B No. 5, pp. 403-414, 1986

Hien Nguyen, Frank Montgomery, Patterns of discharge flow at traffic signals and implications in motorcycle traffic, Journal of the Eastern Asia Society for Transportation Studies, Vol. 7, 2007

Hsu, Tien-Pen, Ahmad Farhan Mohd Sadullah, Nguyen Xuan Dao, A comparison study on motorcycle traffic development in some Asian countries – case of Taiwan, Malaysia and Vietnam, The Eastern Asia Society for Transportation Studies (EASTS) 2003

Lawrence W. LAN, Chiung-Wen Chang, Motorbike's moving behavior in mixed traffic: particle-hopping model with cellular automata, Journal of the Eastern Asia Society for Transportation Studies, Vol.5, October, 2003

Maerivoet Sven, Bart De Moor, Cellular Automata Models of Road Traffic, http://phdsven.dyns.cx, 2005

Nagel Kai, Cellular Automata Models for Transportation Applications, S. Bandini, B. Chopard, and M. Tomassini (Eds.): ACRI 2002, LNCS 2493, pp. 20–31, 2002.

Wenzhou Jin, Yingli Zheng, Jiang Li, Microscopic Simulation of Traffic Flow at Signalized Intersection Based on Cellular Automata, http://ieeexplore.ieee.org/stamp/stamp.jsp?arnumber=00830635

DEVELOPMENT OF PEDESTRIAN SIMULATOR FOR TRANSFER CENTER OPERATION ANALYSIS

MYUNG-JOO HAN, DAISIK NAM
YOUNG-EUN KANG and YOUNG-IHN LEE
Department of Environmental Planning
Graduate School of Environmental Studies
Seoul National University, Republic of Korea
nds1027@snu.ac.kr

ABSTRACT

A pedestrian simulator for analysis of transfer center operations was developed using novel pedestrian behavior algorithms. We developed a pedestrian behavior algorithm (including an obstacle avoidance behavior algorithm) and a transit center user behavior algorithm (including a transit facility use behavior algorithm that included transit boarding and alighting behavior). To evaluate the operational efficiency of the design of a new transit center and improve the transit center plan, this study used measures of effectiveness (MOE) for pedestrians, the facility, and the simulation. In addition, a prototype was developed to verify the adequacy of the pedestrian behavior and facility use behavior algorithms.

1. INTRODUCTION

1.1 Background and Purpose of the Study

The efficiency of the interconnection systems between means of transportation in current mass transportation transit systems (MTTS) is often inadequate. Long transit times may be required because MTTS have complicated pedestrian traffic lines and there is insufficient information about the facilities in the system (e.g., transit and convenience facilities).

Consequently, there are plans to construct a transit center that will minimize transit time by improving user convenience. However, the current design standards for such a transit center are inadequate. Therefore it is difficult to evaluate transit center design effectively. To improve the design and evaluate the operational plans for a new transit center, an analysis of pedestrian characteristics is required. Accordingly, this study develops algorithms to analyze pedestrian behavior at a microscopic level, including such behaviors as movement, facility usage, boarding and alighting. Such algorithms will enable the evaluation of the operational efficiency of a new transit center design, enable improvements to the design of the transit center, and allow the development of an operation analysis program.

1.2. Scope of the Study

The major objective of this study is to develop pedestrian behavior algorithms for such behaviors as obstacle avoidance, facility use, as well as boarding and alighting, that will allow analysis of transit center operations at the microscopic level.

Thus, the scope of this study includes:

- Development of an obstacle avoidance behavior algorithm
- Development of a transit facility use behavior algorithm
- Development of a means of assessing transit boarding and alighting behaviors
- Development of an operation analysis program (i.e., a pedestrian simulator)
- Presentation of the results of the study

2. STATE-OF-THE-ART OF PEDESTRIAN BEHAVIOR MODELING

2.1. Pedestrian Behavior Model

It is relatively easy to analyze the movement patterns of vehicles since they are required to drive along specific lanes and follow specified regulations, but there are no similar physical or behavioral regulation systems for pedestrians. In addition, analyzing the patterns and regularity of pedestrian behavior is quite difficult because various behavior patterns change according to the pedestrian's mental state and the purpose of their walking behavior.

Few studies have reported on research in this area. J. Fruin (1991) studied pedestrian behavior as it reflected pedestrian traffic flow characteristics and pedestrian mental factors. Another study KHCM (2004), in Seoul, Republic of Korea, analyzed pedestrian behavior and provided pedestrian facility evaluation criteria by examining pedestrian traffic flow characteristics. That study produced a macroscopic level analysis of pedestrian characteristics including assessment of pedestrian speed, density, and volume. However, none of the available pedestrian traffic flow characteristic analyses reflect pedestrian behavior at the microscopic level, such as the examination of sequential behavioral processes used in object recognition and subsequent reaction.

2.2. Pedestrian Simulator Development Cases

The operation analysis program discussed here includes a pedestrian simulator function that reflects facility use and pedestrian behavior algorithms. To date, no local technologies have been developed to simulate the interactions of pedestrian behavior, transportation links, and transit systems. However, there have been a few foreign studies and some commercially available software packages have been developed. SIMPED is a pedestrian simulator model developed in the Netherlands, which analyzes various behaviors generated by pedestrian movements and the interactions between pedestrians. SIMWALK, developed by Savannah Simulations AG, Herrliberg, Switzerland, is a pedestrian simulation software program that may be used to simulate pedestrian flows by traffic planners, urban professionals, and safety managers, and to evaluate facility features. This program analyzes such aspects as walking behavior possibilities, pedestrian comfort, and traffic congestion in various environments. Another pedestrian simulation program, the Uban Analytics Framework (UAF) software from Quadstone Paramics of Edinburg, Scotland, was developed to analyze and evaluate the interactions between road traffic and pedestrians. There are other pedestrian simulators, such as NOMAD (Delft University of Technology, Delft, Netherlands), PEDROUTE (Halcrow Group, London, UK), which were developed for various purposes. However, the analyses and results available from these simulators was not deemed suitable for our study. Thus a locally appropriate simulator was needed.

3. PEDESTRIAN SIMULATOR

3.1. Features and Configuration

The operation analysis program (pedestrian simulator) is an analytic tool which can reproduce the behaviors of major facilities and means (pedestrian, train, etc.) of transit center in a three dimensional (3D) display. Furthermore, it can be used to evaluate and verify a transit center's operational efficiency, its design adequacy, and it can evaluate a variety of pedestrian behavioral aspects at a microscopic level. This type of simulation program can be used to perform transit center pedestrian's behavior analysis, microscopic level analysis of service facilities, and transit center operation evaluations for various situations (e.g., peak time, disaster, etc.). The pedestrian simulator discussed here includes several definitions and algorithms.

3.2. Operation Analysis Algorithm

3.2.1 Pedestrian Behavior Algorithm

Pedestrian Definition

Walking is the basic transportation system in all pedestrian activities and the most important means to connect to other transportation means. The characteristics that differentiate pedestrian traffic and vehicle traffic are:

- Vehicles drive along a fixed lane; pedestrians do not have a fixed route.
- Vehicles move in a single direction in one lane, but there may be many different directions in pedestrian traffic.
- Similar vehicles exhibit similar acceleration rates, but pedestrians may exhibit marked differences in acceleration.

- Vehicles move along a route in a forward direction, but pedestrians may have many direction changes.
- Pedestrians have greater acceleration and deceleration than vehicles.
- Pedestrians have the capability to change course, while vehicles do not.

Pedestrian Characteristic and Class Definitions

We defined directional changes in, and avoidance related aspects of, pedestrians based on a pedestrian's physical body area (Figures 1 and 2).

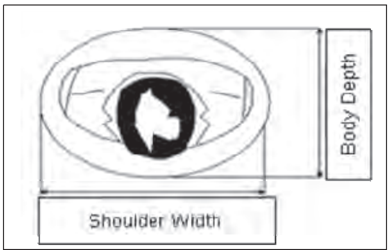

Data from : John J. Fruin 『Pedestrian Space』, 1991

Figure 1: Body Ellipse

	Body Center Point : Base for movement distance calculation, this is a point
	Body Ellipse : Human's minimum occupational space. body center point centered ellipse
	Buffer Space : Personal free action radius buffer (this is volatile)
	Visual Field : Set by person's view scope. (normal value is 70 degree, reduces when using stairway or E/S)
	Recognition Space : Recognition and judgement range for obstacles and route change. differs by individual and congestion

Figure 2: Definition of Pedestrian Characteristic and Class

Pedestrians have various walking speed, and this may differ by sex, age, and physical disability. In addition, pedestrians may show different walking speed according to their purpose. This program divides pedestrians into classes according to sex, age, and other characteristics, and also classifies pedestrians according to whether they are with or without packages (i.e., normal pedestrian with no baggage, normal baggage, backpack, or luggage). Thus, the pedestrians were divided into 64 classes by sex (male/female), ages (<10/10-20/20-60/>60), other characteristics (e.g., degree of haste), diverse physical occupancy characteristics, and recognition range characteristics.

Pedestrian Route Selection Algorithm

The above characteristics may affect a pedestrian's subjective decisions about route selection in a transit center. This study applied a shortest path algorithm and a space syntax theory route searching algorithm to create a mathematical model for pedestrian route selection analysis. The shortest path algorithm (Moore Algorithm) was used to find the shortest route and assumed that the pedestrian is familiar with the facility structure and passage routes in the transit center. The Space Syntax Theory was applied when a pedestrian was not familiar with the facility structure and routes of passage.

Pedestrian Behavior Algorithm

Pedestrians may show instantaneous behavior changes using an individual decision-making process, which may include decisions about walking direction and acceleration, and deceleration changes. Therefore, an algorithm is required to express such microscopic level characteristic changes. This study defined several physical area standards that includes a pedestrian's body ellipse area and a recognition area which, by recognizing other pedestrians and obstacles, allows for obstacle avoidance and direction and speed changes. In addition, we defined a pedestrian avoidance principal according to those standards.

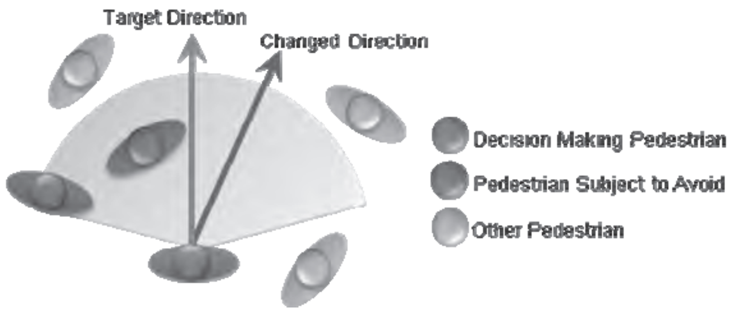

Figure 3: Diagram of direction change and possible speed changes

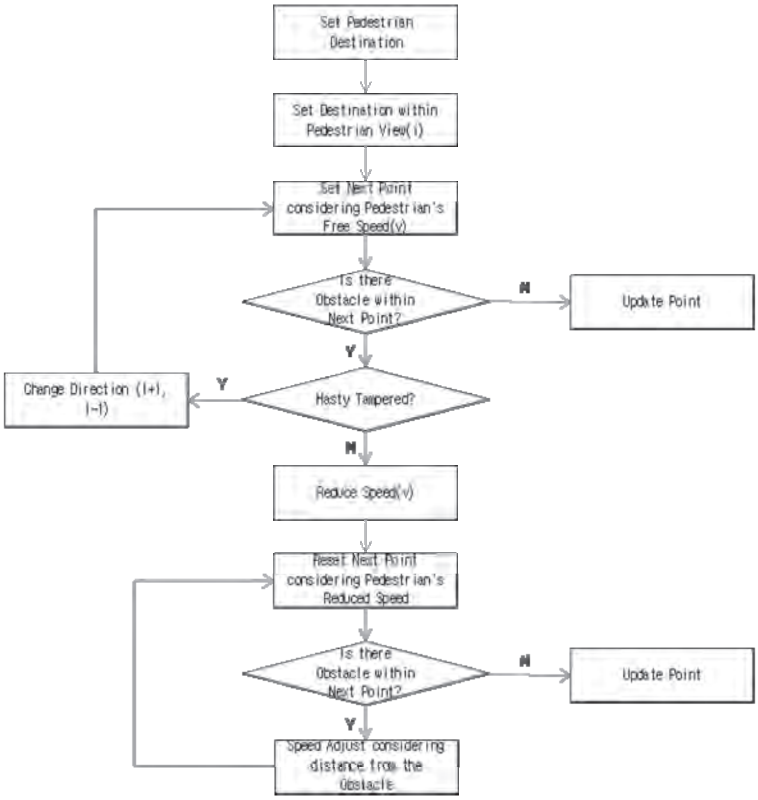

Figure 4: Pedestrian behavior algorithm

Figure 3, which uses the color coding of Figure 2, shows that a pedestrian has a body range, a recognition range, and a current direction. In the pedestrian behavior algorithm, a pedestrian has a 180 degree avoidance range which is based on its physical range. Furthermore, when another pedestrian or obstacle is within recognition area, the pedestrian may adjust both direction and speed within the desired directional range.

3.2.2 Transit Center User Behavior Algorithm

Transit Center Definition

The types of transit centers considered were: large scale (inside and outside), medium scale (general facility type), and small scale (specific area within a Facility) types. In addition, facilities were divided into block types in the operation analysis program, and an established node-link system was used when using the facility usage and pedestrian behavior algorithms.

Table 1: Definition of transit center types

Large Category	Medium Category	Small Category	Large Category	Medium Category	Small Category
Inside Facility	Passenger Facility	Platform	Inside Facility	Other Facility	Ticket Gate
		Waiting Room			Lounge
	Elevator Facility	Indoor Stairway			Function Room
		Outdoor Stairway			Emergency Shelter
		E/S			Flood Prevention
		E/V		Facility for Disabled	
	Passage	General Passage	Outside Facility	Connection Facility	Bus Stop
		Connecting Passage			Bicycle Storage
		Transit Passage			Transit Parking Lot
		New Traffic Connection			Stop Station
	Other Facility	Toilets			

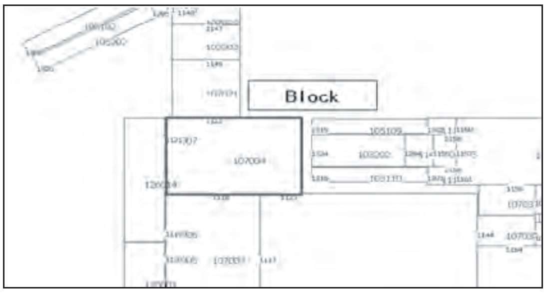

Figure 5: Block System

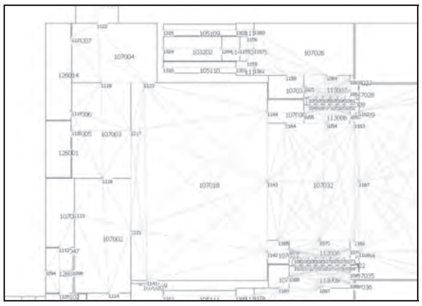

Figure 6: Node-link System

Service Characteristics of the Facility and Queuing Algorithm Application

A service facility can be divided into two types: single and multiple services. Through characteristic analysis on transit customers who use a facility, applied the facility service using characteristic and passenger's queuing algorithm, and reflected transit center user behavior algorithm. Situations in which a pedestrian uses a facility for transit were based on a pedestrian entering into a queue to use the facility. In the simulation model, both entering and exiting the queue are included.

Fundamental factors included in the queuing algorithm

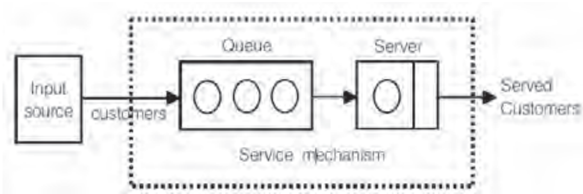

Figure 7: Schematic of queuing algorithm

- Input source: volume of customers entering the service facility
- Queue: customer waiting line before service

- Service discipline: sequence of service
- Service facility: service providing person or facility

The types of queuing sequence used are:

- First in/first out (FIFO) : Ticketing Office, Ticket Gate, E/S
- LIFO: E/L
- Random: Toilet, Entrance Gate, Stairway

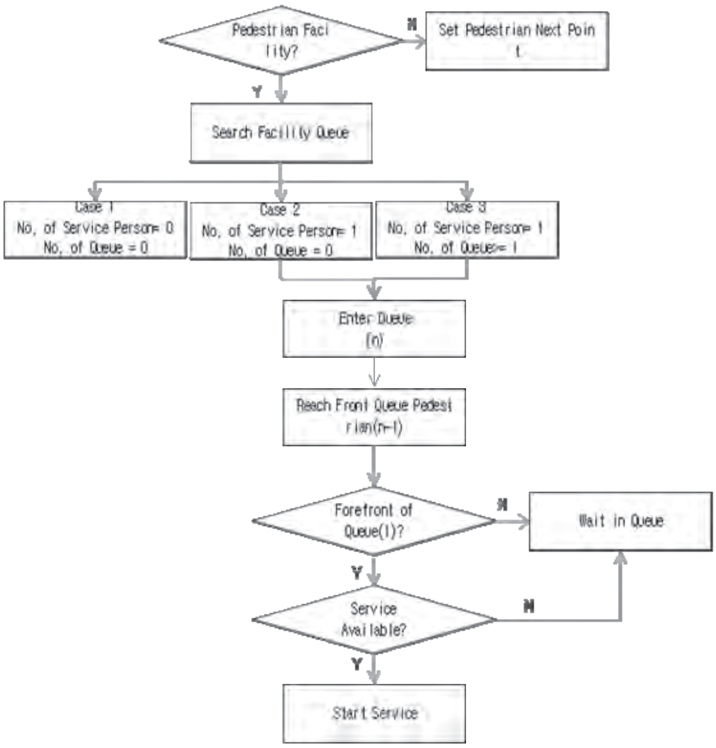

Figure 8 Facility Usage Algorithm

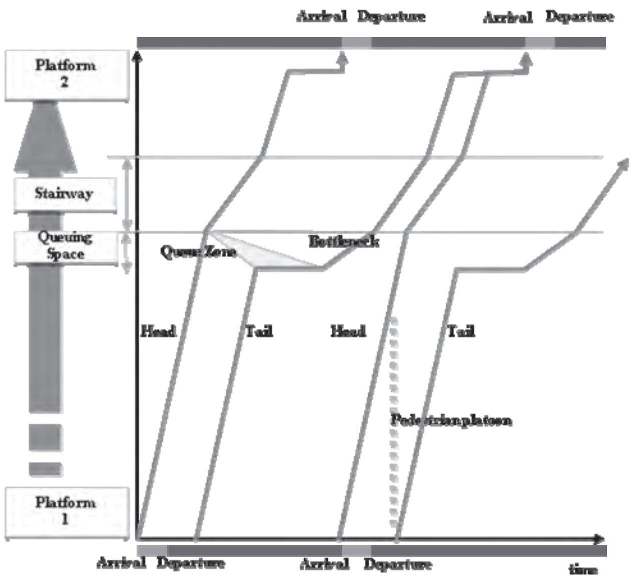

Figure 9 Time-Space Diagram In Transfer Center

Within the operation analysis program it is necessary use the above algorithms to classify each facility's characteristics, define the service patterns for the facility, and establish the sequence by which pedestrian's enter and exit a queue to use the facility and receive service.

3.2.3. Space Expansion

Vehicle Simulation

An applied car-following theory and a lane change model that reflect car and bus moving characteristics were used in the operation analysis program. In addition, it includes simulation of pedestrians' behaviors outside of a pedestrian service facility (e.g. at a bus stop or on a sidewalk or pedestrian crossroad).

Mass Transportation Boarding and Alighting Model

The operation analysis program included both bus stop and subway platform information to assess transit customer behavior and reflect pedestrian boarding and alighting behaviors. This included a boarding and alighting algorithm to model queuing behavior at bus stops, and included information on boarding & alighting intervals.

3.2.4. MOE Setup

Measures of effectiveness (MOE) for transit center efficiency analysis can be derived through the operation analysis program, as well as through assessment of the pedestrian and facility information at each simulation time step. This study establishes MOE for pedestrians, facilities, and for the simulation.

- Pedestrian related MOE: based on basic information on the pedestrian (i.e., pedestrian ID, age, sex, propensity, baggage), and on the pedestrian's current speed, as well as the free flow speed, travel time and distance, etc.
- Facility related MOE : Facility basic information on the facility (i.e., facility ID, facility type, server number), and on the number of users, the average service and queue times, and queue length, etc.
- Simulation MOE : Assesses total simulation time, total pedestrian occurrence, totals of pedestrian moving distance and moving time, pedestrian average speed, pedestrian movement traces, etc.

<table>
<tr><td colspan="9">Pedestrian related MOE</td><td>Facility related MOE</td></tr>
<tr><td>MOE</td><td>Route</td><td>Person</td><td>MOE</td><td>Route</td><td>Person</td><td>MOE</td><td>Route</td><td>Person</td><td>Facility</td></tr>
<tr><td colspan="3"><u>Personal MOE</u>
Person ID:
Current Speed:
Desired Speed:
Travel Distance:
Travel Time :</td><td colspan="3"><u>Route Information</u>
Person ID:
Origin Node:
Destination Node:
Current Block:
Block Type:
Current Point : (x, y, z)</td><td colspan="3"><u>Person Information</u>
Person ID:
Age:
Sex :
Personality:
Baggage:
State:
Walk/Wait/Service</td><td><u>Facility MOE</u>
ID :
Facility type :
# of Server :
Mean Service Time :
Mean Waiting Time :
# of used person :
Queue length :
Occupancy :</td></tr>
</table>

Figure 10: Simulator MOE

<table>
<tr><td>Simulation MOE</td><td>Pedestrian Trace Display</td></tr>
<tr><td>
</td><td>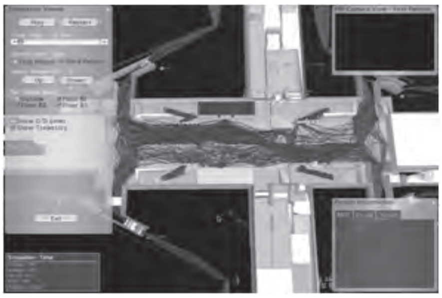</td></tr>
</table>

Figure 11: User Interface of Pedestrian Simulator

3.3. Program Development

3.3.1 Development of a Prototype for Algorithm Verification

A prototype was developed to verify the adequacy of the pedestrian behavior and facility use behavior algorithms. The prototype was developed with object oriented properties that divide the environmental components into homogeneous characteristic and feature performing objects and responds to each event specified for simulation. It was developed using the Visual C++ Program from Microsoft Corporation, Redmond, WA, USA, and was based in the Microsoft Windows XP operating system.

Establish Input Data
(Generate Pedestrian, OD, Facility Operation/Use Status)

↓

Perform Simulation(Time Step)

. Pedestrian Generate/Disappear
. Network Update(Network → Transit Center Update → Each Floor Update → Facility Block Update → Pedestrian within Block Update)
. Calculate MOE

↓

Output Result

Figure 12: Flow of data through the simulation process

<table>
<tr><td>Pedestrian Characteristic
(Recognition Space, Body Ellipse)</td><td>Facility Usage Behavior</td></tr>
<tr><td>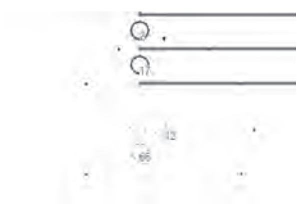</td><td>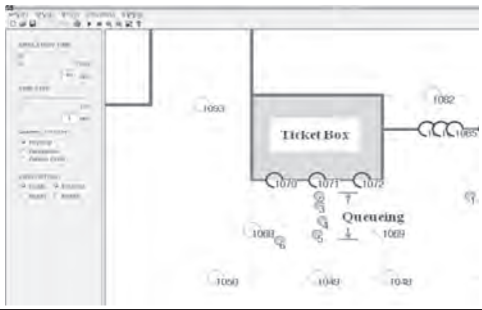
</td></tr>
<tr><td>Pedestrian Class(Pedestrian with baggage)</td><td>Boarding and Alighting Behavior</td></tr>
<tr><td>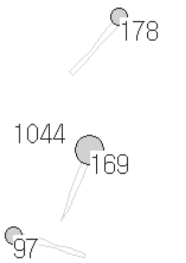
</td><td>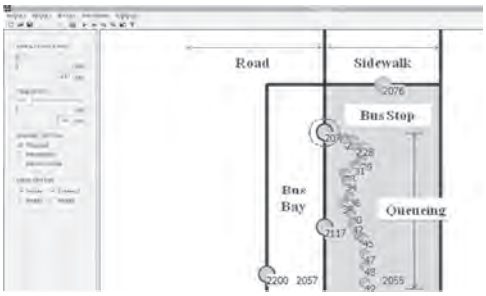
</td></tr>
</table>

Figure 8: Pedestrian Classification

3.3.2. Two-dimensional Transformation and Processing of the Prototype

A 3D model generating process is performed using pedestrian behavior two-dimensional (2D) data analysis. An additional animation process was required in order to produce a realistic 3D image. Motion data (walking motion) is justified to a static 3D pedestrian model and displayed as a 3D animation vision using this as a framework.

3.3.3. 3D Operation Analysis Program Development

The 3D operation analysis program was developed using the aforementioned pedestrian behavior algorithms.

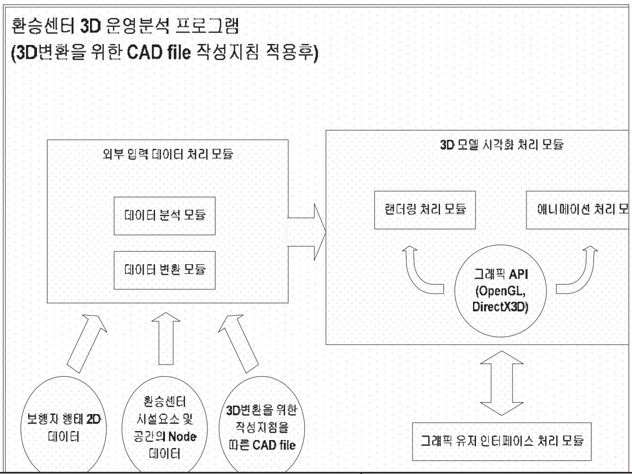

Pedestrian 3D	Display Pedestrian Property
	
3D View of Sadang Station	Operation Analysis Program UI

Figure 14: 3D Operation Analysis Program(Pedestrian Simulator) Development

Write Normalized CAD File(including 3D Transform Guideline)

↓

Design Operation Analysis Program Framework

↓

Design detailed Module, Functions

↓

Develop Operation Analysis Program UI, Establish Input Variable, MOE, Data Storage System

↓

Develop 3D Operation Analysis Program

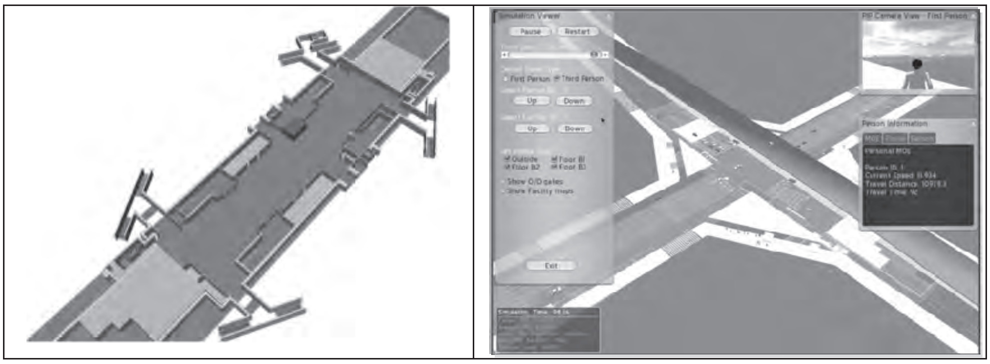

Figure 15: Pedestrian Simulator

4. STUDY AVAILABILITY

The transit center operation analysis program performs transit center operation efficiency evaluations that can reflect microscopic level pedestrian behaviors within the transit center. At present, this program is under development and is being designed to use or be based on the following features.

- Simulation tests and MOE analyses of various scenarios (e.g., unexpected incidents, peak time usage, future demand changes, etc.)
- Analyze transit behavior according to pedestrian demand (e.g., transit time and transit distance)
- Transit behavior analysis of various pedestrian types, including those that are transportation vulnerable
- Dynamic and microscopic level individual pedestrian simulation tests for transit center design plan evaluations
- Analysis of Korean style transit centers including the consideration of local pedestrian characteristics

5. FUTURE STUDY DIRECTION

This transit center operation analysis program is under development, and there are still many items to complete. First, there is a need to complete the pedestrian behavior algorithms. That step requires verification through field surveys. Second, there is a need to reflect various pedestrian behaviors in the model through the use of an appropriate pedestrian characteristic classification system, and the need to complete an algorithm that effectively considers various facility use behaviors. Third, the program should be developed as a user friendly program. Accordingly, this study will use a normalized computer assisted design (CAD) writing guide function to automatically extract program input data. The CAD function is currently under development. Finally, this program should be able to produce various MOE estimates. The following types of MOE are to be included.

- Transit passenger mobility (e.g., transit distance, transit time, movement path, etc.)
- Transit passenger convenience (e.g., waiting time, boarding and alighting time, etc.)
- Facility adequacy (e.g., facility usage density, capacity adequacy analysis, disposition adequacy evaluation, etc.)
- Moving convenience for the transportation vulnerable (e.g., transit distance, transit Time)
- Transit center walking (moving) space usage rate distribution
- Number of pedestrian interactions
- Time-space trace according to transit paths and the transit path diagram

ACKNOWLEDGEMENTS

This research is one of several national transport projects in South Korea sponsored by the ‘Korea Ministry of Land, Transport and Maritime Affairs.’ The authors thank the members of the ‘Korea Ministry of Land, Transport and Maritime Affairs’ for their assistance

REFERENCES

MOCT, Supplementary and Design Guideline for City Railway and Transit, Convenience Facility, 2002.

MOCT, KHCM, 2004.

Park DongJu, Study on Pedestrian Traffic Flow Characteristic according to Walking Purpose, SNU Master's Thesis

Lee JinUk, Study on Pedestrian Traffic Flow Characteristic and its application, Yeungnam University Master's Thesis

Transportation Research Board, Transit Capacity and Quality of Service Manual, 2nd Edition, 2003.

John J. Fruin, Pedestrian Space : Theory and Design, 1991

Daamen, W., Modelling Passenger Flows in Public Transport Facilities, PhD thesis, Delft University of Technology, 2004.

EXPLORING IMPACTS OF COUNTDOWN TIMERS ON THROUGH MOVEMEN AT A SIGNALIZED INTERSECTION IN BANGKOK

THIRAYOOT LIMANOD,
PRAMUK PRABJABOK and KRAISI TIPPAYAWONG
School of Transportation Engineering
Suranaree University of Technology, Thailand
tlimanond@yahoo.com

ABSTRACT

This study aimed to explore the impacts of the countdown timer during various stages of the signal cycle using two approaches: a traffic analysis and a public opinion survey. The traffic analysis made a comparison of traffic characteristics during an off-peak day time at a selected intersection when the countdown timer was on operation against when it was switched off. A public opinion survey was conducted among more than 300 local drivers who drive regularly and are familiar with the timer. It was found that the presence of the countdown timers at the intersection would help reducing the start-up lost time during the beginning of the green phase by 22 percent and reducing the number of red-light violations during the beginning of the red phase by 50 percent. Furthermore, more than half of the local drivers consented that the timers would help relieving their frustration from stopping for uncertain amount of time during the red phase. However, the timer was also found to slightly reduce the saturation flow rate during the green phase. The public opinion survey showed that the majority of the local drivers were favorable towards the system, and would support the municipality to install more of such device on the street network.

1. INTRODUCTION

The applications of signal countdown timers have been increasingly popular in several traffic-congested cities in Asia. The timer is a digital clock, installed next to the signal head, continuously displaying the number of seconds remaining for each phase of the cycle. It informs an exact cue of the onset of the next phase, so drivers are able to make a better decision on how they should react to the signal. The countdown timers are often claimed to offer many benefits, among others, to improve the vehicle flow at the intersection, to provide drivers extra times for making judgment to stop or to proceed through the intersection, to increase safety conditions at the intersection, and to relieve frustration of those drivers waiting in the queue (Kasetsart University, 2004). Nevertheless these claimed benefits have been rarely justified in the field.

It is less than a decade that the continuous countdown timers have been employed in the field, thus the research works on this device are still limited. Kidwai et al (2005) found a reduction in the average throughput (in a unit of pcu/h) after the installation of the timers at a non-CBD intersection in Malaysia. An experiment with an intersection in Singapore by Lum and Halim (2006) found that the installation of the device reduced the number of the red-light violations by 65% at 1.5 months of the installation. However, such impact does not sustain over time; the number of the red-light violations was rebounded to the usual level after 7.5 months of the installation. The device was also found to increase the number of vehicular stops within 2 seconds into red, and this effect seems to sustain over the long period. The study of Ibrahim et al (2008) comparing the queue discharge patterns at the three intersections with timers and the three intersections without timers, found that the timers tend to reduce the discharge headways of the first six vehicles in the standing queue.

Although these studies demonstrate some evidence of countdown timers' benefits, each focused on different characteristics without substantiation from another geographical area, where driving mentality and behavior might be different. In addition, to authors' knowledge, driver opinions on countdown timers have never been reported anywhere. The objectives of this research are to explore the impacts of the countdown timers occurred during different stages of the full signal cycle, and to investigate opinions of the local commuters on the countdown timers installed on the street network.

2. METHODOLOGY

Table 1 below summarizes the potential impacts of the countdown timer anlayzed in this study as well as the methodologies used. This research primarily investigated traffic patterns between the 'with timer' and the 'without timer' conditions, and utilized descriptive statistics and statistical tests to analyze whether the device instigates any impacts on traffic during various stages of the cycle. Apart from the traffic analysis, this study also conducted a public opinion survey among local drivers for their opinions on the countdown timer device.

The intersection of Kaset-Navamin Road/Lad Pra Kao Road was selected to be the project site since it met all of the pre-defined conditions. It is a major intersection located in a non-CBD area in Bangkok and equipped with the countdown timers on all four approaches. The signal countdown timers are on operation throughout the day except for the morning and evening peak hours when traffic polices take control and manually adjusted traffic signals themselves. During these peak periods, the countdown timers are switched off and display nil. It is a typical situation of all major intersections in Bangkok. This circumstance prevents the researchers from making a comparison between the "with timers" and "without timers" conditions during the peak periods. The present study, thus, focuses on the comparisons of traffic characteristics during the off-peak day time, starting from 10:00 – 15:00.

Table 1: Potential impacts of the countdown timer at various stages of the signal cycle

Stage during the cycle	Potential impact of countdown timers	Methodology
Beginning of the green phase	Reduce the start-up lost time	Descriptive statistics, t-test
During the green phase	Improve the saturation flow rate	Descriptive statistics, t-test
During the amber phase	Reduce the no. of vehicles entering during the amber time	Descriptive statistics
Beginning of the red phase	Reduce the no. of red-light violations	Descriptive statistics
During the red phase	Relieve frustration of drivers	Public opinion survey
Other benefits of countdown timers		Public opinion survey

This study analyzes the through movement on the eastbound approach along Kaset Navamin Road. This approach comprises of two left-turn lanes (free-flow), three through lanes and one right-turn lane. We particularly focused on the vehicular flow on the second and the third through lanes, since traffic stream on these lanes were not much affected by motorcycles (which primarily drive on the first lane). Furthermore, the researchers carefully selected and removed the headways of those large vehicles, *e.g.*, large trucks, buses and the subsequent vehicles from the analysis to ensure that our study strictly analyzed the headways of normal passenger vehicles.

A video camera was set up on a building located adjacent to the intersection, for recording the vehicular flow at the intersection during the off peak day time (10:00 to 15:00). Exactly a week later, the researchers requested the department of highways to switch off the countdown timers without any modifications of the traffic signal and its timings, then recorded the flow of traffic at the same intersection for the same period. The later case was used to represent the without countdown timer conditions, as drivers have no knowledge of the remaining time of the upcoming phase change, similar to the situation when the timer was not installed. We intended to experiment at the same intersection to avoid any uncontrollable factors that could happen when two different intersections were analyzed.

Table 2 below summarizes the signal operations and some traffic parameters observed on the eastbound through lanes for both the “with timer” and the “without timer” conditions. The signal consistently operated with a cycle length of 230 seconds with a green time of 102 seconds for the eastbound through movement during the off-peak day time. The ranges of observed queue length on both experiment days were comparable: 14 – 33 vehicls on the “with timer” day (25 April 2007) and 14 – 37 vehicles on the “without timer” day (2 May 2007) implying that traffic demand on both days were similar.

Table 2: Summary of the signal operations and traffic parameters of the eastbound through lanes during the off-peak period (10:00 – 15:00)

Conditions	Date of survey	No. of cycles analyzed	Cycle length/ green time (minutes)	Range of observed queue length (vehs/cycle)
With timer	25 Apr 2007	78	230/102	14-33
Without timer (or timer off)	2 May 2007	78	230/102	14-37

In this study, the saturation flow rate and the start-up lost time were determined based on the conventional approach, presented in the Highway Capacity Manual (Transportation Research Board, 2000). That is, the first few vehicles in the queue generally take a few extra moments to make a decision and react to the signal change by proceeding through the intersection. The headway of successive vehicles gradually decreases until it finally reaches a relatively stabilized interval through the rest of the queue. This stable interval is referred to as the saturation headway.

The determination of the i^{th} vehicle in the queue that begins to sustain the saturation headway state is a challenging task. This study utilized a similar approach to the previous studies of Joseph and Chang (2005) and Raksutorn (2004). It performed a series of statistical t-tests to determine whether the headway of the first few vehicles in the queue is significantly different from the average headways of the rest of all vehicles in the standing queue. That is, it starts by comparing the headway of the first vehicle with the average headway of the second vehicle to the last vehicle in the queue. If they are significantly different, then we proceed to test the difference between the headway of the second vehicle and the average headway of the third vehicle to the last vehicle in the queue, and so on. The test terminates when it finds the i^{th} vehicle that its headway is not statistically different from the average headway of all subsequent vehicles. Then, the i^{th} vehicle is presumably the first vehicle of the queue that sustains the saturation headway. The start up lost time is determined as the summation of the extra seconds over the saturation headway that the first few vehicles (exactly from the first to the $(i\text{-}1)^{th}$ vehicles) in the queue experienced.

Apart from the traffic analysis, the researchers conducted an interview of more than 500 local drivers randomly selected in front of the key spots, *e.g.*, large shopping mall,s, department of lane transport, in the city. Given that the countdown timers have been utilized in Bangkok since 2002, and currently being installed at more than 400 intersections all over the Bangkok area, local commuters are fairly familiar with the device and presumably have a firm opinion on the system. The questionnaire requested the personal data of the respondents, the frequency of their driving in Bangkok, and their specific opinions on the signal countdown device. The dataset was later reduced to include only those who drive at least 2-3 days per week.

This study categorized the sample into two groups: passenger car drivers and motorcycle drivers. Motorcycles are usually small, have maneuverability flexibility while driving, and have ability to sieve through and stall in front of the standing queue while the approach receives a red light. Thus, the two groups might have different opinions on the timers. The final sample includes 368 respondents, composing of 116 regular motorcycle drivers and 252 regular car drivers.

The distribution of sexes, age groups, income groups of the samples are shown in Table 3. In general, the gender of the sampled car drivers is equally split between male and female, while that of the motorcycle drivers are predonminantly male. The sampled car driver group tends to be older and have higher income than the motorcycle driver group.

Table 3: summarizes general characteristics of the respondents.

	Motorcycle drivers		**Car drivers**	
Total no. of sample	**116**		**252**	
Characteritics	**Amount**	**Share**	**Amount**	**Share**
Sex				
Famale	21	18.1%	119	47.2%
Male	95	81.9%	133	52.8%
Age group				
<18 yrs.	6	5.2%	1	0.4%
18-22 yrs.	11	9.5%	22	8.7%
22-30 yrs.	49	42.2%	95	37.7%
30-45 yrs.	35	30.2%	101	40.1%
45-60 yrs.	11	9.5%	31	12.3%
>60 yrs.	4	3.4%	2	0.8%
Income group				
<5,000 baht	23	19.8%	10	4.0%
5,000-10,000 baht	52	44.8%	56	22.2%
10,000-20,000 baht	31	26.7%	118	46.8%
20,000-40,000 baht	9	7.8%	55	21.8%
40,000-60,000 baht	0	0.0%	9	3.6%
60,000-80,000 baht	1	0.9%	0	0.0%
80,000-100,000 baht	0	0.0%	0	0.0%
>100,000 baht	0	0.0%	4	1.6%

3. RESULTS

3.1 Impacts on saturation headway and saturation flow rate during the green phase

Table 4 summarizes descriptive statistics of saturation headway as well as saturation flow rate under the “with timer” and the “without timer” conditions. It was found that the average saturation headway of the “with timer” condition (1.88 seconds per vehicle) was larger than the saturation headway of the “without timer” condition (1.85 seconds per vehicle). One plausible explanation is that, while the queue is proceeding through an intersection (without countdown timers) during the green phase, the drivers are uninformed of the exact termination of the green phase, thus, they likely to follow the front vehicle closely to improve their chance of proceeding through the intersection before the green phase ends. With the presence of the countdown timers, however, the drivers know the exact remaining time before the green time ends, and can comfortably follow the front vehicle to proceed through the intersection with larger headways. Thus, we observed larger headways on traffic stream at the intersection with countdown timers. However, the t-test showed that the mean saturation headways between the "with timer" and the "without timer" conditions are not statistically different at a 95% interval (with a p-value of 0.261).

Table 4: Comparisons of saturation headway and saturation flow rate

Study period	first veh. to sustain saturation headway	No. of data in the saturation headway state	Saturation headway		Equivalent Saturation flow (vehicles/hour)
			Mean	Std dev	
With timer	8	2,469	1.88	0.82	1,918
W/O timer	10	2305	1.85	0.80	1,946

The larger saturation headway of the "with timer" condition leads to a decrease in the saturation flow rate from 1,946 vehicles per hour without the presence of the timer to 1,918 vehicles per hour when the countdown timer is presented. It implies that the installation of countdown timers at a signalized intersection would not improve, but rather reduce the saturation flow rate of the intersection. Although it is contradict to our presumption, this is consistent with the result of Kidwai *et al* (2005) that found a reduction in the average throughput (in a unit of pcu/h) after the installation of the timers at a non-CBD intersection in Malaysia.

3.2 Impacts on the start-up lost time during the beginning of the green phase

The analysis of start-up lost time (SULT) requires some adjustments to the previous computations in order to make a comparison between the "with timer" and the "without timer" conditions with the same basis. First, the order of the vehicle in the standing queue that first sustains the saturation headway has to be equal between the two conditions, otherwise one sums more headway data than the other. Second, the saturation headways of the two conditions must be assumed to be of the same magnitude, or else it is difficult to justify whether the estimated SULTs of one condition is higher than the other. The adjusted values utilized in the analysis as well as the estimated SULTs are shown in Table 5.

Table 5: Comparisons of start-up lost time

Cases	First veh. to sustain saturation headway (i^th^)	weighted average saturation headway (sec./veh.)	No. of cycles analyzed	Start-up lost time (seconds)	
				Mean	Std dev
With timer	8	1.87	139	6.53	1.76
W/O timer	8*	1.87	122	8.32	2.06

*adjusted vehicle to sustain saturation headway state, to make the comparison based on the same basis.

As shown in Table 5, the mean SULT with countdown timers is less than its without timer counterpart. The average SULT decreases from 8.32 to 6.53 seconds (or 22 percent reduction) when the countdown timers are present at the intersection. A t-test proved that the mean SULTs between the two conditions were statistically different at a 95% confidence interval (with a p-value of less than 0.001). This is logical given that queuing drivers anticipate the upcoming phase change from the countdown timers, so they are ready to proceed through the intersection without much delay compared to when the countdown timers are in use. This results in a decrease in the SULT with the operation of the countdown timers. In fact, this favorable effect of the countdown timer has been well perceived by most of general public. According to the public opinion survey, 69.4 percent of the sampled motorcycle drivers and 63.2 percent of the sampled car drivers agree that the timing information given by the countdown timers assists them prepare to proceed through the intersection when the green phase begins.

To further explore the impacts of countdown timers on individual vehicles in the standing queue, the researchers analyzed the paired individual headways between with and without timers, as summarized in Table 6 and plotted on Figure 1. The impact of the countdown timers in reducing individual headways are largest on the first vehicle (1.24 seconds). The impact, however, quickly dissipated on the second vehicle, and was further reduced for subsequent vehicles. A series of statistical tests demonstrated that the differences in individual headways are significant at a 95 percent confidence interval for the first vehicle, while are insignificant for the rest of the queue. This indicates that the countdown timers have significant effects on the headway of the first vehicle only. It should be noted that this finding was disagree with the results from the Ibrahim *et al* (2008) study, which found that the countdown timers tended to reduce the discharge headways of the first six vehicles in the standing queue. The difference could be perhaps due to a number of locality factors, such as, driving behavior, drivers' mentality, level of traffic congestion.

Table 6: The difference in mean individual headways of the first few vehicles in the standing queue for the with and without timer conditions

		mean headway (seconds)							
	i^{th} vehicle	**1**	**2**	**3**	**4**	**5**	**6**	**7**	**8**
Day	**With timer**	5.66	2.67	2.50	2.33	2.26	2.05	2.10	1.98
	Without timer	6.90	2.87	2.44	2.46	2.24	2.25	2.19	2.01
	Difference	-1.24	-0.20	0.06	-0.13	0.02	-0.20	-0.09	-0.03
	Sig. at 95% CI?	Yes	No	No	No	No	No	No	No

Note: Sig. – significant , CI – confidence interval

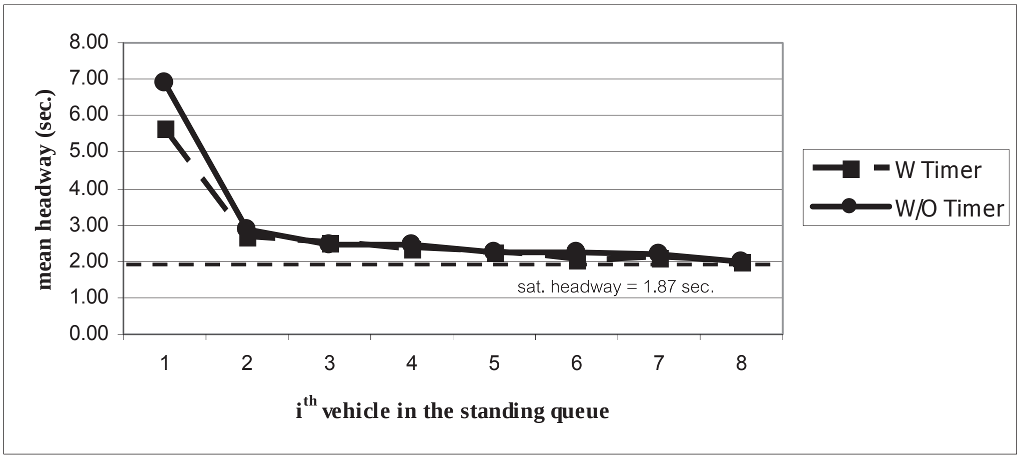

Figure 1: Comparison of headway patterns of the first few vehicles in the standing queue

3.3 Impacts on traffic characteristics during the amber phase

Table 7 summarizes the number of vehicles entering the intersection during the amber phase as well as the entering time observed under the two conditions. It was found that the numbers of vehicles entering the intersection during the amber phase were comparable between the two conditions, 101 vehicles under the "with timer" condition and 104 vehicles under the "without timer" condition. It was also found that the average entering time during the amber phase was 1.34 seconds after the beginning of the amber phase under the "with timer" condition, slightly less than 1.52 seconds under the "without timer" condition. Nevertheless, a t-test showed that the difference was not statically different at 95% confidence interval (with a p-value of 0.153). Thus, from the finding of this research, the countdown timers have no or little impact on traffic characteristics during the amber phase.

Table 7: Comparisons of the number of vehicles entering the intersection during the amber phase and the entering time

Cases	No. of cycles analyzed	Total no. of vehicles entering during the amber light	Avg. no of vehicles entering during the amber light per cycle	Entering time (seconds after the beginning of amber)	
				Mean	Std dev
With timer	78	101	1.29	1.34	0.87
W/O timer	78	104	1.33	1.52	0.92

.

3.4 Impacts on red-light violations during the beginning of the red phase

Table 8 summarizes the number of red-light running occurrence and the maximum violation time (in seconds) observed under the two conditions. It was found that the red-light violations under the "with timer" condition occurred 35 times, half of the number of red-light violations under the "without timer" case (70 times). Furthermore, we found a reduction in the maximum violation time when the countdown timer is used. Under the "without timer" condition, the maximum violation time was 4.13 seconds after the onset of the red phase, while it reduced to 3.08 seconds under the "with timer" condition. In summary, the countdown timers would help reducing the number of red-light running occurrence as well as reducing the maximum violation time a vehicle entering the intersection after the onset of the red phase. These two impacts of the timer would help creating a safer environment for driving, and reduce the likelihood of the right-angle collisions at the intersection.

Table 8: Comparison of the number of red-light violations and maximum violation time between with and without timer conditions.

Cases	No. of cycles analyzed	Total no. of red-light violations observed	Avg. no of vehicles entering during the red light per cycle	Maximum violation time (seconds after the beginning of red)
With timer	78	35	0.45	3.08
W/O timer	78	70	0.90	4.13

Given that the countdown timers were installed at the study intersection in early 2006, the researchers still found the reduction in the red-light violations in 2007, which is approximately one year after the installation of the devices. Thus, the impacts of reducing the number of red-light violations seemed sustain over at least one year. This contradicts to the Lum and Halim (2006) study, which found that the countdown timers effectively reduce the red-light violation incidents only for a short term (1.5 month after the installation).

3.5 Public opinions on countdown timers

From a public opinion survey conducted on 252 car drivers and 116 motorcycle drivers, it was found that the majority of local commuters are favorable towards the countdown timers. More than 95 percent of the car drivers interviewed recognized that the countdown timers are somehow beneficial to them, and almost all of them would encourage Bangkok Metropolitan Administration to install more countdown timers on the street network. The attitude of motorcycle drivers is also highly positive, but to a lesser extent. Approximately 74 percent of motorcycle drivers interviewed appreciate the countdown timers, and would support the municipality to install more countdown timers in the city.

The summary of local drivers' opinions on the key impacts of countdown timers is reported in Table 9. The majority of both car driver and motorcycle driver groups consented that countdown timers would help relieving their frustration from stopping for long and uncertain amount of time during the red phase (64.4% and 51.8%, respectively), assisting them to promptly proceed through the intersection when the signal turns green (63.2% and 69.4%, respectively), and ensuring them confidence in driving through intersection during the green phase (62.8% and 54.1%, respectively). Approximately half of both groups also agreed that the timers would assist them in making a better judgment to stop during the phase change to red (54.4% and 47.1 %, respectively). Less than half of respondents utilize information from the timers for better usage of waiting time spent during the red phase, or for switching off the car engine while waiting in the standing queue.

Table 9: Summary of public opinions on specific impacts of countdown timers.

Opinion on specific impacts of timers	Car drivers		Motorcycle driers	
	Agree	Not Agree	Agree	Not Agree
Relieve frustration from stopping for long and uncertain amount of time during the red phase	64.4%	35.6%	51.8%	48.2%
Assist to promptly proceed through the intersection when the signal turns green	63.2%	36.8%	69.4%	30.6%
Ensure confidence in driving thru intersection during the green phase.	62.8%	37.2%	54.1%	45.9%
Assist better judgment to stop when the signal turns red	54.4%	45.6%	47.1%	52.9%
Better use of waiting time spent during the red phase	34.7%	65.3%	40.0%	60.0%
Turn off the engine while waiting in the standing queue	25.9%	74.1%	42.4%	57.6%

For those respondents who think that the countdown timers will help relieving their frustration during the red phase, the interviewers further requested them to rate the average level of frustration they usually experienced while driving under the "without timer" and the "with timer" situations. The rating is in a scale of 0 to 4, where it denotes 5 levels of frustration from none, little, moderate, severe, to maximum, respectively. It was found that when the countdown timers were in use, the average frustration level of car drivers would reduce from the score of 2.68 to 1.34. For motorcycle drivers, the level of frustration decreased from the average score of 2.41 to 1.71. That is, the countdown timers would help reducing the overall frustration of the drivers due to the long and unknown waiting during the red light from a "moderate to severe" level to a "little to moderate" level.

4. DISCUSSION AND CONCLUSION

The present study aimed to explore various impacts of the countdown timers occurred throughout the full signal cycle using two approaches. First, the researchers made comparison of traffic flow characteristics of the through movement at an intersection in Bangkok when the countdown timer was on against when the timer was switched off. Due to some technical difficulties preventing us from making a comparison of the traffic conditions during the peak hours, the traffic analysis of this study focused on the conditions during the off-peak day time (10:00 to 15:00). Second, a public opinion survey was conducted to interview local drivers on their opinions regarding the countdown timer device. The final data set include opinions of those who drive regularly on Bangkok streets, comprising 116 motorcycle drivers and 252 car drivers. They all are supposed to be fairly familiar with the device and presumably have a clear opinion on the system, since the countdown timers have been utilized in Bangkok for more than 6 years, and currently being installed at more than 400 intersections all over the Bangkok area.

The impacts of the countdown timers found in this study are summarized in Figure 2 and described below per stage of the cycle.

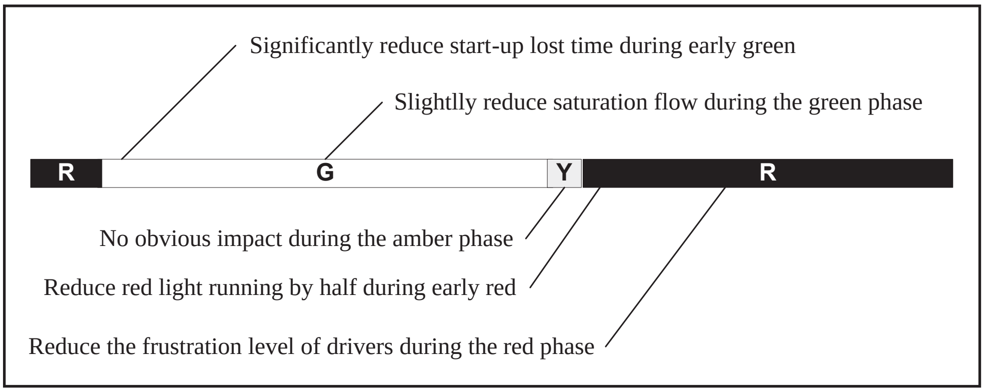

Figure 2: Summary of the impacts of countdown timers

At the beginning of the green phase, the installation of the countdown timers at an intersection would help reducing the start-up lost times experienced by the first few vehicles in the standing queue. It was found that the SULT of through movement decreased from 8.32 seconds under the "without timer" condition, to 6.53 seconds under the "with timer" condition. This is equivalent to 22 percent reduction in SULT when the timer was on. The saving in SULTs contributes moderate improvement on the overall flow at signalized intersections. The countdown timers would reduce SULTs by 1.79 seconds per cycle per lane, or equivalent to 1 extra vehicle/cycle/lane. Given a cycle length of 230 seconds utilized at the intersection, an hour comprises of 15.6 repeated cycles. Thus, the countdown timers can be reasonably expected to increase the throughput of the through movement by 15 vehicles/hour/lane. An intersection with a total of 8 through lanes (6 lanes on the east-west approach plus 2 lanes on the north-south approach) can reasonably expect to accommodate up to 120 extra vehicles per hour on the through movement of all approaches combined.

During the green phase, the information from the countdown timer will give drivers confident in proceeding through the intersection before the green phase ends, thus drivers tend to use a larger headway at the intersections where the countdown timers are presented. This leads to a slight reduction in the saturation flow rate. In this study, the saturation flow rate of the through movement under the "without timer" condition was 1,946 vehicles per hour, decreasing to 1,918 vehicles per hour under the "with timer" condition. This equals to a reduction of 28 vehicles/hour/lane. Assuming a green time of 102 seconds for through movement with a cycle length of 230 seconds, the throughput of the through movement is expected to reduce by 12.4 vehicles/hour/lane. An intersection with a total of 8 through lanes can reasonably expect to accommodate 99 fewer vehicles per hour on the through movement of all approaches combined.

Note that the reduction in the saturation flow rate would offset the benefits of saving in SULT, so that the overall benefits of the countdown timers on traffic flow become marginal. From the calculation above, the presence of a countdown timer would be able to accommodate 21 extra vehicles on the 8 through lanes of the intersection in an hour.

This study does not found any obvious impact of countdown timers on traffic characteristics during the amber phase. The numbers of vehicles entering during the amber phase between the "without timer" and the "with timer" conditions were comparable, and the average entering times between the two conditions were not statistically different.

At the beginning of the red phase, the countdown timers would reduce the number of red-light running occurrences, since it provides timing information of the end of the green phase beforehand so drivers have more time to make a proper decision. In this study, the number of red-light violations under the "with timer" condition was a half of the amount found under the "without timer" condition. The reduction in red-light running incidents would help decreasing the likelihood of right-angle collisions at the intersection. Nevertheless, it should be noted that the countdown timers could potentially cause another safety impact at the intersection. As discussed above, the countdown timers help reducing the SULT so the first vehicle in the standing queue enters the intersection earlier than before. It could hit the vehicle running red light from the previous phase, causing a right angle collision. A personal communication with a traffic police indicates no increasing trend of such accident. However, future studies are needed to substantiate this presumption when adequate accident statistics become available.

Finally, the countdown timers potentially help relieving drivers' frustration from stopping for long and uncertain amount of time during the red phase. From the public opinion survey, 64.4 percent of the sampled car drivers and 51.8 percent of sampled motorcycle drivers agree that the timers help alleviating their frustration. The timing information given by the countdown timer would let the drivers aware of the exact waiting time in advance.

ACKNOWLEDGMENTS

The authors would like to thank Suranaree University of Technology for the funding of this research project.

REFERENCE

Ibrahim MR, Karim MR, Kidwai FA. (2008). The effect of digital count-down display on signalized junction performance. American Journal of Applied Science 5 (5): 479-482.

Joseph J, Chang GL. (2005). Saturation flow rates and maximum critical lane volumes for planning applications in Maryland. ASCE Journal of Transportation Engineering, December 2005: 946-952.

Kasetsart University (2004). The development, the administration and the management of Intelligent Transportation System: a review report. For the Office of traffic and transport planning and policy, Bangkok, Thailand, 2004.

Kidwai FA, Karim MR, Ibrahim MR. (2005). Traffic flow analysis of digital count down signalized urban intersection. Journal of the Eastern Asia Society for Transportation Studies, 5, 1301-1308.

Lum KM, Halim H. (2006). A before-and-after study on green signal countdown device installation. Transportation Research Part F, 9, 29-41.

Raksutorn W. (2004). Saturation flow rate and start-up lost time of motorcycles at signalized intersection. Proceeding of the 6^{th} National Convention on Civil Engineering, Petchburi, Thailand.

Transportation Research Board. (2000). Highway Capacity Manual. Transportation Research Board, National Research Council. Washington D.C. 2000.

A MATHEMATICAL MODEL FOR TRANSIT NETWORK ASSIGNMENT

YONGTAEK LIM
Dept. of Transportation & Logistics
Chonnam National University, Korea
limyt@chonnam.ac.kr

JUN-SEOK JANG
Dept. of Transportation & Logistics
Chonnam National University, Korea
jjs1982@live.co.kr

ABSTRACT

In this paper, a transit assignment model in stochastic environment is proposed. The model is expected to overcome some existing limits of conventional transit models, which have adopted the optimal strategy of Spiess et al.(1989). The proposed model contains in-vehicle congestion effect as well as in-vehicle travel time and waiting time. A simple example was also given to test the model

1. INTRODUCTION

A public transport including railroad has been increasingly drawing more attention amid growing interest in green growth, environmental pollution and energy conservation. Since KTX launched its operation in 2004, the demand for railroad transport, not to mention high-speed rail, has been on the rise in line with positive recognition to the transit. However, the effect of transit network or effect on other transport means have yet to be fully considered due to insufficient analysis model necessary for evaluating and planning the behavior of the transit passengers, and even the existing transit assignment model fails to fully incorporate the reality. On the contrary, network-level analysis techniques considering the connectivity between the highways and network effect developed for extended time have been practically applied to the expressway or highway, and consequently, the projects have been planned based on prediction on potential effect in network aspect. The study was first intended to analyze the challenges with the existing transit assignment model, thereby presenting the transit assignment model that would deal with such challenges. The model proposed in the study was structured in stochastic model to incorporate the perceived travel cost error that might be incurred when the passengers choose the transit route. In the following Chapter, the challenges with the transit travel cost function and the transit assignment model were evaluated, and in Chapter III, a transit model proposed was introduced. Lastly in Chapter IV, the model proposed in the study was assesses though the examples.

2. TRANSIT TRAVEL COST FUNCTION AND EXISTING TRANSIT ASSIGNMENT

2.1. Transit travel cost function

In general, the travel cost of the public transport such as railroad and bus is represented by generalized travel cost, which is a sum of travel time from the start point to end point and the out-of-pocket money paid for transport means. the out-of-the-pocket-money refers to the cost in cash such as fare and the travel time includes access time, in-vehicle travel time, transfer time and waiting time. A travel cost function has been presented in many ways and in case of TransCAD, a commercial program, it includes boarding time and dwelling time in travel time. De Cea et al.(1993) proposed the travel cost function for route section as formula (1). The route section refers to the section between transfer points.

$$c_s = t_s + w_s + \phi_s(f_s) \tag{1}$$

Where, the first term refers to in-vehicle travel time of the route section s and the second term refers to waiting time and the last term is the congestion cost resulting from tin-vehicle passengers, which used to be excluded because of difficulties in estimating.

2.2. Problems with transit assignment using optimal strategy

2.2.1 Transit assignment using optimal strategy

The optimal strategy widely used today was developed by Spiess et al.(1989), which is the transit assignment technique of EMME/2, the commercialized transport demand program. This method comprises the 1st stage to seek the optimal strategy and the 2nd stage for loading the transport demand to the section selected by optimal strategy. The optimal strategy is to choose the route at the minimal cost when selectable routes were known at the start point. When a route is determined using the optimal strategy, a traffic demand is assigned to the section in proportion to the headway of the routes passing each node. The optimal strategy is outlined as follows.

[Step 0] Definition of start node

[Step 1] Move from the start node on a vehicle arriving the earliest among the routes belonging to attractive line

[Step 2] Getting off at the node predetermined according to optimal strategy

[Step 3] If not arrived at the destination, the getting-off node is defined as new start node, and start again from [step 1] and repeat until arrive at the destination.

2.2.2 Problems with transit assignment according to optimal strategy

The problems with transit assignment using optimal strategy could be categorized into the two. As seen in [step 1] it's modeled to get on the vehicle arriving the earliest, causing frequent transfer against the reality, which are indicated in other experimental studies, resulting from the principle of the optimal strategy.

The second problems, which is more critical, is unrealistic assignment of transport demand to the route. To explain such problem, the example using optimal strategy suggested in Emme/2 in <Fig 1> was evaluated. The figures at each section refer to in-vehicle travel time and section number and it was assumed that 2 routes are provided from start point (Node A) and end point (Node B) and the unit transport demand exists. Fig 1(b) and Table 1 indicate the travel volume and travel time by route. As indicated in Table, despite route #2 & #4 required less travel time, less assignment was given to the section #4 & #5 where two paths are located as seen in Figure 1(b), indicating unrealistic transit assignment based on optimal strategy.

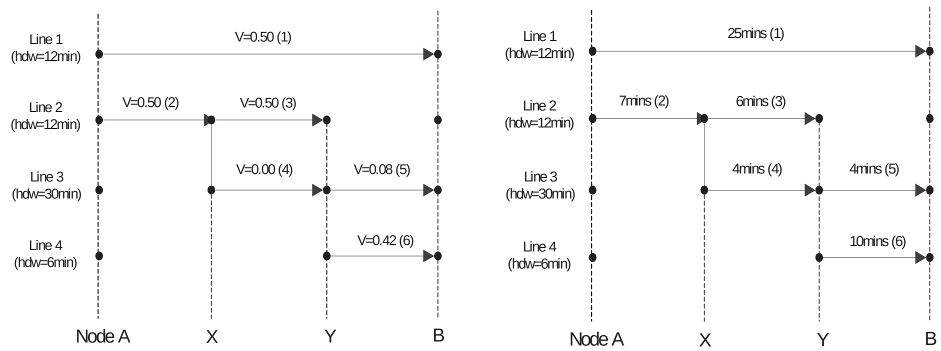

(a) Example transit network

(b) Assigned transit volumes by optimal strategy

Figure 1: An example transit network and its assigned volumes (in Emme/2 user manual)

Table 1: Travel times for each path

path	**Route composition**	**Travel time of the path**		
		In-vej t/time (A)	**Waiting time(B)**	**Total (A+B)**
1	line 1	25	0	25.00
2	line 2-Y-line 3	7+6+4	2.5	19.50
3	line 2-Y-line 4	7+6+10	2.5	25.50
4	line 2-X-line 3	7+4+4	4.3	19.30
5	line 2-X-line 3-Y-line 4	7+4+10	4.3+2.5	27.80

3. STOCHASTIC TRANSIT ASSIGNMENT MODEL

The study, in a bid to ease the limit with transit assignment using optimal strategy, was aimed at proposing the new transit assignment model, which is stochastically structured using a logit model. A stochastic user equilibrium assignment has the benefit to ease the unrealistic assumption which the deterministic user equilibrium assignment has. That is, It enables to ease the assumption that all passengers have the same travel characteristics and determine the route when a complete travel information. In stochastic transit assignment, unlike the deterministic user equilibrium assignment, the error term or the difference in perceived cost by user, is added to the travel cost of the link, and each user tends to choose the route to minimize their perceived cost. Thus, in stochastic user equilibrium (SUE), it may be defined as the state that any user is not able to reduce the perceived travel cost by changing the route at its discretion. The stochastic transit assignment model proposed in the study is as formula (2) below.

$$f_k^{rs} - q_{rs} p_k^{rs} = 0 \qquad (2)$$

Where, f_k^{rs} is the travel volume using the route k between the start and end point, rs. q_{rs} is travel demand between the start and end point, rs. p_k^{rs} is the probability of using the route k between the start and end point, which uses logit model as formula (3)

$$p_k^{rs} = \frac{\exp(-\theta c_k^{rs})}{\sum_i \exp(-\theta c_j^{rs})} \qquad (3)$$

θ in formula (3) is the scale parameter of logit model, and , c_k^{rs} is the travel time of the route k between rs, which is represented as formula (4)

$$c_k^{rs} = t_k^{rs} + w_k^{rs} + \alpha\left(\frac{f_k^{rs}}{u_k^{rs}}\right)^{\beta} \qquad (4)$$

Where, t_k^{rs} is the in-vehicle travel time of the route k between rs while, w_k^{rs} is expected waiting time and u_k^{rs} is the capacity of the route k between rs . Thus, the last term on right in formula (4) is the cost term reflecting in vehicle congestion. (α, β is the parameter) Thought there are several methods to resolve the proposed model (formula 2), A direct logit assignment method of Lim Yongtaek (2003) was adopted. This direct logit method has a single balanced solution according to the fixed point theory and seeks the solution through repeated procedures.

4. ASSESSMENT OF THE MODEL

4.1 Examples of transit assessment

The study, in a bid to assess the transit assignment model proposed, was aimed at evaluating the methods in two different ways that considers the in-vehicle congestion as well as without considering the congestion. The case without considering the congestion has not the last term on the right of formula (4) The parameter of logit model was $\theta = 0.1$, coefficient of the cost function was $\alpha = 0.5$, $\beta = 2.0$, and the travel demand was set as $q_{rs} = 1.0$.

4.2 Outcome of the analysis

Figure 2 shows the result of the case without considering the in-vehicle congestion and when compared to the assignment using the optimal strategy in Fig 1(b), the travel demand appeared to have been broadly distributed and particularly, a considerable travel volume was assigned to section #4 and #5 where the route #2 and #3 requiring less travel time were located. And in case of the route #1 requiring more travel time, it was significantly reduced when comparing to the assignment based on the optimal strategy, which indicates the proposed model assigned the travel demand to the network more realistically. Fig 3 shows the result of the case considering the in-vehicle congestion. (route capacity $u_k^{rs} = 0.1$). As indicated in figures, it looks similar with the case without considering the congestion effect, but in case of section 5 to which the most travel volume was assigned, the travel volume was reduced from 0.564 to 0.515 due to congestion effect and part of the travel volume was shifted to other routes. Table 2 compares the travel time by route in two cases. The cases considering the capacity (congestion was considered) appeared to have had extended travel time, which was attributable to the travel cost function incorporating in-vehicle congestion caused by limited capacity into the travel cost.

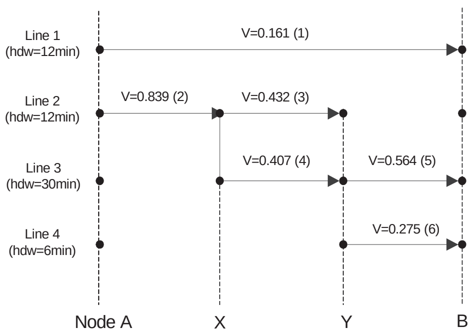

Figure 2: Assigned volumes without congestion effect

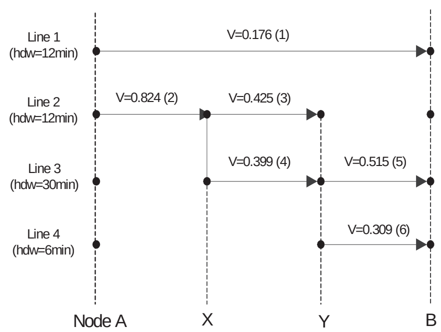

Figure 3: Assigned volumes with congestion effect

Table 2: Comparison of path travel times for each case

Capacity	Route	Route composition	Time
Without considering	1	line 1	25.00
	2	line 2-Y-line 3	19.50
	3	line 2-Y-line 4	25.50
	4	line 2-X-line 3	19.30
	5	line 2-X-line 3-Y-line 4	27.80
Considering	1	line 1	26.54
	2	line 2-Y-line 3	22.78
	3	line 2-Y-line 4	26.93
	4	line 2-X-line 3	22.66
	5	line 2-X-line 3-Y-line 4	28.78

5. CONCLUSIONS AND FUTURE STUDY

The study was intended to propose and evaluate the new transit model in an attempt to ease the problems with the existing transit assignment model. The travel time of the model proposed is in the generalized form which includes in-vehicle travel time, waiting time and the congestion cost, and to consider the perceived error by the passengers, it was structured in a stochastic user balanced transit assignment model. This model could be considered the more realistic model than the transit assignment model using the optimal strategy. As a result of evaluating the model proposed in the study through the example, the proposed model proved to be able to produce the more realistic resolution that the method using the optimal strategy. However, the study, which is still at the early stage, has a various modeling limits, which is first the clear interpretation of the travel cost function of the public transport and the need of realistic estimate of the parameters included. Furthermore, the field test to apply the transit assignment model to the large scale real network is also needed.

REFERENCES

Yongtaek Lim, 2003. An analysis algorithm of the stochastic logit transit assignment model, *Journal of Koreran Society of Transportation, Vol 21*, *No2*, 95-105, Apr 2003.

De Cea, J. and J. E. Fernandez, 1993. Transit Assignment for Congested Public Transport System : *An Equilibrium Model, Transportation Science*, *Vol. 27*. No. 2. 133-147.

Emme/2 user's manual, INRO, http://www.inro.ca/en/index.php

Spiess H. and M. Florian, 1989. Optimal Strategies : *A New Assignment Model for Transit Networks, Transportation Research 23B. No. 2*, 83-102.

Traveldemand modeling with TransCAD, Caliper, http://www.maptitude.co.uk/transcad.htm

HIERARCHICAL SHORTEST PATH ALGORITHM WITH PROBABILISTIC TRAVEL TIME

THEONETTE RUBA MARIBOJOC and HYUNMYUNG KIM
Transportation Engineering
School of Engineering and Technology
Asian Institute of Technology
st106067@ait.ac.th

ABSTRACT

It has long been aimed by transportation researchers to select the path which can make drivers move to their destination at a least cost. With the development of Route Guidance System (RGS) and telecommunication technology, travelers' route choice behaviors change rapidly but the existing modeling methods could not follow the speedy change. For example, most route choice models regard travel time as a deterministic value so the uncertainty of travel time is ignored. In addition, many of the previous route choice models were formulated without integrating the driver's attitude and preference in detail. Customizable route guidance system is not yet available nowadays. In this paper, a new route choice model which deals with the mentioned topics is proposed. With the combined concepts of hierarchical road classification and resource constraints, non-overlapping paths are enumerated in the real network. After then, the model calculates the path choice probabilities with respect to the given preferred arrival time. In addition, the idea is also expanded to the general case without preferred arrival time. Using a network in Bangkok, Thailand, the proposed model was tested and the calculated path choice probabilities are compared to the True Success Rate (TSR_k) and deterministic hierarchical MNL.

1. INTRODUCTION

1.1 Background and Purpose of the Study

A route choice problem has been one of the core study topics in transportation network analysis. In traffic assignment, forecasting the route choices of drivers is a fundamental requisite. In addition, a route choice problem is a rising issue in Intelligent Transportation System (ITS). In the last decade, a car navigation system (CNS) is prevalent and many commercial companies are devoting themselves to develop a better route finding algorithm. Although there have been significant developments on this topic, the existing models for the route choice problem are not so satisfactory and still have numerous flaws to be improved. The main difficulty in modeling the route choice problem is that it consists of various influencing factors. The influencing factors included in the route choice problem can be classified into two groups; 1) user behavior and 2) system uncertainty.

First, each driver in the real world has heterogeneous characteristics and travel demand. For example, the attitudes of drivers to uncertainty or danger are different from one another. Some drivers are risk-averse; while others are risk-taking. In addition, the travel time budgets of travelers differ even if their origin and destination is the same. Second, the supply side of road system also has some uncertainties. As we can observe in the real world, travel time between two locations is ever-fluctuating and the variation depends on the time of day and day of week. There would be various recurrent and non-recurrent sources of the fluctuation. As a result, the variables included in the route choice problem are not deterministic but probabilistic ones. The need for a better model which incorporates the behavioral aspects into the route choice is among the highlights of recent ITS applications (Beckhor et al, 2006).

This study aims to develop a hierarchical path enumeration algorithm that overcomes the Independence of Irrelevant Alternatives (IIA) problem while reducing the computational costs and to calculate the choice probabilities of the generated paths considering the driver’s arrival time preferences.

1.2. Scope and Limitations of the Study

The study includes the formulation of the path enumeration algorithm, the simulation of the link travel times and the determination of the path probability density functions, a survey and analysis of the OD (Suvarnabhumi Airport to Victory Monument route) travel time PDF, the formulation of the route choice model and the checking of the model’s reliability. . The proposed model application is limited to transportation networks where link travel times are stochastic but not time-dependent. The study is applied to single OD pair and passenger car vehicle travel only. The study does not include the evaluation of the computation efficiency of the algorithm.

2. LITERATURE REVIEW

2.1. Shortest Path Problems and Algorithms

A shortest path algorithm plays an important role in route choice problems. Generally, shortest path algorithms are based on Bellman’s principle of optimality which states that:

“Any optimal policy has a property that whatever the initial state and initial decisions are; the remaining decisions must constitute an optimal policy with regard to the state resulting from the first decision.”

The most basic algorithm for finding the shortest path is Dijkstra’s algorithm (Dijkstra, 1959) which can identify paths from one origin to *more* destinations. Contrarily, Floyd (1962) formulated an algorithm that finds paths from multiple origins to multiple destinations. Finding the shortest paths from all origins to all destinations is beneficial to traffic assignment problem with a non-sparse OD table.

However, in this study, a single OD pair is considered, so Dijkstra's algorithm is employed as a path finding algorithm. In terms of the randomness of link attributes, shortest path algorithms can be classified into two categories: deterministic and stochastic. The deterministic shortest path (Dijkstra, 1959; Sharma, 2001; Nepal, 2002) uses one exact value, usually the mean travel time for transportation networks, in determining the shortest path. On the other hand, the stochastic shortest path (Frank, 1969; Mirchandani, 1976) uses random variables, the link travel time probability distribution function (PDF), in determining the shortest path. For real transportation networks, the stochastic approach is recommended since it is similar to how drivers perceive their path travel time. However, stochastic problem is more complex and more difficult.

2.2. Path Enumeration Algorithms

In the route choice problem, multiple paths are provided and the choice probability of each route is calculated in general. For the problem, the preparation of choice alternatives (i.e. routes) is the most important work since a false definition of alternatives will bring out false choice probabilities. Therefore, it is important to enumerate the plausible alternative paths for a given OD pair. In this study, the existing path enumeration algorithms are grouped into two categories; namely, *k*-shortest path algorithm and path enumeration algorithm.

The first *k*-shortest path algorithms was introduced by Bock et al (1957). All possible paths from an origin to a destination are enumerated and sorted based on the travel cost. Pollack (1961) calculated the *k* -shortest path set by subjecting the links of the *k*-1 links to infinity. Eppstein (1998) formulated a *k*-shortest path algorithm using heap-ordered tree. To overcome the excessive calculation burden of the aforementioned *k*-shortest path algorithms, Yen (1971) introduced an algorithm that eliminates the nodes used by the enumerated shortest path to find the next shortest path. In this algorithm, overlapping among enumerated paths, well-known as IIA (Independence of Irrelevant Alternatives) problem, arises.

Column generation method is popular in path enumeration algorithm. This method uses a revised Simplex method in solving the problem over a subset of columns. Bell (1995) suggested a capacity-oriented column generation method while Thomas (1991) introduced a label collecting algorithm that updates its predecessor nodes and finds the multiple paths by combining predecessor nodes. Park and Rillet (1997) presented two heuristic algorithms that identify multiple and reasonable alternative paths defining reasonable alternative paths as those having acceptable attribute values and dissimilar in terms of links used with respect to the previously identified paths. The first uses link penalty to minimize the link overlaps. The second classified the network according to road classification function or hierarchy and uses link penalty as well. Both algorithms use a node-based Dijkstra algorithm in finding the shortest path. Sharma (2001) identified multiple alternative routes by pruning the network using resource and route constraints to maintain uniqueness of identified paths. Nepal (2002) introduced algorithms that consider multiple and conflicting objectives in the shortest path formulation. Lim and Hydecker (2006) illustrated a full path enumeration method but it cannot be applied to a practical problem without constraints since the required memory for storing the full path set is tremendous. Lim and Kim (2006) introduced a link-based algorithm that considers path overlap and turn prohibitions in enumerating reasonable paths.

2.3 Route choice problem

In this paper, the way for incorporating the uncertainty of travel time into the route choice problem is the main concern. According to the inclusion of travel time uncertainty, the types of route choice problems can be grouped into two categories; the deterministic and stochastic. The deterministic approach assumes that the travel times of the available routes are deterministic. The travelers in the network know exactly the times on these routes and each traveler chooses a route with the least travel time from his origin to his destination. In reality, assuming travel times as deterministic and exactly known to the travelers is not reasonable. On the other hand, the stochastic approach analyzes the network travel time and travelers' perception as random variables (Sheffi, 1985). Analytically the perceived travel time, C_k^{rs} on route k between origin r and destination s, is computed as:

$$C_k^{rs} = c_k^{rs} + \xi_k^{rs} \qquad \forall k, r, s, k \in K^{rs} \tag{1}$$

where c_k^{rs} is the measured or deterministic travel time and ξ_k^{rs} is the random error. K^{rs} is the set of paths for OD pair rs. Mirchandani and Soroush (1987) proposed a generalized traffic equilibrium model with probabilistic link travel times and perceptions. They classified the travelers into three categories: namely, risk-*neutral*, *risk-averse* and *risk prone*.

Assuming that the travel time is the most important attribute of concern to travelers in their choices of travel routes, the probability that a route is chosen, P_k^{rs} is given by

$$P_k^{rs} = \Pr(C_k^{rs} \le C_l^{rs}, \forall\, l \in K^{rs}) \qquad \forall k, r, s; l \ne k \in K^{rs} \tag{2}$$

The probability that a given route is chosen is the probability that its travel time is perceived to be the lowest among the alternative routes (Sheffi, 1985).

The process of selecting alternative paths for a stochastic network can be based on the theory of discrete choice models, where an individual's preferences towards each alternative is described by the attractiveness or utility measure associated with each alternative. The most common discrete choice models are the multinomial logit (MNL) and the multinomial probit

(MNP) models. The former is based on the assumption that the utilities of the alternatives in the choice set are identically and independently distributed (i.i.d) Gumbel variates and can be derived (assuming the utility of using the k^{th} path between origin r and destination s, U_k^{rs}) as follows.

$$U_k^{rs} = -\theta \cdot c_k^{rs} + \xi \qquad \forall k, r, s \tag{3}$$

The logit choice probability is then computed as

$$P_k^{rs} = \frac{e^{-\theta \cdot c_k^{rs}}}{\sum_l e^{-\theta \cdot c_l^{rs}}} \qquad \forall k, r, s \tag{4}$$

where θ is a coefficient that scales the perceived travel time. The STOCH method or Dial's algorithm is known to implement a logit route choice model. However, the logit model does not account the correlation between the perceived travel times of the various routes to properly reflect the topology of the network. The probit route choice model alleviates many difficulties associated with logit-based network loading at increased computational costs. In this model, the perceived travel time is assumed to be normally distributed that leads to a multivariate normal distribution of the perceived travel times on all paths of the given OD pair. Monte Carlo simulation is used in loading the probit choice probabilities.

2.4 Travel Time Reliability

The effectiveness of a route choice model is dependent on how close is imitates the real network. The drivers' route preference in uncongested ideal traffic condition may solely be based on the path travel distance. Oppositely, in congested real traffic condition, the drivers may consider travel time variations due to the variation of travel demand and supply, accidents, poor weather, etc. In this regard, the reliability of travel time on the path is an important decision factor in the real route choice problem. The network reliability has two aspects; namely, connectivity and travel time reliability (Wakabayashi and Iida, 1989). The concept of connectivity evaluates the probability that the driver reaches a given destination by all means, while travel time reliability evaluates the probability that the driver reaches a given destination within a given time. In this study, the authors focus on the second aspect.

Asakura (1998) proposed a model that evaluates the travel time reliability between an OD pair in the case of natural disasters. Using a stochastic travel time, a reliability measure is defined as a probability that one can travel between an OD pair within an acceptable level of travel time. Lee et al. (2000) formulated a reliability traffic assignment model where travel time reliability is determined by the degree of travel time variation on the paths chosen by the motorists. In their study, travel time reliability is a function of both road capacity and traffic demand. Asakura and Hato (2000) formulated a behavioral model in a deteriorated network focusing on the difference between the recognized network and the actual network for non-informed and informed drivers. Fan and Nie (2006) proved the monotonic property of successive approximation sequences for routing problems with recourse. The study further showed that the deterministic shortest path and *k*-shortest path problems are equivalent to the special case of the stochastic on-time arrival (SOTA) problem where link travel time probability densities are delta functions.

Kim (2008) used PDFs of OD and route travel time for an activity scheduling and route choice problem, respectively. In the study, reliable travel time and travel time margin were introduced in order to model the risk-averse behavior of travelers. A traveler who has a preferred arrival time at a destination would consider it for deciding one's departure time. If necessary, the preferred travel time can be reflected in one's route choice. In this paper, the integration of personal travel preference will be discussed in detail.

3. MODELING FRAMEWORK

3.1 Path enumeration problem and Hierarchical Road Network Classification

The concept of the hierarchical algorithm proposed in this study is based on Park and Rillet's (1997). The algorithm identifies *k* reasonable shortest paths in the hierarchical network in which arterial and highway network is denoted as a major network and drivers find independent corridors on it. In reality, human beings recall major corridors first and only consider them when choosing and changing their routes since the memory capacity of human beings are not sufficient for storing a whole minor network topology. Therefore, the first process of hierarchical path enumeration is an independent corridor finding problem. In order to find the corridors in the major network, a normal k-path algorithm is used. The link similarity among enumerated paths has been an issue in the generation of multiple paths. In this study, a penalty method is employed (Lim and Kim, 2006) in which the links used by previously identified paths are penalized to minimize the chances of generating the *k*-shortest path set with similar links used. As explained, the corridor finding process on the major network copies the cognitive process of human beings. In addition to the hierarchical corridor finding, the maximum detour of path is restricted for building up a reasonable path set. After enumerating all feasible paths, the enumerated paths were further subjected to the travel time constraint. Based on the driver's perspective, paths with costs higher than a driver's acceptable limit would not be included in the *k*-reasonable path set. In this study, the maximum travel time is 2.5 times higher than the minimum OD travel time. After finding a corridor, a driver has to connect one's origin and destination with the closest points on the corridor because most original origins and destinations are not located on the highway or main corridor. The original origin and the destination should be connected with the closest entering and exiting locations on the corridors. Dijkstra's algorithm is used for finding the shortest connection.

The corridor-based hierarchical path searching algorithm has an advantage for modeling the effect of traffic information via VMS (Variable message sign) or radio. In reality, traffic information disseminated through broadcast systems only reports traffic condition along main corridors. Accordingly, most drivers cannot perfectly identify travel time on their paths since traffic condition between their trip ends and corridor in/out points is still unknown. If a hierarchical network structure is used for modeling traffic information evaluation, then the imperfect information can be considered in such a way that the travel times of corridors on the major network are updated and given to drivers. To check the properties of the identified corridors, two measures of effectiveness (MOE) were conducted. The total travel time ratio (TTTR) is the first, which is the ratio of the travel time of alternative path *p* to the travel time of the fastest path *k*. The TTTR shows a pair-wise comparison of relative efficiency between two routes *k* and *p* in terms of travel times. The second is the route similarity (RS), which is the ratio of the length of the route *k* repeatedly used while traversing through the alternative path *p*.

$$TTTR_{kp} = \frac{TT_p}{TT_k} \tag{5}$$

$$RS_{kp} = \frac{\sum_{a \in A}^{n} d_a \cdot \delta_{a,kp}}{d_{\min}^{rs}} \tag{6}$$

where $TTTR_{kp}$ = TTTR between route k and p; TT_k = travel time on route *k*; RS_{kp} = RS of route *k* to route *p*; d_a = distance on link a; $d_{\min}^{rs}$ = distance of the shortest route for OD pair *rs*; $\delta_{a,kp}$ = 1 if link *a* is used by route *k* and route *p*, 0 otherwise; and *n* = number of links in the network.

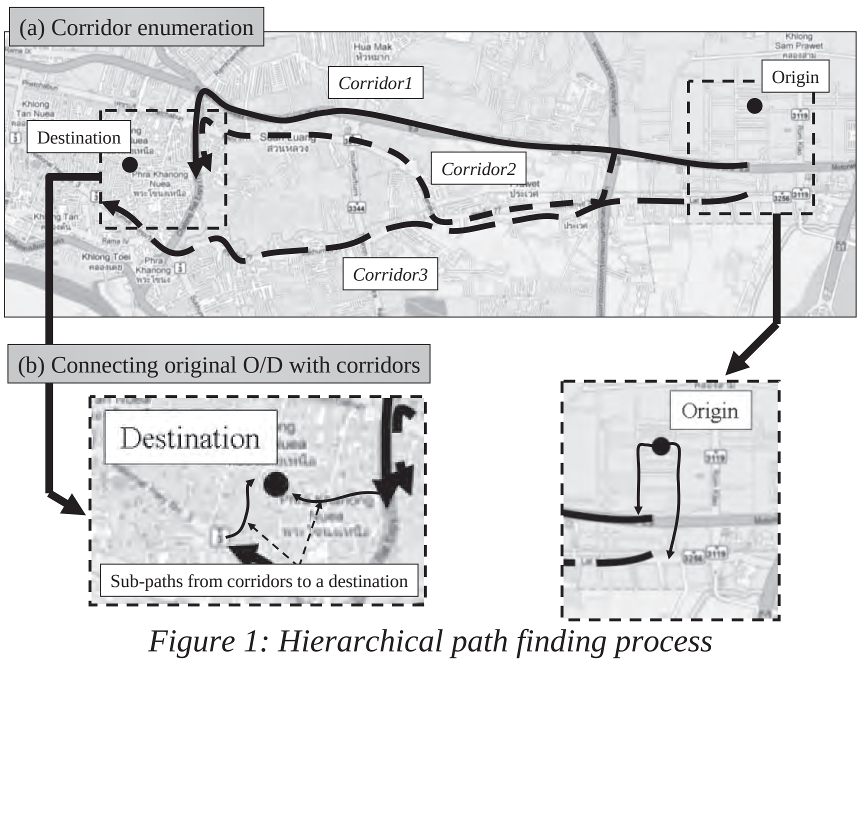

Figure 1: Hierarchical path finding process

3.2 Path choice problem with probabilistic travel time distribution

3.2.1 Link travel time

The first step of the modeling procedure for probabilistic path travel time is the generation of random link travel time. Generally, the link travel time is dependent on the traffic flow on the link. However, incorporating traffic flows to the route choice model requires a huge calculation burden, thus affecting the efficiency of the model. To simplify the problem while considering the link travel time variation, the actual link travel time t_a is considered as a random variable with a normal PDF $N(TT_a, \sigma_a)$, where TT_a (7) is the average link travel time and σ_a (8) is the standard deviation of the link travel time, which is dependent on the road functional classification of the link, $\varphi_{RF(n)}$. It should be noted that link travel times in arterial roads are more variable compared to freeways.

$$TT_a = \frac{d_a}{E(SPD_a)} \tag{7}$$

$$\sigma_a = \varphi_{RF(n)} \cdot TT_a \tag{8}$$

where d_a and $E(SPD_a)$ is the length and average travel speed of link a, respectively.

In randomly generating the actual link travel time, t_a, Monte Carlo simulation method is used. Monte Carlo simulation is a technique in which an output of random numbers is related to an assumed probability distribution (in this study, a normal distribution) so that a set of probable values for the basic variables of the function is obtained (Smith, 1986). This method is used to generate a sample of link travel time, t_a.

$$t_a = TT_a + \sigma_a \sqrt{-2 \ln TT_a} \cdot \sin 2\pi \cdot TT_a \tag{9}$$

3.2.2 Path travel time

In reality, drivers recognize a path as a whole instead of dividing it into independent links. Therefore, the uncertainty of path travel time is also modeled with respect to a path instead of a link. It is therefore reasonable not to include the perception errors of the links in computing the path travel time. Instead, perception errors should be considered path-based not link-based as in Mirchandani and Soroush's (1987) formulation. Accordingly, path travel time c_k^{rs} is calculated by summing random link travel times t_a along path k as shown in Eq. (10). In other words, a sample of path travel time is calculated as a sum of random link travel times.

$$c_k^{rs} = \sum_{a=1}^{n} t_a \cdot \delta_{a,k} \quad \text{where } \delta_{a,k} \begin{cases} 1 & if \quad a \in k \\ 0 & otherwise \end{cases} \tag{10}$$

The addition of the random link travel times might be questionable because it does not consider the correlation of subsequent links. In reality, traffic congestion and delay between two connecting links are interrelated. Due to computational complexities, however, the inclusion of link correlation is left for the future study.

After a number of simulation trials m, the range and frequencies of each path travel time are determined for estimating the distribution of path travel time. To test the goodness of fit of the distribution, a chi-square test was conducted. All path travel time distribution functions should satisfy Eq. (11).

$$\sum_{i=1}^{m} \frac{(n_i - e_i)^2}{e_i} < c_{1-\alpha, f} \tag{11}$$

where n_i is the observed frequency of $c_{k,i}^{rs}$ values and e_i is the corresponding frequency from the assumed theoretical distribution; $f = m - 1$; $c_{1-\alpha, f}$ is the value of the approximation of Chi-square (χ_f^2) distribution at a cumulative probability (1-α) and; α is the significance level.

The mean travel time of path k, μ_k and the standard deviation, σ_k of the enumerated paths were determined using Eq. (12) and Eq. (13), respectively.

$$\mu_k = \frac{1}{m} \cdot \sum_{i=1}^{m} c_{k,i}^{rs} \tag{12}$$

$$\sigma_k = \sqrt{\frac{\sum_{i=1}^{m} (c_{k,i}^{rs} - \mu_k)}{m-1}} \tag{13}$$

With the calculated path mean travel time and standard deviation, the path normal distribution function curve was drawn. The distribution function was calculated using Eq. (14).

$$f_x(x) = \frac{1}{\sigma_k \sqrt{2\pi}} e^{-\left(\frac{(x-\mu_k)^2}{2\sigma_k^2}\right)} \tag{14}$$

where $x = z \cdot \sigma_k + \mu_k$ and -4.0 $\leq z \leq$ 4.0. The path travel time distribution is used for generating random path travel time samples in the developed route choice model.

A statistical test for a normal distribution of a path travel time would be unnecessary because the path travel time is the sum of normal link travel times. The main purpose of above the procedure is for the application to real link travel time data. If link travel time is collected from the real road network, the sum of the travel time would not follow a normal distribution. Therefore, in that case, a statistical test for other probability distributions is required. In addition, neglecting the link travel time correlation is acceptable when the surveyed link travel times are used for path travel time modeling since the link travel times already include the interaction.

3.3 Formulation of a new route choice model

Two alternatives were considered in the calculation of the route choice probability; namely, 1) with travel time budget and 2) without travel time budget. For the with travel time budget case, it is assumed that there is a known preference arrival time at the destination; while for the without travel time budget case, the route choice probabilities of a typical driver is calculated.

3.3.1 Route choice with travel time budget

Some drivers demand a specific arrival time or maximum acceptable travel time for their travels. Existing route choice models have not reflected this demand which is, in reality, an important influencing factor on the route choice decision. In this study, the path choice probability is calculated based on the user's maximum acceptable travel time and it is denoted as the "reference time." As hypothesized by Fuji and Kitamura (2004), the path choice probabilities can be calculated considering the reference travel time within the users' time frame. Usually, the drivers recall the route travel time in ranges; that is, from a minimum to maximum value. To imitate the perception process of path travel time, in their study, it is assumed that the drivers believe that the path travel time of path *k* would not be less than t_{min} or greater than t_{max}..

In calculating the path choice probability, this study accounts for the PDF function of the path travel time. As shown in Figure 2, the probability that the traveler arrives at a destination within a reference time *t* is determined by the shaded area. The greater the shaded area, the higher is the probability of arriving on time using the path. In addition, the reference time *t* differs from one person to the other in reality. Accordingly, the perceived travel time distribution is surveyed in order to reflect the real distribution of the reference time. The path choice calculation is taken as the probability that a given path *k* is the shortest path at a particular reference time *t*. Eq. (15) shows the probability that path *k* becomes the shortest path given a minimum OD travel time π^{rs}. That is, when path *k*'s travel time is shorter than those of the other alternative's and mathematically represented by

$$pr(C_k^{rs} = \pi^{rs}) = pr(c_k^{rs} < c_1^{rs} \text{ and } c_k^{rs} < c_2^{rs} \text{ and} \ldots\ldots\ c_k^{rs} < c_n^{rs}) \quad \forall 1,2,\ldots,k,\ldots,n \in P^{rs} \qquad (15)$$

where P^{rs} is the path set for OD pair *rs*. The probability that the path *k* becomes the shortest path is calculated by Eq. (15). All paths found by a hierarchical finding algorithm do not have serious overlapping links, so their travel times can be assumed to be independent one another. Accordingly, the choice probability is further simplified as follows:

$$pr(c_k^{rs} = \pi^{rs}) = pr(c_k^{rs} < c_1^{rs}) \cdot pr(c_k^{rs} < c_2^{rs}) \cdot \ldots\ldots \cdot pr(c_k^{rs} < c_n^{rs}) \quad \forall 1,2,\ldots,k,\ldots,n \in P^{rs} \qquad (16)$$

Analytically, the calculation of choice probability $pr(c_k^{rs} = \pi^{rs})$ for path *k* by Eq. (15) and (16) requires a big calculation burden especially in the real-size network since all cases have to be compared pair by pair. Let's assume that there are only two independent paths. In order to calculate the choice probabilities of the two paths, the probability distributions of two paths should be considered simultaneously. In addition, the cases in which the minimum travel time is shorter than the reference time (c_{ref}^{rs}) are only taken into account because travelers do not want to arrive later than their maximum acceptable time. If both of paths cannot give a travel time shorter than the reference time, then it is regarded as a fail. The choice probability of path 1 only in the success cases can be calculated as Eq. (17).

$$pr(c_1^{rs} < c_2^{rs} \mid success) = \frac{pr(c_1^{rs} < c_2^{rs})}{pr(\min(c_1^{rs}, c_2^{rs}) < c_{ref}^{rs})} = \frac{pr(c_1^{rs} < c_2^{rs})}{pr(c_1^{rs} < c_{ref}^{rs}) + pr(c_2^{rs} < c_{ref}^{rs})} \qquad (17)$$

The calculation of Eq. (17) is not so difficult in the case of two paths. However, a calculation burden increases sharply as the number of paths in the network increases. In addition, the calculation of $pr(c_1^{rs} < c_2^{rs})$ requires analytical manipulation.

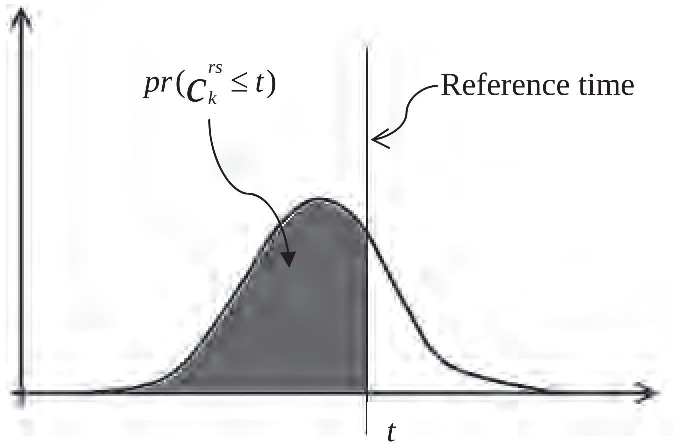

Figure 2 Path Probability of On-time Arrival

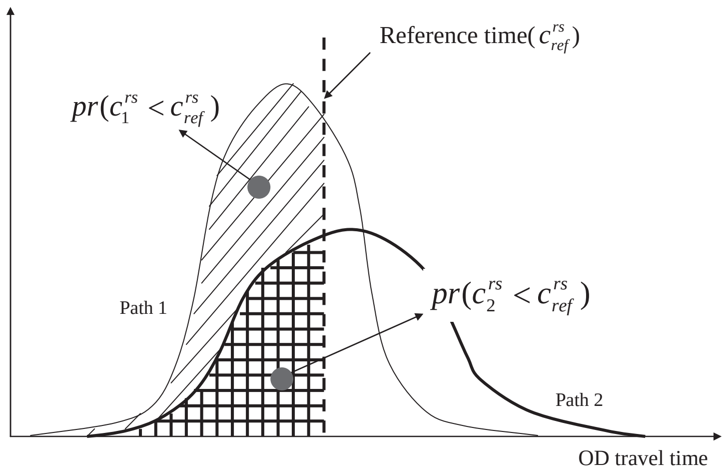

Figure 3 Pair by Pair Path Choice Probability Comparison

In this study, a simplified approach in approximating the path choice probability of Eq. (15) is presented. Using the Monte Carlo simulation technique, the travel time of each path in the path set is generated and the feasibility of the minimum travel time under the reference time is checked. In other words, if the minimum travel time of paths at a trial is longer than the reference time, then the trial is considered fail and it would not be included in the probability calculation. The number of times that a path travel time c_k^{rs} is the shortest is denoted, N_k^{rs}, where $c_k^{rs} \leq \pi^{rs}$ is counted and the choice probability of path *k* is estimated as follows:

$$pr(c_k^{rs} = \pi^{rs}) = \frac{N_k^{rs}}{N_{total\_success}} \tag{18}$$

where $N_{total\_success}$ is the number of trials where the shortest path has a path travel time less than or equal to the reference time c_{ref}^{rs}. The feasibility of arriving at the destination within c_{ref}^{rs} is also calculated as

$$SR(c_{ref}^{rs}) = \frac{N_{total\_success}}{Total\ Trials} \tag{19}$$

where $SR(c_{ref}^{rs})$ is the success rate where the shortest path has a travel time less than c_{ref}^{rs} (also known as *Expected Satisfaction Rate*) and *Total Trials* is the total number of Monte Carlo trials.

3.3.2 Route choice without travel time budget

In some cases, the traveler does not declare a specific arrival or it is unknown to a route choice model. In this condition, the reference travel time which has been introduced in the previous case cannot be defined as a deterministic value. If the reference time is uncertain, the driver's reference travel time is assumed as an interval or probability distribution. This assumption is based on the study of Fuji and Kitamura (2004). As in the previous formulation, the probability that the driver arrives at the destination on time is calculated as

$$pr(c_k^{rs} = \pi^{rs}) = pr(c_k^{rs} = \pi^{rs} \mid c_{ref}^{rs} = t) \tag{20}$$

In this case, *t* is unknown but has a probability distribution which can be determined from an interview survey. Analytically, equation (20) could be elaborated as follows:

$$pr(c_k^{rs} = \pi^{rs}) = \frac{\int_{t_{\min}}^{t_{\max}} pr(c_k^{rs} = \pi^{rs}) \cdot pr(c_{ref}^{rs} = t)}{\int_{t_{\min}}^{t_{\max}} pr(c_{ref}^{rs} = t)} \tag{21}$$

For simplicity, the path choice probability by Eq. (21) can be approximated by Eq. (22).

$$pr(c_k^{rs} = \pi^{rs}) = \frac{\sum_{t_{\min}}^{t_{\max}} pr(c_k^{rs} = \pi^{rs}) \cdot pr(c_{ref}^{rs} = t)}{\sum_{t_{\min}}^{t_{\max}} pr(c_{ref}^{rs} = t)} \tag{22}$$

where t_{min} and t_{max} represent a temporal framework for route choice problem and they are set as t_{min} = 5 minutes and t_{max} = 120 minutes, respectively. In other words, drivers only consider their reference travel time within this time frame. The calculation of the term $pr(c_k^{rs} = \pi^{rs})$ is the same to the solution in the previous section; while the value of the term $pr(c_{ref}^{rs} = t)$ is taken from the probability distribution function of the perceived OD travel time which is an Erlang distribution and is given by

$$pr(c_{ref}^{rs} = t) = \frac{v(vx)^{k-1}}{(k-1)!} e^{-vx} \tag{23}$$

where v and k are parameters.

3.4 Measure of the Model Performance

For the performance evaluation, the proposed model was compared to the true success or hit ratio (TSR_k) shown in Eq. (24) and the Multinomial Logit (MNL) model. TSR_k has the nearly same concept with Eq. (18) but the success and the fail of arrival by the reference time is not considered in Eq. (24). Another data set for calculating the true probability to be the shortest path is generated for the model evaluation. The events of N_k^{rs} is randomly calculated using the path travel time distributions (see Eq. (14)).

$$TSR_k = \frac{N_k^{rs}}{N_{total}} \tag{24}$$

where, N_{total} is the total number of events for a comparison.

On the other hand, the choice probability of path k by a conventional MNL model P_k^{rs} was also calculated as

$$P_k^{rs} = \frac{e^{-\theta \cdot c_k^{rs}}}{\sum_{l \in P^{rs}} e^{-\theta \cdot c_l^{rs}}} \tag{25}$$

where the c_k^{rs} is the mean travel time on path k and the optimal value of scale parameter θ was calibrated based on TSR_k in a heuristic way. Note that all paths found by the hierarchical method should be sufficiently independent. Therefore, a requisite in applying MNL, known as IIA (Independence of irrelevant alternative), is satisfied and MNL can show desirable capability in the route choice problem.

3.5 Survey design for perceived travel time

In order to determine the probability distribution function of the reference time, a survey was conducted on the test route (Suvarnabhumi Airport to Victory Monument in Bangkok, Thailand). Respondents were asked regarding their expected travel time for the OD pair and they gave answers as an interval. The interval of travel time was standardized and plotted in a histogram. The number of bins, k is assumed using the following criterion (Hahn and Shapiro, 1967).

$$4 \cdot [0.75(n-1)^2]^{1/5} \le k \le \frac{n}{5}, \qquad \text{where: } n = \text{number of samples} \tag{26}$$

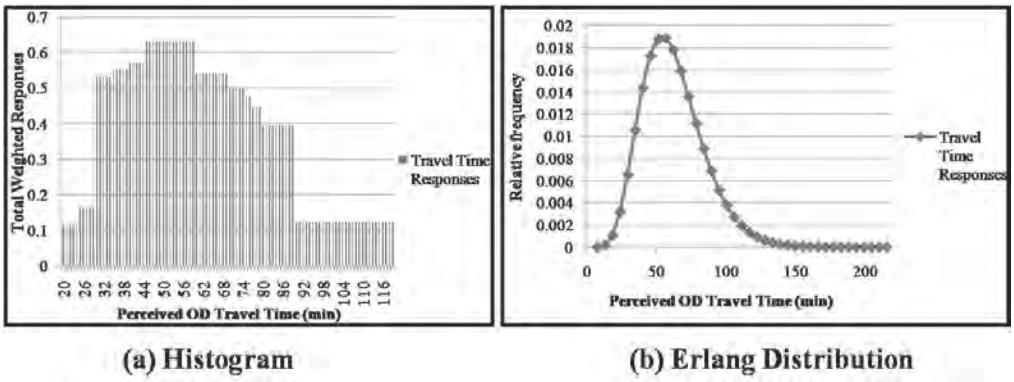

Figure 4: Perceived OD Travel Time Distribution

Table 1: Chi-square goodness-of-fit Test Results

Distribution	Parameters	Chi-squared value (w)
1. Normal	μ = 61.149 σ = 11.343	158.185 > 75.624; Rejected
2. Lognormal	**λ = 3.596** **ζ = 0.967**	**50.808 < 75.624; OK**
3. Gamma	α = 29.059 β = 0.475; 1/β = 2.104	660.701 > 75.624; Rejected
4. Erlang	**α = 15** **β = 0.245; 1/β = 4.077**	**31.526 < 75.624; OK**
5. Beta	**α = 2.0** **β = 3.5**	**44.224 < 75.624; OK**

The chi-square *goodness-of-fit* test is used for a statistical test. The chi-square test statistic, *w* is obtained using Eq. (27). Note that high values of *w* signify that the observed data contradicts the assumed model.

$$w = \sum_{i=1}^{k} \frac{(n_i - e_i)^2}{e_i} < c_{1-s,f} \quad (27)$$

where: n_i=observed frequencies, e_i= corresponding frequencies from an assumed theoretical distribution, $c_{1-\alpha,f}$ is the value of the appropriate chi-square distribution at the cumulative probability (1 - α), degree of freedom, $f = k - r - 1$ *and* r = number of parameters. The assumed test distribution models include normal, lognormal, gamma, Erlang and beta. The appropriate probability distribution for the perceived OD travel time is used in the calculation of the route choice probability. The perceived OD pair travel time was taken from the survey conducted. The perceived OD travel time responses were in ranges. In increments of 1 minute; the data were plotted and the histogram of the OD travel time was obtained as shown in Figure 4 (a). The length of range can be different in person to person, so the weight of each response for the range is normalized. From the data gathered, a chi-square *goodness-of-fit* test was conducted. The results of the test is shown in Table 1; where n = 37 samples, sample mean, μ = 61.149 min, standard deviation, σ = 11.343 and $chi_{(0.05,\ dof\ =\ 57)} \leq 75.62375$. The Erlang distribution best represents the perceived travel time distribution function, as shown in Figure 4 (b).

4. TEST RESULTS

4.1 Test area and path enumeration

An OD pair in Bangkok, Thailand (see Figure 5) is selected as a test network. The origin-destination (OD) pair chosen is the Suvarnabhumi Airport-Victory Monument route. The network consists of 314 links and 102 nodes. The generalized cost is taken from the average travel speed and length of each link. Using the hierarchical path enumeration model, five sufficiently independent paths are found as shown in Figure 5. In order to access the performance of the path enumeration algorithm, two Measures-of-Effectiveness were used; namely, the total travel time ratio (TTTR) and the route similarity (RS).

In the final path set, TTTR of the longest path is 2.003 with respect to the shortest path; which means that the worst path is 200.3% longer than the shortest one. Similarly, TTTR of the second, third, and fourth paths are 1.191, 1.284, and 1.448, respectively. In the case of the RS, most path pairs have a trivial value. The biggest one is between path 3 and 1 in which the RS value is 0.041; which implies that only 4.1% of the total distance of path 3 overlaps with path 1. The second biggest RS is 0.039 and it is occurred between path 5 and path 4. As a result, all five paths are sufficiently independent.

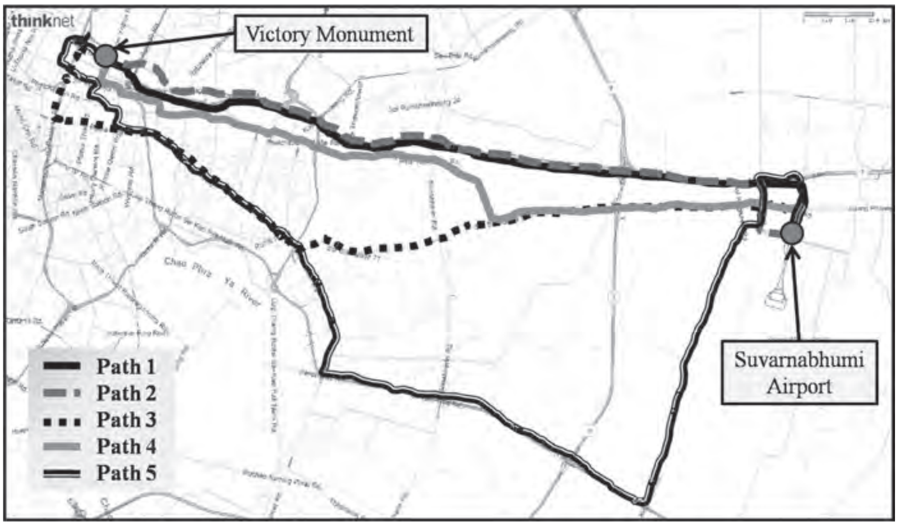

Figure 5 Study area in Bangkok, Thailand

4.2 Travel time generation for paths

Using Monte Carlo technique, the travel time of the enumerated path links were generated ($\varphi_{RF(1)}$ = 0.75 and $\varphi_{RF(1)}$ = 1.5). The road function coefficient, φ_{RF} serves as the standard deviation of the link travel time during the simulation process. In every trial, the sample path travel time is taken as the summation of the link travel times along the path. After then, the probability distribution of path travel time is assumed to be normal and a chi-square goodness-of-fit test was conducted.

The Chi-square value (w) for the test is ($Chi_{(0.05,6)} \leq 23.685$). In the test, a normal distribution well fits for the five paths. The w value of path 2 is the lowest (6.175) and the biggest occurs on path 3 (15.514). Figure 6 depicts the normal distribution of path travel time for the five paths. Path 1 shows the smallest average travel time (22.664 min). In addition, the SD of travel time on path 1 is also the smallest (6.831). The second best path is path 3. The average and SD of travel time on path 3 are 28.650 (min) and 8.758, respectively. Contrarily, Path 5 gives the worst travel time with an average travel time of 60.842 and SD of 13.23 minutes. Therefore, path 5 has the least possibility to become the shortest path.

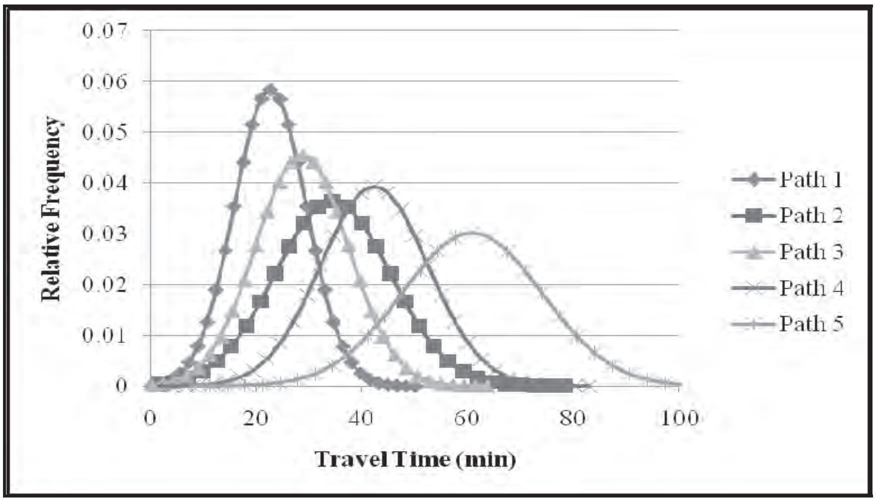

Figure 6 PDF of path travel time

4.3 Calculation of path choice probability

4.3.1 Route choice probability with travel time budget

Some drivers demand a specific travel time to arrive at the destination. For instance, travelers might have important appointments, meeting, or even the regular office check-in times. For this case, the probability that a traveler arrives at the destination on time was determined by calculating the cumulative distribution function (CDF) of the path actual travel time for a particular reference travel. Accordingly, the probability of arriving on time increases as the reference time increases (see Figure 7). If the on-time arrival probability is very low, the driver has to delay his arrival time target so as to have sufficient probability for on-time arrival.

The total number of events where the shortest travel time is less than or equal to the given reference time is set to 500, also known as the *total number of successful trials* in this study. The total number of trials regardless of whether the shortest path is less than or equal to the reference time is also noted to determine the feasibility of arriving at the destination denoted as the *Expected Satisfaction Rate* (see Figure 7). If a traveler wants to arrive at the destination within 35 minutes or less, the probability that at least one path would have such travel time is less than 100%. On the other hand, if the traveller demands a travel time greater than 35 minutes, at least one path (mainly path 1) that could give such travel time.

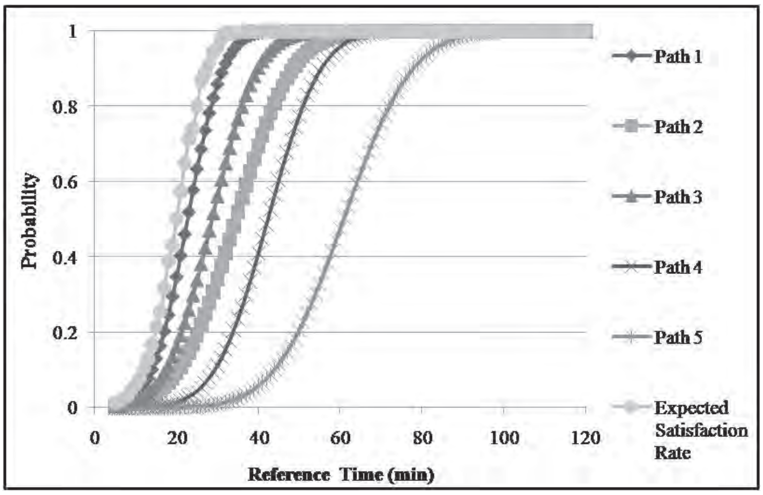

Figure 7 On-time arrival probabilities and Expected Satisfaction Rate with increasing reference time

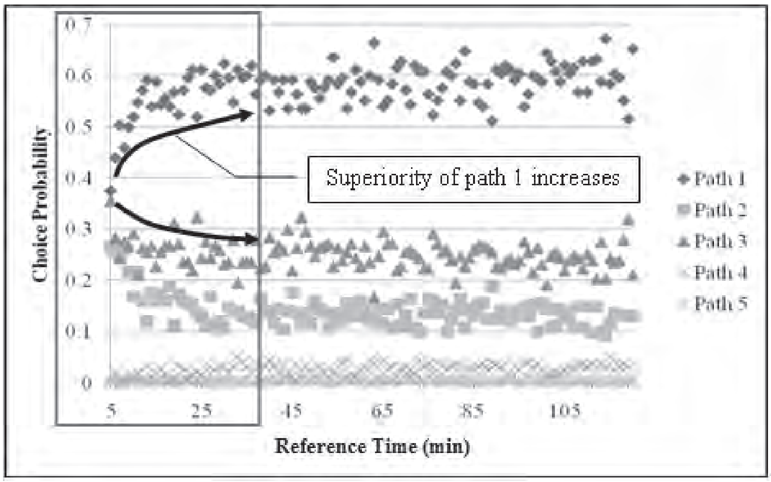

Figure 8 Path Choice Probabilities at Different Demand Travel Time

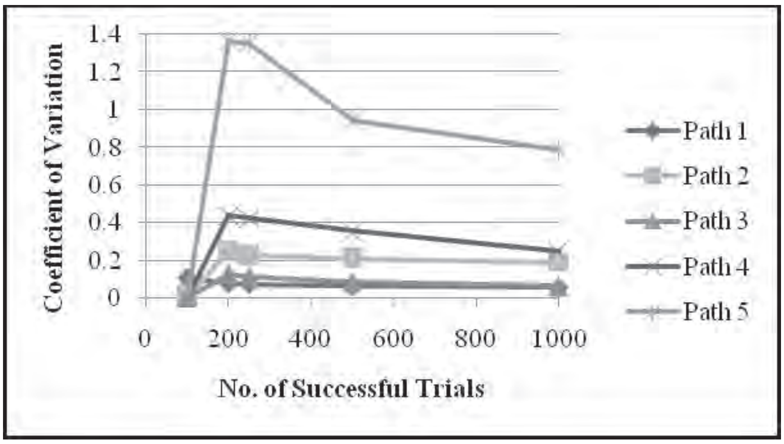

Figure 9 Coefficient of Variation of the path choice probabilities with increasing successful trials

Figure 8 shows the probability of being the shortest path at a specific reference time using 500 successful trials. When the reference time is very short, such as 5 minutes, paths 1, 2, and 3 have similar probabilities. As shown in Figure 7, the on-time arrival probability of the three paths are very small, so the paths show similar performance. However, the superiority of path 1 increases as the reference time is extended. In Figure 7, path 1 provides more than 60% probability for arriving on time at 25 minutes reference time. Oppositely, those of path 2 and 3 are less than 35%. The superiority keeps increasing until the reference time reaches 25~40 minutes. After then, path choice probabilities are stablized.

Moreover, some fluctuations in the path choice probabilities are observed with increasing reference time (see Figure 8) mainly because the choice probabilities are calculated using Monte Carlo simulation. When the number of trials in the simulation increases, the choice probabilty fluctuation can be decreased. The variance change of the path choice probabilities is shown in Figure 9. Visibly, the variance is inversely proportional to the number of successful trials; that is, increasing the successful trials decreases the variation of the path choice probabilities. As shown in Figure 9, 500 successful trials give a satisfactory path choice probability variance and is therefore used in this study.

4.3.2 Route choice probability without travel time budget

The path choice probability without travel time budget is calculated using Eq. (22). This case is particularly applicable for travelers who perceive an uncertain travel time as an interval. In this case, the perceived travel time is unknown but its probability distribution is available from the survey conducted. Figure 10 shows the trend of the path choice probabilities with varying reference time. In the test, the path choice probabilities are calculated from t_{min} = 5 minutes to t_{max} = 120 minutes. Drastic changes in path choice probabilities were observed when the maximum acceptable travel time is relatively low; 5 to 30 minutes. Since the calculation of the choice probability is accumulated from t_{min} to t_{max}, the values are dependent on the maximum reference time. The longer the maximum reference time; the more stable is the path choice probability. From the survey, the maximum perceived travel time from Suvarnabhumi Airport to Victory Monument was known to be 120 minutes. Figure 11 shows the path choice probability of the proposed model, as well as the comparison to the True Success Rate (TSR_k) and Multinomial Logit (MNL) model results.

The path choice probabilities of the proposed route choice model were then compared to the True Success Rate (TSR_k) and multinomial Logit (MNL) model. As shown in Figure 12, both the proposed and the hierarchical MNL models have strong positive linear relationship to TSR_k; 0.9975 and 0.9972, respectively. Moreover, the coefficient of determination, r^2 values are relatively close to 1; 0.9951 and 0.9943 for the proposed model and Hierarchical MNL, respectively. This means that 99.51% and 99.43% of the variance or fluctuation in the path choice probabilities of the proposed model and the Hierarchical MNL respectively can be predicted from the TSR_k. Therefore, we can conclude that the route choice probabilities of TSR_k, MNL, and the developed method are nearly similar at the aggregate level. Note that there is no IIA problem for MNL. It means the test condition is very suitable and ideal for MNL model. Therefore, the performance of the developed model is very promising. In addition, in the case of MNL, utility coefficients should be calibrated with the real choice of travelers. It means that the developed model can give very accurate forecasting result without calibration. It is an attractive advantage when applying the developed model to the real-time route guidance system.

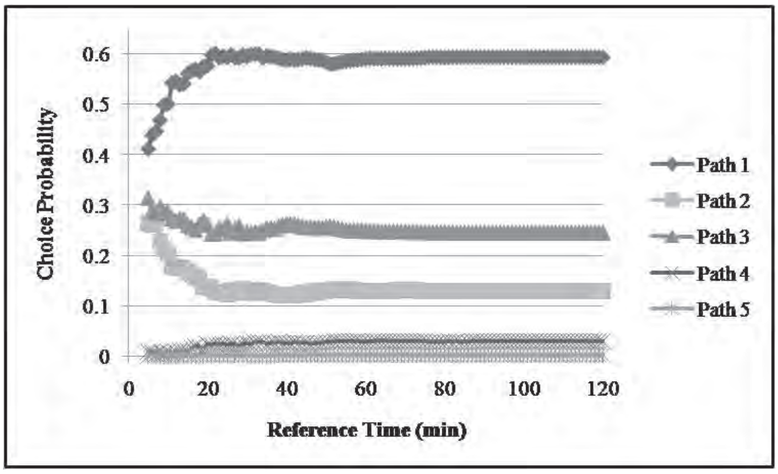

Figure 10 Path choice probabilities with increasing maximum reference travel time

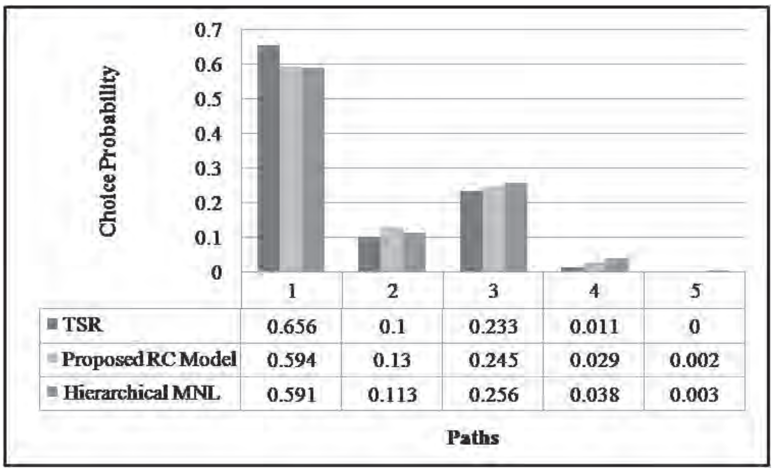

	1	2	3	4	5
TSR	0.656	0.1	0.233	0.011	0
Proposed RC Model	0.594	0.13	0.245	0.029	0.002
Hierarchical MNL	0.591	0.113	0.256	0.038	0.003

Figure 11 Path Choice Probabilities between the Proposed Model, TSR and MNL

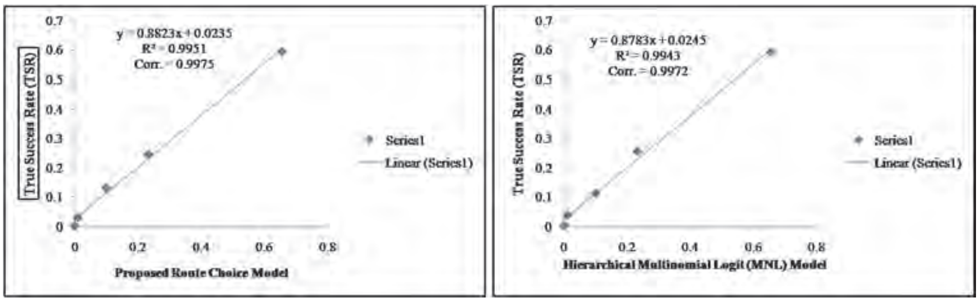

Figure 12 Correlation of the TSR to the Proposed Model and MNL

5. CONCLUSION

Understanding the variable transportation network characteristics and travelers' behavior are the keys to achieve an efficient route choice model. Route choice models have played an important role in solving the unmanageable urban congestion problem. This study presents a route choice model consisting of two parts; the path enumeration algorithm and the route choice formulation. The path enumeration algorithm is used for generating the reasonable path set. Both efficiency and flexibility to transportation network conditions are considered in the formulation of the algorithm. Among the issues addressed in the establishment of the algorithm are excessive link overlapping and path resource constraint.

On the other hand, a new route choice model is formulated in order to consider the probabilistic definition of path travel time and the perceived OD travel time. Through the Monte Carlo simulation technique, the link travel times were generated and then the path travel time mean and variance are calculated. From the Chi-square test, a normal distribution is selected for path travel time distributions. Moreover, the perceived travel time of drivers is formulated by a PDF (Erlang distribution) based on the survey data. Taking both the path actual and the perceived travel time PDFs, path choice probabilities were calculated for the two case scenarios: with and without travel time budget. The route choice model was evaluated and compared to the True Success Rate (TSR_k) and the deterministic Multinomial Logit (MNL) model.

There are several important academic contributions of this study. First, a route choice model for the PDF of path travel time is proposed. Previously, a discrete choice model assuming the uncertainty of path travel time has been used. For example, a logit model assumes that an error term in the utility function follows a Gumbel distribution. Oppositely, the developed model does not need any assumption on the travel time uncertainty. Instead, it can handle the travel time distribution without any manipulation.

Second, the developed model can calculate route choice probabilities without calibration. Most route choice models have to be calibrated with real survey data. Conversely, the developed model does not have any coefficient to be calibrated. Even without calibration, however, the developed model gives the same route choice probabilities with MNL. It is a big advantage for practical applications.

Thirdly, the drivers' time budget can be taken into account in the route choice problem. Existing route choice models and route guidance systems does not consider the arrival time demanded by drivers. In reality, however, many travelers have preferred arrival time in their travels. For example, if a driver has an appointment 50 minutes later, the driver's reference time is 50 minutes. Hence, his request for route choice is a conditional problem in which he wants to find the shortest path for arriving at his destination within 50 minutes. The developed model also shows that the route choice probability is dependent on the reference time when the path travel time is uncertain. In addition, the developed model can calculate the success rate for on time arrival with given reference time. If the methodology is embedded in the car navigation system, drivers can adjust their scheduled appointments with the information.

Fourthly, a hierarchical multi-path enumeration method is presented. All paths found by the model are sufficiently independent so it is useful for applying MNL to a real-size network. The concept of building two-layer network is also consistent with the cognitive process of human beings.

To further improve the proposed route choice model, it is suggested to extend the application to dynamic and stochastic traffic assignment problem. It is further recommended to apply the model to integrated transportation networks where turn prohibitions and/or multimodal conditions exist. A mathematical approach in calculating the path utility choice function is also recommended to eliminate the burden of Monte Carlo simulation.

REFERENCES

Asakura, Y. (1998) Reliability Measures of an Origin and Destination Pair in a Deteriorated Road Networks with Variable Flows, Recent Methodological Advances, 273-287.

Asakura, Y. and Hato, E. (2000) A Route Recognition Model for Transport Networks Reliability Analysis, Reliability of Transport Networks, 203-216.

Behkor, S. et al (2006) Evaluation of Choice Set Generation Algorithms for Route Choice Models, Annals of Operations Research, Vol. 144, 235-247 (13).

Bell, M.G.H. (1995) Stochastic User Equilibrium Assignment in Networks with Queues, Transportation Research part B 29B, 125-137.

Bock, F. et al (1957) An Algorithm for Finding and Ranking Paths Through a Network, Research Report, Armour Research Foundation, Chicago, Illinois, November 15, 1957.

Dijkstra, E.W. (1959) A Note on Two Problems in Connection with Graphs, Numerical Mathematics 1, 269-271.

Eppstein, D. (1998) Finding the k-shortest Paths, SIAM Journal Computing, 28 (2), 652-673.

Fan, Y. and Yu Nie (2006) Optimal Routing for Maximizing the Travel Time Reliability, Networks and Spatial Economics, Vol. 6 (3), 333-334.

Floyd, R. (1962) Algorithm 97: Shortest Path, Communications of the ACM 5 (6), 345.

Frank, H. (1969) Shortest Paths in Probabilistic Graphs, Operations Research, Vol. 17 (No. 4), 583-599.

Fuji, S. and Kitamura, R. (2004) Driver's Mental Representation of Travel Time and Departure Time Choice in Uncertain Traffic Network Condition, Networks and Spatial Economics, 243-256.

Hahn, G. and Shapiro, S. (1967) Statistical Models in Engineering. USA. John Wiley and Sons Inc.

Kim H. (2008) New dynamic travel demand modeling methods in advanced data collecting environments, Ph.D. dissertation, University of California, Irvine.

Lee, S. et al (2000) Reliability Analysis and Calculations on Large Scale Transport Networks, Reliability of Transport Networks, 173-189.

Lim Y., B. Heydecker (2005) Dynamic departure time and stochastic user equilibrium assignment, Transportation Research Part B 39 (2), 97-118.

Lim, Y. and Kim, H. (2006) A Shortest Path Algorithm for Real Road Network Based on Path Overlap, Journal of the Eastern Asia Society for Transportation Studies, Vol. 6, 1426-1438.

Mirchandani, P. (1976) Shortest Distance and Reliability of Probabilistic Networks, Comput. And Operations Research, Vol. 3, 347-355.

Mirchandani, P. and Soroush, H. (1987) Generalized Traffic Equilibrium with Probabilistic Travel Times and Perceptions, Transportation Science, Vol. 21, No. 3, 133-152.

Nepal, P. K., (2002) Median shortest path problems in the design of transportation networks, Master thesis, Asian Institute of Technology, Bangkok.

Park, D. and Rillet, L.R. (1997) Identifying Multiple and Reasonable Paths in Transportation Networks, A Heuristic Approach, Transportation Research Record, 1607, 31 – 37.

Pollack, M (1961) The kth Best Route Through a Network, Operations Research, Vol. 9, 578.

Sharma, S. L., (2001) Identifying Multiple Reasonable Alternative Routes in Transportation Networks Using Efficient Vector Labeling Approach, Master thesis, Asian Institute of Technology, Bangkok.

Sheffi, Y. (1985) Urban Transportation Networks Equilibrium Analysis and Mathematical Programming Methods. New Jersey, Prentice Hall.

Thomas, R. (1991) Traffic Assignment techniques, Avebury technical.

Yen, J.Y. (1971) Finding the k shortest Loopless Paths in a Network, Management Science, Vol. 17, No. 11, 712-716.

Wakabayashi, H. and Iida, Y. (1989) An Approximation Method of Terminal Reliability of Road Networks Using Partial Minimal Path and Cut Set, Proceedings of the 5thWorld Conference on Transportation Research, Vol. 4, pp. 367-380. Yokohama, Japan.

DEVELOPMENT OF MULTI-CLASS PEDESTRIAN ASSIGNMENT ALGORITHM

JUNG-YUB LEE, HYUN-HO CHANG,
HYUN-SUB LIM, and YOUNG-IHN LEE
Graduate School of Environmental Studies
Seoul National University
urrruk@naver.com

ABSTRACT

Walking is a fundamental means of transport for humans, and a primary means to connect between other forms of transportation. Even though the number of studies on pedestrians and on pedestrian demand analysis have increased, there are few studies on pedestrian assignment. The object of this study is to develop a pedestrian assignment algorithm that is applicable to mega-buildings and general sidewalks, and to investigate its application possibility. This paper comprises a literature review of vehicle and pedestrian assignment, a section on pedestrian assignment methodology, a section with experiment results and analysis, and closes with a conclusion and suggestions for future studies.

1. INTRODUCTION

Walking is a human's fundamental means of transport, and a primary transport method used to connect with other forms of transportation. Most existing studies have investigated traffic assignment in order to analyze the traffic demands of passengers. Recently, there has been an increase in the number of studies on pedestrian traffic and an increase in the need for pedestrian demand analysis. However, there are few studies on pedestrian assignment within pedestrian demand analyses.

In the existing vehicle traffic assignment methods, the transportation capacity used to calculate travel cost is fixed. However, the capacity of the facilities that pedestrians use varies with facility type and pedestrian demand. There are also equilibrium and non-equilibrium states that may co-exist and may relate to pedestrian class. Such co-existence limits the application of existing traffic assignment methods that use the Node-Link system. Accordingly, a multi-class pedestrian assignment algorithm, which considers variation in capacity related to directional demands and mixed directionality of pedestrians, was developed in this study.

The multi-class pedestrian assignment algorithm considered pedestrian space characteristics and was configured using a Node-Link-Block network system where the Block, a pedestrian space unit, has been added to the existing Node-Link system. A travel cost function was also developed. Furthermore, pedestrian's preferred or enforced travel types were included in the assignment algorithm. Using the developed Node-Link-Block network system, along with the travel cost function and the pedestrian assignment algorithm, a final pedestrian status is obtained in which user equilibrium or user non-equilibrium states related to each pedestrian class can co-exist.

This paper consists of a review of the literature regarding vehicle and pedestrian assignment, a section on the development of pedestrian assignment methodology comprising five portions: 1) pedestrian assignment; 2) definition of multi class pedestrians and facilities; 3) a description of the Node-Link-Block network system; 4) a definition of the travel cost function; and 5) a pedestrian traffic assignment technique. This is followed by a section containing experiment results and analyses. The paper ends with a conclusion and suggestions for future study.

2. LITERATURE REVIEWS

2.1 Existing Traffic Assignment

Existing studies on traffic assignment typically consider passenger cars and/or public transit, and their objectives are to analyze traffic demand to allow system optimization or to determine user equilibrium states. An assumption in traffic assignment studies based on user equilibrium is that no passenger can select another path from origin to destination (O-D) without increasing the total cost of all vehicle passengers. A characteristic of user equilibrium is that all travel path costs are the same for all O-D paths, and that the cost of the selected path is less than that of the unselected path. The purpose of system optimization is to minimize the system's overall travel cost rather than to optimize passenger travel cost. Study on the traffic assignment algorithm is continuously on the progress to link base and path base, from static to dynamic traffic assignment.

A typical traffic assignment transportation system has specific paths that are based on unidirectional directionality within a path. However, each pedestrian may move with differential directionality in a pedestrian space and may move along an infinite number of paths. Accordingly, there are significant limitations when applying existing Node-Link vehicle traffic assignment systems to pedestrian assignment systems.

2.2 Pedestrian Assignment

Even though there are many local and foreign studies regarding traffic assignment, there are very few studies on pedestrian assignment. Ahmed Abdelghany studied an American football field stadium, a crowded facility, using a cell unit based discrete space structure system and an A* algorithm. However, there are no known reports on pedestrian assignment among the reviewed traditional traffic assignment studies. Accordingly, the object of this study is to develop a pedestrian assignment algorithm that is applicable to mega-building and general sidewalk situations, and to investigate its application possibilities.

3. PEDESTRIAN ASSIGNMENT METHODOLOGY

Development of a methodology for pedestrian assignment consisted of establishing the main items of consideration based on the traditional traffic assignment system, establishing a network system for pedestrian spaces, establishing the criteria for multi-class pedestrians, developing a travel cost function for specific facilities, and altering the traffic assignment algorithm based on the aforementioned items.

3.1 Considerations for Pedestrian Assignment

There are four key limitations to applying existing assignment methods to pedestrian traffic. Accordingly, the following items were included during development of the pedestrian assignment algorithm.

- Pedestrians use various facilities. Therefore, facilities in the pedestrian space need to be defined.
- The capacity of the Block used in this study varies according to pedestrian directionality and pedestrian demand varies by direction.
- Different from the unidirectional link system used for vehicle traffic, a pedestrian's movement direction within the pedestrian space varies from 1~∞.
- Pedestrians can be divided according to facility usage types, such as those who are required to use a specific facility, those who prefer to use it, as well as those who attempt to optimize the travel time to a specific facility.

3.2 Multi-Class Pedestrian and Facility Groups

Distinct from vehicle characteristics, pedestrians consist of a variety of classes that may be grouped according to facility usage, as well as by social or biological characteristics. Pedestrian class has been divided mainly based on types of items being carried or accompanying the pedestrian. In addition, if there is a specific facility in a specific pedestrian space, then the pattern of use of that facility and the time to pass through that facility can differ by pedestrian class. For example, a pedestrian with a specific accompanying item may prefer to use an escalator rather than a stairway. Thus, pedestrians were grouped into five classes to reflect these characteristics (Table 1).

Table 1: Multiple classes of pedestrians

		Groups
Pedestrian class	k_1	General Pedestrian
	k_2	Pedestrian with briefcase
	k_3	Pedestrian with BagPack
	k_4	Pedestrian with Carrier
	k_5	Pedestrian with baby

There are various types of facilities in pedestrian use areas, and the patterns of use of these facilities are different. These types were categorized according to the travel cost similar to the approach used in vehicle traffic assignment. A travel cost model was developed for each facility type to reflect these characteristics. Table 2 presents the list of facilities that was included in the development of the pedestrian assignment.

Table 2: Facilities included in the pedestrian assignment process

	Items
Facilities included in Pedestrian Traffic Assignment	Stairway
	Escalator
	Moving Walk
	Passage

3.3 Node-Link-Block System

The network system used in this study differed from the network system used for vehicle traffic assignment in that specified size of pedestrian using block which is called facility. Vehicles follow a fixed direction path in the traffic assignment network system; however, pedestrians may use an infinite number of paths. Accordingly, the system used in this study added the Block item to the Node- Link system used for vehicle traffic assignment.

Figure 1 presents the basic structure of the Node-Link-Block system for use in multi-class pedestrian assignment, and shows the attributes used for pedestrian assignment. There are more than two Nodes in the pedestrian network system, and Links connect those Nodes. The number of Nodes and Links also differ according to the Block's characteristics. The Link indicates the passage within a Block along which pedestrians can move. There are two Nodes and a single Link for some facilities, such as an escalator, because the direction of pedestrian movement in that facility is only in one directional.

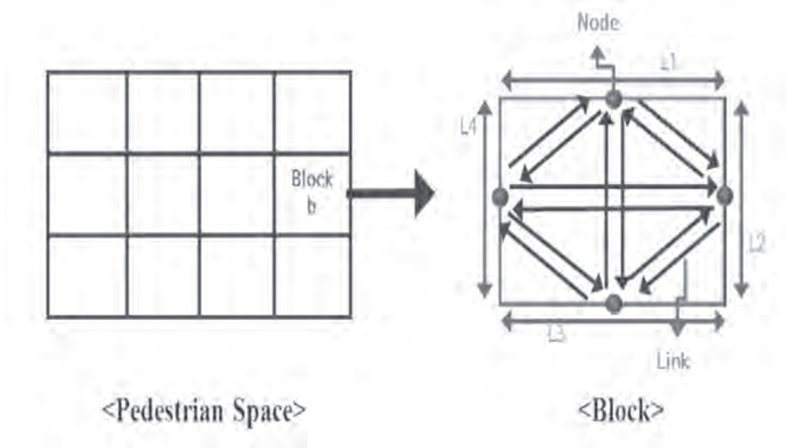

Figure 1: The Node-Link-Block system used in pedestrian assignment

The variables used to define the Node-Link-Block system, including travel cost, pedestrian traffic demand, etc., are as follows:

- $\mathbf{S} = \{\mathbf{S_1},\ \mathbf{S_2},\ \mathbf{S_3},\ \mathbf{S_4}\} = \mathbf{S_a}$: the pedestrian space which includes four facility types
  $\mathrm{S_1}$: Stairway, $\mathrm{S_2}$,: Esclaltor, $\mathrm{S_3}$: Moving Walk, $\mathrm{S_4}$: Passage
- $\mathbf{B_{a,b}}$: the $\mathrm{b^{th}}$ Block which constitutes a facility or pedestrian space $\mathrm{S_a}$
- $\mathbf{d_{a,b,e}}$: the length (m) of the line that constitutes the $\mathrm{e^{th}}$ of $\mathrm{B_{a,b}}$
- $\mathbf{N_{a,b,e}}$: a set of nodes at the $\mathrm{e^{th}}$ outline of $\mathrm{B_{a,b}}$
- $\mathbf{N}$: a Node set the consists of n components, $\mathrm{N_{a,b,e}} \in \mathrm{N}$
- $\mathbf{l_{b,i,j}}$: a Link length i which connects Node i to the Node of $\mathrm{b^{th}}$ Block, $\mathrm{j} \in \mathrm{N}$
- $\mathbf{t_{b,i,j,k}}$: the $\mathrm{k^{th}}$ pedestrian class traffic at Node i and Node j connected to a Link in $\mathrm{b^{th}}$ Block
  $\mathrm{k} = \{\mathrm{k_1}, \mathrm{k_2}, \mathrm{k_3}, \mathrm{k_4}\}$ the pedestrian class group (see Table1)
- $\mathbf{F_{b,i,j,k}}$: free traffic flow speed (m/s) of the $\mathrm{k^{th}}$ pedestrian class at Node I and Node j connected by a Link in $\mathrm{b^{th}}$ Block
- $\mathbf{C_{b,i,j,k}}$: the travel cost of the $\mathrm{k^{th}}$ pedestrian class at Node i and Node j connected by a Link in the $\mathrm{b^{th}}$ Block

3.4 Establish Travel Cost Function

As explained previously, the road capacity to calculate travel cost is fixed in a vehicle traffic assignment system. However, the Block capacity in pedestrian assignment varies according to the total of each possible directional pedestrian demand in the pedestrian assignment system. To consider the volatile characteristics of the Block capacity, the capacity and demand of the Block at the each iteration is calculated through an incremental assignment, and the Link's travel cost is calculated using the V/C of the Block, where the V/C of each Block iteration is calculated using the accumulated pedestrian traffic demand in equations (1) and (2), and the capacity calculation from above. Thus

$$V_b = \sum_{i,j,k} t_{b,i,j,k} \tag{1}$$

$$C_b = \frac{\sum_{i,j,e} t_{b,i,j,k} \times d_{a,b,e}}{\sum_{e} d_{a,b,e}} \times C_{bo} \tag{2}$$

$$X_b = V_b / C_b \tag{3}$$

- $\mathbf{V_b}$: is the pedestrian demand using the bth Block
- $\mathbf{C_b}$: is the capacity of the bth Block
- $\mathbf{C_{b0}}$: is the unit capacity of Block b by type (persons/minute/meter)

Pedestrian facilities were classified as in Table 2 and equation (4) was used to determine the travel cost function in each pedestrian class according to the facility classification.

$$c_{b,i,j,k} = (F_{b,i,j,k} + d_b) \times (1.0 + \alpha(v_b/c_b)^{\beta}) \tag{4}$$

where d_b is the pedestrian demand for use of the bth Block and α and β are derived through pedestrian surveys. Here, the values were from survey data obtained at the Sadang Station where subway lines 2 and 4 cross. A total of 6 h of surveying [2 h at the morning peak time (07:00~09:00), 2 h during the evening peak time (17:00~19:00), and 2 h of non-peak time (12:00~14:00)] were used. The non-linear feedback analysis from the SPSS statistic package, was used to estimate the α and β parameters.

Table 3: Estimates of the α and β parameter values of the travel cost function for each facility type

	α			β			R-square
	Estimate	Confidence Interval (Asymptotic 95%)		Estimate	Confidence Interval (Asymptotic 95%)		
		lower	upper		lower	upper	
Stairway	0.80	0.79	0.82	2.92	2.76	3.08	0.95
Escalator	0.02	0.01	0.02	4.11	4.05	4.16	0.97
Elevator	0.10	0.09	0.10	6.49	6.32	6.66	0.95
Transit Passage	0.72	0.71	0.73	2.38	2.30	2.47	0.97

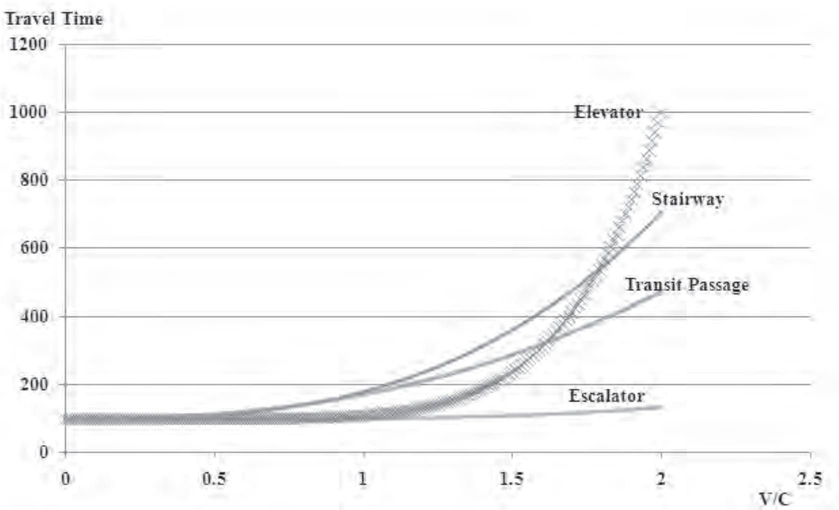

Figure 2: Travel time by facility type

3.5 Traffic Assignment Method

The pedestrian use of a Block's capacity varies according to the directionality of pedestrian travel and the pedestrian demand in each direction. One problem is that the assignment may not reach equilibrium because of pedestrian class differences between enforced and preferred use characteristics of the facility type being used. Therefore, applying existing vehicle traffic assignment methods to reach user equilibrium was deemed inappropriate. Accordingly, a Block's capacity at the each iteration is revised through an incremental assignment method. We speculated that those who are required to select a facility reach non-equilibrium, while those showing a preference for a facility reach equilibrium. The variation in capacity at the each iteration is primarily related to the percentage of traffic along the O-D multi class pedestrian path which requires minimum cost. Based on this, the capacity is calculated according to the demands of the pedestrian's Block usage, and this capacity is used to update the travel cost function. This takes into consideration the often marked and rapid changes in pedestrian demand for facilities in a subway station, which in reality, does not reach equilibrium.

Considering these disciplinary limitations and the applicability to the study site, an incremental pedestrian assignment method was implemented in this study. There was little difficulty in the calculation operation because the selected traffic assignment network was for a relatively small network. The preference selection pedestrian class reaches equilibrium but the pedestrian assignment is made in a non-equilibrium state for mandatory or forced users of a facility.

Figure 3 shows the multi-class pedestrian assignment procedure. The procedure performs pre-loading along the shortest initial path at a V/C=0 state using equation (5), and with the $P_{r,s,k}$ initial assignment ratio from each class traffic between pedestrian classes origin (r) and destination (s) at Iteration = 0. This is the initial traffic assignment stage for pedestrians who use the facility as a result of mandatory, forced, or preference reasons. At the iteration >0 stage the shortest path for each pedestrian traffic is calculated using equation (6) for each iteration.

The V/C at iteration (i), along with the demand and capacity are calculated using the Link demand included in the Block, and the outline length of the Block. The Link travel time at iteration (i+1) is calculated using the V/C at iteration (i). Equations (1) through (4) are used for these iterations. The search for the shortest path uses $C_{b,i,j,k}$ and the Dijkstra Algorithm, which reflects the Link cost by pedestrian class between each iteration's origin (r) and destination (s).

- $T_{r,s,k}$: the k^{th} pedestrian class traffic from the r to s
- $P_{r,s,k}$: the k^{th} pedestrian assignment ratio for the initial shortest path from r to s (where $0.0 \le P_{r,s,k} \le 1.0$)
- Initial (Iteration = 0) shortest path assignment value:
  $$T_{r,s,k} \times P_{r,s,k} \qquad (5)$$
- Loading traffic per iteration:
  $$\{T_{r,s,k} \times (1 - P_{r,s,k})\}/i \qquad (6)$$

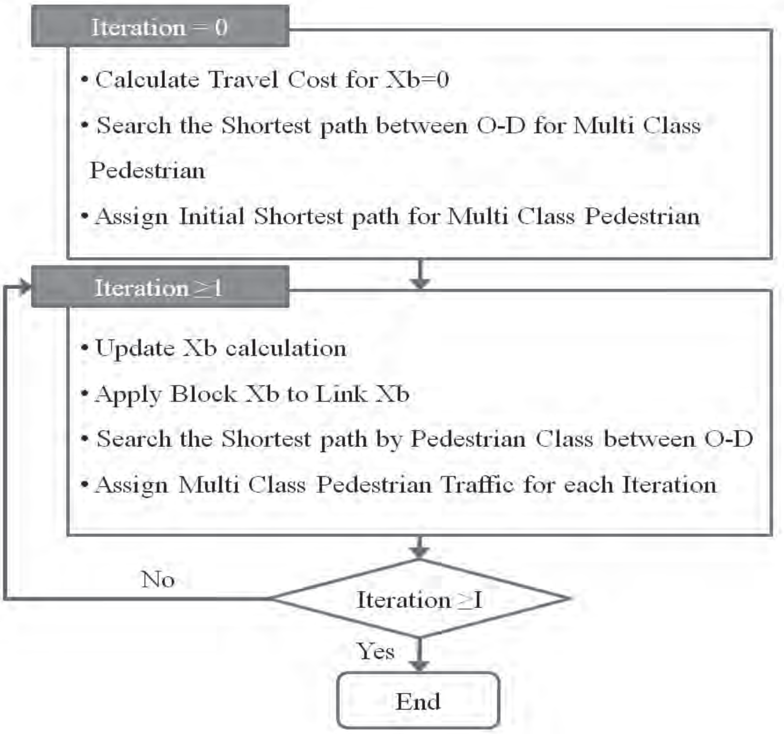

Figure3: The traffic assignment method used for multi-class pedestrians

4. IMPLEMENTATION RESULTS

4.1 Network and Input Data

Figure 4 presents a schematic of the network used to implement multi-class pedestrian assignment in a specified pedestrian space. The network has three types of facilities with the stairway and escalator forming two vertical transport facilities. A pedestrian's vertical transport facility type selection varies because of the pedestrian class characteristic. For example, a pedestrian with accompanying children prefers the escalator to stairway. In consideration of this variation, a pedestrian's initial shortest path selection ($P_{r,s,k}$) was set close to actual.

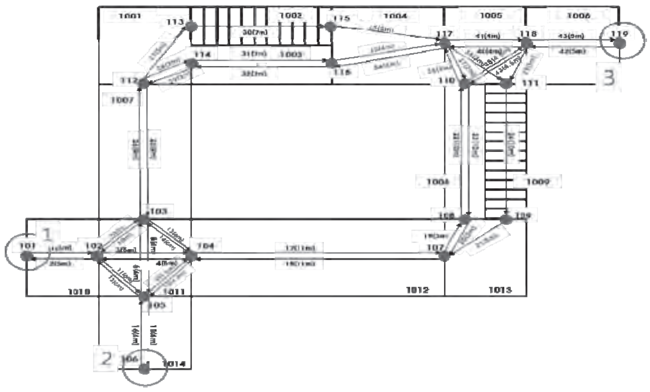

Figure 4: Sample network

Table 4 Sample network facility components

Facility Type	Block No.	Link No.
Passage	10 ea	39 ea
Escalator	2 ea	2 ea
Stairway	2 ea	4 ea
Total Number	14 ea	45 ea

The network used in this analysis consisted of 3 Zones, 14 Blocks, 16 Nodes, and 45 Links. The configuration ratio of traffic and pedestrian class between origin and departure points for traffic assignment was randomly selected (Table 5).

Table 5: Origin and destination information used for pedestrian assignment

Orig	Dest	Traffic (Person /Hr)	Pedestrian Class Ration between O-D				
			k1	k2	k3	k4	k5
1	2	1,000	0.45	0.15	0.20	0.05	0.15
1	3	2,000	0.40	0.20	0.20	0.05	0.15
2	1	1,500	0.45	0.15	0.15	0.15	0.10
2	3	2,500	0.35	0.15	0.20	0.15	0.15
3	1	3,000	0.50	0.15	0.15	0.05	0.15
3	2	3,000	0.45	0.10	0.10	0.20	0.15

4.2 Traffic Assignment Result

Multi-class pedestrians were assigned to the sample network with the maximum iteration number set at 60 in the incremental assignment method. The O-D traffic demand was set to 1 h, and the fluctuation in pedestrian demand was set to 1 min. The actual demand fluctuation, according to data obtained from train arrivals in the subway facility, was longer than 1 minute. Thus, the setting used in this study may be regarded as realistic.
Table 6 indicates the results for the final path travel time for a general pedestrian and a pedestrian with a baby and travelling from origin point 1 to destination point 3.

Table 6: Traffic assignment result: path travel time for two pedestrian classes.

Orig. 1->Dest. 3	O-D Travel Time(Min.)	
	General Pedestrian	Pedestrian with baby
path 1(Stairway)	1.30	1.97
path 2(Escalator)	1.29	2.67
path 3(Stairway)	1.28	2.05

The travel time using the escalator was longer than stairway for the baby accompanied pedestrian. Regardless of the longer travel time, restricted pedestrians with carriers or those with an accompanying child prefer to use an escalator rather than a stairway. Furthermore, the restricted pedestrians used the escalator more, even when there is increased pedestrian demand for the escalator. Accordingly, the travel time for pedestrians accompanying child does not reach equilibrium.

General pedestrians do not have any such restrictions, and they select facility type by preference. Accordingly, when there are many pedestrian demands in the escalator Block, using a stairway results in the optimum travel time since the escalator then requires more travel time. According to these general pedestrian's characteristics, final travel time reaches equilibrium within the measured error range, regardless of the presence of an escalator.

Consequently, a pedestrian of a specific class may or may not reach travel time equilibrium. User equilibrium or non-equilibrium status is related to pedestrian class and thus, the overall network includes a non-equilibrium system.

5. CONCLUSION AND FUTURE STUDY PROJECTS

5.1 Conclusion

Since Block capacity varies according to directional pedestrian demands, the equation used to calculate capacity must consider such volatile characteristics. For parameter traffic assignment, the α and β parameters of the travel cost function in each facility are estimated using a non-linear feedback method. According to the pedestrian class characteristic, the travel time for restricted pedestrians, such as those with carriers or with an accompanying child, does not reach equilibrium along any of the available paths. However, for general pedestrians that are without facility selection restriction, travel time will reach equilibrium along each available path.

5.2 Future Study Projects

This study introduced an assignment algorithm for multi-class pedestrians in a specified pedestrian space. It is expected that pedestrian traffic assignment may be possible following the analysis of pedestrian traffic surveys in actual pedestrian spaces. In this study, the travel cost function's α and β parameters were decided by facility type. It is expected that higher accuracy could be achieved by reflecting survey based estimates of the α and β parameters by pedestrian class.

ACKNOWLEDGEMENTS

This South Korea national transport research project was sponsored by the Korean Ministry of Land, Transport and Maritime Affairs. The authors thank the members of the Korea Ministry of Land, Transport and Maritime Affairs for that support.

REFERENCES

Ahmed Abdelghany, Khaled Abdelghany, Hani S. Mahmassani and Saad A. Al-gadhi(2005) Microsimulation Assignment Model for Multidirectional Pedestrian Movement in Congested Facilities: **Transportation Research Record** pp.123-132

Srinivas Peeta and Hani S. Mahmassani(1995). Multiple User Classes Real-time Traffic Assignment for Online Operations: A Rolling Horizon Solution Framework, **Transportation Research** Part B

Lee Jun, Lim KangWon, Lee YoungIn, Lim YongTaek(2004) Development of Multi-Class Assignment For Dynamic path Guidance Strategy, Korean Society of Transportation Journal, Vol. 22-7, **Korean Society of Transportation** pp. 91-98

Lim YongTaek(2002), Multiple User Class Traffic Assignment based on Variational Inequality Formulation in Variable demands , Korean Society of Transportation Journal, Vol. 20-5, **Korean Society of Transportation**, pp. 153-161

THE APPLICATION OF STOCHASTIC ASSIGNMENT TECHNIQUE TO NETWORK DESIGN PROBLEMS

HYUNMYUNG KIM[1] and TAWIN TIRATANAPAKHOM[2]
Transportation Engineering
School of Engineering and Technology
Asian Institute of Technology, Thailand
[1] khclsy@gmail.com, [2] tawinhkt@gmail.com

ABSTRACT

In this study, the effect of demand uncertainty in the transportation system is investigated with network design problems. A network design problem (NDP) finds a solution for the best network improvement with making use of optimization techniques. It provides important information for building up the best investment plan with a given budget constraint. Therefore, it has been a core topic in transportation planning. However, existing frameworks for NDP have some limitations. Among various shortcomings, the most important flaw is that the uncertainty existing in the real transportation system has been ignored and all attributes included in the model are considered in a deterministic way. In this paper, one of the uncertainties, the probabilistic property of travel demand is incorporated with NDP. In order to deal with the probabilistic travel demand, Monte Carlo simulation technique is employed and new probabilistic definitions of OD and link flows are also given. The main academic contributions of this study are following three. 1) Traffic congestion is defined in terms of a probability concept, 2) A new objective function for NDP in the stochastic network analysis is developed, and 3) The probabilistic version of Braess' paradox is found.

1. INTRODUCTION

A network design problem (NDP) is a popular research topic in transportation planning. Starting from building a new road to find the optimal congestion toll, it has provided valuable information with decision makers. Nonetheless, the existing methodologies for transportation network design have some limitations. First, most of them do not consider the uncertainty existing in the transportation system. A transportation system consists of two parts, the supply side and the demand side of the system. In reality, the attributes of the two transportation system components have variations everyday. For example, the travel demand realized in the network has a daily fluctuation. Kim (2008) explained the reason of the daily demand fluctuation from an activity-based perspective. Even in the morning peak in which daily mandatory trips take more than 50% out of a whole travels, the number of total travels and the departure profiles of them are ever-changing. Moreover, the supply side of transportation system also has a variation. The representative example is the drop of link capacity because of rainfall. In a rainy day, the surface of road is slippery and it makes running vehicles slow down (Lam et al., 2008). Among the both, a demand variation is more important factor for explaining uncertainty in the transportation network. The variation of link flow, density, and travel speed mainly comes from the daily change of incoming travel demand to the network.

Many researches have realized the importance of demand variation for transportation planning problems (Waller et al., 2001; Chen et al., 2003; Clark and Watling, 2005; Sumalee et al, 2006; Siu and Lo, 2007; Ukkusuri et al., 2007). They have assumed that travel demand has a probabilistic property and proposed several methodologies in order to deal with the stochastic behavior of network. However, most of the studies do not come up with a comprehensive framework for analyzing the stochastic network problem. Most transportation planning studies still regard that network attributes such as link flows and travel times as deterministic values in the analysis. The elements in the OD table are still defined as deterministic values. In addition, no proper objective function for NDP in the stochastic case has been developed.

In this study, the authors develop a new comprehensive framework for a stochastic network analysis. A new definition for probabilistic traffic congestion is proposed by means of a probabilistic link flow distribution. In order to estimate the probabilistic distribution of link flows, Monte Carlo technique is used. After then, a new objective function which can consider the probabilistic properties of link flows is proposed for a stochastic NDP. The capability of the developed framework is investigated with test networks. In addition, a probabilistic Braess' paradox is also found. The static version of the paradox is well-known to the transportation field but the probabilistic version of it is newly identified in this paper.

2. HISTORICAL REVIEW

2.1 Stochastic traffic assignment

The stochastic traffic assignment so far has been paid attention to the uncertainty of travelers' behavior such as the perception error of travel time. One of the stochastic techniques that play a major role in traffic assignment model is the stochastic user equilibrium (SUE). In the SUE, travelers choose their route based on their perceived travel time. This travel time is considered as a random value. In addition, unlike the deterministic user equilibrium (DUE), the assumption, that travelers have perfect information about travel time and they make correct decisions regarding route choice, can be relaxed (Sheffi, 1985). To load the OD demand onto a transportation network, the discrete choice model associated with a random utility is generally adopted for the SUE basic. Generally, there are two different forms of discrete choice model: logit model and probit model. The logit model assumes that the random components of travel utility are independent while the probit model considers the joint density function of these random components. By using the stochastic network loading mechanism (Sheffi, 1985) associated with either logit or probit model, the assignment under SUE can be achieved.

2.2 Network design problem

Network design problem (NDP) plays a major role in transportation planning and decision making processes. The solutions of NDP can tell us which segments of the transportation network can be optimally improved or added (Abdulaal and LeBlanc, 1979). From Bell and Iida (1997), network design problem can be considered into two forms: the continuous network design problem and the discrete network design problem. Given network topology, the continuous network design, taking link parameters such as capacity and user charge into account, generally considers the trade off between user benefit and costs of introducing network improvement. For example, the continuous network design problem is used to determine the improvement of a link such as capacity expansion by adding new lanes into the network. On the other hand, the discrete network design problem considers the topology of the network into such trade off. For example, the discrete network design problem is used to find the addition or removal of a link in the network. Therefore, the problem of transportation network design is defined as to select which links in the network should be improved or added in order to maximize social welfare while accounting for the route choice behavior of network users (Suwansirikul et al., 1987) or in order to minimize total network cost subject to a budget constraint while the flows satisfy the user equilibrium (UE) condition (Ukkusuri et al., 2007). In addition to the deterministic user equilibrium (DUE), other objective functions such as the nonlinear objective functions whose solutions satisfy the system optimal (SO) condition and the linear objective functions are also exist in NDP (Abdulaal and LeBlanc, 1979; Chen and Alfa, 1991). Furthermore, the SUE discussed in previous section can also be applied to NDP as presented by Chen and Alfa (1991). They stated that considering the SUE is more realistic than the DUE but it requires more computational effort. In their study, the heuristic approach was adopted to solve the NDP with logit based SUE problem.

2.3 Uncertainty in the network analysis

The uncertainty on the road network comes from various reasons such as uncertainty in OD demand, link capacity, travel time, etc. In this study, the uncertainties are categorized into three groups in terms of the source of them; supply uncertainty, demand uncertainty and travel time uncertainty.

2.3.1 Uncertainty in supply side

Supply uncertainty comes from several uncertain disturbances on the road such as accident, road work, illegal parking, rainfall, etc. In addition, such phenomena affect a driving condition and cause a variation in the road capacity (Lam et al., 2008). For example, road capacity may degrade in a rainy day because of poor driving conditions such as visibility and pavement friction. Link capacity degradation would also happen as a result of some major and minor events and incidents (Siu and Lo, 2007). On one hand, major events such as earthquakes cause a network connectivity problem. On the other hand, some minor events such as accident, vehicle failure cause stochastic link capacity degradation.

Likewise, Chen et al. (2002) considered such events as the sources of network disruption. Recurrent and non-recurrent disturbance are used to refer these events. For example, congestion is referred as recurrent disturbance since it could repeat almost everyday. On the other hand, non-recurrent disturbance can be further classified into two types; an abnormal and a normal failure. An abnormal failure such as earthquake causes system damage whereas a normal failure such as a traffic accident does not involve system damage. In addition, Lam et al. (2008) classified the sources of road capacity uncertainty into two categories, predictable and less-predictable. In their study, events such as a poor weather condition or a road work are considered as a predictable source. On the other hands, a road accident or a vehicle breakdown is regarded as a less-predictable source.

2.3.2 Uncertainty in demand side

Recently, demand uncertainty has become fashionable in transportation planning. For example, Chen et al. (2003) developed a mean-variance model for finding the optimal toll and road capacity of the build-operate-transfer roadway project by considering the uncertainty of demand for travel. Ukkusuri et al. (2007) introduced a robust network design problem (RNDP) which takes demand uncertainty into account. According to Sumalee et al. (2006), travel demand variation mainly results from travelers' behavior uncertainty and day-to-day variation in activity patterns. Lam et al. (2008) proposed a new traffic assignment model which can consider the impact of weather condition with uncertainty in both supply and demand.

Travelers' Behavior Uncertainty

Uncertainty from travelers' behavior such as route choice variability plays an important role in demand uncertainty (Sumalee et al., 2006). For example, Asakura and Hato (2001) addressed that in degraded network, a traveler's knowledge of the network influences his or her route choice behavior. In their study, when network is degraded, non-informed travelers will randomly recognize whether a link will be closed or not. He or she may change routes several times or may not continue to finish their trips after some wasted trials.

Day-to-Day Variation

Daily variations in activity patterns are one of the main sources of uncertainty in travel demand (Clark and Watling, 2005; Kim, 2008). For example, Siu and Lo (2007) classified travel demand into two main groups: commuters and infrequent travelers. They assumed that the traffic flows of commuters are stable since they travel regularly on the same OD pair. Conversely, infrequent travelers irregularly make their trips, so their traffic flows are subject to higher uncertainty. Kim (2008) explained the properties of travel demand variation over time of day from an activity perspective. As researched by Lam et al. (2008), weather also can be an important factor for the variability of day-to-day OD travel demand. For example, to avoid a possible congestion during raining, travelers may change their plans to travel after receiving the weather forecast information.

2.3.3 Uncertainty in travel time

Uncertainty in travel time results from the interaction between supply and demand variations of transportation system. The mean and standard deviation of OD travel time increase as a result of higher travel demand (Chen et al., 2002). Lo and Tung (2003) considered the variation of daily travel time caused by minor traffic incidents. In addition, they also showed that in heavy traffic, travel time variability is higher than that in light traffic. Travel time variation or travel time reliability influences travelers' route choice behavior (Siu and Lo, 2007; Lee et al., 2000, Kim, 2008). Hence, travel time uncertainty can also influence the travel demand. As stated by Lee et al. (2000), travelers prefer the path on which the travel time variation is minimized. Furthermore, Lo and Tung (2003) introduced probabilistic user equilibrium (PUE) to characterize route choice behavior in the face of uncertainty travel time. They believed that travelers settle into a long-term equilibrium pattern after they learn and experience their trips. Kim (2008) introduced the concept of travel time uncertainty into the generation of activity schedule. In his study, the reliability of travel time is defined as a probability that an OD travel time is less than a reference value. In addition, he found that the variation of travel time is proportional to the length of travel and the level of congestion.

3. MODELING FRAMEWORK

3.1 Modeling method of demand variation

A stochastic OD table is proposed to capture the variation of OD travel demand. For a given OD pair, the number of trips is regarded as a random variable. In the previous studies (Hazelton, 2003), the same assumption was used and a normal distribution was proved as the most prevalent probability distribution for modeling a variation in travel demand (Chen et al., 2003; Lam et al., 2008). Other probability distributions such as Poisson distribution (Hazelton, 2003; Sumalee et al., 2006), uniform distribution (Ukkusuri et al., 2007) also have been used for modeling a demand variation. Furthermore, Lam et al. (2008) assumed that the standard deviation of OD travel demand is an increasing function with respect to the mean OD demand. Hazelton (2003) proposed the mean-variance relationship modeled by $\mathrm{Var}(Q_{rs}) = \alpha \mathrm{E}[Q_{rs}]^{\beta}$ where Q_{rs} represents the number of random day-to-day OD trips, and α, β are positive parameters (see Hazelton, 2003). Ukkusuri et al. (2007) and Waller et al. (2001) assumed that OD demand varies uniformly around mean value. Chen et al. (2003) used a half of expected OD demand as a standard deviation. In this study, a stochastic OD table is assumed to consist of random elements following a normal distribution.

$$N(q_{rs}, \sigma_{rs}^2) \tag{1}$$

where, q_{rs} is a mean of travel demand between OD pair rs and σ_{rs}^2 is a variance of travel demand between OD pair rs. The OD table, as shown in Table 1, is called a stochastic OD table. Note that the correlations among OD flows are ignored when generating a random OD table. In reality, some OD pairs have correlations because they share a common origin or destination. However, no information regarding the correlations is available for the hypothetical networks used in this study, so all OD flows are assumed independent.

Table 1: A general form of a stochastic OD table

	Destination				
Origin	1	2	3	…	…z
1	$N(q_{11}, \sigma_{11}^2)$	$N(q_{12}, \sigma_{12}^2)$	$N(q_{13}, \sigma_{13}^2)$	…	… $N(q_{1z}, \sigma_{1z}^2)$
2	$N(q_{21}, \sigma_{21}^2)$	$N(q_{22}, \sigma_{22}^2)$	$N(q_{23}, \sigma_{23}^2)$	…	… $N(q_{2z}, \sigma_{2z}^2)$
3	$N(q_{31}, \sigma_{31}^2)$	$N(q_{32}, \sigma_{32}^2)$	$N(q_{33}, \sigma_{33}^2)$	…	… $N(q_{3z}, \sigma_{3z}^2)$
$\vdots$					
i	$N(q_{i1}, \sigma_{i1}^2)$	$N(q_{i2}, \sigma_{i2}^2)$	$N(q_{i3}, \sigma_{i3}^2)$	…	… $N(q_{iz}, \sigma_{iz}^2)$
$\vdots$					
z	$N(q_{1z}, \sigma_{1z}^2)$	$N(q_{2z}, \sigma_{2z}^2)$	$N(q_{1z}, \sigma_{1z}^2)$	…	… $N(q_{zz}, \sigma_{zz}^2)$

3.2 Stochastic traffic assignment by Monte Carlo technique

To simulate the demand uncertainty, Monte Carlo technique is used for producing the number of travels in each element of OD table. For generating a random variable with assumed probability distribution, Monte Carlo simulation has been used as a sampling technique (Sumalee et al., 2006; Waller et al., 2001; Clark and Watling, 2005). In addition, other sampling techniques also can be employed. For example, Chen et al. (2003) used Latin hypercube sampling (LHS) technique to simulate demand uncertainty. To generate multiple OD tables, the mean and standard deviation of each OD demand are assumed to be known. In this paper, 30% of OD flow volume is assumed as a standard deviation.

Figure 1 shows the framework of traffic assignment used in this study. From the given stochastic OD table, multiple OD tables are generated randomly and loaded onto the network. In the tests, the number OD table is set as 30. As a result, each link has 30 OD flow samples. In this study, a standard traffic assignment method, UE (user equilibrium) model is used for the OD flow loading with BPR (U.S. Bureau of Public Roads) function is

used as a link performance function. Finally, a probability distribution of link flow is estimated from the sample link flow set.
In the study, a link flow is assumed as a random variable. Accordingly, a link flow distribution can be estimated from the link flow samples. For the purpose, the histogram of sample link flows should be constructed. After then, a best-fit distribution would be found by a Chi-square (χ^2) test. From Blank (1980), the general form of hypothesis for the test is shown as follows.

H_0: sample is from a specified distribution
H_1: sample is not from a specified distribution

A goodness-of-fit test is a test of H_0 versus H_1. The test can be performed by measuring the relative difference between observed (O_i) and expected (E_i) frequency values as shown in Eq. (2).

$$\chi^2 = \sum_{i-1}^{k} \frac{(O_i - E_i)^2}{E_i} \tag{2}$$

where (O_1, O_2,…, O_k) are observed frequencies and (E_1, E_2,…, E_k) are expected or theoretical frequencies from assumed distribution.
The frequency values, E_i, are:

$$E_i = nP_i \tag{3}$$

where n is the sample size and P_i is the probability from the assumed distribution.

Moreover, to test the fit by determining the acceptance region, the degree-of-freedom parameter (4) of the χ^2 probability distribution function (PDF) must be determined.

$$v = k - r - 1 \tag{4}$$

where r is the number of parameters of the assumed distribution. The acceptance region for H_0 is area to the left side of the Chi-square value ($C_{1-\alpha, v}$) or the CDF at $1-\alpha$. That is, if $\chi^2 < C_{1-\alpha, v}$, then the assumed theoretical distribution is acceptable with the significant level, α. For this experiment, the significant level, α, is set to 5 percents and the best fit distribution provides the lowest value of χ^2.

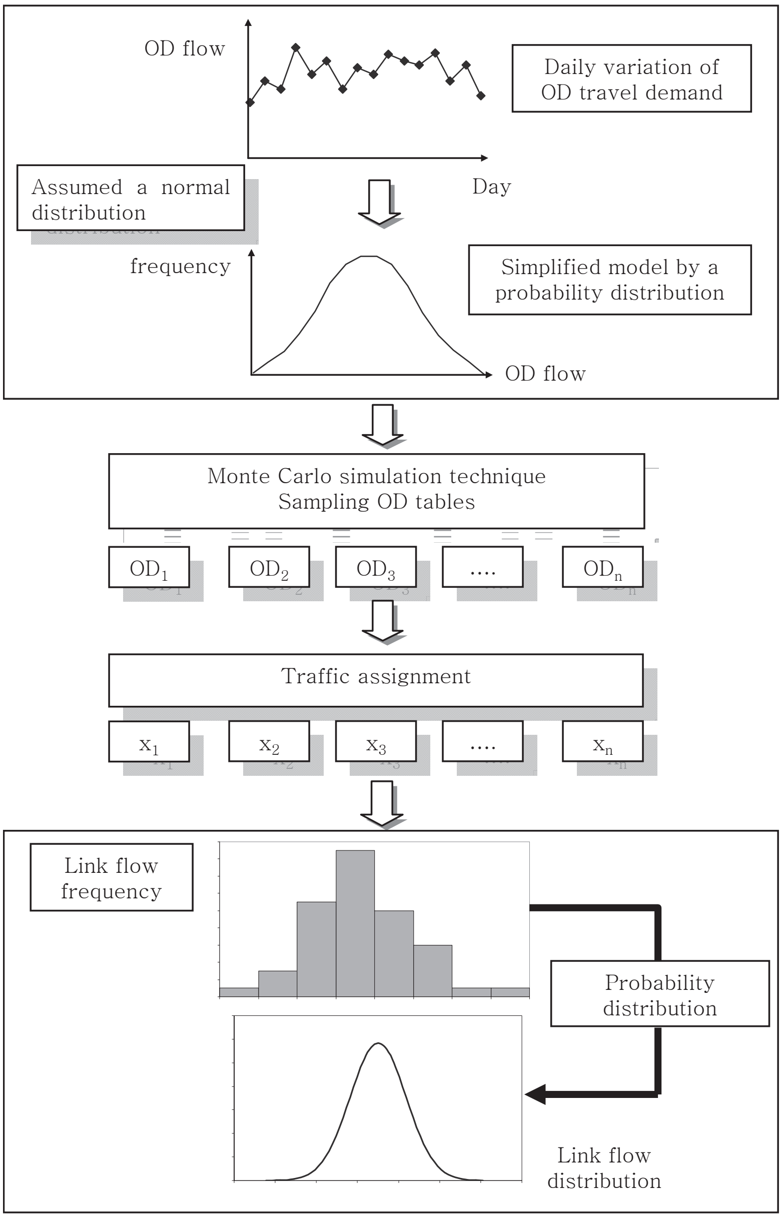

Figure 1: Monte Carlo simulation framework for link flow distribution

3.3 Probabilistic definition of traffic congestion

In the developed framework, a new definition for traffic congestion arises. As shown in Figure 2, each link has the distribution of flow as a probability density function. In the conventional traffic assignment, a link traffic flow is defined as a deterministic value and the level of congestion can be assessed by comparing the flows to the deterministic link capacity (c_a). However, in the stochastic assignment, link flow has randomness, so comparing the average flow to capacity is insufficient for assessing the level of congestion. Therefore, the probability of congestion at the link a is introduced and denoted as $P(x_a>c_a)$.

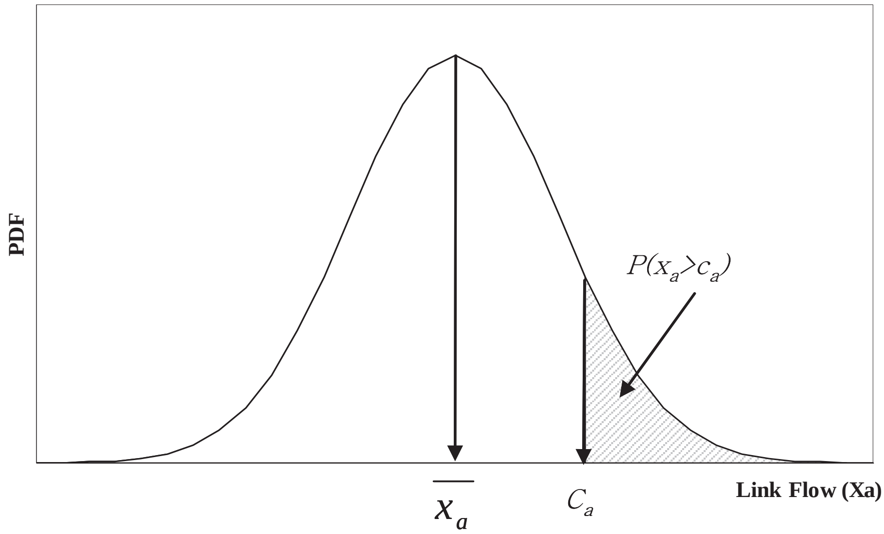

Figure 2: The probability of traffic congestion

For a conventional definition of traffic congestion, v/c ratio (x_a/c_a) has been used prevalently. In this case, x_a is the average link flow. Accordingly, the conventional method only uses the average link traffic for evaluating the level of congestion on the link. However, in the stochastic traffic assignment, not only an average link flow rate, but also a link flow variance should be taken into account. The new definition for traffic congestion can capture the probabilistic property of link flow. The probabilistic definition of traffic congestion is useful for explaining the behavior of real traffic congestion. In the real world, we have different levels and locations of traffic congestion. The fluctuations in the supply and demand side of transportation system makes very complex demand-supply interactions on the road network. However, if an average OD table is used with deterministic network attributes, the fluctuation of traffic congestion cannot be explained. In addition, the *v/c* ratio (x_a/c_a) cannot explain the feature of probabilistic traffic congestion comprehensively.

Figure 3 shows the difference in the definition of traffic congestion between probabilistic and deterministic cases. If the variances of flows on the two links are the same, then v/c is a complete measure for evaluating a congestion level. However, if two link flows have the difference magnitudes of variances, the level of congestion cannot be compared in terms of *v/c*. In the figure, the path 1 has a higher average flow than the path 2 but the probability of congestion of the link 1 is smaller than that of the link 2.

Note that the probability of congestion is a more user-oriented measure. Let's assume that there are two daily commuters who use the given two paths, respectively. In that case, the commuter on the path 2 would experience traffic congestion more frequently than the commuter on the path 1. However, the *v/c* ratio cannot reflect the reality and expects the path 1 is more congestion-prone. Considering a current traffic surveillance system, the calculation of *v/c* is easier than that of congestion probability because the variance of flows requires traffic surveillance for a sufficient number of days. This is a reason why *v/c* has been preferred to date. However, the consideration of congestion probability should be included in transportation planning and engineering because it show the actual traffic situation with which drivers face in reality.

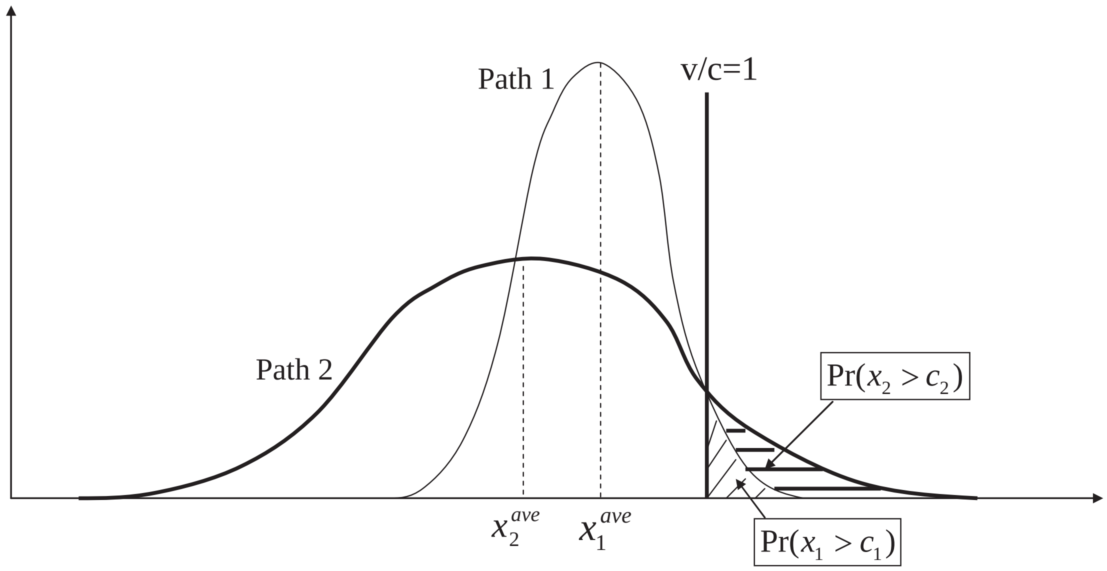

Figure 3: Deterministic and probabilistic definitions of traffic congestion

3.4 Formulation of objective function for a stochastic NDP

As mentioned above, in the conventional NDP, the impact of new network design is evaluated by means of the average link flows and the average link travel time. However, in the real world, since travel demand randomly changes consistently, the flow on each link cannot be a deterministic value but a random value. In this stochastic case, how can we evaluate the performance of new network design? How can we minimize the random traffic congestion with the network design change?

In order to improve the performance of network under uncertainty, a new objective function for a NDP is proposed. The concept of new objective function for a stochastic NDP is to determine the additional capacity of each link which can be improved so that the probability of congestion in the system is minimized. At first, the probability of congestion on the link *a* should be defined in terms of the CDF of normal distribution.

$$P(x_a > c_a) = 1.0 - \Phi\left(\frac{c_a - x_a^*}{\sigma_a}\right) \tag{5}$$

where, $\Phi(\,)$ is the cumulative distribution function (CDF) of normal distribution. x_a^* and σ_a are the average and standard deviation of link flow on the link *a*.

After then, the probability of congestion in the system representing the whole network's congestion situation can be defined mathematically by adopting the concept of weighted average. That is, in order to reflect the average probability of congestion for a whole network, the probability of congestion of all links need to be taken into account. In addition, since each link has different amount of flows, the average link flow (x_a^*) is taken into account as a weighting parameter to the probability of congestion. For finding the optimum capacity improvement, as stated above, the mathematical optimization program is established as presented in Eq. (6).

$$\min Z(y_a) = \frac{\sum_{a \in P} \overline{x_a}^* \left[1.0 - \Phi\left(\frac{(c_a + y_a) - x_a^*}{\sigma_a} \right) \right] + \sum_{a \in E} x_a^* \left[1.0 - \Phi\left(\frac{(c_a + y_a)}{\sigma_a} \right) \right]}{\sum_a x_a^*} \tag{6}$$

where, y_a is additional capacity for improvement, P is the set of links proposed for improvement, and E is the set of remaining links (no improvement). In this regard, y_a is a decision variable for link a.

3.5 Solution algorithm for NDP

To solve the above objective function, several global optimum searching methods are available nowadays. In this paper, the Hooke and Jeeves' method is adopted since it is simple and sufficient for the experiments.

Hooke and Jeeves' Method

Hooke and Jeeves algorithm consists of two main steps: exploratory move and pattern move, running repeatedly in order to search for optimum objective value. Briefly, first, *exploratory move* searches the better objective function value along the decision variable axes either positive or negative direction with a fixed step size. Second, *pattern move* searches the better objective function value by stepping off from the best point of exploratory move. This is in the trend of optimizing the objective function by using the extrapolation technique with a fixed step size. Then, this point is considered as a start point for the next exploratory move. Following the steps discussed in Abdulaal and LeBlanc (1979), the overview of Hooke and Jeeves algorithms is dicussed as follows.

Step 1: *Initialization*: Choose a starting point $(y_1^0, y_2^0, ..., y_i^0)$, and initial step size (Δ_i^0) which is equal to a current decision value multiplied by step size reduction factor.

Step 2: *Exploratory move*:

2.1 Move to positive direction with a step length $(y_i^{k+1} = y_i^k + \Delta_i^k)$.

2.2 Evaluate objective function value. If $Z(y_i^{k+1}) < Z(y_i^k)$, go to step 3. Otherwise go to step 2.3.

2.3 Move to negative direction $(y_i^{k+1} = y_i^k - \Delta_i^k)$ and then evaluate objective value like in step 2.2. If the result is successful, go to step 3. Otherwise, go to step 2.4.

2.4 Go back to origin point and reduce the step size by reduction factor. After that start step 2.1 again.

Step 3: *Pattern move*:

3.1 Set $y_i^k = y_i^{k+1}$

3.2 Extrapolation by $y_i^{k+1} = 2y_i^k - y_i^{k-1}$ and evaluate the objective function value. If success, go to step 3. Otherwise, go back to origin like step 2.4.

3.3 If step size is satisfied the convergence criteria, stop. Otherwise, reduce the step size by reduction factor and go to step 2.

The solution here is the additional capacity which will be added to the links proposed for improvement. After improvement, the link's characteristic has been changed. Accordingly, the equilibrium of the system is replaced. Then, the traffic assignment problem needs to be conducted for finding the new equilibrium of the network again. Consequently, the solving procedure returns to find the new global optimum over again. This solving procedure conducts iterative process between global searching method and traffic assignment problem until satisfying the convergence criteria.

4. SIMULATION RESULTS OF STOCHASTIC TRAFFIC ASSIGNMENT

4.1 Test network 1

Nguyen-Dupius network (Ukkusuri et al., 2007) is selected as the first test network. It has 13 nodes and 19 links and is shown in Figure 4. There are four OD pairs: 1→2, 1→3, 4→2 and 4→3. The outcome of stochastic traffic assignment is the probabilistic flow distributions of links. In Monte Carlo simulation, 50 samples of link traffic flows are generated for each link. From the samples, a probabilistic distribution of link flow is estimated.

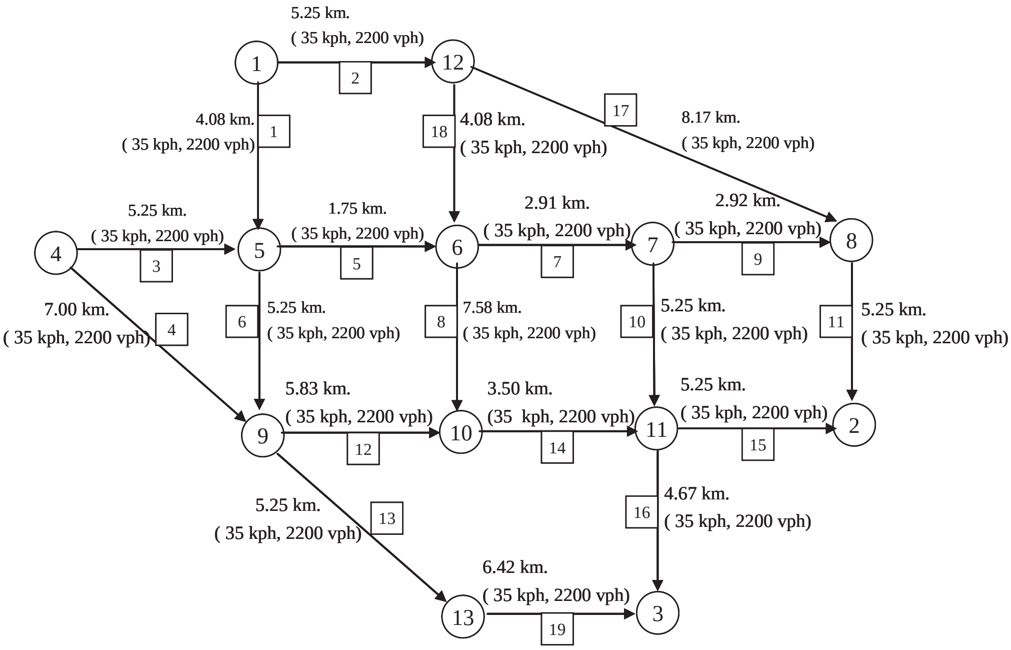

Figure 4: Nguyen-Dupius Network

In order to determine the appropriate distribution of link flows, three plausible candidates for the probability distribution: normal, log-normal, and Gamma distribution, are selected. After then, each distribution is tested by means of the Chi-square goodness-of-fit.

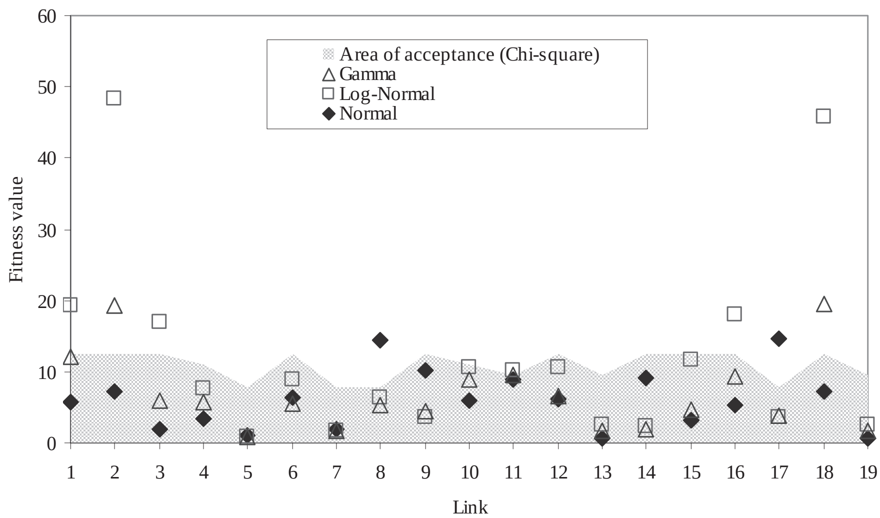

Figure 5: Comparison of the results from the Chi-Square Goodness-of-Fit test

According to Figure 5, a normal distribution is selected as the most appropriate distribution. At the all links except link 8 and 17, a normal distribution is accepted. There are twelve links showing that a normal distribution is superior to other two distributions. In summary, 63% of the best fit cases in this network are achieved by a normal distribution. In the

Chi-square test, a normal distribution is accepted at the 89% of links. The probability of congestion, herein, is defined as the probability that traffic flow exceeds capacity on the particular link. Figure 6 shows the relationship between the probability of congestion and v/c. As illustrated in the figure, there are two independent tendencies. Up to 0.6 v/c level, the probability of congestion is nearly zero, so v/c and congestion probability have no correlation up to the level. Beyond 0.6 v/c level, however, the probability of congestion steeply goes up with the increase of v/c. This figure implies there is a critical v/c ratio in order to keep the probability of congestion low.

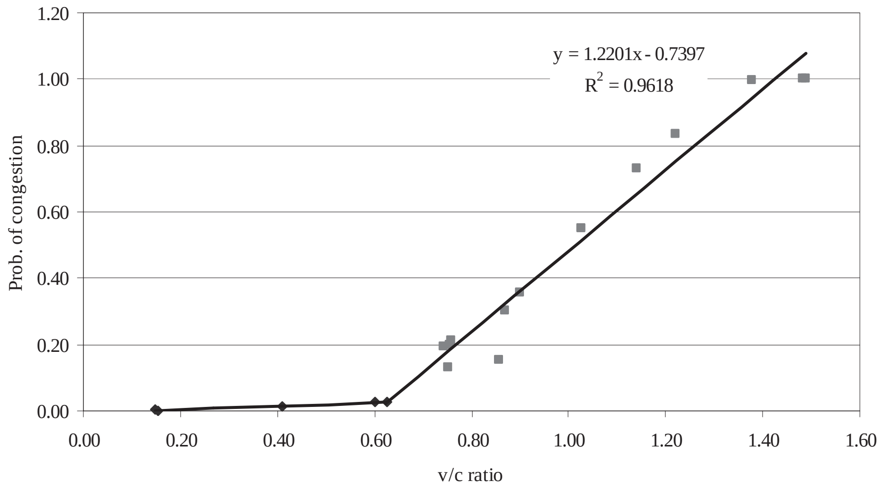

Figure 6: v/c ratio and probability of congestion for Nguyen-Dupius Network

4.2 Test network 2

In order to test the developed model under more general condition, Sioux Falls network shown in Figure 4 is selected. It consists of 24 nodes, 76 links, and 552 OD pairs. The network characteristics and OD demands follows Suwansirikul et al. (1987). In order to find the best probability distribution for link flows, a normal and a log-normal distribution are tested. The results of test are summarized in Figure 8 in which both distributions are accepted for all links beside the link 28 and 48. In addition, a log-normal distribution is rejected at the link 21 and 59. In summary, the results demonstrate that most of the best fits (i.e. lowest of fitness value) are achieved with a normal distribution which is accepted for 97 percents of number of links.

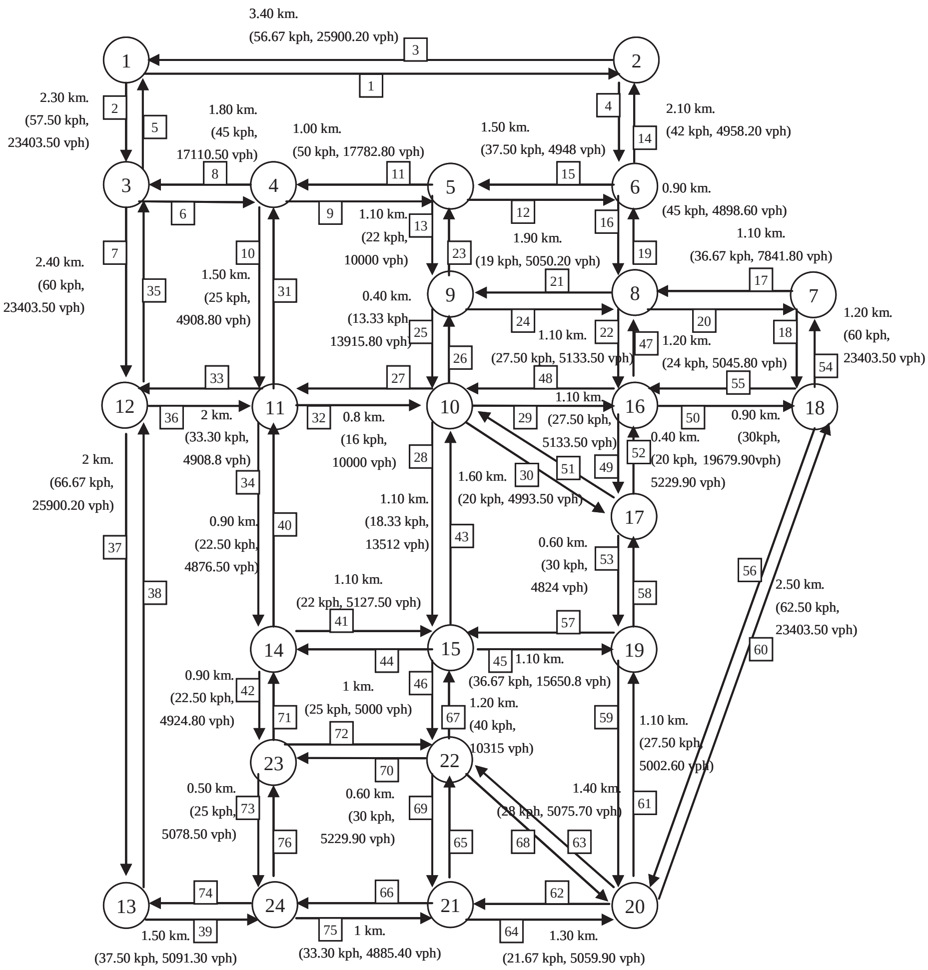

Figure 7 Test network 1

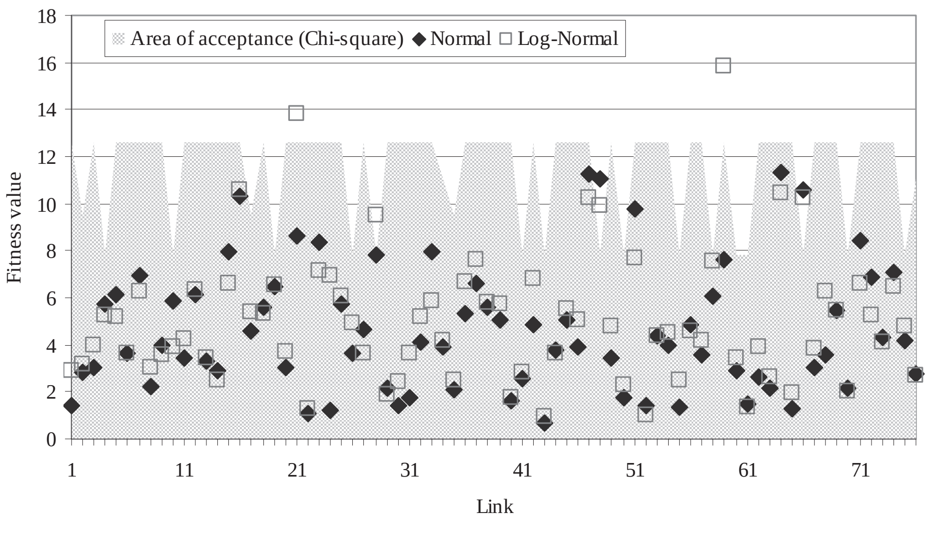

Figure 8 Comparison of the Results from the Chi-Square Goodness-of-Fit Test

As shown in Figure 9, *v/c* and congestion probability have a proportional relationship when *v/c* is near or beyond capacity range. However, the two values might be inconsistent each other. In order to examine it, the probability distribution of link flow is plotted against the *v/c* ratio of link as shown in Figure 9. The link 26 and the link 51 are selected for illustration. The *v/c* ratios of link 26 and link 51 are 0.9234 and 0.8603 respectively, so the link 26 shows the higher congestion level. However, the area of PDF curve beyond capacity (i.e., v/c>1.0) for the link 51 is larger than that for the link 26. That is, the link 51 is more likely to have traffic congestion than the link 26. The probability of congestion for the link 51 and the link 26 are 0.1599 and 0.1197, respectively. This example proves that the probability of traffic congestion and *v/c* are different measures. As explained, drivers on the link 51 will undergo traffic congestion more frequently than drivers on the link 26. Therefore, the consideration of congestion probability is more appropriate and user-oriented measure when investigating a traffic congestion problem.

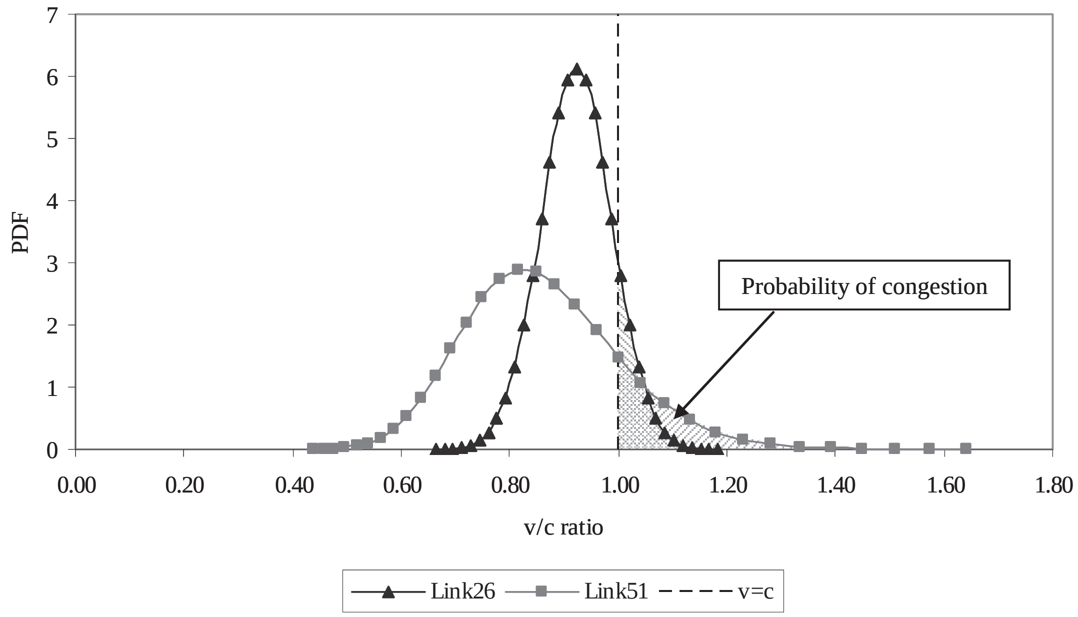

Figure 9: v/c ratio and the probability of congestion

5. NDP IN STOCHASTIC TRAFFIC ASSIGNMENT

In this chapter, the features of the new traffic assignment model are investigated. In order to consider the probabilistic property of link flow, a new objective function for NDP is proposed as shown in Eq. (6). The comparison between a conventional objective function (i.e., total network travel time, TNTT) and the Eq. (6) will be given.

5.1 Test network 1: Harker-Friez (HF) Network

As shown in Figure 10, the HF network consists of 6 nodes and 16 links and there are two OD pairs; from the node 1 to the node 6 with 15 flow units and from the node 6 to the node 1 with 30 flow units. In this experiment, three test cases were conducted. First, the conventional NDP with a deterministic traffic assignment is denoted as “Case 1.” The conventional NDP means the optimal network design is calculated in terms of the minimization of TNTT. In the Case 1, the average OD flows of the multiple OD tables used for the Case 2 and 3 is used. The number of OD tables is 30. Second, the conventional NDP with the new stochastic assignment technique is denoted as “Case 2.” For the purpose, multiple traffic assignments are executed and the average link flow value is used for minimizing the TNTT. It means that the average TNTT is minimized in the Case 2. Third, the objective function (6) with the new stochastic assignment technique is named as “Case 3.”

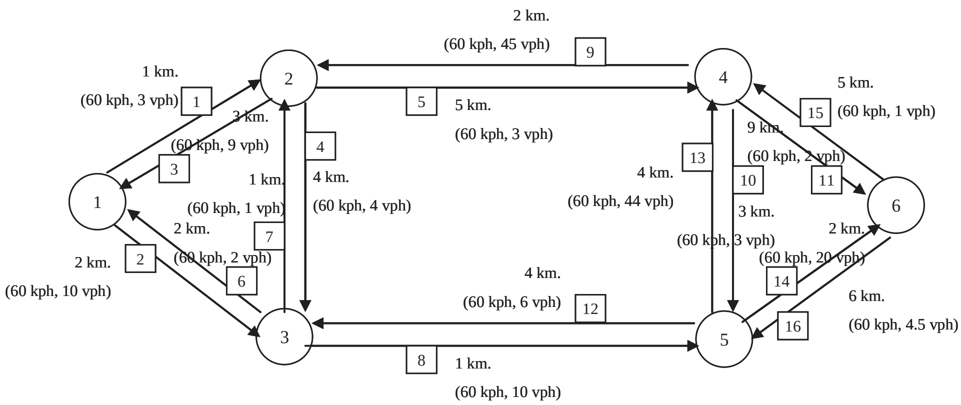

Figure 10: Harker-Friez (HF) network

The scenario in this experiment is that all links in this network can have additional capacity at the same time and the maximum capacity to be added for each link is assumed as 5 flow units. In order to find the optimal capacity improvement, Hooke and Jeeves algorithm is employed. For simplicity, no budget constraint is considered. The results of this experiment are depicted in Figure 11.

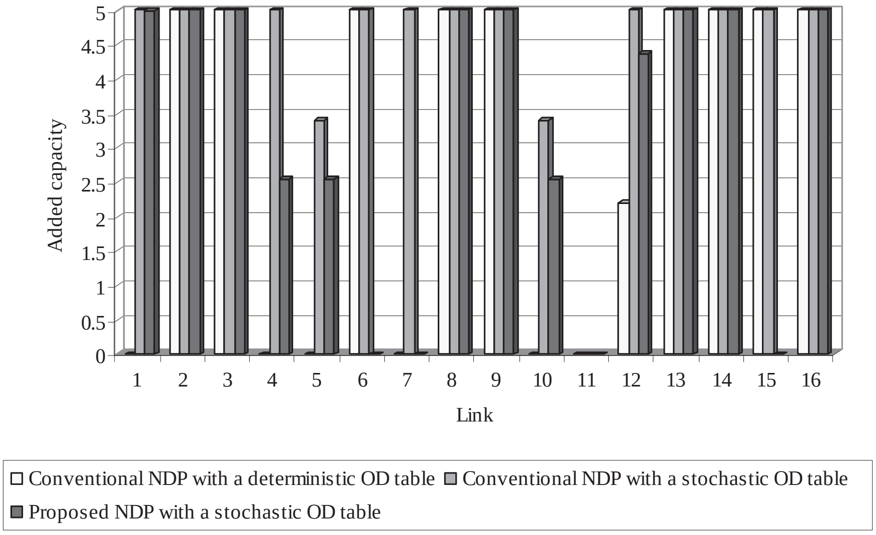

Figure 11: The comparison of the three cases

The first interesting finding is that the optimal increases of links are significantly different among the cases. For example, the capacity of link 7 is fully increased in the Case 2, but other cases do not add capacity. At the link 5, the link capacity is increased in the Case 1 and 2, but there is no capacity increase in the Case 3. It means that the extra capacity on the link 5 can decrease TNTT, but would increase or at least cannot decrease the probability of traffic congestion.

Table 2 Comparison of values of system travel time (TSTT) and probability of congestion in the network (PCN) between Case 1, 2 and 3

Case	**TNTT**		**PCN**	
	Before[1]	**After[1]**	**Before**	**After**
Case 1	412.521 (796.834[1])	14.7055 (21.5721[1])	- (0.6187[1])	- (0.5775[1])
Case 2	796.834	21.2802	0.6187	0.5702
Case 3	796.834	71.7505	0.6187	0.4813

[1] Note: Originally, the PCN of Case 1 cannot be calculated because it executes a single assignment. The above number in the cell shows it. For comparison, the TNTT and PCN value for the Case 1 is calculated with the multiple OD tables used in the Case 2 and 3. It is shown in the parenthesis.

Furthermore, the values of TNTT and the probability of congestion in the network (PCN) in each case were compared in Table 2. According to the table, the TNTT of all cases are substantially reduced after the improvement. In term of improved TNTT, the Case 2 provides the best solution. On the other hand, if solely the PCN is taken into account, Case 3 gives the best solution. In addition, as observed from this table, the improved TNTTs of Case 1 and Case 2 are very similar. Note that the objective function of the Case 1 and 2 are the minimization of TNTT. This result implies that the role of objective function is critical in NDP.

Another important thing to be discussed is the TNTT calculated from the average OD table is significantly lower than the average TNTT calculated from multiple OD tables. The distinct between deterministic TNTT from the average OD table and the expected TNTT from multiple OD tables is consistent with the study of Waller et al. (2001). In the study, this situation was explained through Jensen's inequality (i.e. $E[g(x)] \geq g[E(x)]$) in their study.

In this study, another reason is provided by means of the nonlinear characteristic of BPR function. The underestimation of TNTT with the average OD table can be explained as shown in Figure 12. From the average link flows (X-AVE), the average link travel time can be decided as T-AVE. Let's assume that link flow has some fluctuations. In that case, the increase of link flows gives a bigger impact on link travel time than the decrease of link flows as shown in Figure 12. In other words, (T-max – T-AVE) is larger than (T-AVE-T-min) although (X-max – X-AVE) is equal to (X-AVE – X-min).

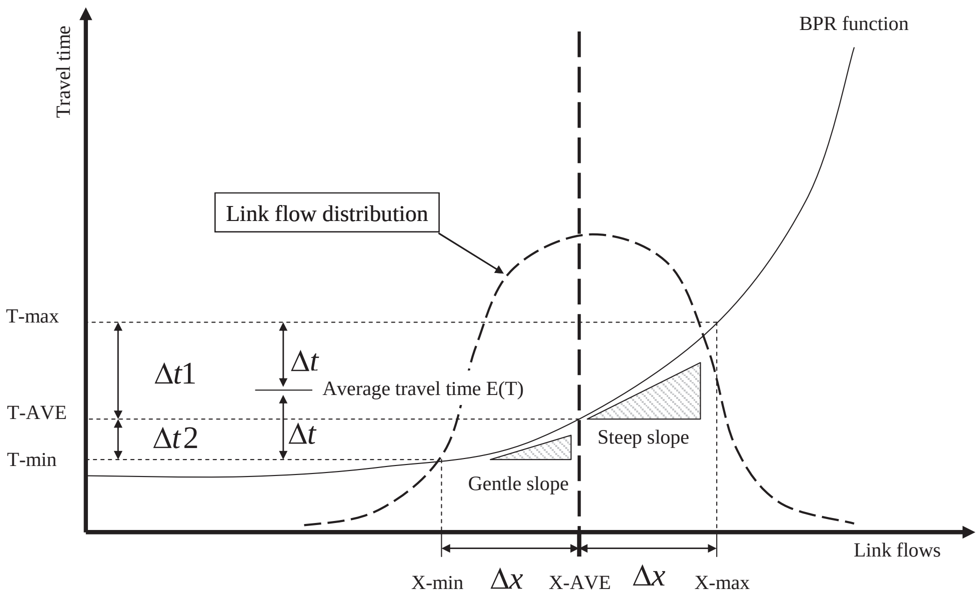

Figure 12: The effect of link flow variation on travel time in BPR function

It is because of the non-linearity of BPR function. As shown in Figure 12, the slope of BPR function in the right side is always steeper than that in the left side. Therefore, $\Delta t1$ is always larger than $\Delta t2$ and the average travel time, E(T) is also always bigger than T-AVE. In the same vein, the bigger travel time from multiple OD tables is reasonable and the discrepancy between the two TNTT in the Case 1 can be increased as the variance of link flows goes up. In reality, the monotonic increase of travel time with respect to link flows is plausible. It implies that the use of average OD table in transportation planning can underestimate the level of traffic congestion significantly.

The superiority of Eq. (6) to TNTT is worth noting. In TNTT, there is no big difference among the three cases. Oppositely, the Case 1 and 2 give over than 57% congestion probability but the congestion probability of Case 3 is 45%. Therefore, the new objective function can give a similar amount of TNTT reduction and significantly bigger reduction in SPC.

5.2 Test network 2: Nguyen-Dupius Network

In this experiment, the maximum extra capacity to be added to each link is equal to 2200 flow units. All attributes of the Nguyen-Dupius network are the same with previous case beside OD travel demand. Three OD demand levels of four OD pairs were selected for this experiment: Q_{12} = {2100, 2600, 3100}, Q_{13} = {2300, 2800, 3300}, Q_{42} = {2500, 3000, 3500}, and Q_{43} = {1900, 2400, 2900}, respectively.

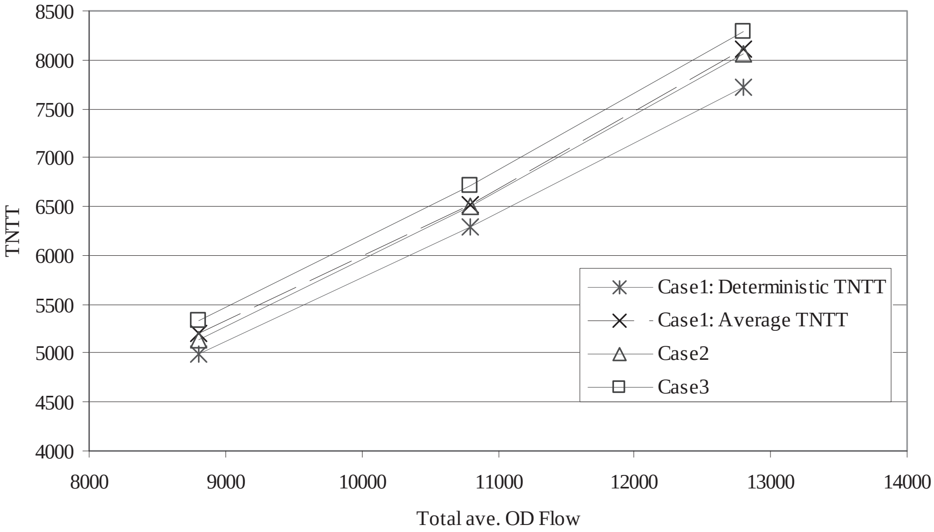

Figure 13: Comparison of Average TNTT between Case 1, 2 and 3 at different OD demand levels

Figure 13 shows the discrepancies of the three cases in terms of TNTT. As expected, there are trivial discrepancies so the performances of TNTT minimization and congestion probability minimization are similar.

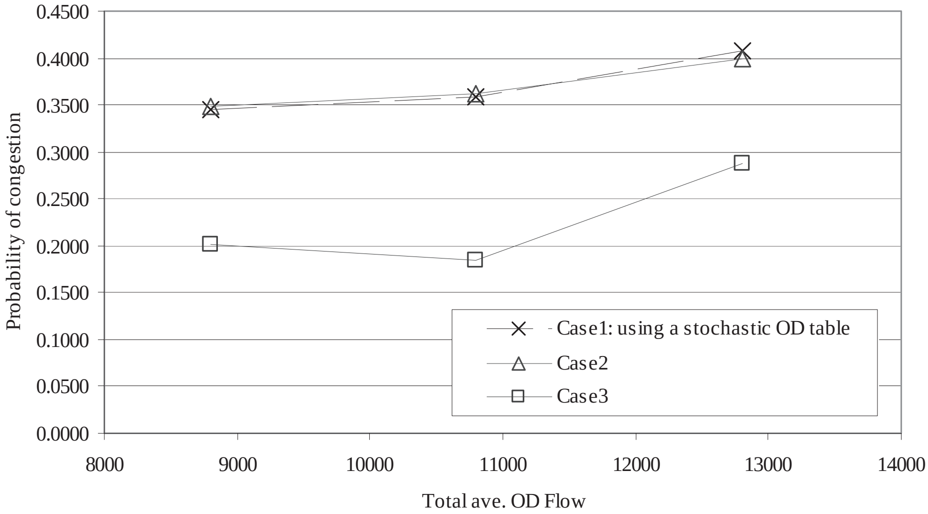

Figure 14: Comparison of PCN between Case 1, 2 and 3 at different OD demand levels

However, the two objective functions reveal significantly different performances in resulted PCN. At all travel demand level, the Case 3 reduces the probability of congestion greater than other two cases do. Nonetheless, the Case 1 and the Case 2 show nearly the same performance. It confirms that the objective function plays a crucial role in NDP and the consideration of multiple OD table (i.e., OD flow variance) without making use of the new objective function would not bring a big improvement in the network design. Based on these properties, the solution for NDP from the new objective function seems to be the best for both aspects.

6. BRAESS' PARADOX IN STOCHASTIC TRAFFIC ASSIGNMENT

In order to check out the properties of the new assignment technique further, a famous problem in transportation planning is tested with a stochastic traffic assignment. The problem is Braess' Paradox in which the addition of new link aggravates the travel time of drivers. The classical Braess' paradox observes the failure of improvement in term of increasing total travel time after adding new link. In this study, differently, the failure of improvement can be explained in terms of congestion probability. This new paradox, namely "*Probabilistic Braess' Paradox*" is described as follows.

Figure 15 presents the improvement of simple network from four-link network to five link network, and the network characteristics, length, free flow speed and capacity are also shown in the figure. The improvement scenario is to add a new link between node 2 and node 3 with intention to reduce the system probability of congestion.

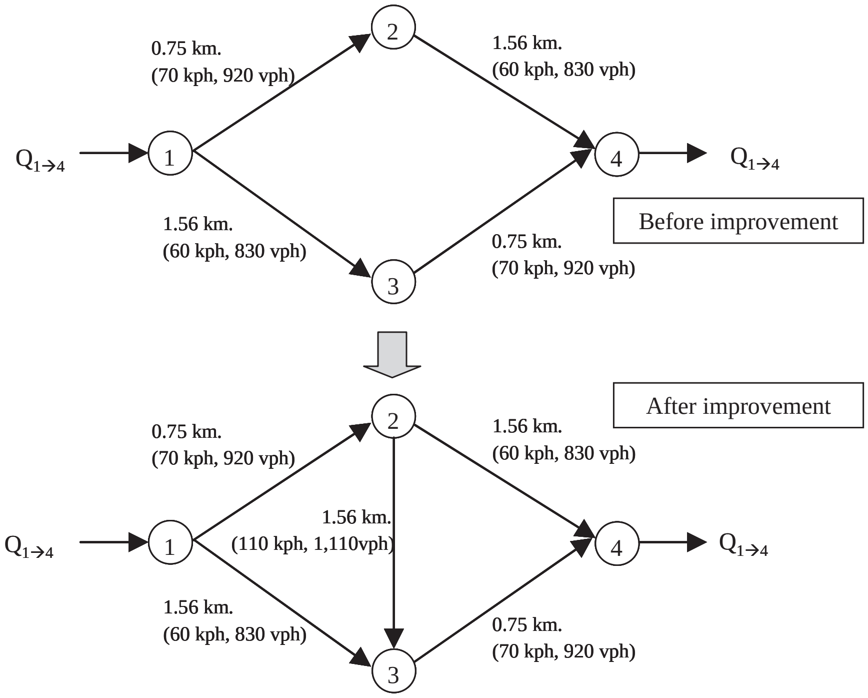

Figure 15: Improvement scenario for showing Braess' Paradox principle

To show the probabilistic Braess' Paradox, suppose that the demand from the node 1 to the node 4 ($Q_{1\to4}$) is 1200 flow units. By performing the traffic assignment with a stochastic OD table, the results show that before improvement, the probability of congestion in the network (PCN) is equal to 0.0826, but after improvement the PCN is 0.23. That is, the improvement makes the occurrence of congestion more likely to happen than before.

6.1 Experiment on Different Demand Levels

The additional experiment was conducted to several demand levels and the results were compared with the classical Braess' paradox from both deterministic OD table and stochastic OD table. Table 3 presents the results from this experiment. According to Table 3, the shaded cells in the table indicate Braess' paradox occurrence. For the deterministic case, the paradox occurs in the demand range between 800 and 1200, and for stochastic case, the demand around 800 presents the paradox situation. On the other hand, the probabilistic Braess' paradox happens in wider range (600 to 1600) and covers the range of classical Braess' paradox as presented in this table.

Table 3 Comparison of TNTT and PCN between before and after improvement

Demand ($Q_{1\to4}$)	**Deterministic TNTT (hrs)**		**Average TNTT (hrs)**		**PCN**	
	Before	**After**	**Before**	**After**	**Before**	**After**
400	14.6924	14.3044	14.7861	14.4588	0	0
600	22.0794	21.8241	22.2681	22.1625	0	0.0105
800	29.5857	29.9512	30.0100	30.0716	0.0002	0.0400
1000	37.3681	37.6485	38.3539	38.3103	0.0119	0.1036

1200	45.6841	45.7091	47.8606	47.4279	0.0826	0.2300
1400	54.9164	54.4577	59.3648	58.2310	0.2254	0.3627
1600	65.5987	64.5702	74.0292	71.5927	0.3925	0.4546
1800	78.4401	76.3319	93.3999	88.7467	0.5417	0.5291
2000	94.3508	90.7065	119.4605	111.4089	0.6585	0.5953
2200	114.4669	108.725	154.6874	141.6219	0.7447	0.6541

Note that the occurrence of Braess' paradox is dependent on the level of travel demand. This is not a new finding in transportation study. Pas and Orincipio (1997) asserted that the occurrence of Braess' paradox is closely related with the level of travel demand and the behavior of network supply. More comprehensive investigation was done in Yang and Bell (1998).

They found that the occurrence of Braess' paradox is dependent not only the level of travel demand but also the route choice behavior of traveler. According to the study, the range of Braess' paradox is wider when SUE (Stochastic user equilibrium) is used as a route choice principle. Another important finding is that the potential or reserved capacity might be reduced by a link addition.

More important finding from this test is that the probabilistic Braess' paradox exists. When travel demand is 1200~1600 flow unit, the probability of traffic congestion increases significantly after the link addition. In addition, the amount of aggravation in congestion probability is also dependent on the level of travel demand. In this example, the probability increase reaches at maximum when travel demand is around 1200~1400 flow unit.

In order to investigate the influence of OD demand variance on Braess' paradox, above test is executed at the various levels of OD flow variance. In addition, three different demand levels: 800, 1200 and 1600 are selected and loaded in order to compare the change of the paradox situation on various demand levels. For comparison, the changes of PCN after improvement used to identify the probabilistic Braess' paradox situation in such that the positive value indicates the occurrence of paradox while the negative value presents no paradox situation. These PCN changing values were plotted against the levels of OD variation as demonstrated in Figure 16.

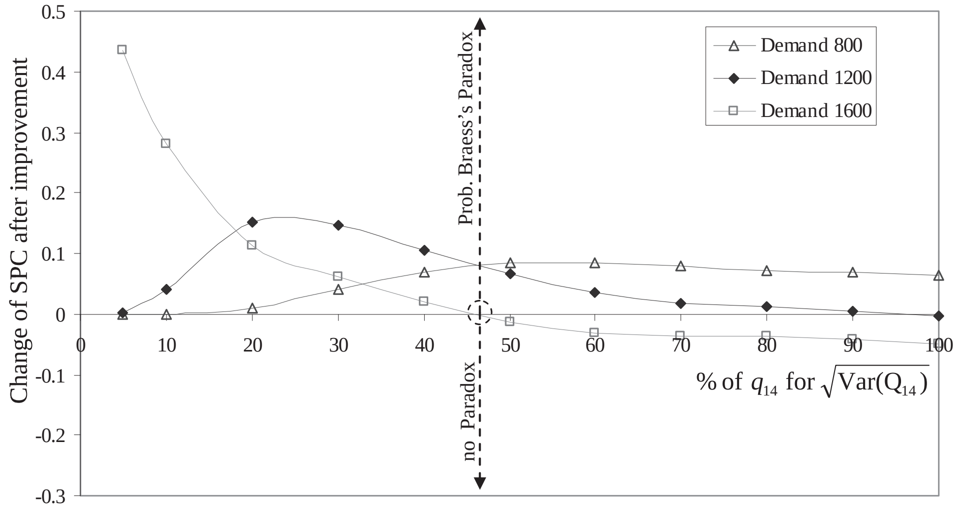

Figure 16: Probabilistic Braess's paradox with various demand levels and variations

According to Figure 16, when the demand is low (demand: 800 flow unit), the peak of PCN change can be observed at the greater level of OD variation (around 50% of q_{14}). Conversely, when the level of demand is high (demand: 1600 flow unit), the highest change of PCN can be observed at the lower level of OD variation (close to 0% of q_{14}). In addition, when demand equals to 1200 flow unit, the peak of PCN changing value can be observed when the level of OD variation is about 23 %. Moreover, it was observed that when the OD variation is high, the severity of probabilistic Braess' paradox tends to decrease. For higher demand level (e.g. 1600 flow unit), the probabilistic Braess' paradox disappears when the OD variation is around 47%, while for lower demand level (e.g. 1200 flow unit), the paradox situation cannot be observed when the OD variation is almost 100%.

7. CONCLUSION

In this study, uncertainty of travel demand is modeled in a way that OD flows are defined as random variables. From the stochastic framework, the new definitions of link traffic flow and congestion for a stochastic network analysis are also introduced. The new measure for probabilistic traffic congestion can reflect the real experience of travelers in the congested network, so it is more user-oriented congestion measure than *v/c*.

The concept of the probabilistic traffic congestion is employed in the NDP. A conventional NDP only considers TNTT, so the uncertainty of travel demand has not been taken into account in the optimal design calculation. For overcoming the flaw, a new objective function which can reflect the probabilistic network congestion is developed. The new objective function shows similar performance to a conventional TNTT minimization function in terms of TNTT. However, it shows a significant superiority to the conventional function in terms of PCN. As a result, the new objective function is a more appropriate measure for a NDP under travel demand uncertainty.

Another important contribution of this paper is the identification of Braess' paradox existence in the stochastic network case. The probabilistic Braess' paradox is defined with probabilistic traffic congestion and the behavior of the paradox is investigated with the various levels of travel demand and its variance. According to simulation tests, the range of Braess' paradox occurrence is wider in the case of stochastic network. In addition, the range of probabilistic Braess' paradox is wider than that of deterministic one. It implies that if travel demand is fluctuating, then more Braess paradox can be happen and the identification of occurrence condition can be found more efficiently with the probabilistic definition of traffic congestion. In other words, if we use TNTT for finding Braess' paradox occurrence, then some cases which increase the probability of network congestion can be unidentified.

Although many significant contributions are achieved in this study, there are some tasks left for the future study. First, a more comprehensive stochastic traffic assignment model should be developed. In this study, Monte Carlo technique is used with static UE traffic assignment, but it requires multiple assignment runs. In addition, the used simulation framework cannot consider the correlation of OD flows. Second, if the proposed probabilistic concept of traffic congestion is combined with a dynamic traffic assignment, a complete network analysis would be possible. One important factor for the occurrence of traffic congestion is the temporal convergence of travel demand. Therefore, a dynamic framework for modeling traffic congestion is inevitable. Third, the probabilistic characteristics of OD travel demand should be investigated with the real data. The variance, appropriate distribution, and correlations among OD flows are the most basic prerequisites for applying the developed model and concepts to in practice.

REFERENCES

Abdulaal, M. and LeBlanc, L.J. (1979). Continuous equilibrium network design models. Transportation Research Part B, 13, 19-32.

Asakura, Y. and Hato, E. (2001). A route recognition model for transport network reliability analysis. In Bell, M. G. H. and Cassir, C. (Eds.), *Reliability of Transport Networks* (pp.203-216). Research Study Press.

Bell, M.G.H. and Iida, Y. (1997). Transportation network analysis. Chichester: John Wiley and Sons.

Blank, L. (1980). Statistical procedures for engineering, management, and science. McGraw-Hill, Inc.

Chen, A., Subprasom, K., Ji, Z.W., (2003). Mean-Variance model for the Build-Operate-Transfer scheme under demand uncertainty. Transportation Research Record 1857, 93-101.

Chen, A., Yang, H., Lo, H. K., and Tang, W. H. (2002) Capacity reliability of a road network: an assessment methodology and numerical results. Transportation Research Part B, 36:225-252.

Chen, M. and Alfa, A.S. (1991). A network design algorithm using a stochastic incremental traffic assignment approach. Transportation Science, 25(3), 215-224.

Clark, S.D., and Watling D.P. (2005). Modelling network travel time reliability under stochastic demand. *Transportation Research, 39* (B), 119-140.

Hazelton, M.L., 2003. Some comments on origin-destination matrix estimation. Transportation Research Part A, 37, 811-822.

Kim H., 2008. New dynamic travel demand modeling methods in advanced data collecting environments, Ph.D. dissertation, University of California, Irvine.

Lam W.H.K., Shao H., Sumalee A. (2008). Modeling impacts of adverse weather conditions on a road network with uncertainties in demand and supply. *Transportation Research Part B*, 42, 890-910.

Lee, S., Moon B. and Asakura Y. (2000). Reliability Analysis and Calculation on Large Scale Transport Networks. In Bell, M.G.H. and Cassir, C. (Eds.), *Reliability of Transport Networks* (pp.173-190). Research Study Press.

Lo, H.K. and Tung Y.K., (2003). Network with degradable links: Capacity analysis and design, *Transportation Research Part B* 37, pp. 345–363

Pas E.I., S.L. Principio (1997) Braess’ paradox : some new insights, Transportation Research Part B 31 (3), pp. 265-276.

Sheffi, Y. (1985). Urban transportation networks. New Jersey: Prentice-Hall.

Siu, B.W.Y., Lo, H. K. (2007). Doubly uncertain transportation network: Degradable capacity ans stochastic demand. *European Journal of Operational Research*, 191, 166-181.

Sumalee A., Watling D.P., and Nakayama S. (2006) Reliable Network Design Problem: the case with stochastic demand and total travel time reliability, *Transportation Research Record*, 1964, p 81-90.

Suwansirikul C., Friesz, T.L., and Tobin, R.L. (1987). Equilibrium decomposed optimization: A heuristic for the continuous equilibrium network design problem, Transportation Science, 21, No.4, 254-263.

Ukkusuri, S.V., Mathew, T.V., Waller, S.T., 2007. Robust transportation network design under demand uncertainty. Computer-Aided Civil and Infrastructure Engineering, 22, 6-18.

Waller, S.T., Schofer J.L. and Ziliaskopoulos A.K. (2001). Evaluation with traffic assignment under demand uncertainty. *Journal of the Transportation Research Board***,** 1771**,** 69–75.

Yang H., M. G. H. Bell (1998) Models and algorithms for road network design: a review and some new developments, Transportation 18 (3), pp. 257-278.

ESTIMATION OF LAND SURFACE WATER COVERAGE (LSWC) WITH AMSR-E AND MODIS

SHUMON MORI, WATARU TAKEUCHI and HARUO SAWADA
Institute of Industrial Science, University of Tokyo
morishumon@gmail.com

ABSTRACT

This research focuses on estimation of land surface water coverage by using AMSR-E and MODIS sensors. The main point in this study is to calibrate the two data, NDPI (normalized difference polarization index) and LSWC (land surface water coverage) obtained by AMSR-E and NDWI (normalized difference water index) of MODIS correspondingly and finally we mapped the inundated land surface distribution.

1. INTRODUCTION

In recent years, overpopulation and human activities are causing water problems such as water shortage, increase of flood disasters. Also, climate changes influence the water cycle and water resources due to global warming. Paddy fields and marshes are presumed to be a major emission source of methane recognized as global warming gases (IPCC), and they are distributed extensively in global scale. It requires the observation methods for paddy fields and marshes and scientific analysis solution for water cycle in global scale. Since it is difficult to investigate the natural field over the extensive area, remote sensing is one of the very useful tools to observe the land surface conditions globally.

AMSR-E is a microwave sensor and its spatial resolution is in scale of kilometers, not high resolution but it can observe the land surface with low cloud interruption (that means high temporal resolution). On the other hand MODIS sensor is a visible infrared sensor and its spatial resolution is in scale of hundreds meter (high spatial resolution) but its observation is frequently interrupted with cloud contamination. In order to overcome the above mentioned problems, the combined utilization of AMSR-E and MODIS is conducted in observing the distribution of the paddy field at the global scale (Takeuchi 2006). These researches focus on the spatial-temporal features of AMSR-E and MODIS that can complement their spatial-temporal weak point each other.

The objective of this study is to investigate the spatial-temporal difference of inundated land surface properties obtained from both AMSR-E and MODIS sensors. The more precise calibration between AMSR-E and MODIS is conducted to find the relationship between AMSR-E NDPI and

MODIS LSWC. The uniqueness of this study is found on the calibration of index (AMSR-E NDPI) and physical quantity supplemented by MODIS.

2. METHODOLOGY

2.1. Flowchart to produce LSWC distribution map with AMSR-E and MODIS

Figure 1 shows a flowchart to produce land surface water coverage (denoted as LSWC) distribution map by combining AMSR-E and MODIS.

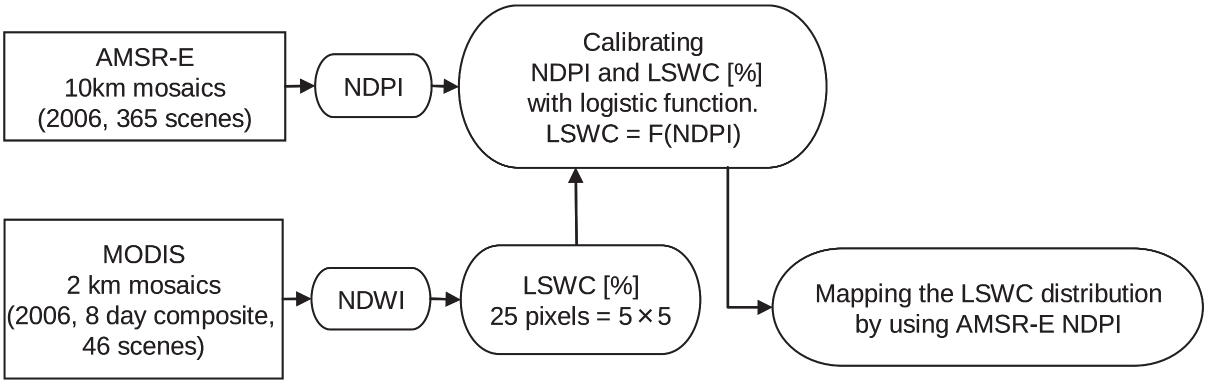

Figure1: Flowchart to produce LSWC distribution map by combining AMSR-E and MODIS

AMSR-E data was obtained from National Snow and Ice Data Center (NSIDC) in United States of America, and a series of preprocessing was carried out including radiance calibration, geometric correction, spatial mosaic and subset. Normalized difference polarization index (NDPI) was computed as shown in Equation (1).

$$NDPI = \frac{T_v - T_h}{T_v + T_h} \qquad (1)$$

T_v : 36.5 GHz brightness temperature vertical
T_h : 36.5 GHz brightness temperature horizontal

MODIS data rebuilding was carried out by Linlle-University group (Dr. Louis Gonzalez, personal communication) based on NASA's 8-day global mosaic composite product (MOD09A1). The idea is to remove clouds by spatio-temporal filtering technique on a pixel-basis processing. Normalized difference water index (NDWI) was computed as shown in Equation (2).

$$NDWI = \frac{VIS - SWIR}{VIS + SWIR} \qquad (2)$$

VIS : Reflectance of visible (630 nm, channel 1)

SWIR : Reflectance of short wave infrared (1620 nm, channel 6)

2.2. Study area

Figure 2 shows an area of interest in this study highlighted by red square, centered at latitude 54-17`59, 95”N, longitude 90-52`0.20”E. The area is 10,000 square kilometers (10x10 pixels) covered by seasonal dynamics of open water, natural wetlands and paddy fields. In this study, above ground vegetation contribution is neglected.

Figure2: Area of interest in this study is highlighted by red square, centered at latitude 54-17`59, 95”N, longitude 90-52`0.20”E and the area is 100 square kilometer known as open water area.

2.3. Setting the inundated pixel threshold

In this study land surface water coverage is strongly dependent on the inundated threshold. To estimate the precise inundated threshold we build the global land coverage histogram by utilizing MODIS NDWI images. After that, we simulated the histogram’s curve behavior with Gaussian function:

$$f(x) = \frac{a}{\sqrt{2\pi c^2}} \exp\left(-\frac{(x-b)^2}{2c^2}\right) \quad (3)$$

The parameter ‘a’ expresses the height of the curve’s peak and ‘b’ expresses the center of curve’s peak and ‘c’ controls the width of peak. In this study we simulated 36 NDWI histograms.

Then we processed 3 steps:

First step is to classify the part of histogram such as vegetation, soil, and mixture of water and soil.

Second step is to confirm the dependence of temporal series of the threshold by verifying the fluctuation of the peaks.

Third step is to classify the distribution of inundated area in order to set the inundated threshold more precisely.

2.4. LSWC (Land Surface Water Coverage)

Figure 3 shows a schematic diagram between AMSR-E and MODIS footprints. One pixel of AMSR-E (10 square km) corresponds to the 5x5 block of MODIS pixels.

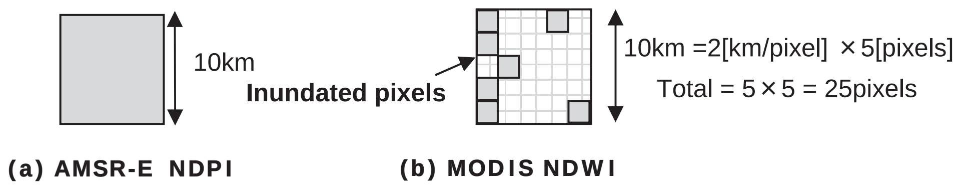

Figure 3: Spatial correspondence between AMSR-E and MODIS.

LSWC between AMSR-E and MODIS was estimated by following the three steps:

1. To select the threshold of MODIS NDWI images to distinguish between inundated and non-inundated pixels aided by histogram curve.

2. To produce the inundated distribution map in 2 km and spatially aggregate the inundated distribution map 2 km into the fractional coverage of land surface water coverage in 10 km (MODIS LSWC).

3. To find out the relationship between AMSR-E NDPI and MODIS LSWC. Logistic function as shown in Equation (4) is expected to fit well between those (Takeuchi, 2006). The coefficients a, b and c are estimated by using the least squares method.

$$LSWC = \frac{a}{1 + b \cdot \exp(-c \cdot NDPI)} \tag{4}$$

3. RESULTS

3.1. Spatial correspondence between AMSR-E NDPI and MODIS NDWI

Figure 4 shows comparison of MODIS NDWI 2 km, MODIS LSW map 2 km, MODIS LSWC 10 km and AMSR-E NDPI 10 km. Brighter pixels indicate high abundance of inundated area.

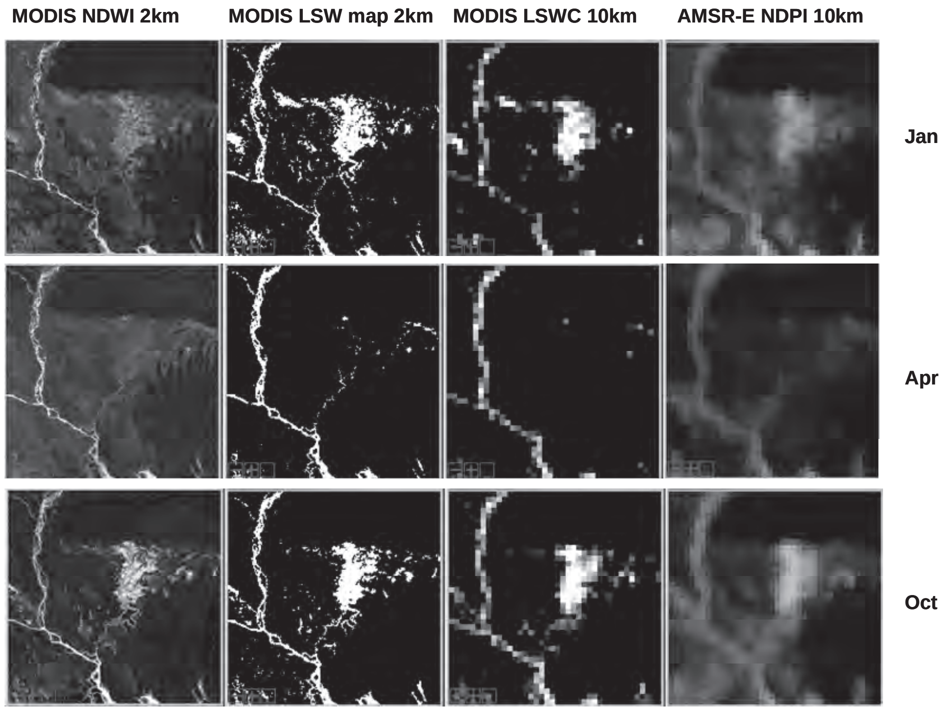

Figure 4: Comparison of MODIS NDWI 2km, MODIS LSW map 2km, MODIS LSWC 10 km and AMSR-E NDPI 10km. Brighter pixels indicate high abundance of inundated area.

3.2. Select the inundated threshold

Figure 5 shows a MODIS NDWI histogram in 2006 characterized by 4 peaks including vegetation (peak1), soil (peak2), mixture of soil and water (peak3), and water and snow (peak4).

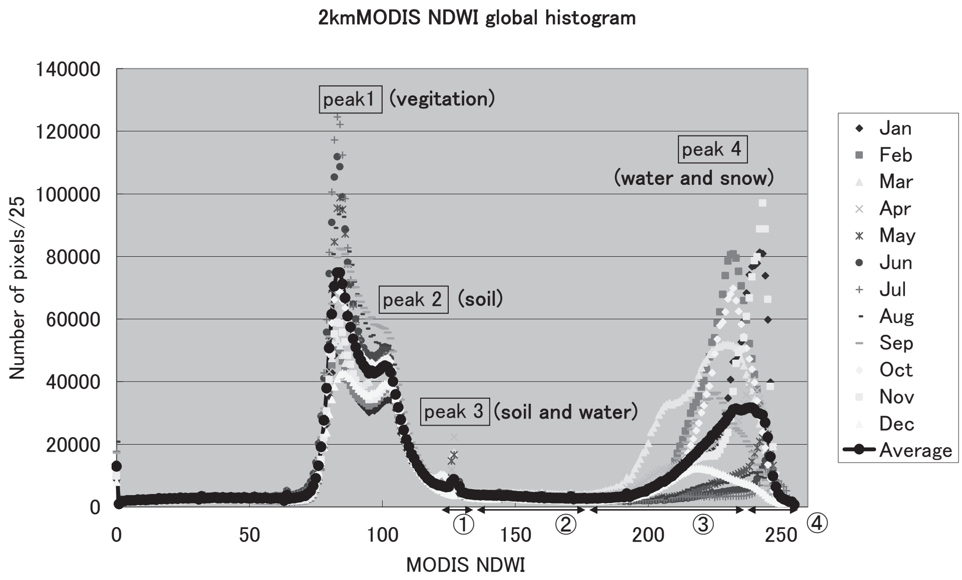

Figure 5 : MODIS NDWI histogram in 2006

In first step, we classified the peak1, 2 and 3 by matching the Gaussian function with them and we demonstrated approximately their land cover type according to NDWI values. Then, the result was that peak1 represents the vegetation area, that peak2 represents the soil area and that peak3 represents the mixture of soil and water area. The results are summarized in Table 1 and in Figure 6.

Table 1: details of 3 peaks

	averaged center of peak	S.D. of peak	S.D. of center
Peak1	83.0	5.2	0.7
Peak2	100.3	7.8	1
Peak3	126.8	3.3	1.5

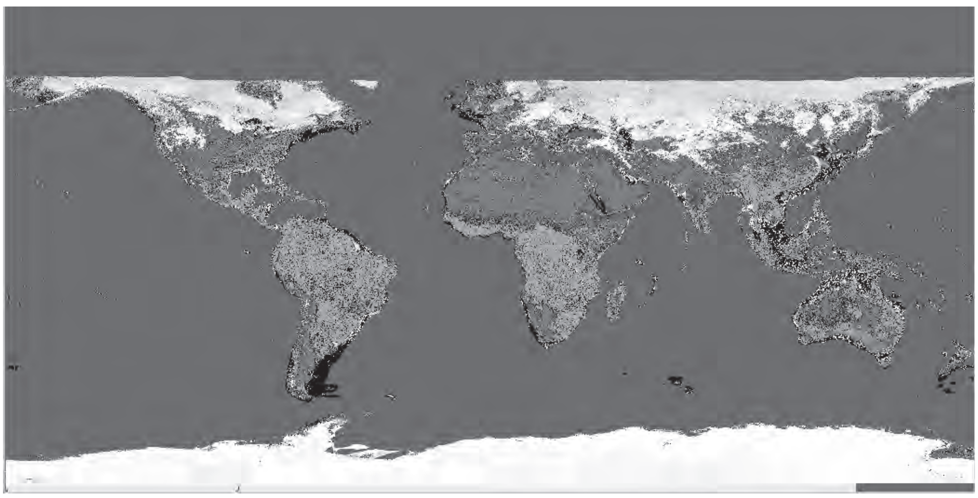

Figure 6: Global NDWI histogram mapping. The green pixels whose range o f [78, 81] shows vegetations, The brown pixels whose range of [92, 108] shows soils and the yellow pixels range of [123, 130].

In second step, we found the slight-fluctuation of the peaks as shown in Table 1 and in Figure 5. Therefore we suggested the independence of the inundated threshold on temporal series.

In third step, we investigated the inundated range, NDWI = [121, 255], to determine the precise inundated threshold by classifying the range to 4 areas, NDWI = [121, 136], [137, 178], [179, 239], [240, 255], as mentioned in the above Figure 5. The results are shown in the figure 7- (b).

Then we comprised the NDWI maps with MODIS visible map in Bangladesh and we determined that inundated threshold=121 represents the inundated areas most precisely as shown in MODIS visible image.

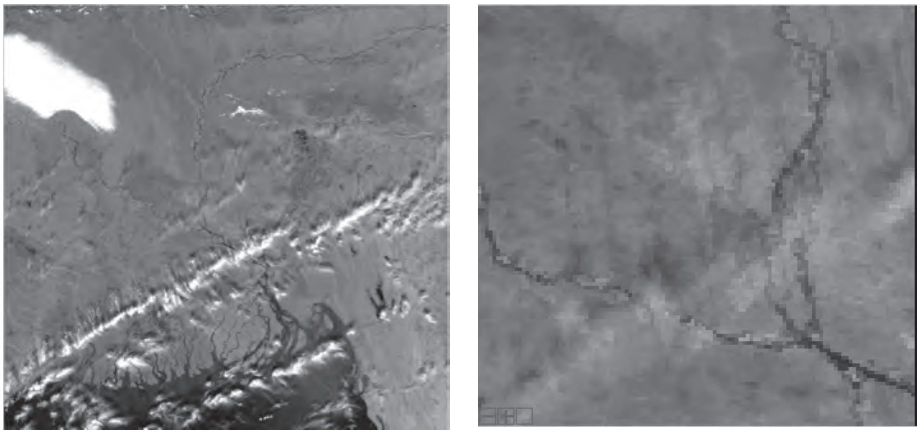

(a) MODIS visible image 20060106 as a reference

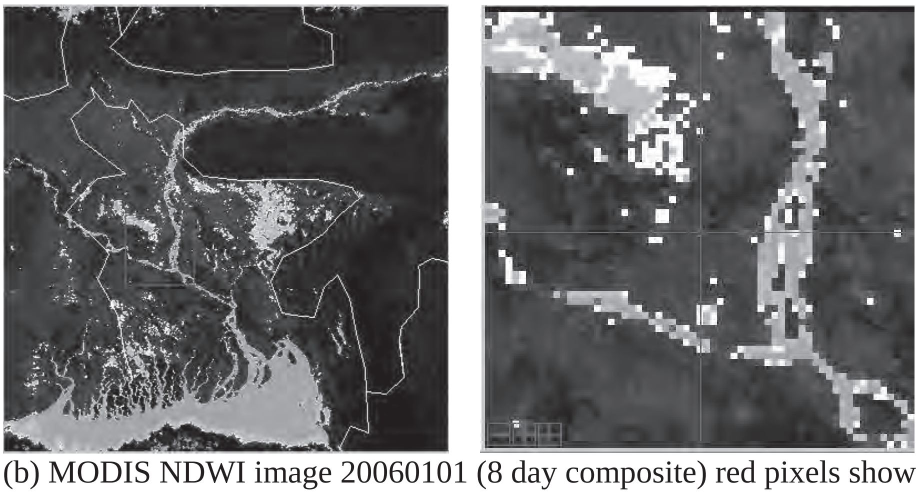

(b) MODIS NDWI image 20060101 (8 day composite) red pixels show range of [240, 255], green pixels show range of [179, 239], cyan pixels show range of [137, 178] and white pixels show range of [121, 136].

Figure 7: Comparison between MODIS visible image and MODIS NDWI image

3.3. Relationship between NDPI and LSWC

Figure 8 shows the scatter plot representing the relationship between AMSR-E NDPI and MODIS NDWI. We used the data on 2006, Jan 01 and on 2006, July 04 in area mentioned above and after applying least squares method we received the following scatter plot, coefficients and standard deviation:

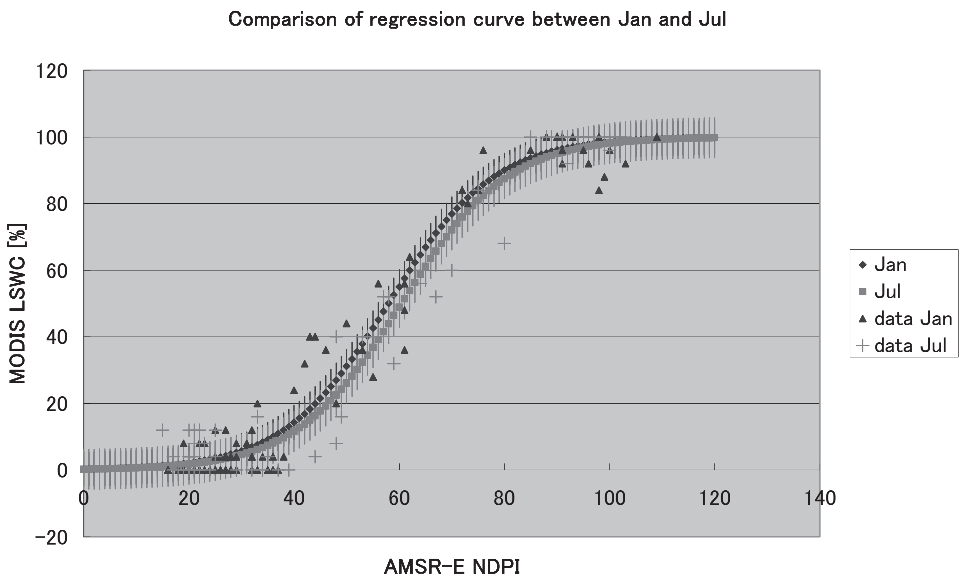

Figure 8 : Scatter plot representing the relation between AMSR-E NDPI and MODIS LSWC

Table 2 : Results of coefficients a, b, c and standard deviation after application of least method

20060101

a	100.0
b	323.5
c	0.1
S.D.	7.1

20060704

a	100.0
b	404.6
c	0.1
S.D.	6.0

For your attention, the data is quantized to 4%. Then, the minimum standard error is 4 % (because MODIS image has 25 pixels in 10 square km area and then minimum scale of data is 4%).

We can find that the two regression curves are modeled similarly within the standard error 4%. Thus, we can hypothesize that theses regression curves represent precisely the LSWC in independent on temporal series.

3.4. Spatial correspondence between AMER-E NDPI LSWC distribution map and MODIS NDWI LSWC distribution map

Figure 9 shows the spatial correspondence between AMSR-E NDPI LSWC distribution map and MODIS NDWI LSWC distribution map. Brighter pixels indicate high abundance of inundated area. There is high correspondence between two maps as shown.

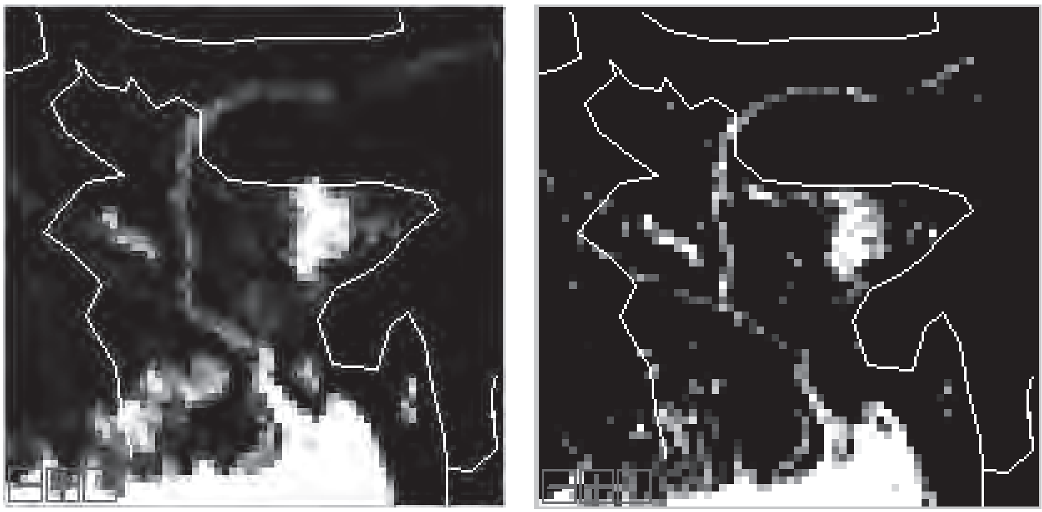

(a) LSWC distribution map of AMSR-E NDPI

(b) LSWC distribution map of MODIS NDWI

Figure 9 : Spatial correspondence of AMSR-E NDPI LSWC distribution map with MODIS NDWI LSWC distribution map

4. CONCLUSION

In this study we built the NDWI histogram in global scale by MODIS 8-day composite data and we classified the main 3 peaks to assume the water-soil mixture NDWI range. Then, we classified more precisely the water NDWI range. Finally, we succeeded to hypothesize the inundated threshold with comparison of MODIS visible image.

Based on the threshold we processed the sub-pixel analysis in 10,000 square km open water area, and then we modeled the logistic regression curve by using 100 points data of this object area.

By comparing with two days regression curve, we found that their difference distance is closely 4% (the our data is quantized to 4% then the minimum standard error is 4 %) then we arrived to the conclusion that our logistic regression curve represent precisely and independently of temporal-series Land Surface Water Coverage in open water area.

Finally we mapped the LSWC distribution by using AMSR-E. By applying these results we can assume the inundated period and produce flood disaster map and so on.

In this study we focus on only open water area. Then for the future work we need to investigate the arboreal vegetation influences on microwaves and visible infrared waves to improve and apply the logistic regression curve for Amazon or other similar area.

REFERENCES

Wataru Takeuchi, Daisuke Komori, Taikan Oki and Yoshifumi Yasuoka, 2006. An integrated approach on rice paddy irrigation pattern monitoring over Asia with MODIS and AMSR-E . American geophysical union fall meeting 2006 (AGU): San francisco, USA, 2006 Dec. 5.

Sippel, S. J. et al., 1994. Determination of inundation area in the Amazon river flood plain using the SMMR 37 GHz Polarization difference, Remote Sens. Environ, 70-76, 48.

COMPARATIVE ANALYSIS OF PLANNED AND ACTUAL DISASTER MANAGEMENT OPERATIONS PERFORMED DURING AND JUST AFTER THE 2007 CYCLONE SIDR IN BANGLADESH

TAIKI KOU[1] and KIMIRO MEGURO[2]
[1]Department of Civil Engineering, The University of Tokyo
[2]International Center for Urban Safety Engineering,
Institute of Industrial Science, The University of Tokyo, Japan
kou@risk-mg.iis.u-tokyo.ac.jp

ABSTRACT

The authors have analyzed "Standing Orders on Disaster", which is the basic plan to implement the disaster management operations in Bangladesh, and compared it to actual operations performed during and just after the Cyclone Sidr in 2007. Information on actual operations was collected by the authors and researchers in the Bangladesh University of Engineering and Technology based on briefing papers at that time and field surveys. The Orders were also sorted out according to the categories of Basic Disaster Prevention Plan in Japan in order to figure out a framework of the Orders. Further, by using the framework, the authors have proposed a continual revision process of the disaster management plan.

1. INTRODUCTION

1.1 Background

Standing Orders on Disaster (SOD), which is equivalent to the Basic Law on Natural Disasters, was published in 1997 in Bangladesh. The principal thinking behind the formulation resulted from the experiences of devastating flood and cyclone damages during the 1980s and 1990s. The experiences intensely highlighted the insufficiencies of disaster management operations that mainly stressed on response and rehabilitation.

More than 10 years have passed since the Orders were put into effect; several controversial points have been noted in that time, and the momentum of revision that has recently gathered.

1.2 SOD –Bangladesh Disaster Management Plan–

What is SOD?

SOD is a basic disaster management plan in Bangladesh to implement the disaster management operations. The Orders comprehensively describe the total disaster management plan for each of the 38 actors which are related to the disaster management operations, and each phase such as "Normal Times", "Alert Stage", "Warning Stage", "Disaster Stage" and "Rehabilitation Stage".

Significance of formulating SOD

Before formulating SOD, it should be remembered that each disaster management plan (such as flood or cyclone) rarely has uniformity in the plan. So the total disaster management plan was formulated, which was adoptable even though he types of disasters are different. This plan clarified the disaster management operations actors, and the proposed operations which were described based on the phase made it straightforward for the actors who implement the disaster management operations to grasp the contents of operations easily by checking up the papers.

Recent Controversial points of SOD

Ten years have passed after publishing the document, and SOD has noted following controversial implementation points immediately preceding and following the disaster management operations. These arguments increase the momentum towards upgrading the Orders into further practical steps.

- Planned operations are only listed, and a time axis is not considered
- Obscurity of coordination and linkage of operations / information with other agencies
- As the total picture of disaster management operations is not described in the Orders, the orientation of each disaster management operation is hard to figure out in the total framework of disaster management.
- Not updated since the publication in 1997

1.3 Purpose of the Study

In this study, the authors have analyzed Standing Orders on Disaster, which is the basic plan to implement the disaster management operations in Bangladesh, and compared it to actual operations during and just after the 2007 Cyclone Sidr. The study focuses on public sectors, Cyclone Preparedness Programme (CPP), Bangladesh Red Crescent Society (BDRCS), and is based on briefing papers at that time and field survey conducted by the authors and Bangladesh University of Engineering and Technology (BUET). Based on the Comparison, the authors have overviewed the actual disaster management situations mainly focusing on Public Sectors in Bangladesh.

In addition, the contents of the disaster management plan described in the Orders have been sorted out by the disaster management operations' categories of Basic Disaster Prevention Plan in Japan. This analysis made it possible to figure out a framework of the Orders by comparing it with Japanese disaster management. Further, by using the framework, this study put forward a proposal of a continual revision process of the disaster management plan.

2. METHODOLOGY

2.1. Database Setting

Database setting of SOD

The authors built up the database of SOD and newly added two attribution data noted on ***Figure 1*** to overcome the controversial points that are illustrated above.

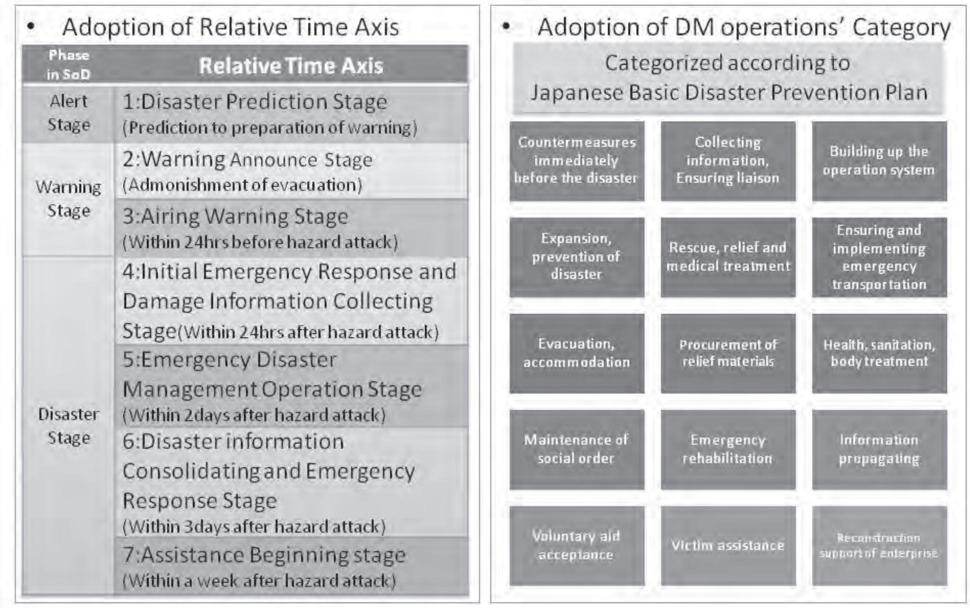

Figure 1: Two attribution data newly added

Introduction of relative time axis

To express the disaster management operations in time axis, we recently added the seven phases, from disaster foreseeing phase to assistance beginning phase.

Adoption of operation categories

The proposed operations in SOD were sorted out by the categories of disaster emergency management and recovery and rehabilitation described in the Basic Disaster Prevention Plan in Japan.

2.2. Three Dimensional Analysis

Three dimensional analysis was done by choosing the actor, time axis, amounts of operations' description from the Database illustrated above. This analysis made it possible to visualize the each actor's amounts of operations relative to time.

2.3. Operation Category Analysis

Operation category analysis was done by choosing an actor and operation category from the database. This analysis made it possible to figure out each description of operation in the total framework of disaster management operations and actors who would implement cognate disaster management operations.

It was important to set an empirically-selected category to embrace disaster management operations, therefore this study adopted the category of Japanese Basic Disaster Prevention Plan. It would be preferable to adopt other categories to analyze the SOD in different ways too.

3. ANALYSIS AND RESULT

3.1 Analysis of SOD

Estimation of operation amounts by three Dimensional Analysis

From the analysis (***Figure2***), the following controversial points became apparent.

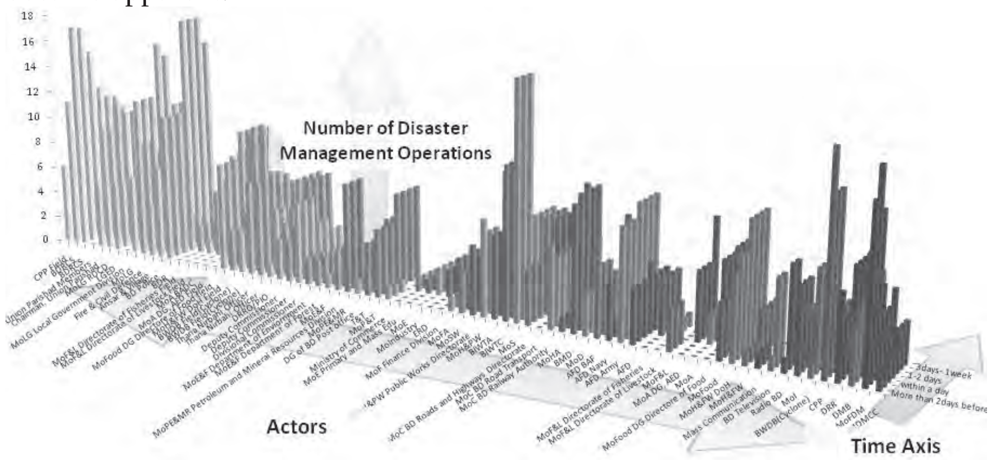

Figure 2: Estimation of operation amounts by three dimensional analysis

1: Planned operations were described based on the four disaster phases as mentioned in section two, so it is difficult to be clear about the orders of operation in each phase
2: Existence of terms when sudden increase of operations are required. It would be better to implement some operations in advance which can be done before the arrival of the hazard
3: The amounts of descriptions of operations are significantly different from each actor. These disagreements come from the concreteness of operations' contents. These disagreements make the responsibility of each actor ambiguous.

Clarification of disaster management operation field of each actor based on Operation Category Analysis

To grasp the total framework of disaster management, which is hard to judge only by the text written in the Orders, we conducted the operation category analysis. Adopting the Disaster management operation actors in Bangladesh and categories of disaster management operations in Japan illustrated in the Basic Disaster Prevention Plan as two axes, this analysis made it possible to grasp the disaster management operation categories of each actor. From the ***Figure 3***, it can be seen that some plans of disaster management operations were fully described to implement comprehensive disaster management operations, such as Ministry of Home Affairs (MoHA), Ministry of Shipping(MoS), Ministry of Health and Family Welfare(MoH&FW), Ministry of Local Government(MoLG). At the disaster stage during which every actor faces the scarcity of both the artificial and the physical, it is quite important for each actor to describe not only disaster management operations related to its usual operations but also disaster particular operations such as rescue, relief operations excepting the particular operations which requires some authorities or abilities, such as the distribution of relief aid, rehabilitation of the infrastructure system or medical relief as a description of orders.

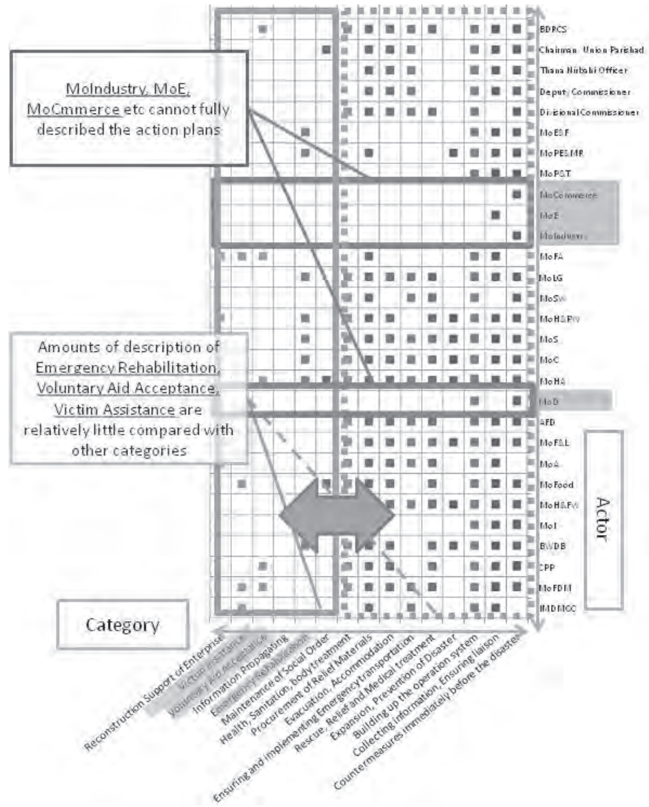

Figure 3: Clarification of disaster management operation field of each actor based on operation category analysis

However, the problem is that "Is it possible or not to implement the whole operations illustrated in the Orders during the disaster stage which faces the crucial scarcity"

If not, the Orders would be an all-round less effective plan. At the stage of comparison with actual disaster management operations, the Orders have to be checked against whether the Orders was formulated with taking consideration of that point.

3.1 Actual Disaster Management Analysis in 2007 Cyclone Sidr

Follow-up period

This study sets from 13th to 22nd November as a follow-up period of disaster management operations led by the government and public administration of Bangladesh for the following reasons:

Situation Report about Cyclone Sidr had been published on 13th November (15:30, 13th Nov, '07). After 22nd November, international coordination relief operations called "Cluster Approach" which both described actors and not described actors in SOD committed had started. This was triggered by the Disaster Emergency Response (DER) Meeting which government, donor, international organization and NGO participated in.

Limited information of disaster management operation

Before starting the analysis, there are some controversial points about disaster management operation records: partial and limited records of disaster management, no detailed description of time and date, amount of time required or head-count required.

For setting the feedback and update system of disaster management operation in place, it will be also required to amend how to the data. is recorded

Comparative analysis of planned and actual disaster management by three Dimensional Analysis

In this analysis related to the above example, some problems occurred.There were several records which could not count as actual disaster management operation records since they lacked description of operations' detail, which made it difficult to do comparisons with the Order "SOD". These ambiguous points were confirmed by the field surveys conducted by the authors and BUET research members. The results of field surveys were reflected to this analysis as much as possible along with the operations defined in SOD.

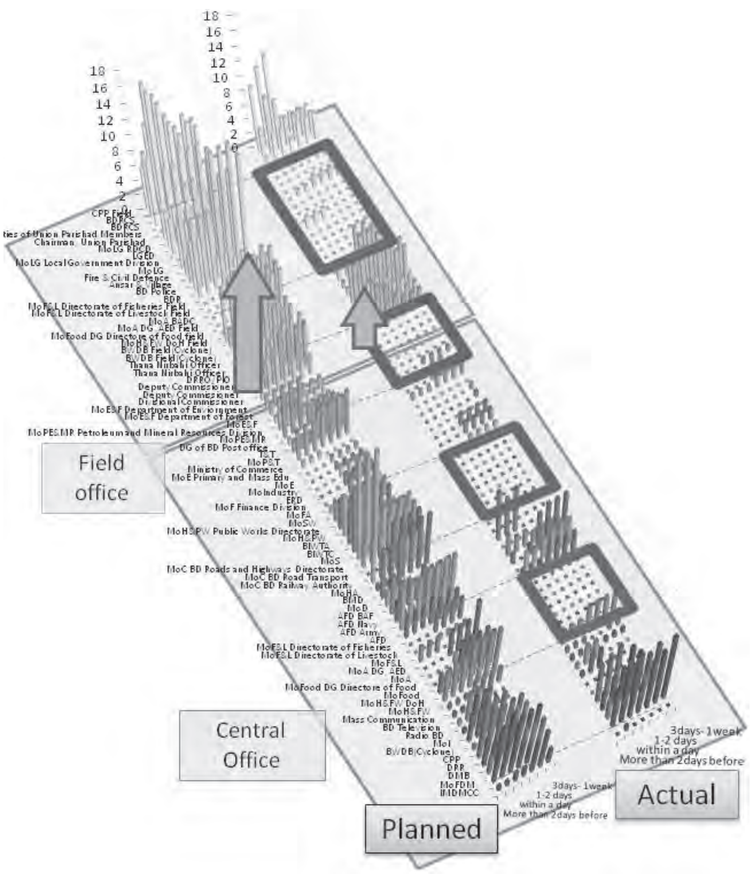

Figure 4: Comparative analysis of planned and actual disaster management by three dimensional analysis

Figure 4 is the result of comparison of actual and planned operations (Left: planned, Right: actual).

From the result of analysis and field survey, the following points can be indicated:

1) Disaster management operations were not or could not be implemented, nor was there a mechanism of information transmittance to the upper organization even though the operations were done
2) Generally, operations were not fully achieved
3) A small portion of central organizations were forced to implement more operations than the Order provisioned

From the insight of field survey, the reason for point 1) and 2) could be divided into two aspects. One was a human resource problem, involving insufficient numbers of public officers or officer's affliction. The other was physical problem: insufficient number of motor boats to distribute the relief materials or shortage of budget to keep up a distribution operations.

Situation like point 3) could be seen at the central disaster management organizations such as Ministry of Food and Disaster Management (MoFDM) or Disaster Management Bureau (DMB). It was confirmed by the field surveys, coordination operations of foreign assistance by several donors or UN agencies, operation works at Barisal were concentrated on these organizations.

Comparison of actual operations and planned operations by using Operation Category Analysis

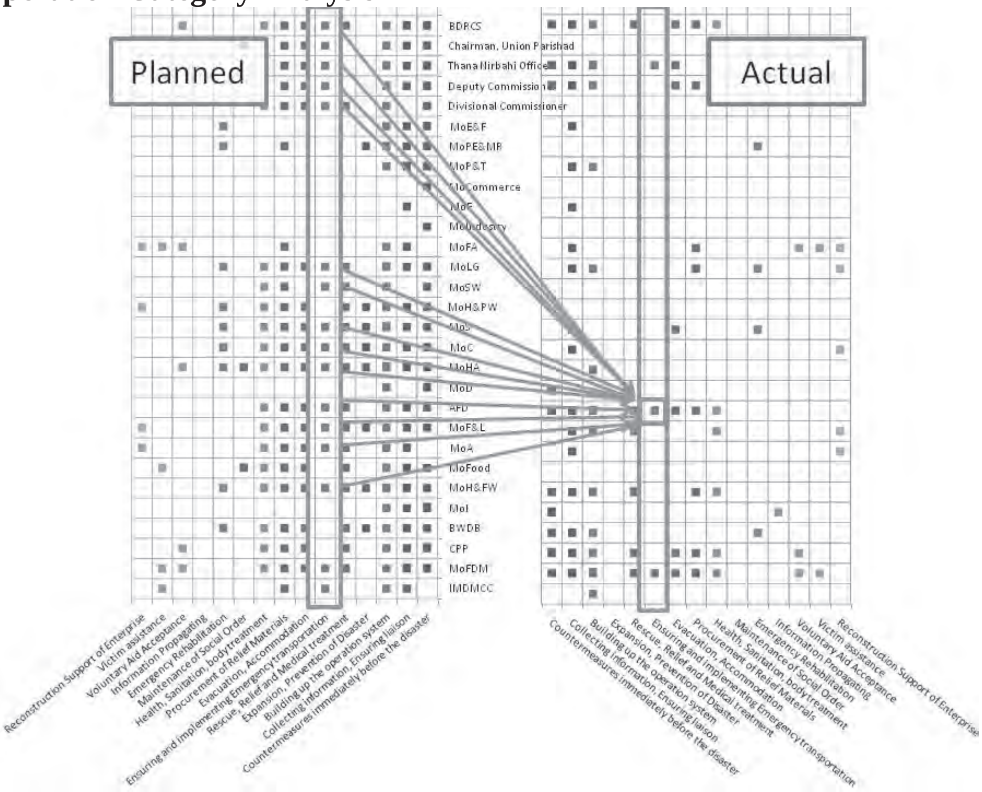

Figure 5: Comparison of actual operations and planned operations by using operation category analysis

Figure 5 is the result of a comparison of actual and planned operations sorted out by the categories of disaster management operations (Left: planned, Right: actual).

From the result of analysis and field survey, the following points can be indicated:

1) Disaster management operations were not or could not be implemented, nor was there a mechanism of information transmittance to the upper organization even though the operations were done
2) Disaster management operations were mainly done within normal time's operation fields of each organization
3) Only limited organizations were able to implement measures in the operation field while several organizations were supposed to implement the operation.

About points 1) and 2), the reason the organization could not implement operations were due to the human and physical issues.

Related to 2), it could be indicated that there was no room to enlarge the operation field to disaster-particular operation fields, such as rescue or relief operations for the problem of the scarcity of human or physical resource problem.

About 3), in 2007 Cyclone Sidr case, Armed Force Division (AFD) played a leading role of operations in the field just after the cyclone. Especially, long-range transportation of relief materials was almost totally implemented only by AFD.

Besides, the blank areas of the right figure, which means that planned operations were not done, were substituted by internal/international aid agencies, NGOs or NPOs.' relief operations. These situations could be realized by analyzing not only records but also field surveys.

4. CONCLUSIONS

Comparison of planned and actual operations by using category analysis enables us to review and evaluate the total disaster management figure in Bangladesh, which had not been done sufficiently before.

The approach to effectively verify the causes of unfulfilled operations was set, such as clarifying the actors which could not fully operate, or the categories which were not fulfilled, by checking up the controversial points of both orders and organizations (***Figure 6***).

At the present stage such disaster management operations described in the Order could not be achieved, therefore it is necessary to set priorities on the Orders under the human, physical resource and time limitation.

In concrete terms, conducting the following validations enables us to renew the orders into more actual suited orders:

- Figuring out whether each actor could conduct the disaster management operations along with the Orders or not, through looking around the whole situation of disaster management
- About the blank areas which can be seen in right side of Figure*, confirming the capacity of implementing disaster management operations of each actor planned in the Order
- If there is sufficient capacity, clarifying and ensuring the implementation framework of the orders for upcoming disaster. If not, confirming which actor could substitute the operations, and re-allocating the operations
- Considering which is adoptable and efficient for the actual situation, coming to terms with the concentrated situation or seeking alternative solutions (Ex: concentration on AFD to transform the relief materials)

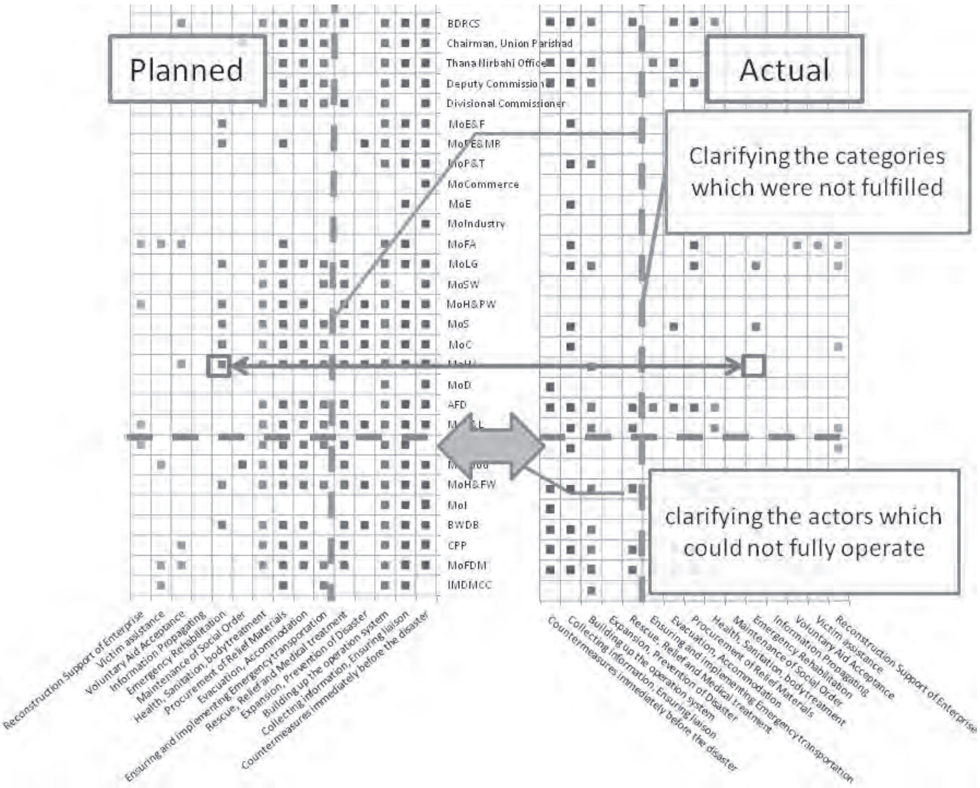

Figure 6: Reviewing Process of disaster management operations by using Operation Category Analysis

Further, as illustrated in ***Figure 7***, continual implementation of this evaluation process whenever the experience is accumulated can reflect sequentially the disjunction of plan and fact. This evaluation process enables us to continually revise the disaster management plan.

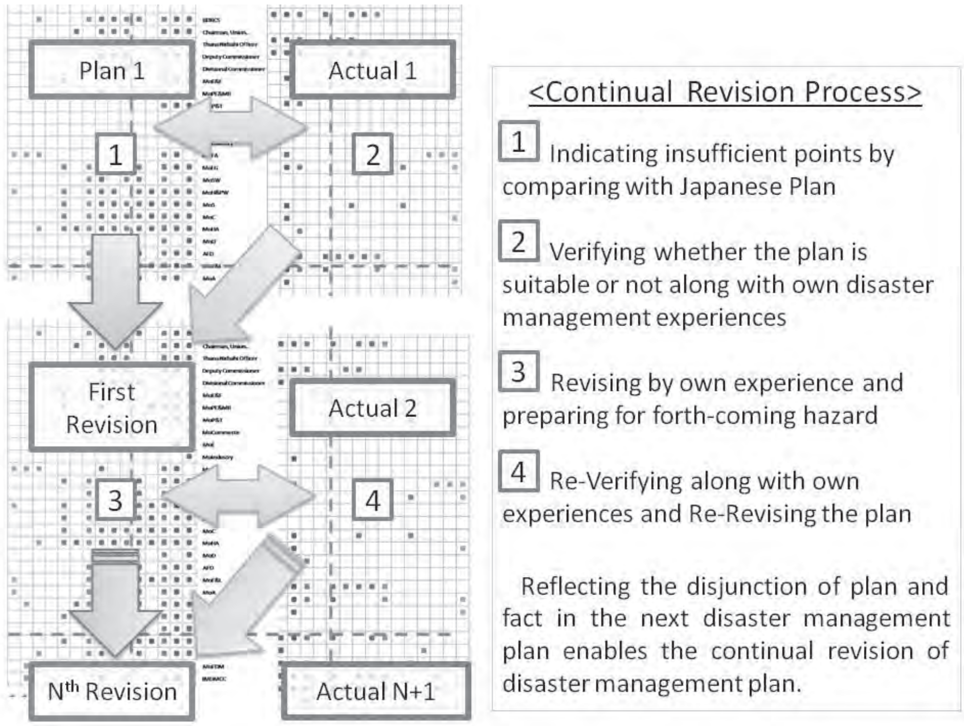

Figure 7: Continual Revision Process of Disaster Management Plan

ACKNOWLEDGEMENT

The authors would like to express their sincere gratitude for all the support by Prof. Mehedi Ahmed Ansary and Ms. Researcher Afifa Imtiaz, Urban Safety Engineering Department, BUET for conducting the field surveys

REFERENCES

Shinya KONDO, 2002. Development of New Style Disaster Information Database for Implementation of Efficient Disaster Countermeasures

Yoshiki HIRUMA, Kimiro MEGURO, 2007. Analysis of Record for Disaster Response Activities of Local Government Officials of NIIGATA Prefecture after The 2004 NIIGATAKEN-CHUETSU Earthquake

Mehedi Ahmed Ansary, Rubel Das, Afifa Imtlaz, 2008. *Role of Logistics during Cyclone SIDR*, BNUS, BUET, USMCA 2008, 249-254

World Bank Report, 2008. *Cyclone SIDR in Bangladesh*, April, 2008.

Government of the People's Republic of Bangladesh, 1999. Standing Orders on Disaster

ENVIRONMENTAL FLOW IN WATER RESOURCES MANAGEMENT: STATUS IN SOUTH ASIA

MD. REAZ AKTER MULLICK and MUKAND S BABEL
School of Engineering and Technology
Asian Institute of Technology, Thailand
reazmullick@gmail.com

ABSTRACT

The concept of environmental flow (EF) is central to achieving sustainable water resources management. This paper reviews the current status on adoption and use of EF approach in water resources management in South Asian countries. Issues explored in this study also include the ongoing challenges in achieving sustainable water resources management since the region is growing fast and freshwater becomes scarce which pushes the region towards environmental water scarcity. The review finds some progress in assessment and adoption of EF into water resources management in Sri Lanka, Pakistan and India; however, Bangladesh and Nepal show an early stage progressing status. At the end, suggestions are made on some key issues to be considered for recognizing EF as an effective tool in integrated water resource management while meeting the water needs for South Asian countries.

1. INTRODUCTION

Water pervades life on earth, determines the ecosystem pattern and deeply embeds civilization while providing numerous services to mankind. The multi-sectoral development and multi-interest utilization criteria of water need to be acknowledged and managed in an integrated approach. Agenda 21 recognizes the issue of ensuring water supply for societal need while preserving the functions of ecosystem. The Millennium Ecosystem Assessment (MEA) identifies *"any progress achieved in addressing the Millennium Development Goals (MDGs) of poverty and hunger eradication, human health and environmental protection is unlikely to be sustained if the ecosystem services on which humanity relies continue to be degraded"*[1]. However, increasing population, growing urbanization and accelerated industrial activities result an enormous appropriation of freshwater resources leading to serious degradation of aquatic ecosystem in much of the world (King & Brown, 2006; Tharme, 2003; Bunn & Arthington, 2002). Degradation of aquatic ecosystem bears a far reaching impact not only by losing ecosystem integrity but also to a large community who directly depends on instream flow for livelihood. Growing demand and competition

---

[1] Millennium Ecosystem Assessment Synthesis Report 2005

for water in developmental needs in one hand with increasing concern on environmental sustainability in another, the concept of 'environmental flow' (EF) is central to the dilemma in achieving sustainable water resources management (WRM).

South Asia, the home of about one-fifth of the world's population, is the most populous and densest yet economically poor region in the world. Dissimilarities observed among different organizations in delineation of South Asia's boundary; however, considering present member states of SAARC (South Asian Association for Regional Cooperation; http://www.saarc-sec.org/) is considered as the basis to find the region. The entire region has many diverse physical characteristics offering a geographical variety from deserts to swamplands, forests to grasslands, mountains to coastal areas. Bounded by the Himalayas in the north, South Asia's southern border is the Indian Ocean. The region spreads up to Afghanistan in the west where as it bounds India-Myanmar border and the Bangladesh-Myanmar border to the east. Several large rivers keep this region 'live'. With the agro based economy of the region, more than fifty percent of the countries population is directly or indirectly dependent on agriculture where water is the key factor to production. Rivers are the major sources of water for agriculture in these countries. Rivers are also vital as the cheapest mode of communication and transportation. However, the region is faced with significant changes and challenges in sustainable water resource management. At the national level, it is expected that Afghanistan, India, Iran, and Pakistan will fall below the threshold of 1500 m^3 per capita of water availability by the year 2030 (Yang, 2003). With the overall growth of population and urbanization in these countries, freshwater ecosystems is under continued pressure due to water withdrawals for increased food production, by building of dams for hydropower to meet energy demand, by making reservoirs to supply drinking water to large cities and by navigational improvement projects to improve trade between countries.

This paper provides a quick overview on environmental water need in water resources management and reviews the status of EF approach in water resources management in South Asia Region including its adoption and implementation. The paper describes briefly on consideration of EF as a tool in Integrated Water Resource Management (IWRM) within this region from current available literature. Issues explored in this study also include the ongoing challenges of achieving sustainable water management since freshwater becomes scarce and the region moves towards environmental water scarcity condition.

2. WATER FOR HUMAN AND NATURE

In late ninth century, Queen Sammu-Ramat (who ruled Assyria, presently northern Iraq), inscribed on her tomb (cited in Postel & Richter, 2003): "*I constrained the mighty river to flow according to my will and led its water to fertilize lands that had before been barren and without inhabitants*". Alike the history, political leaders still are in practice of showing their power and legitimacy with endeavor of winning their constituencies' favor by creating the provision of economic development of their country using the water resources. Globally, fresh water supports 40% of the food production, 20% of fish yield through aquaculture (FAO, 1996) and 20% of power supply (Gleick, 1998). However, direct economic contribution of water resources at regional level can still be higher (Saleth and Dinar, 2004). To make increase the gross benefit from water resources human intervention on the natural flow is a common phenomenon. Following the developed world, natural flow alteration is growing rapidly in the developing region (Richter et al., 2006). Flow that meets the sea is often viewed as wastage from an effective management perspective and in several places water is shared between the offstream users leaving the rivers dry proves once again the well known quote from Winston Churchill in 1908 (cited in Postel & Richter, 2003), *"One day, every last drop of water which drains into the whole valley of the Nile … shall be equally and amicably divided among the river people, and the Nile itself … shall perish gloriously and never reach the sea."*

Human interventions on natural flow through dams, reservoirs, diversions or commercial afforestation and land use change have serious and far reaching consequences on the original flow regime of rivers (Hughes, 2003; King & Brown, 2006). These activities change the dynamic movement of water and sediment of a free flowing water body, which result an alteration of habitats for aquatic and riparian species with an ultimate loss of ecosystem goods and services those flowing river provides (Poff et al., 1997; King & Brown, 2006). Richter et al. (2006) cited several literatures on river ecosystem health deterioration due to alteration of natural flow in the rivers.

However, water requirement for the natural environment has rarely been considered and almost ignored in the traditional water management and planning (IWMI, 2005; Gleick, 2003; Gleick, 1996) even though the environment is showing a continuous degradation. The circumstances urged the scientists started thinking on provision of flow for the natural water bodies with the view of defining a development space and imposing a limit up to which flow can be diverted for human use while maintaining the integrity of the ecosystem or an accepted level of degradation (Tharme, 2003). Hence, environmental flow (also termed as minimum flow or instream flow) is the provision of flow in a regulated river towards maintaining a specified level of ecosystem integrity through mimicking the natural flow regime in order to ensure ecosystem goods and services on which human rely in myriad ways.

3. CONSIDERING ENVIRONMENTAL FLOW IN THE FRAMEWORK OF IWRM

IWRM is a process that 'promotes the coordinated development and management of water, land and related resources, in order to maximize the resultant economic and social welfare in an equitable manner without compromising the sustainability of vital ecosystems' (Global Water Partnership 2000). Environmental flow identifies the environment as an individual sector with its own right of using water at basin scale.

In addition to its intrinsic value, flows in river carry significant economic and socio-cultural values. In particular the riparian communities crucially depend on river flow for their livelihood. Environmental flow is therefore an important tool for balancing the relationship between functioning healthy ecosystems and sustainable livelihoods for a large community. Within the framework of IWRM environmental flow helps ensuring water allocation to the environment in development planning, especially involving large infrastructure, and is seen as an integral to sustainable water management. With a better understanding of environmental requirements and the potential trade-offs with other uses, decision-makers are able to make informed decisions on water allocation to competing users. Environmental flow approach provides a roadmap for defining negotiated instream flow requirements, considering the implications for infrastructure development, assessing costs and benefits, nurturing a supportive institutional and policy framework and generating political consensus for changes.

4. WATER NEED – CONFLICT BETWEEN HUMAN AND NATURE

Despite a substantial work has already been done on instream water requirement, rivers are still drying up. Inefficient, over appropriation and misuses of water resources are still in practice within all off-stream water use sectors generate extra pressure on increasing demand for water. As a consequence, water resources sector is clearly showing an era of scarcity (Saleth, 2002) which results severe ecological degradation with reduced flow of ecosystem goods and services including loss of industrial and agricultural production (Postel et al., 1996). Reallocation of water from off-stream use to environmental use has also been taken place in different places (Hollinshead & Lund, 2006); however, conflicts based on the perceived needs of ecosystems versus human for fresh water are increasingly reported in the news and came in several literatures e.g. Johnson & Adams, 1988; Poff et al., 2003; Hollinshead & Lund, 2006. Aquatic ecosystems are under a real threat all the world around in spite of taking some measures. Gleick (1996) noted that in global scale there are more than 700 species of fish which are considered to be threatened with extinction. Smakhtin et al. (2004) might be the first in estimating the global environmental water scarcity; they stated that about 1.4 billion people live in river basins where current water uses are in conflict with environmental water demand. Higher demand for the growing population and developmental needs along with climate change effects are exacerbating the situation by acting synergistically. In particular higher agricultural water demand results environmental water scarcity for developing countries and it becomes a critical concern to meet about a double irrigation water demand by 2050 as forecasted by some estimates (Falkenmark & Galaz, 2007). In second World Water Forum 2000, this issue was raised by the two groups of people, one ‘water for food’ and another ‘water for nature’ – both stressed on significant water requirement for their respective fields. The Global Water Partnership’s Framework for Action concluded that (GWP, 2000): *“On the one hand, the fundamental fear of food shortages encourages ever greater use of water resources for agriculture. On the other, there is a need to divert water from irrigated agriculture to other users and to protect the resources and the ecosystem. Many believe this conflict is one of the most critical problems to be tackled in the early 21st century.”*

5. USE OF ENVIRONMENTAL FLOW IN WRM IN SOUTH ASIA

The South Asian rivers, mostly originated from the Himalayas act as the cultural and economic backbone of this region while support livelihood to millions of people and irrigate millions of hectares of land as well as they own very rich ecosystem. These rivers are, however, also a source of conflict between countries and people in the region because of their transboundary nature. Ganges, Indus, Brahmaputra, Krishna, Godavari, Cauvery, Mahi Tapti are some of the major rivers among lots in this region. Almost all rivers in South Asia are heavily exploited mainly for irrigation and hydropower neglecting the environment. India alone has 4011 large dams (registered at ICOLD [International Commission On Large Dams]) on several of its rivers sharing 9% of world’s total number of dams (Tharme, 2003). Almost all the river basins in South Asia therefore fall in the category of environmental water scarcity defined by Smakhtin et al., 2004. In *Pilot Global Assessment of Environmental Water Requirements and Scarcity*, Smakhtin et al. 2004 provided a preliminary estimate of mean Environmental Water Requirements (EWR) as a percentage of mean annual runoff (MAR) for the major basins and drainage regions of the world. The estimated EWR indicates the basic flow requirement to maintain a river system at “fair” on a conservation status scale of natural-good-fair-poor. The estimated EWR for highly variable monsoon-driven rivers in South Asia are lower (20 to 30 percent of the MAR) which is presented in Table 1. Basins to be managed for higher levels of ecosystem health would require higher EWRs. One critical justification for greater concern for aquatic ecosystem health for this region is the dependence on fisheries as a source of food and local economy. The share of fish protein in total animal protein consumption in Sri Lanka and Bangladesh in 1993 was high (51.5% and 46.7%, respectively), while that in India was relatively low (12.7%). The per capita fish consumption in South Asia in 1993 ranged from 0.2 kg (Bhutan) to 15.4 kg (Sri Lanka) (de Silva and Smith, 2005).

Table 1: EWR for some major rivers in South Asia

River basin	Countries	EWR (% of MAR)
Brahmaputra	Bangladesh, China, India	27
Brahmari	India	24
Cauvery	India	25
Chotanagpui	India	25
Eastern Ghats	India	26
Ganges	Bangladesh, India, Nepal	23

River basin	Countries	EWR (% of MAR)
Godavari	India	24
India East Coast	India	25
Indus	India, Pakistan, Afghanistan	25
Krishna	India	24
Luni	India	21
Mahi Tapti	India	23
Sahyada	India	21
Sri Lanka	Sri Lanka	26

Source: adopted from Smakthin et al., 2004

There are enough evidences of EF adoption into IWRM approach particularly in developed world; however, developing countries are also showing interest in this field (Moore 2004). South Africa is the pioneer from the developing world in adopting EF in water resources management. Tharme and Smakhtin (2003) reported clear evidence of increasing research and practice in EF assessments in south Asian countries of Nepal, Pakistan and Sri Lanka, where as India is in the early stage. This paper reports the interest, adoption and implementation of EF approach in water resources management for different countries in South Asia in detail (Table 2). The South Asian countries of India, Nepal and Pakistan have adopted the approach and, in some cases, have included EF in national legislation and policies. Emerging areas of interest and adoption in EF include Bangladesh and Sri Lanka. However, evidence of implementation is generally limited. Countries where there was no evidence of EF included Afghanistan, Bhutan, and Maldives.

Table 2: Status and use of environmental flow in South Asian countries

Country	EF status and use
Afghanistan	No evidence of using EF is found as a tool for IWRM. One recent study is found on estimating environmental flow for Hari Rod river and subsequent simulation of Salma dam operation to satisfy environmental requirement by Atef, 2009.
Bangladesh	Evidence of interest in adopting the EF approach in Bangladesh is found; however, the approach is not mainstreamed into river basin management. Three studies are found estimating EF requirements for Ganges by Rahman (1998), for Surma by Zobeyeer (2004) and for Surma-Kushiyara, Teesta and Gorai by Bari & Marchand (2006). The *National Water Policy 1999* and *National Water Management Plan 2001* do not explicitly mention EF but strongly mention the requirements of ecosystem to be provided. However, National Water Plan (1986, 1991) argued that if discharge is maintained for navigation, then water for environment and ecosystem would be met.
Bhutan	The review did not find any evidence of EF being used as a tool for IWRM.
India	Environmental flow approach has been adopted in India to some extent. First scientific attempt to assess EF (in fact volume of EF) is by Amarasinghe et al., 2005. Smakhtin & Anputhas, 2006 examine and evaluated the EF demand for Brahmaputra, Cauvery, Ganga, Godavari, Krishna, Mahanadi, Mahi, Narmada, Pennar, Periyar, Tapi, Sobarmati and Subarnarekha. The *National Water Policy 2002* provides for EF as does the *National Environmental Policy 2006*.

Country	EF status and use
	Adoption of EF is occurring at varying scales and levels of governance. Barriers to the implementation of the EF approach include, lack of funding and institutional mechanisms for IWRM, and awareness about the approach.
Maldives	No evidence of EF is found being used.
Nepal	Environmental flow approach is considered in the *Water Resources Strategy Nepal 2002*, the *National Water Plan*, and the *National Wetland Policy 2003*. Smakhtin et al., 2006 estimated EF for East Rapti River using desktop method. However, using EF as a tool is in its infancy in terms of implementation.
Pakistan	Environmental flow approach has been adopted in Pakistan in particular for lower Indus basin (Acreman et al., 2000). The *National Water Policy* (draft) takes note of the necessity of EF for the Lower Indus delta in no ambiguous terms. However, the adoption and implementation of EF appears to be occurring slowly.
Sri Lanka	Progress of Sri Lanka in adoption of environmental flow is observed well with several evidences of interest. Tharme (2003) mentioned different methods under use in Sri Lanka to assess EF. However, national legislation or policies do not reflect yet.

6. CONCLUSION AND WAY FORWARD

This study attempted to review the trend and current status of EF approach in water resources management in South Asian countries. Some progress in assessment and adoption of EF into water resources management is observed in Sri Lanka, Pakistan and India; however, Bangladesh and Nepal are in early stage progressing. It is a contemporary need to initiate EF assessment and adopt EF in national water resources management strategy for all countries. In particular for India, EF assessment projects need to initiate at several sites in cooperation with downstream countries like Bangladesh which is most likely to be affected by the planned National River Linking Project (NRLP) inter-basin water transfer.

Several methods are already developed to assess EF; however, it needs to be tested in a specific context of flow regime, ecology and water resources development at a particular area. Type of EF assessment methods have to be selected based on the type of proposed development, level of impact of the proposed development, ecological importance and sensitivities of the river, the degree to which it is already developed, the socioeconomic importance of the river and its proposed development. Large transboundary river basins present a special challenge in assessment and application of EF. Cross-border collaboration is therefore important, but also results in an increased expenditure of effort in addressing EF in river restoration and other projects (Tharme 2003).

Factors likely to limit the adoption of EF in the region include lack of awareness from the key stakeholders. In addition to just recognition of the concept, awareness should extend to various aspects including awareness of the costs and benefits of implementation, the consequences of not considering EF and the trade-offs between social, economic and environmental objectives within a river basin. It is therefore extremely important to realize the societal cost and benefit from environmental water allocation by all the stakeholders. This concept gets reinforcement when analyzing the reasons behind successful implementation of EF in some countries where importance of flows to local livelihoods is taken with due regards (Moore 2004). Community members and social organizations, as well as other key actors within a river basin, therefore need to be meaningfully engaged in the development of an EF program.

REFERENCES

Acreman M.C., Farquharson F.A.K., McCartney M.P., Sullivan C., Campbell K., Hodgson N., et al., 2000. *Guidelines for artificial flood releases from reservoirs to restore and maintain downstream wetland ecosystems and their dependent livelihoods*. Final report to DFID and World Commission on Dams. Centre for Ecology and Hydrology, Wallingford, United Kingdom.

Amarasinghe, U. A., Sharma, B. R., Aloysius, N., Scott, C., Smakhtin, V. U., De Fraiture, C. et al. 2005. *Spatial variation in water supply and demand across the river basins of India*. Colombo, Sri Lanka: International Water Management Institute. 37 pp. (IWMI Research Report 83).

Atef, S. S., 2009. *Reservoir operation considering environmental flows: a case study in Hari Rod river basin, Afghanistan.* M. Engg. Thesis, Water Engineering and Management, Asian Institute of Technology, Thailand.

Bari, F. M. & Marchand, M., 2006. *Introducing Environmental Flow Assessment In Bangladesh: Multidisciplinary Collaborative Research.* BUET-DUT Linkage Project, Phase III, Capacity Building in the Field of Water Resources Engineering and Management in Bangladesh. Research Project No. 2 – Management of Rivers for Instream requirement and ecological protection.

Bunn, S. E. & Arthington, A. H., 2002. Basic Principles and Ecological Consequences of Altered Flow Regimes for Aquatic Biodiversity. *Environmental Management.* 30 (4), 492–507

De Silva, S. S. & Smith, S. F., 2005. *A review of stock enhancement practices in the inland water fisheries of Asia.* Asia-Pacific Fishery Commission. RAP PUBLICATION 2005/12. Food and Agriculture Organization of The United Nations Regional Office for Asia and The Pacific, Bangkok, Thailand.

Falkenmark, M. & Galaz, V., 2007. *Agriculture, Water and Ecosystems.* Swedish Water House Policy Brief Nr. 6.

FAO, 1996. *Food production: the critical role of water*. Technical background document for the world food summit: 7, Rome: FAO.

Gleick P. H., 1996. Basic water requirements for human activities: Meeting Basic Demand. *Water International.*, 21 (2), 83 – 92.

Gleick, P. H., 1998. *World's water 1998–1999: The biennial report on freshwater resources.* Island Press, Washington, DC, 319 pp.

Gleick, P. H., 2003. Water Use. *Annual Reviews on Environmental Resources*. 28, 275-314.

Global Water Partnership (GWP), 2000. *Framework For Action: Towards a Water Secure World.* Global Water Partnership, Stockholm.

Hollinshead, S. P. & Lund, J. R., 2006. Optimization of environmental water purchases with uncertainty. *Water Resources Research.,* 42 (8), art no. W08403.

Hughes, D., 2003. Environmental flow requirements in water resource planning and operation. *Water Resources Systems—Hydrological risk, management and development.* (Proceedings of symposium HS02b held during IUGG2003 at Sapporo, July 2003). IAHS Publ. no. 281, 2003.

IWMI, 2005. *Environmental flows: Planning for environmental water allocation.* Water policy briefing, Issue 15. International Water Management Institute. October 2005.

Johnson, N. S. & Adams, R. M., 1988. Benefits of Increased Streamflow: The Case of the John Day River Steelhead Fishery. *Water Resources Research.*, 24 (11), 1839-1846.

King, J., & Brown, C., 2006. Environmental Flows: Striking the Balance between Development and Resource Protection. *Ecology and Society.* 11 (2): 26.

Millennium Ecosystems Assessment, 2005. *Ecosystem and Human Well-being Synthesis*, Island Press, Washington DC, USA.

Moore, M., 2004. *Perceptions and interpretations of Environmental Flows and implications for future water management – A Survey Study.* Master Thesis, Department of Water and Environment Studies, Linkoping University Sweden.

Poff, N. L., Allan, J. D., Bain, M. B., Karr, J. R., Prestegaard, K. L., Richter, B. D., et al., 1997. The natural flow regime. *BioScience.* 47, 769–784.

Poff, N. L., Allan, J. D., Palmer, M. A., Hart, D. D., Richter, B. D., Arthington, A. H., et al., 2003. River flows and water wars: Emerging science for environmental decision making. *Frontiers in Ecology and the Environment.* 1 (6), 298-306.

Postel, S. L., & Richter B. D., 2003. *Rivers for Life: Managing Water for People and Nature.* Island press, Washington DC.

Postel, S. L., Daily, G. C. & Ehrlich, P. R., 1996. Human appropriation of renewable fresh water. *Science*. 271, 785 – 788.

Rahman, M., 1998. *A hydrologic determination of instream flow requirement of the Ganges River.* M. Engineering Thesis, Department of Water Resources Engineering, Bangladesh University of Engineering and Technology, Dhaka.

Richter, B. D., Warner, A. T., Meyer, J. L. & Lutz, K., 2006. A collaborative and adaptive process for developing environmental flow recommendations. *River Research and Application.* 22, 297-318.

Saleth R. M. & Dinar A., 2004. *The Institutional Economics of Water A Cross-Country Analysis of Institutions and Performance.* A co-publication with the World Bank. Edward Elgar, UK & USA. pp. 398.

Saleth R. M., 2002. (Edited) *Water resources and economic Development.* Edward Elgar publishing limited, UK & USA. pp527.

Smakhtin, V. & Anputhas, M. 2006. *An assessment of environmental flow requirements of Indian river basins*. Colombo, Sri Lanka: International Water Management Institute. 42p. (IWMI Research Report 107).

Smakhtin, V., Shilpakar, R. L. & Hughes, D. A. 2006. Hydrology-based assessment of environmental flows: an example from Nepal. *Hydrological Sciences Journal*. 51 (2), 207 – 222.

Smakhtin, V., Revenga C. & Doll, P., 2004. A pilot global assessment of environmental water requirements and scarcity. *Water international.* 29 (3), 307 – 317.

Tharme, R. and Smakhtin, V., 2003. Environmental Flow Assessment in Asia: Capitalizing on Existing Momentum. *Proceedings of the First Southeast Asia Water Forum*, 17-21 November 2003, Chiang Mai, Thailand.

Tharme, R. E., 2003. A global perspective on environmental flow assessment: Emerging trends in the development and application of Environmental flow methodologies for rivers. *River Research and Applications.* 19, 397–441.

Yang, H. P. Reichert, K. Abbaspour and A.J.B. Zehnder, 2003. A water resources threshold and its implications for food security. *Environ. Sci. Technol.* 37, 3048–3054.

Zobeyer, A. T. M. H., 2004. *Application of Physical Habitat Simulation Approach for instream flow requirement in the Surma river*, M. Sc. Engineering Thesis, Department of Water Resources Engineering, Bangladesh University of Engineering and Technology, Dhaka.

EXPERIMENTAL STUDY ON SHAKING TABLE TEST OF A CONCRETE GRAVITY DAM

SUMETEE CHAROENWONGMIT,
EKACHAI YOOPRASERTCHAI, BUPAVECH PHANSRI,
PENNUNG WARNITCHAI and KYUNG-HO PARK
School of Engineering and Technology
Asian Institute of Technology, Thailand
sumethee_joe@hotmail.com

ABSTRACT

This study deals with the shaking table testing conducted on small-scale concrete gravity dam models. Two models of the prototype dam with 118 m high and 94 m width at 1:100 scale are tested on a 1.2 m x 1.0 m shaking table. The bentonite-concrete material is developed to match the material similitude requirements between the prototype and the model. The scaled models typically employ two types of excitation: resonance and ambient testing. The resonance frequency of two models showed obviously different mode due to the effect of material properties. The propagation of the cracks was observed in the neck area until the failure at the base acceleration of about 0.55g-0.60g.

1. INTRODUCTION

Many concrete gravity dams have been designed with static and seismic loading, to make sure that this structure will be able to resist a maximum earthquake without the full and uncontrolled cracks. However, some concrete gravity dams have been damaged due to the strong ground motion, for example Koyna Dam, India, 1967; Hsingfengkiang Dam, China, 1962; Sefi-Rud Dam, Iran, 1990 and Pacoima Dam, California, 1971 and 1994.

For concrete gravity dams designed according to current design criteria, the static and earthquake compressive stresses are generally much less than the compressive strength of the concrete. However, linear dynamic analyses of gravity dams show that the earthquake ground motion can produce tensile stresses that exceed the tensile strength of the mass concrete. Therefore, the nonlinear tensile cracking must be considered in the seismic response of concrete gravity dams.

In order to predict the earthquake response of gravity dams, the experimental shaking table tests have been conducted on small-scale models (Bakhtin & Dumenko 1979, Niwa & Clough 1980, Donlon 1989, Hall 1989, Donlon & Hall 1991, Lin et al. 1993, Zadnik & Paskalov 1992, Zadnik 1994, Mir & Taylor 1995, 1996, Harris et al. 2000, Tinawi et al. 2000). These studies considered special materials and length scale for investigation of the nonlinear aspects of dam response (cracking, joint opening, sliding behavior under high compression, and cavitation in the water).

This study deals with the shaking table testing of a concrete gravity dam, which is planed for the construction in the northern Thailand or Myanmar. Two small-scale models were designed to maintain similitude relationships and be constructed and tested on the shaking table.

2. MODEL DEVELOPMENT

2.1 Similitude requirements

To simulate the nonlinear behavior of a small scale model corresponding of its prototype or full scale, it is necessary follow the laws of similitude requirements. These laws are determined by dimensional analysis according to Buckingham's Pi thorem. Using the scale factor definitions, $F_p / F_m = S_F$, $t_p / t_m = S_t$, $m_p / m_m = S_m$ and $l_p / l_m = S_l$, the model and prototype relation give the formulas:

$$S_F = S_l S_m / S_t^2 \quad (1)$$

$$S_r = S_l^{\,2} S_m / S_t^2 \quad (2)$$

where F, t, m and l are force, time, mass and length, respectively. Subscript p and m represent the prototype and model. A summary of the similitude requirements established for this investigation is presented in Table 1.

Table 1: Scale factors for nonlinear seismic response analysis

Physical Quantity	Notation	Dimensions	Scale Factor
Acceleration due to gravity	g	LT^{-2}	1
Linear dimension	l	L	S_l
Modulus of elasticity	E	FL^{-2}	S_r
Stress	σ	FL^{-2}	S_r
Strain	ε	-	1
Poisson's ratio	υ	-	1
Ultimate strength	σ_{cu}, σ_{tu}	FL^{-2}	S_r
Time	T	T	$\sqrt{S_l}$

Frequency	f	T^{-1}	$\frac{1}{\sqrt{S_l}}$

In this study, the length scale is set at 1/100 by considering a model size that could be constructed and tested on shaking table. According to similitude requirement, the properties of prototype and model are shown in Table 2.

Table 2: Similitude requirements and model material properties

Physical Property	Unit	Prototype	Scale Factor	Model
Density	kg/m^3	2400	1	2400
Ultimate strength				
compressive, f'_c	MPa	10-15	100	0.1-0.15
tensile, f_t	MPa	2.5	100	0.025
Young's modulus, E	MPa	18200	100	182
Ultimate strain				
compressive, ε_c	-	0.003	1	0.003
tensile, ε_t	-	0.00012	1	0.00012

2.2 Development of material

One of the important works is to develop a material having appropriate strength and elastic modulus. The unit weight is not considered in the material development. This study used bentonite as a component to reduce strength and elastic modulus.

2.2.1 Concrete mix design and material properties

In order to find the suitable mixture proportions, the trial mix was separated into two phases. In the first phase, five mixtures were proportioned with zero (control mixture), 10, 15, 20, and 25 % bentonite by mass of cement plus bentonite (Table 3). The trial mixes were made in the laboratory. Standard 10×20 cm cylinders were made from each batch to identify required properties. The modulus of elasticity and Poisson's ratio are determined by attaching two strain gages (vertical and horizontal direction) at 7 and 28 day's age.

Based on the test results of the first phase, the second concrete mixture proportions were prepared to develop the materials such that their properties are matched to similitude requirements by varying other components, for example, content of fine or coarse aggregate. The mix and properties used for the model are shown in Table 4.

Table 3: Bentonite-concrete mixture proportions

	Mix1 (kg/m^3) (Control)	**Mix2 (kg/m^3)**	**Mix3 (kg/m^3)**	**Mix4 (kg/m^3)**	**Mix5 (kg/m^3)**
Water	258	309	314	332	332
Cement	178	160	151	142	95
Bentonite	0	18	27	36	24
Bentonite (%)	0%	10%	15%	20%	25%
Fine Aggregate	866.00	798.00	797.00	773.00	810.00
Coarse Aggregate	873.00	806.00	804.00	780.00	820.00
w/c	1.45	1.93	2.08	2.34	3.49
w/b	1.45	1.74	1.76	1.87	2.79
Weight (kg)	2175	2091	2093	2063	2081

Table 4: Model concrete mix components

Component	**Actual model mix**	
	Model mix, kg/m^3	**Volume in mix per 0.065 m^3 batch**
Water	404.46	26
Cement	81.23	5.28
Bentonite	36.46	2.37
Fine Aggregate	1056.92	68.70
Coarse Aggregate (No.4-3/8"): *wet*	1060.00	68.90
w/c	4.98	
w/b	3.44	
Weight(kg)	2639.08	171.54

In this study, two dam models were constructed. Three batches were mixed in each model and nine standard 10cm x 20cm cylinders were collected from each batch to test the physical properties. Compressive strength was given from compression test at 28 days after casting. Ultimate tensile strength of specimens was obtained using two different methods: direct tensile method and splitting tensile method. Also, the physical properties of the mix are shown in Table 5.

Table 5: Properties of model materials

Physical property	Unit	Target value	Actual model mix at 28 days	
			Model 1	**Model 2**
Ultimate compressive strength, f'_c	MPa	0.1-0.15	0.317	0.399
Ultimate tensile strength, f_t	MPa	0.025		
- Direct tensile			0.029	0.054
- Splitting tensile			0.0135	0.0103
Young's modulus, E	MPa	182		
- Ec : Compressive test			1,797.65	905.82
- Et : Tensile test			11.56	14.16
Mass density, ρ	kg/m^3	2,400	1,907.44	1,936.87
Ultimate compressive strain, ε_c	-	0.003	0.00139	0.00262
Ultimate tensile strain, ε_t	-	0.00012	0.00495	0.00429
Poisson ratio	-	-	0.2026	0.1930

3. EXPERIMENT SET-UP AND PROCEDURE

3.1 Model construction and instrumentation

For the experiment the model was constructed on the floor, mounted on a shake table, and then tested at the time of 35 days for model 1 and 28 days for model 2. The 1/100 scale chosen resulted in a 1.18 m tall model weighing 263 kg. Figure 1 shows the dam model mounted on the shake table. Instrumentation was designed to measure displacements and accelerations on the model and from the input actuator. The lateral bracing with two plastic rollers were conducted to prevent transverse vibrating. Also, the general instrumentation locations and detailed is shown in Figure 1.

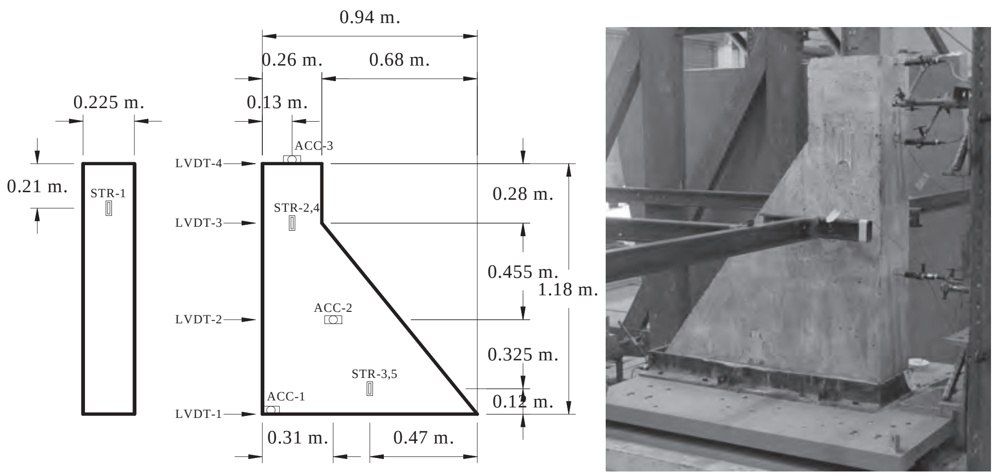

Figure 1: Configuration of a small-scale concrete gravity dam

3.2 Input motion

In order to determine resonant frequencies of the modal, model response was recorded at even frequencies from 2 to 30 Hz with a constant input acceleration of 0.05g. Figure 2 shows the acceleration of the top of the model along the excitation axis at even frequencies from 10 to 30 Hz. The normalized displacement at the top of model at even frequencies from 2 to 30 Hz is shown in Figure 3.

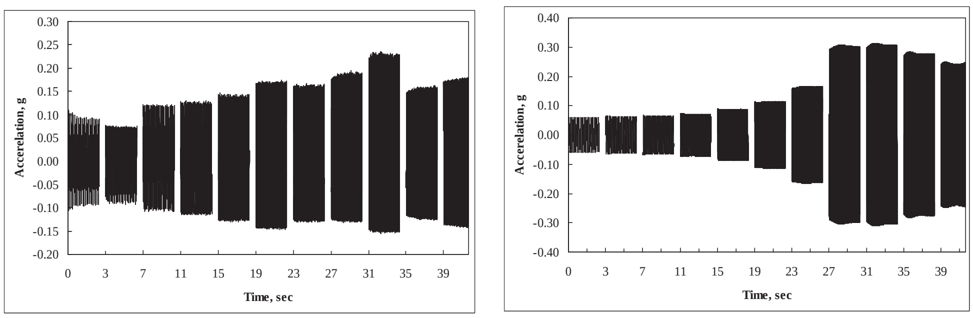

(a) Model 1 (b) Model 2

Figure 2: Resonance testing: horizontal acceleration at the top of the model

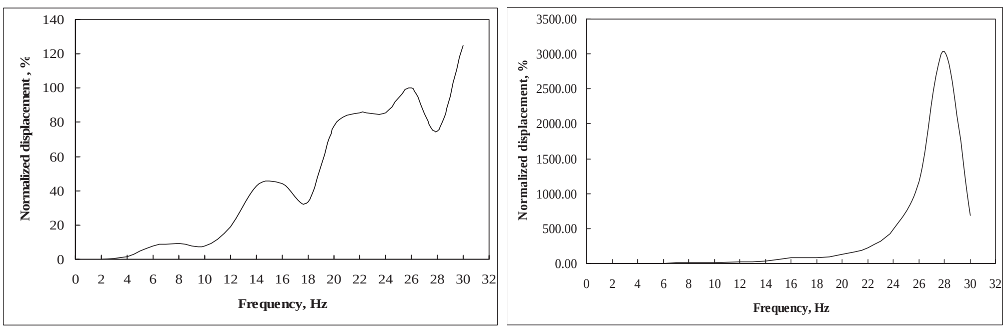

(a) Model 1 (b) Model 2

Figure 3: Normalized displacement at the top of model at frequencies from 2 to 30 Hz

In the model 1, the first excitation frequency which showed an amplification of acceleration above the input was 14 Hz. A sinusoidal motion of 14 Hz was chosen as the excitation frequency for all subsequent tests. For the model 2, acceleration with the frequency 24-28 Hz at base of model showed the excitation of the model. Therefore, the sinusoidal motion of 28 Hz was chosen as the excitation frequency for all subsequent tests. In summary, the test program consisted of two phases: (1) the determination of the lowest resonant frequency by shaking the model at 0.05g at even frequencies from 2 to 30 Hz, and (2) the failure of the model by shaking it at the lowest resonant frequency, increasing the acceleration amplitude from 0.05g to failure in 0.0125g steps holding at each step for 5 seconds.

4. TEST RESULTS

For ambient testing, the maximum amplitude accelerations at the base are 0.55g-0.60g and 0.60g-0.65g for the first and second models, respectively. Crack was initiated at the changing slope point and developed around the neck of model below the crest 30-40 cm. Figure 4 shows crack patterns of two models.

(a) Model 1 (b) Model 2

Figure 4: Crack pattern at the top of dam model

5. CONCLUSION

(1) A new concrete mix design was proposed. The mix used benotite to reduce strength properties of the concrete. From the results of mix properties, it is obvious that not all parameters meet the similitude requirement simultaneously.

(2) An experimental study was conducted on the shaking table. The propagation of the cracks was observed in the neck area until the failure at the base acceleration of about 0.55g-0.60g.

REFERENCES

Bakhtin BM, Dumenko VI, 1979. Seismic stability of a concrete gravity dam having a lightweight profile. *Hydrotechnical Construction*. 5, 445-450.

Donlon WP, 1989. Experimental investigation of the nonlinear seismic response of concrete gravity dams. Earthquake Engineering Research Laboratory. *Report No. 89-01*. California Institute of Technology, Pasadena.

Donlon WP, Hall JF, 1991. Shake table study of concrete gravity dams: Shake table tests and numerical analyses. *Earthquake Engineering and Structural Dynamics*. 20, 769-786.

Hall JF, 1989. The dynamic and earthquake behaviour of concrete dams. *Soil Dynamics and Earthquake Engineering.* 7, 58-121.

Harris DW, Snorteland N, Dolen T, Travers F, 2000. Shaking table 2-D models of a concrete gravity dam. *Earthquake Engineering and Structural Dynamics*. 29, 769-787.

Lin G, Zhou J, Fan C, 1993. Dynamic model rupture test and safety evaluation of concrete gravity dams. *Dam Engineering*. IV(3), 769-786.

Mir RA, Taylor CA, 1995. An experimental investigation into earthquake-induced failure of medium to low height concrete gravity dam. *Earthquake Engineering and Structural Dynamics*. 24, 373-393.

Mir RA, Taylor CA, 1996. An investigation into the base sliding response of rigid concrete gravity dams to dynamic loading. *Earthquake Engineering and Structural Dynamics*. 25, 79-98.

Niwa A, Clough RW, 1980. Shaking table research on concrete dam models. Earthquake Engineering Research Center. *Report No. UCB/EERC-80-05*. College of Engineering, University of California, Berkeley, California.

Tinawi R, Leger P, Leclerc M, Cipolla G, 2000. Seismic safety of gravity dams: from shake table experiments to numerical analyses. *Journal of Structural Engineering*. 126(4), 518-529.

Zadnik B, Paskalov T, 1992. Dam stability and time-dependent coefficient of friction. *Proceedings of the 10th World Conference on Earthquake Engineering*, Balkema, Rotterdam, The Netherlands. 4633-4638.

Zadnik B, 1994. Motions of rigid unsymmetric bodies and coefficient of friction by earthquake excitations. *Structural Engineering and Mechanics*. 2(3), 257-267.

TUNNELING-INDUCED GROUND MOVEMENT IN TWIN-TUNNELS OF BANGKOK MRT SUBWAY PROJECT

TRAN VIET DUNG and KYUNG-HO PARK
School of Engineering and Technology, Asia Institute of Technology
vietdungtran82@gmail.com

ABSTRACT

This study deals with tunneling-induced ground movement in twin-tunnel of Bangkok MRT Blue Line subway project. First the measured longitudinal surface settlements are evaluated. Second the simplified 3D numerical simulations, based on 2 main parameters (the partial stress release factor α_{dec} and the length of unlined zone L_{dec}), are examined for drained and undrained cases. The results of the numerical simulation may be used for the prediction of tunneling-induced ground movements in the planned South Blue Line Extension subway project.

1. INTRODUCTION

Generally three methods (analytical, empirical and numerical methods) have been used for the prediction or estimation of tunneling-induced ground movements. Among those methods, numerical simulation of EPB (Earth Pressure Balance) tunneling requires complex aspects, such as the soil excavation, the overcut or annular space, the application of the face pressure, the installation of the definitive supports, the grouting of the annular space, non-linear behavior of the soil, and the soil-structure interaction. In particular, in order to take into account the boundary condition around the opening during the tunnel construction process, two approaches have been used (Cheng et al., 2008): the force controlled approach and the displacement controlled approach (Sagaseta, 1987; Longanathan and Poulos, 1998; Park, 2004, 2005).

The force controlled approach simulates tunneling by removing nodal forces corresponding to the initial soil stress state. However, the method predicts wider surface settlement trough accompanied with higher far field settlement than field or centrifuge test (Simpson et al., 1979; Dasari, 1996; Leca, 1996; Stallebrass et al., 1996). Recently Mroueh and Shahrour (2008) proposed a simplified modeling technique by applying the convergence-confinement concept to 3D numerical simulation. In this way, the out-of-balance forces, developed by tunnel excavation, are not entirely released but partially released at each construction stage.

The measured longitudinal surface settlements in the single tunnel of the MRT Blue Line subway project were evaluated and the corresponding 3D numerical simulations were conducted (Tran, 2008). This study deals with the evaluation of the measured longitudinal surface settlement and the simplified 3D numerical simulation for twin-tunnel.

2. EVALUATION OF THE MEASURED SURFACE SETTLEMENT DATA

In Zone 23 from Thiam Ruamit to Pracharar Bumphen, there were total 46 ground surface makers, installed along the centreline of the tunnel alignment. The primary object of the measurements with settlement makers was to measure the maximum surface settlements above the centreline. In addition, the reading was taken over time covering a period before shield approaching and after shield passing. The location of the ground settlement maker is shown in Figure 1.

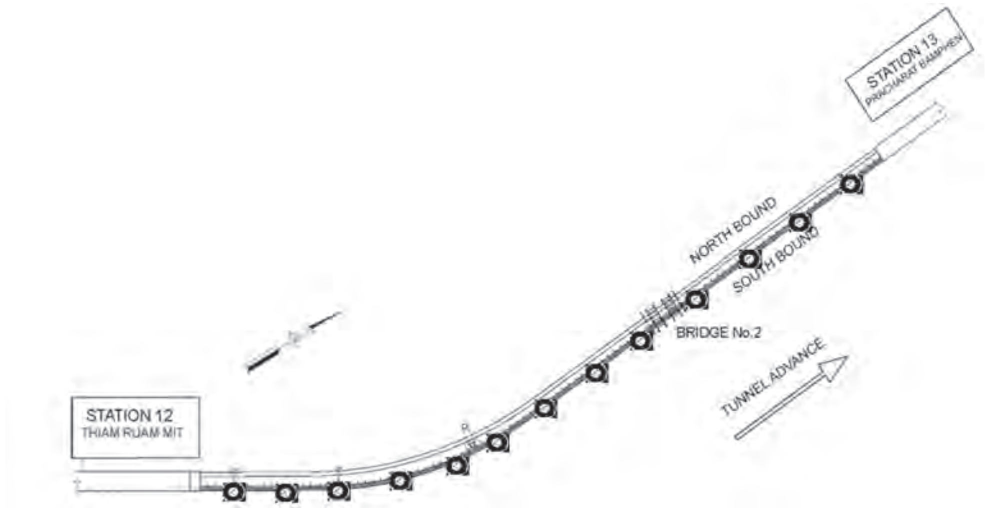

Figure 1: Location of ground settlement makers

The surface settlement data of total 46 points are collected. Among those, the data of only 23 points are selected for the further study to avoid the possible measurement error from other points.

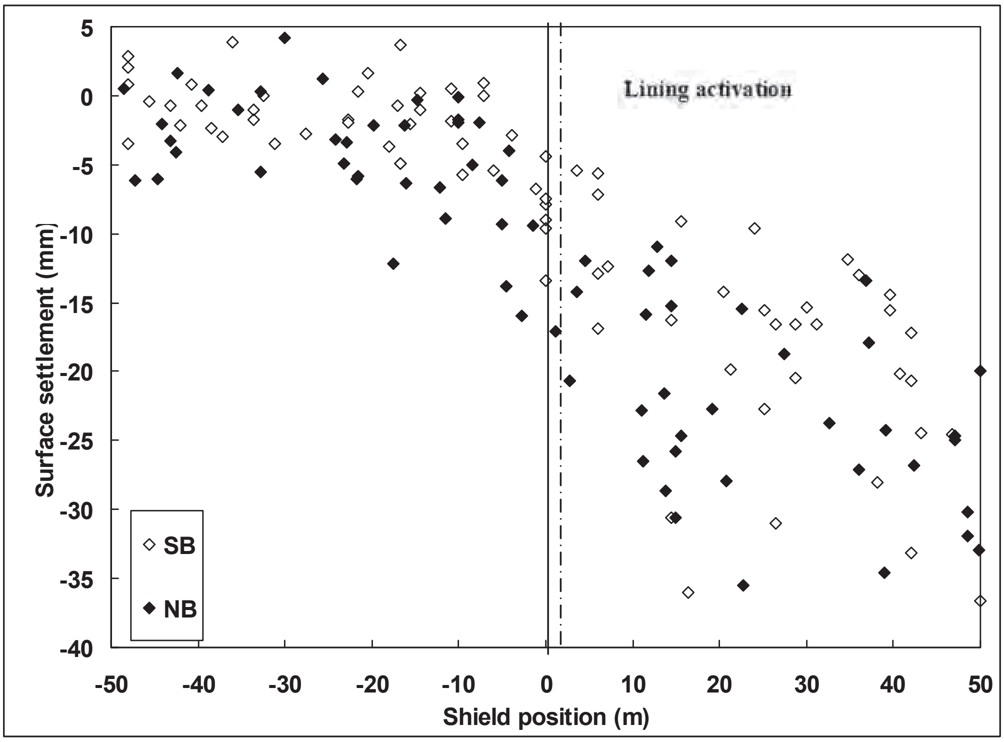

Figure 2: Measured surface settlement

Figure 2 shows the summary of the surface settlement measurements of the Southbound (SB, the first excavated tunnel) and the Northbound tunnel (NB, the second excavated one). In both tunnels, the longitudinal surface settlement mostly occurred between 40 m (≈ 7D) to – 40 m (≈ 7D) and can be divided into three zones: Zone 1, about 30 m distance, the ground begins to deform but the shield not reached; Zone 2, about 15 m distance, starts from the distance in front of the shied face and develops significantly during the shield passing; Zone 3 begins after the performance of the tail void grouting. For the Southbound tunnel, the maximum surface settlement varied from 14 mm to 33 mm and the surface settlement at the tunnel face (w_a), w_a = 4 ~ 16 mm, the surface settlement induced in the unlined zone (w_b), w_b= 2 ~ 6 mm and the surface settlement due to complete released stress of the confinement (w_c), w_c = 8 ~ 22 mm. And for the Northbound tunnel, the maximum surface settlement varied from 14 to 36 mm. The value of w_a = 6 ~ 19 mm, w_b = 2 ~ 7 mm, and w_c = 5 ~ 18 mm. Due to the excavation of the Southbound tunnel (the first tunnel) the initial settlement of about 4 ~ 6 mm was recorded.

3. 3D NUMERICAL SIMULATION

Numerical simulation has been conducted using the commercial finite different code FLAC^{3D}. Figure 3 and 4 show the ground condition and the modelling mesh. The constitute law used for the soil element is the elasto-plastic associated Mohr-Coulomb model. The left right boundaries are hinged to prevent the movement in horizontal direction but are free to allow vertical direction. The width of the left through the right boundaries is set to prevent boundaries effect on the perimeter of the tunnel. At the bottom, the boundary is fixed against vertical movement.

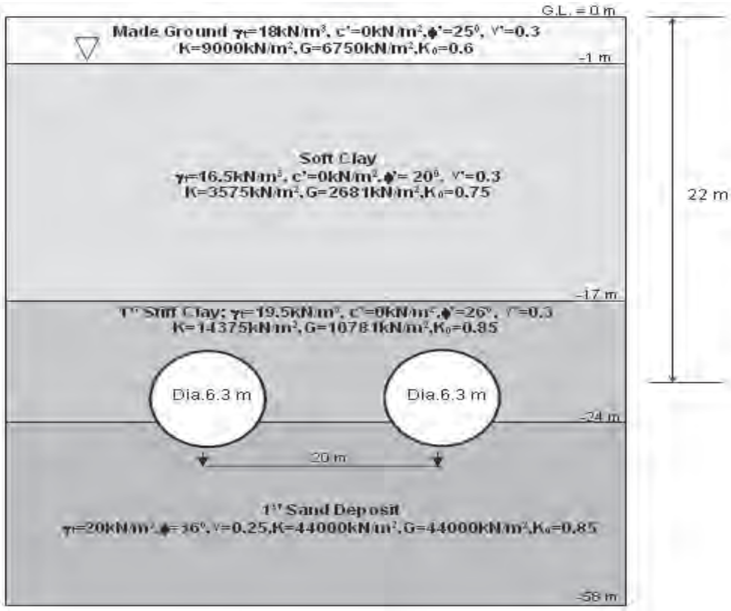

(a) Drained case

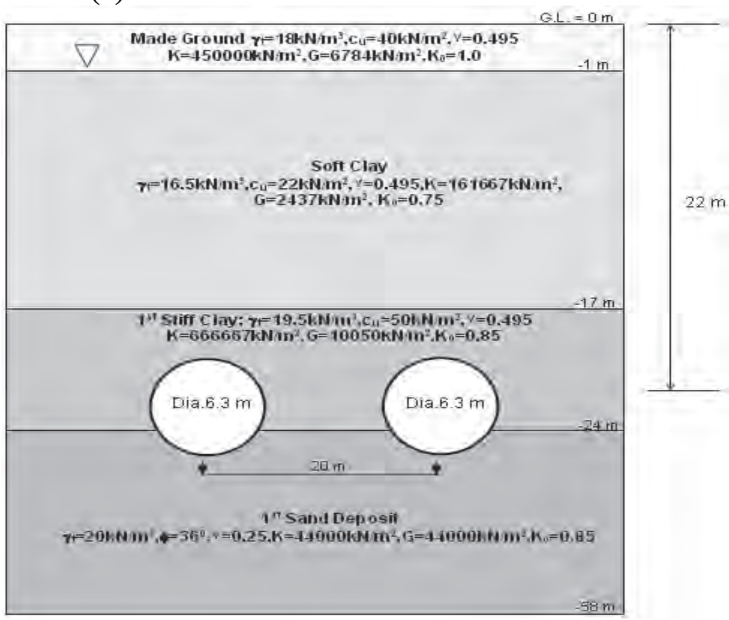

(b) Undrained case

Figure 3: Typical subsoil conditions in Zone 23

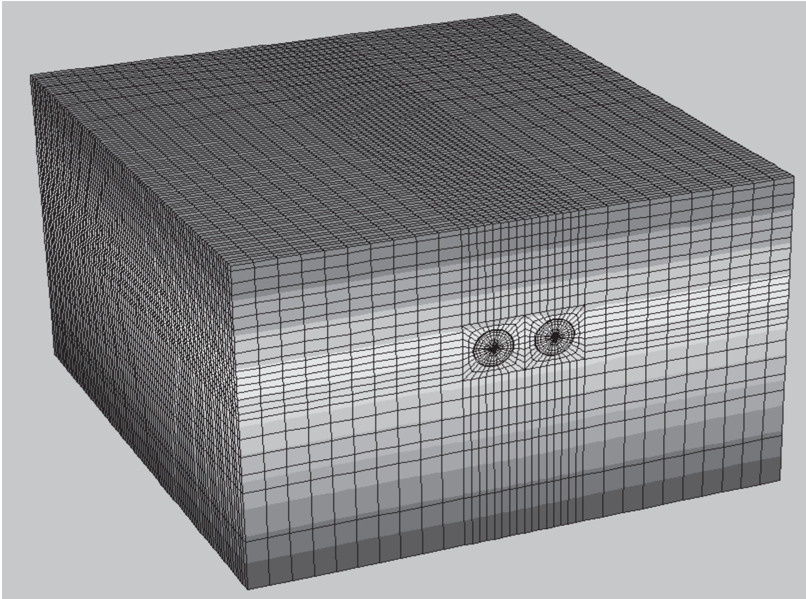

Figure 4: Modelling mesh

Excavation and the shield advance are simulated through the step by step procedure as follows:

In the first step of excavation, (a) remove the ring of soil element equal to 7 m ahead of the shield (6m for length of the shield and the length of the unlined zone and 1 m for the supported zone where the lining will be installed), (b) release stress around the tunnel, (c) grout the removed area, (d) install lining 1 m at the end of the excavated and measure the displacement at the tunnel boundary and at the surface, (e) back fill material and apply face pressure to prepare for the next excavation.

In the step of tunnel face advance, (a) remove the ring of soil element ahead of the tunnel face, (b) release the stress using α_{dec} and L_{dec}, (c) grout the removed area, (d) activate the lining element in removed are with the length of L_{lin} and take the measurement for the element displacement, (e) apply the pressure at the tunnel face. Then repeat from (a) to (e).

4. RESULTS

4.1 Drained case

Figure 5 shows the numerical results of the longitudinal surface settlement using α_{dec} = 0.4 and 0.6, together with the measured one. L_{dec} is fixed to 1D (D: diameter of the EPB). Similar to the measured surface settlement, a portion of ground settlement occurred due to the excavation of the first tunnel. The value of α_{dec} highly affects to the simulated results (value of w_a, w_b, w_c or the maximum surface settlement value). The maximum surface settlements vary from 27 to 37 mm.

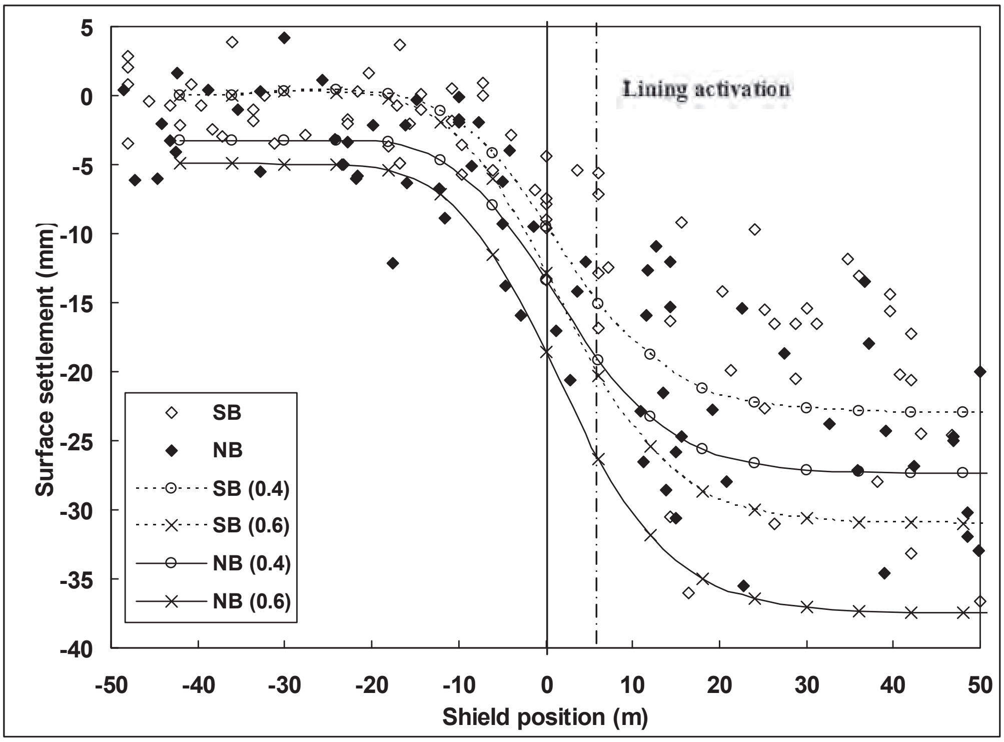

Figure 5: Simulated results (Drained case)

4.2 Undrained case

Figure 6 shows the numerical results for undrained case. In undrained case, the value of α_{dec} = 0.4, 0.5, 0.6 and L_{dec} is fixed to 1D. Similar to the drained case, the ground settlement mostly occurred between -4D ~ 4D and a small portion settlement occurred at the beginning of the excavation due to the excavation of the first tunnel. The value of α_{dec} is also the key parameter and mainly affect to the simulated results. The maximum surface settlements vary from 27 to 40 mm.

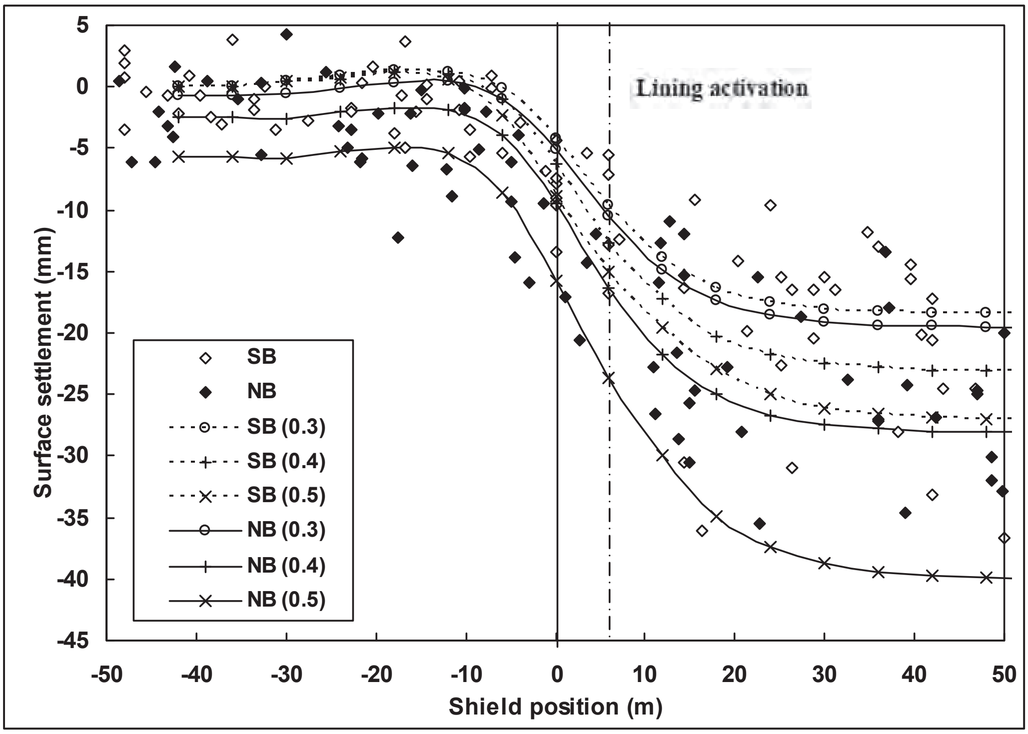

Figure 6: Simulated results (Undrained case)

5 CONCLUSION

In this study, measured longitudinal surface settlements were evaluated and the corresponding 3D numerical simulations were conducted for twin-tunnel. The following conclusions can be drawn:

(1) The maximum surface settlements varied from 14 mm to 36 mm: w_a = 6 ~ 9 mm, w_b= 2 ~ 7 mm and w_c = 5 ~ 18 mm. The excavation of the first tunnel causes 4 ~ 6 mm in the settlement of the second one.

(2) The longitudinal surface settlement mostly occurred between 40 m (≈ 7D) to – 40 m (≈ 7D) and can be divided into three zones.

(3) The parameter α_{dec} highly affects the maximum surface settlement. As α_{dec} increases, the maximum surface settlement increases. The measured surface settlements can be ranged within α_{dec} = 0.4 ~ 0.6 in drained case and 0.3 ~ 0.5 in undrained case.

REFERENCES

Cheng, C.Y., Dasari, G.R., Chow, Y.K., Lueng, C.F., 2008. Finite element analysis of tunnel-soil-pile interaction using displacement controlled model. *Tunnelling and Underground Space Technology*, 22, 450-466.

Leca, E., 1996. Modelling and prediction for bored tunnels. *Proceedings of International Symposium on Geotechnical Aspects of Underground Construction in Soft Ground*, Balkema, London, 27–42.

Longanathan, N., Poulos, H.G., 1998. Analitical prediction for tunneling induced ground movement in clay. *Journal of Geotechnical and Geoenviromental Engineering*, 124(9), 846-856.

Mroueh, H., Shahrour, I., 2008. A simplified 3D model for tunnel construction using tunnel boring machine. *Tunnelling and Underground Space Technology*, 23, 38-45.

Park, K.H., 2005. Analytical solution for tunnelling-induced ground movement in clays. *Tunnelling and Underground Space Technology*, 20(3), 249-261.

Park, K.H., 2004. Elastic solution for tunnelling-induced ground movement in clays. *International Journal of Geomechanics ASCE*, 4(4), 310-318.

Sagaseta, C., 1987. Analytical of undrained soil deformations due to ground loss. *Geotechnique*, 37(3), 301-320.

Simpson, N.J., O'Riordon, Croft, D.D., 1979. A computer model for the analysis of ground movements in London clay. *Geotechnique*, 29(2), 149–175.

Stallebrass, S.E., Grant, R.J., Taylor, R.N., 1996. A finite element study of ground movements measured in centrifuge model tests of tunnels. *Proceedings of International Symposium on Geotechnical Aspects of Underground Construction in Soft Ground*, Balkema, London, 595–600.

Tran, V.D. 2008. A simplified 3D numerical simulation for subway tunnel construction in Bangkok. *AIT Master Thesis*.

Student Report

REPORT FROM STUDENT PARTICIPANTS ON 2nd JOINT STUDENT SEMINAR ON CIVIL INFRASTRUCTURES

Venue: Asian Institute of Technology, Pathumthani, Thailand
Date: July 6-7, 2009

AIT Center

BRT terminal

Participants (from left to right, above picture): Shumon Mori; Dr. Muyeyoshi Numada; Mari Sato; German Alberto Pardo Rios; Hoang Thuy Linh; Tae Soo Tang; Vu Viet Hung; Dr. Shinji Tanaka

PRESENTATION SESSION

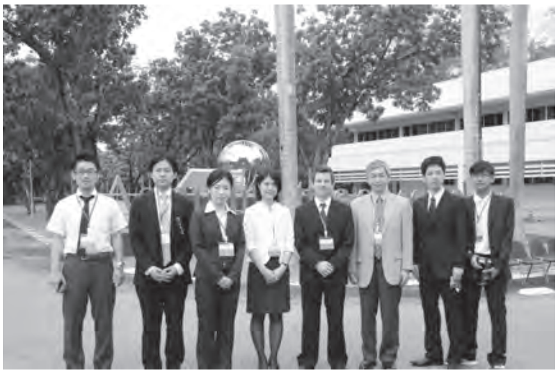

Japan team at AIT

On 06 July, 2009, 2nd Joint Student Seminar on Civil Infrastructures was held at Asian Institute of Technology (AIT) by International Center for Urban Safety Engineering (ICUS) with great success. Although prevalence of new influenza, 34 peoples were gathered from Thailand, Korea and Japan at AIT and shared fruitful time together. The Japan team consisted of 6 members from various nationalities: 1 Colombian, 1 Korean, 2 Vietnamese and 2 Japanese. Although this was first time to meet each other, we shared all the time together in good friendship.

Joint Student Session

In the presentation session 5 professors gave us lectures and then 18 students presented their researches with various fields such as Nano technology, Transportation Engineering, Geotechnical Engineering, Concrete Structure Engineering, Disaster Mitigation Engineering and Applied Remote Sensing. Each of us presented their research theme successfully with great efforts.

The party held by ICUS

After presentation session all members were invited to the party held by ICUS. At the opening of party 3 students from each country were awarded as best presenter voted by all students. The party was so lively and gave us good chance for cultural exchange and friendship.

In this conference we had very precious experiences to study various interesting topics related on civil infrastructure field. Furthermore, toward this conference, we had good opportunities to practice presentation skill in English. Although the session was short, we spent so valuable and unforgettable day.

On The Visit Bangkok's Public Transportation Facilities

At the seminar, Dr. Thirayoot Limanond gave us a very fruitful introduction about the traffic situation and public transportation system in Bangkok. And on the next day, we had a great opportunity to experience this system and visit its facilities. On one day, we had ridden on most of public transportation modes in Bangkok including MRT (subway), BTS (skytrain), taxi, bus, tuktuk and boat. It was very interesting to all of us.

Picture1: Tuk tuk

Picture 2: Taxi

Bus and Taxi are quite popularly used with reasonable price but they face congestion at the peak hour. Tuk tuk - a small size taxi, which made us very impressed and excited for running fast and threading movement, is also very popular. But, frankly speaking, it was quite scary!

Picture3: Boat and Boat Pier in Chao Phraya River

The Chao Phraya River and channel system in the city are also utilized as a very convenient way of transport. The boat which took us from Asokepetchaburi boat pier to Pratunam boat pier was very crowded not only by the tourists but also by local people.

Transportation infrastructure in Bangkok is quite well developed but congestion still occurs everyday. Two BTS routes and one MRT route has been constructed and brought in use. And due to budget constraints, Bangkok is promoting Bus Rapid Transit (BRT) system in near future plan.

To keep our good memories of this trip, we record the route we took by using Bangkok map as following.

List of locations:
A: Chatuchak Park MRT station
B: Phetchaburi MRT station; and Asokepetchaburi boat pier
C: Pratunam boat pier
D: Siam BTS station
E: Non changsri BTS station
F: Sathon Express Boat Pier
G: Tha Chang Wang Luang Express Boat Pier

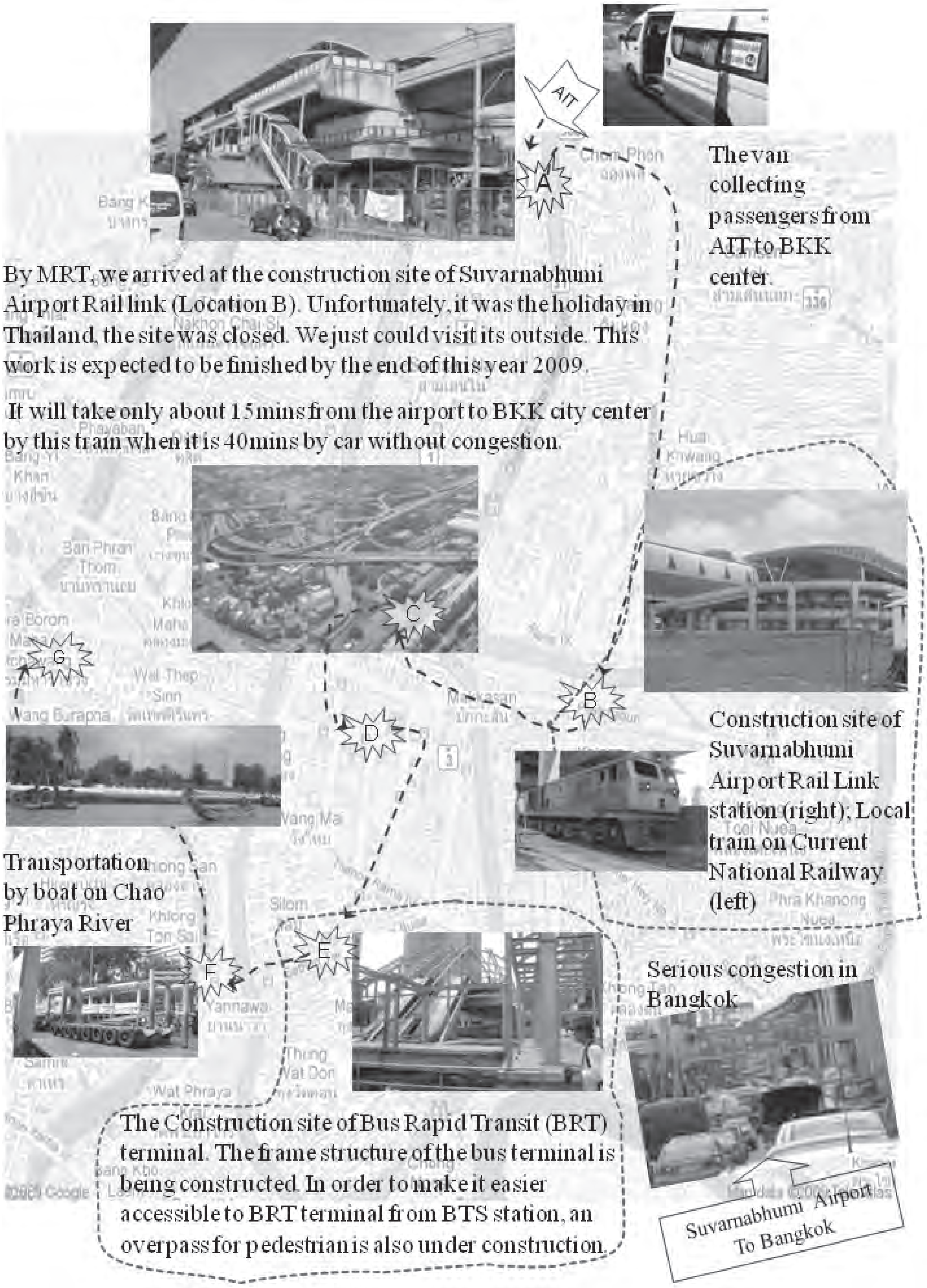

The van collecting passengers from AIT to BKK center.

By MRT, we arrived at the construction site of Suvarnabhumi Airport Rail link (Location B). Unfortunately, it was the holiday in Thailand, the site was closed. We just could visit its outside. This work is expected to be finished by the end of this year 2009.

It will take only about 15mins from the airport to BKK city center by this train when it is 40mins by car without congestion.

Construction site of Suvarnabhumi Airport Rail Link station (right); Local train on Current National Railway (left)

Transportation by boat on Chao Phraya River

Serious congestion in Bangkok

The Construction site of Bus Rapid Transit (BRT) terminal. The frame structure of the bus terminal is being constructed. In order to make it easier accessible to BRT terminal from BTS station, an overpass for pedestrian is also under construction.

IMPRESSIONS FROM THE STUDENT PARTICIPANTS

Mr. German A. Pardo R.

The 2nd Joint Student Seminar on Civil Infrastructure was fruitful in many aspects. First of all, this was my first time giving a presentation about a research in an important event, being this challenging but gratifying in order to acquire experience for futures presentations. Second, I could obtain some useful information from the other presentations which were about different topics, and also notice the different ways of presenting from the speakers. From the field visit I could realized the way Thailand government is facing its traffic congestion problem by implementing different types of transportation systems. Finally the possibility of visiting for the first time this country, and know more about its culture accompanied by my other friends from The University of Tokyo. In summary this experience was great and unique.

Mr. Vu Viet Hung

The 2nd Joint Student Seminar on Civil infrastructures provided me a very good chance not only to share my current research with other students on the same field, but also to taste the special Thai's culture and food. I will memorize deeply all my "hot" experiences I had in this event, such as "hot" seminar, "hot" food and "hot" weather. It was a big surprise for me because of the diversity Bangkok transportation systems and infrastructures even though there is still a lot of works to improve in the future. Another impression is the unique architecture of temples and shrines in Thailand, and the ancient city in Ayutthaya. Finally I really appreciate and want to express my gratitude to all organizers who held this event and all my friends.

Ms. Mari Sato

The 2nd Joint Student Seminar on Civil Infrastructures at the Asian Institute of Technology gave me precious and unforgettable experience. To communicate with students who study different fields was very exciting. From this seminar, I realized that there were various issues in Civil Engineering and that these issues were related with each other. Presentation in English is very hard for me even now. However, I was motivated to study harder in both my research field (Geotechnical engineering) and English. Public transportation tour in Thailand was also interesting. I was so surprised that fee of TukTuk was more expensive than that of taxi. I would like to visit Bangkok again by Airport Rail Link. Finally, I express to all participants my deepest gratitude for your kind attention of my presentation. I am looking forward to seeing you again and discussing with various research topics of Civil Engineering.

Ms. Hoang Thuy Linh

The seminar in AIT and the whole trip in Bangkok were so great and unforgettable to me. It was not only my first opportunity to attend and to be a speaker in an international seminar but also my first chance to Thailand. The seminar gave me a chance to meet, to talk and to share with many friends from other universities who are Korean, Thai and Bangladesh about our research or our concerns. At the presentation session, I have learnt a lot from the professors' lectures and other friends' presentations. On the visiting some public transportation facilities in Bangkok which is close to my major –Traffic engineering, I could experience many types of transportation means and their histories of development. Besides, the trip had made our team members get to know each other better. I did have a very good time in Thailand!

Mr. Shumon Mori

First of all it was my pleasure to participate in 2nd Joint Student Seminar. This Joint Student Seminar was the first international conference for me and I gained precious experience by studying in the presentation session, presenting in English, visiting the construction site and exchanging culture with other foreign students. The most impressive matter for me was the presentation session. Through the session I could learn various interesting fields related on civil infrastructures field. Actually it was not easy to understand others presentation but it stimulated my interest strongly and this experience will help my future works toward urban safety Engineering. Finally, I would appreciate ICUS for giving us this valuable opportunity.

Mr. Taiki Kou

The Joint Student Seminar on Civil Infrastructures bestowed me a good opportunity to share my research topic with the international participants. In the conference, I gave a presentation to the other countries' researchers for the first time and also could discuss the topic with professors and researchers during the question time and after the presentation. These discussions and advices significantly imparted me the insight into the development of my research. In addition, presentations given by other students and professors allowed me to have a chance to grasp other research areas of civil engineering. I would like to express my sincere gratitude for the opportunity I could receive and would like to make the most use of this experience toward my future research and activities I will be devoted to.

INTERNATIONAL CENTER FOR URBAN SAFETY ENGINEERING
Institute of Industrial Science, The Universiy of Tokyo
4-6-1 Komaba, Meguro-ku,
Tokyo 153-8505, Japan
http://icus.iis.u-tokyo.ac.jp
E-mail: icus@iis.u-tokyo.ac.jp

Tel: (+81-3)5452-6472 *Fax: (+81-3)5452-6476*